LECTURE NOTES ON

Nanomagnetism

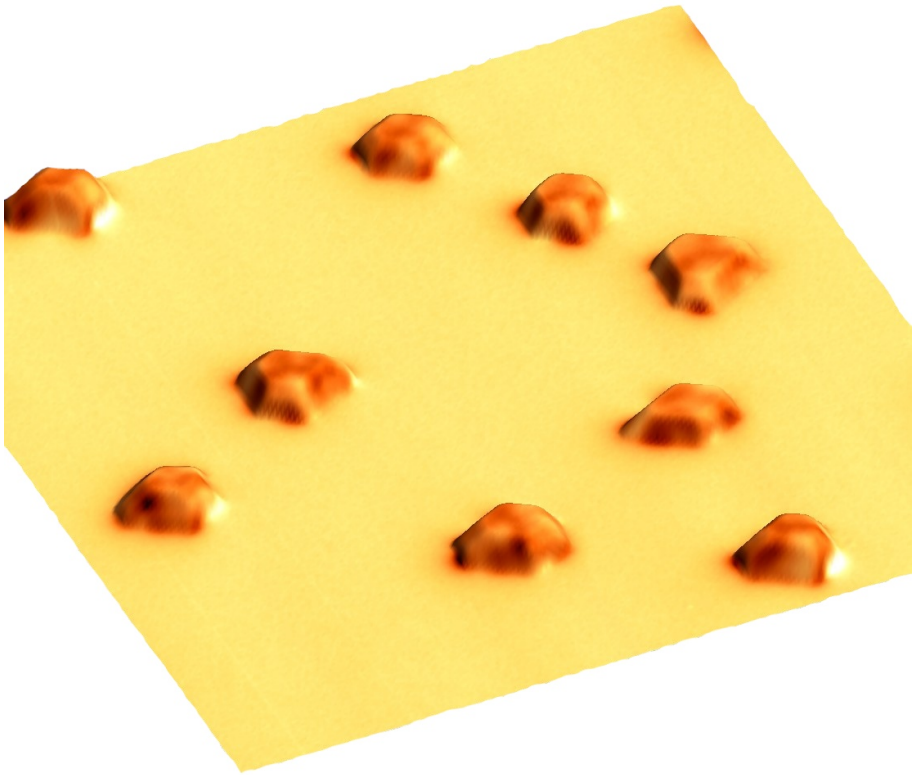

Olivier FRUCHART

SPINTEC (Université Grenoble Alpes, CNRS & CEA)

Version : October 3, 2018

Olivier.Fruchart-at-cea.fr

http://fruchart.eu

Contents

Introduction **6**
Content . . . 6
Notations . . . 7
Formatting . . . 8

I Setting the ground for nanomagnetism **10**
1 Magnetic fields and magnetic materials . . . 11
1.1 Magnetic fields . . . 11
1.2 Magnetic materials . . . 12
1.3 Magnetic materials under field – The hysteresis loop . . . 15
1.4 Domains and domain walls . . . 19
2 Units in Magnetism . . . 20
3 The various types of magnetic energy . . . 22
3.1 Introduction . . . 22
3.2 Zeeman energy . . . 23
3.3 Magnetic anisotropy energy . . . 23
3.4 Exchange energy . . . 24
3.5 Magnetostatic energy . . . 25
3.6 Characteristic quantities . . . 26
4 Handling dipolar interactions . . . 27
4.1 Simple views on dipolar interactions . . . 27
4.2 Various ways to handle magnetostatics . . . 28
4.3 Demagnetizing factors . . . 30
5 The Bloch domain wall . . . 34
5.1 Simple variational model . . . 35
5.2 Exact model . . . 35
5.3 Defining the width of a domain wall . . . 37
6 Magnetometry and magnetic imaging . . . 38
6.1 Extraction and vibrating magnetometers . . . 39
6.2 Faraday and Kerr effects . . . 40
6.3 X-ray Magnetic Dichroism techniques . . . 41
6.4 Scanning probe microscopies . . . 44
6.5 Electron microscopies . . . 48
Problems for Chapter I . . . 52
1. Self-testing . . . 52
2. Short questions . . . 52

3. Demagnetizing coefficients of composite materials 53
4. More about units 55
5. More about the Bloch domain wall 56
6. Extraction and vibration magnetometer 59
7. Magnetic force microscopy 61

II Magnetism and magnetic domains in low dimensions **63**
1 Magnetic ordering in low dimensions 64
1.1 Ordering temperature 64
1.2 Ground-state magnetic moment 66
2 Magnetic anisotropy in low dimensions 67
2.1 Dipolar anisotropy 67
2.2 Projection of magnetocrystalline anisotropy due to dipolar energy 68
2.3 Interface magnetic anisotropy 69
2.4 Magnetoelastic anisotropy 72
3 Domains and domain walls in thin films 74
3.1 Bloch versus Néel domain walls 74
3.2 Domain wall angle 76
3.3 Composite domain walls 77
3.4 Vortices and antivortex 78
3.5 Films with an out-of-plane anisotropy 80
4 Domains and domain walls in nanostructures 82
4.1 Domains in nanostructures with in-plane magnetization . . . 83
4.2 Domains in nanostructures with out-of-plane magnetization 84
4.3 The critical single-domain size 85
4.4 Near-single-domain 86
4.5 Domain walls in strips and wires 87
5 An overview of characteristic quantities 89
5.1 Energy scales 89
5.2 Length scales 89
5.3 Dimensionless ratios 90
Problems for Chapter II 91
1. Self-testing 91
2. Short questions 91
3. Demagnetizing field in a strip 92
4. Three-dimensional micromagnetics: a magnetic nanotube 93
4.3.a. Longitudinal magnetization94 4.3.b. Azimuthal magnetization95 4.3.c. Radial magnetization95
5. The Dzyaloshinskii-Moriya interaction and chiral magnetic structures 95

III Magnetization reversal **99**
1 Macrospins - The case of uniform magnetization 100

1.1 The Stoner-Wohlfarth model . . . 100
1.2 Dynamic coercivity: effects of temperature and waiting time 104
1.3 The superparamagnetic regime . . . 107
1.4 What do we learn from dynamic coercivity and superparamagnetism? . . . 110
1.5 Ensembles of grains . . . 110
2 Magnetization reversal in nanostructures . . . 111
2.1 Near single domains . . . 111
2.2 Large elements of soft magnetic material . . . 116
2.3 Motion of domain walls in one-dimensional elements . . . 118
2.4 Magnetization processes inside domain walls and vortices . 120
3 Magnetization reversal in extended systems . . . 121
3.1 Description of the question at stake . . . 121
3.2 Zero-temperature views . . . 122
3.3 Activation volume . . . 126
3.4 Practical cases and models . . . 127
Problems for Chapter III . . . 131
1. Self-testing . . . 131
2. Short questions . . . 131
3. Herzer model for coercivity in nanocrystalline materials . . . 132
4. A model of pinning - Kondorski's law for coercivity . . . 134
5. Droplet model for nucleation . . . 135

IV Precessional dynamics of magnetization 138
1 Ferromagnetic resonance and Landau-Lifshitz-Gilbert equation . . . 139
1.1 Precession . . . 139
1.2 Ferromagnetic resonance . . . 141
1.3 Damping and Landau-Lifshitz equations . . . 144
1.4 Spin waves . . . 145
2 Precessional switching of macrospins driven by magnetic fields . . . 147
2.1 The role of shape anisotropy . . . 147
2.2 Setting-in in-plane uniaxial anisotropy . . . 149
2.3 Practical conditions: finite damping and pulse length . . . 151
3 Precessional motion of domain walls and vortices driven by a magnetic field . . . 154
3.1 Domain walls – The case of azimuthal isotropy . . . 154
3.2 Domain walls – The case of azimuthal anisotropy . . . 156
Problems for Chapter IV . . . 160
1. Self-testing . . . 160
2. Short questions . . . 160
3. Effective fields . . . 161
4. Precessional switching of magnetization . . . 161
5. Damping . . . 163

Appendices **165**
Symbols 165
Acronyms 166
Glossary 167

Bibliography **169**

Introduction

Content

This manuscript is based on several lectures about *Nanomagnetism*. Parts have been given at the European School on Magnetism, IEEE Magnetics Society Summer School, the École Doctorale de Physique de Grenoble, the Master-2 Nanoscience and Nanotechnology in Grenoble, and in Master-2 lectures at the Cadi Ayyad University in Marrakech.

Nanomagnetism may be defined as the branch of magnetism dealing with low-dimension systems and/or systems with small dimensions. Such systems may display behaviors different from those in the bulk, pertaining to magnetic ordering, magnetic domains, magnetization reversal etc. These notes are mainly devoted to these aspects, with an emphasis on magnetic domains and magnetization reversal.

Spintronics, *i.e.* the physics linking magnetism and electrical transport such as magnetoresistance, is only partly and phenomenologically mentioned here. We will consider those cases where spin-polarized currents influence magnetism, however not when magnetism influences the electronic transport.

This manuscript is only an introduction to Nanomagnetism, and also sticking to a classical and phenomenological descriptions of magnetism. It targets beginners in the field, who need to use basics of Nanomagnetism in their research. Thus the explanations aim at remaining understandable by a large scope of physicists, while staying close to the state-of-the art for the most advanced or recent topics.

Every chapter is followed by a series of questions and problems. There is first a series of *self-testing questions*. These are of use to test your understanding of the basic concepts of the chapter. No calculation nor analysis is needed. Second is a series of *Short questions*. These generally require a bit of thinking and possibly calculation. There both test your understanding of the chapter, and possibly extend the concepts described in the chapter. Finally, a series of problems is proposed. A problem tackles a focused topic, being an application of the concepts covered by the chapter. is consists of a structured list of questions, whose coverage may require typically one hour of work. Many of them were part of Master exams.

Finally, **these notes are never intended to be in a final form, and are thus by nature imperfect. The reader should not hesitate to report errors or make suggestions about topics to improve or extend further**. A consequence is that it is probably unwise to print this document. Its use as an electronic file is anyhow preferable to benefit from the included links within the file. At present only chapters I and II are more or less completed.

It is my pleasure to acknowledge comments on the manuscript from Alberto GUIMARÃES. Several students also contributed to track mistakes and suggest improvements, especially Michal STAŇO, Alexis WARTELLE, Ilja RAUSCH, Rafael MESTRE CASTILLO, David WANDER. Valuable information and feedback was also provided by Hélène BÉA, Ursula EBELS, Daria GUSAKOVA, Jean-Christophe TOUSSAINT, Jan VOGEL.

I welcome all future comments to contribute to the improvement of these notes.

Notations

As a general rule, the following typographic rules will be applied to variables:

Characters

- A microscopic extensive or intensive quantity appears as slanted uppercase or Greek letter, such as H for the magnitude of magnetic field, E for a density of energy expressed in J/m^3, ρ for a density.
- An extensive quantity integrated over an entire system appears as handwritten uppercase. A density of energy E integrated over space will thus be written $\mathcal{E}$, and expressed in J.
- A microscopic quantity expressed in a dimensionless system appears as a handwritten lowercase, such as e for an energy or h for a magnetic field normalized to a reference value. Greek letters will be used for dimensionless versions of integrated quantities, such as ϵ for a total energy.
- Lengths and angles will appear as lower case roman or Greek letters, such as x for a length or α for an angle. If needed, a specific notation is introduced for dimensionless lengths.
- A vector appears as bold upright, with no arrow. Vectors may be lowercase, uppercase, handwritten or Greek, consistent with the above rules. We will thus write $\mathbf{H}$ for a magnetic field, $\mathbf{h}$ its dimensionless counterpart, $\mathfrak{M}$ or $\boldsymbol{\mu}$ a magnetic moment.
- The unit vector linked with coordinate i will be written: $\hat{\boldsymbol{\imath}}$. For example, the set of unit vectors in cartesian coordinates is $(\hat{\boldsymbol{x}}, \hat{\boldsymbol{y}}, \hat{\boldsymbol{z}})$. The set of unit vectors in spherical coordinates is $(\hat{\boldsymbol{r}}, \hat{\boldsymbol{\theta}}, \hat{\boldsymbol{\varphi}})$. A unit vector tangent to a curve will be

written $\hat{\boldsymbol{t}}$. A unit vector normal to a curve or a surface will be written $\hat{\boldsymbol{n}}$.

Mathematics

- The dot product of two vectors **A** and **B** is written $\mathbf{A} \cdot \mathbf{B}$.
- The cross product of two vectors **A** and **B** is written $\mathbf{A} \times \mathbf{B}$.
- The curl of a vector field $\nabla \times \mathbf{A}$ is written **curl A**.
- Einstein notation (implicit summation): $n_i \mathbf{u}_i$ is a shortcut for $\sum_i n_i \mathbf{u}_i$
- i is the imaginary number such that $\exp(i\pi) = -1$
- The elementary integration volume and surface elements are written $\mathrm{d}\mathcal{V}$ and $\mathrm{d}\mathcal{S}$, respectively.
- ∂ means a boundary. For example, while $\mathcal{V}$ is a volume, $\partial\mathcal{V}$ is the surface bounding $\mathcal{V}$.
- A dotted quantity is shortcut for its time derivative: $\dot{\mathbf{m}} = \mathrm{d}\mathbf{m}/\mathrm{d}t$.
- Functions
  - $\cosh x = ([\exp(x) + \exp(-x)]/2$ the hyperbolic cosine
  - $\sinh x = ([\exp(x) - \exp(-x)]/2$ the hyperbolic sine
  - $\tanh x = \sinh x / \cosh x$ the hyperbolic tangent
  - $\coth x = \cosh x / \sinh x$ the hyperbolic cotangent
  - $\mathcal{L}(x) = \coth x - 1/x$ is the Langevin function
  - $\mathcal{B}_{1/2} = \tanh$ is the Brillouin $1/2$ function

Units

- The International system of units (SI) will be used for numerical values. Notations should conform to the recommendations of the Bureau International des Poids et Mesures (BIPM).
- B will be called magnetic induction, H magnetic field, and M magnetization. We will often use the name magnetic field in place of B when no confusion exists, *i.e.* in the absence of magnetization (in vacuum). This is a shortcut for B/μ_0, to be expressed in Teslas.

Special formatting

Special formatting is used to draw the attention of the reader to certains aspects, as illustrated below.

Words highlighted like this are of special importance, either in the local context, or when they are important concepts introduced for the first time.

The hand sign will be associated with hand-wavy arguments and take-away messages.

The slippery sign will be associated with misleading aspects and fine points.

Chapter I

Setting the ground for nanomagnetism

Overview

A thorough introduction to Magnetism[1–3] and Micromagnetism and Nanomagnetism[4–7] may be sought in dedicated books. This chapter only serves as an introduction to the lecture, and it is not comprehensive. We only provide general reminders about magnetism, micromagnetism, and of some characterization techniques useful for magnetic films and nanostructures.

1 Magnetic fields and magnetic materials

1.1 Magnetic fields

Electromagnetism is described by the four Maxwell equations. Let us consider the simple case of stationary equations. Magnetic induction **B** then obeys two equations:

$$\mathbf{curl}\,\mathbf{B} = \mu_0 \mathbf{j} \tag{I.1}$$

$$\mathrm{div}\,\mathbf{B} = 0 \tag{I.2}$$

j being a volume density of electrical current. **j** appears as a source of induction loops, similar to electrostatics where the density of electric charge ρ is the source of radial electric field **E**. Let us first consider the simplest case for an electric current, that of an infinite linear wire with total current I. We shall use cylindrical coordinates. Any plane comprising the wire is a symmetry element for the current and thus an antisymmetric element for the resulting induction (see above equations), which thus is purely orthoradial and described by the component B_θ only. In addition the system is invariant by rotation around and translation along the wire, so that B_θ depends neither on θ nor z, however solely on the distance r to the wire. Applying Stokes theorem to an orthoradial loop with radius r (Figure I.1) readily leads to:

$$B_\theta(r) = \frac{\mu_0 I}{2\pi r} \tag{I.3}$$

This is the so-called Œrsted induction or Œrsted field, named after its discovery in 1820 by Hans-Christian ŒRSTED. This discovery was the first evidence of the connection of electricity and magnetism, and is therefore a foundation for the development of electromagnetism. Notice the variation with $1/r$. Let us consider an order of magnitude for daily life figures. For $I = 1\,\mathrm{A}$ and $r = 10^{-2}\,\mathrm{m}$ we find $B = 2 \times 10^{-5}\,\mathrm{T}$. This magnitude is comparable to the earth magnetic field, around 50 µT. It is weak compared to fields arising from permanent magnets or dedicated electromagnets and superconducting magnets.

We may argue that there exists no infinite line of current. The Biot and Savart law describes instead the elementary contribution to induction $\delta\mathbf{B}$ at point P,

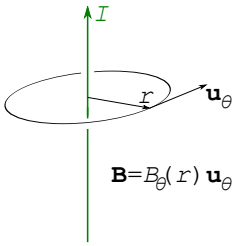

Figure I.1 – So-called Œrsted magnetic induction **B**, arising from an infinite and linear wire with an electrical current I.

Table I.1 – Long-distance decay of induction arising from various types of current distributions

Case	Decay
Infinite line of current	$1/r$
Elementary segment	$1/r^2$
Current loop (magnetic dipole)	$1/r^3$

arising from an elementary part of wire $\delta\ell$ at point Q with a current I:

$$\delta\mathbf{B}(P) = \frac{\mu_0 I\, \delta\ell \times \mathbf{QP}}{4\pi QP^3} \tag{I.4}$$

Notice this time the variation as $1/r^2$. This can be understood qualitatively as a macroscopic (infinite) line is the addition (mathematically, the integral) of elementary segments, and we have $\int 1/r^2 \mathrm{d}r = 1/r + \mathrm{Cte}$. It may also be argued that there exists no elementary segments of current for conducting wirings, however only closed circuits (loops), with a uniform current I along its length. When viewed as a distance far compared to its dimensions, the Biot and Savart law for a small loop of current can be expanded in Taylor series, which to first order reads

$$\mathbf{B}(\mathbf{r}) = \frac{\mu_0}{4\pi r^3}\left[3\frac{(\boldsymbol{\mu}\cdot\mathbf{r})\mathbf{r}}{r^2} - \boldsymbol{\mu}\right]. \tag{I.5}$$

where $\boldsymbol{\mu}$ is a pinpoint magnetic dipole, which is an example of a magnetic moment. For a planar loop $\boldsymbol{\mu} = I\mathbf{S}$ where $\mathbf{S}$ is the surface vector normal to the plane of the loop, oriented accordingly with the electrical current. Here it appears clearly that the SI unit for a magnetic moment is $\mathrm{A}\cdot\mathrm{m}^2$. Also, note now the variation with $1/r^3$. This may be understood as the first derivative of the variation like $1/r^2$ arising from an elementary segment, due to nearby regions run by opposite vectorial currents j (*e.g.* the opposite parts of a loop).

Table I.1 summarizes the three cases described above.

1.2 Magnetic materials

A magnetic material is a body which displays a magnetization $\mathbf{M}(\mathbf{r})$, *i.e.* a volume density of magnetic moments. The SI unit for magnetization therefore appears naturally as $\mathrm{A}\cdot\mathrm{m}^2/\mathrm{m}^3$, thus $\mathrm{A/m}$[I.1]. In any material some magnetization may be induced under the application of an external magnetic field $\mathbf{H}$. We define the magnetic susceptibility χ with $\mathbf{M} = \chi\mathbf{H}$. This polarization phenomenon is named diamagnetism for $\chi < 0$ and paramagnetism for $\chi > 0$.

[I.1] We shall always use strictly the names magnetic moment and magnetization. Experimentally some techniques provide direct or indirect access to magnetic moments (*e.g.* an extraction magnetometer, a SQUID, magnetic force microscopy), other provide a more natural access to magnetization, often through data analysis (*e.g.* magnetic dichroism of X-rays, electronic or nuclear resonance).

Table I.2 – Main features of a few important magnetic materials: ordering (Curie) temperature T_C, spontaneous magnetization M_s, a magnetocristalline anisotropy constant K at $300\,\mathrm{K}$ (The symmetry of the materials, and hence the order of the anisotropy constants provided, is not discussed here). The last column provides the diameter below which a spherical particle of that material is superparamagnetic at room temperature for an observation time of 1 s, a state that will be defined in chap.III, p.104.

Material	T_C (K)	M_s (kA/m)	$\mu_0 M_s$ (T)	K (kJ/m^3)	$D_{300\,\mathrm{K}}$ (nm)
Fe	1043	1730	2.174	48	16
Co	1394	1420	1.784	530	7.2
Ni	631	490	0.616	-4.5	35
$Fe_{20}Ni_{80}$ (Permalloy)	850	835	1.050	≈ 0	–
$Fe_{65}Co_{35}$ (Permendur)	1210	1950	2.45	20	24.7
Fe_3O_4	858	480	0.603	-13	25
$BaFe_{12}O_{19}$	723	382	0.480	250	9.2
$Nd_2Fe_{14}B$	585	1280	1.608	4900	3.4
$SmCo_5$	995	907	1.140	17000	2.3
Sm_2Co_{17}	1190	995	1.250	3300	3.9
FePt $L1_0$	750	1140	1.433	6600	3.1
CoPt $L1_0$	840	796	1.000	4900	3.4
Co_3Pt	1100	1100	1.382	2000	4.6

Diamagnetism arises from a Lenz-like law at the microscopic level (electronic orbitals), and is present in all materials. χ_{dia} is constant with temperature and its value is material-dependent, however roughly of the order of 10^{-5}. Peak values are found for Bi ($\chi = -1.66 \times 10^{-4}$) and graphite along the c axis ($\chi \approx -4 \times 10^{-4}$). Such peculiarities may be explained by the low effective mass of the charge carriers involved.

Paramagnetism arises from partially-filled orbitals, either forming bands or localized. The former case is called Pauli paramagnetism. χ is then temperature-independent and rather weak, again of the order of 10^{-5}. The later case is called Curie paramagnetism, and χ scales with $1/T$. A useful order of magnitude in Curie paramagnetism to keep in mind is that a moment of $1\,\mu_B$ gets polarized at $1\,\mathrm{K}$ under an induction of 1 T.

Only certain materials give rise to paramagnetism, in particular metals or insulators with localized moments. Then diamagnetism and paramagnetism add up, which may result in an overall paramagnetic of diamagnetic response.

Finally, in certain materials microscopic magnetic moments are coupled through a so-called exchange interaction, leading to the phenomenon of magnetic ordering at finite temperature and zero field. For a first approach magnetic ordering may be described in mean field theory modeling a molecular field, as we will detail for low dimension systems in Chapter II. The main types of magnetic ordering are:

- Ferromagnetism, characterized by a positive exchange interaction, end

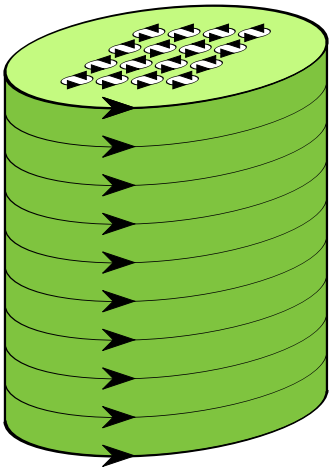

Figure I.2 – Amperian description of a ferro (or ferri-)magnetic material: microscopic currents cancel each other between neighboring regions, except at the perimeter of the body.

favoring the parallel alignment of microscopic moments. This results in the occurrence of a spontaneous magnetization M_s[I.2]. In common cases M_s is of the order of 10^6 A/m, which is very large compared to magnetization arising from paramagnetism or diamagnetism. The ordering occurs only at and below a temperature called the Curie temperature, written T_C. The only three pure elements ferromagnetic at room temperature are the 3d metals Fe, Ni and Co (Table I.2).

- Antiferromagnetism results from a negative exchange energy, favoring the antiparallel alignment of neighboring moments[I.3] leading to a zero net magnetization M_s at the macroscopic scale. The ordering temperature is in that case called the Néel temperature, and is written T_N.
- Ferrimagnetism arises in the case of negative exchange coupling between moments of different magnitude, because located each on a different sublattice[I.4], leading to a non-zero net magnetization. The ordering temperature is again called Curie temperature.

Let us consider the simple case of a body with uniform magnetization, for example a spontaneous magnetization $\mathbf{M}_s = M_s\hat{\boldsymbol{z}}$ (Figure I.2). It is readily seen that the equivalent current loops modeling the microscopic moments cancel each other for neighboring loops: only currents at the perimeter remain. The body may thus be modeled as a volume whose surface carries an areal density of electrical current, whose magnitude projected along $\hat{\boldsymbol{z}}$ is M_s. This highlights a practical interpretation of the magnitude of magnetization expressed in A/m.

Let us stress a fundamental quantitative difference with Œrsted fields. We consider again a metallic wire carrying a current of 1 A. For a cross-section of

[I.2] The s in M_s is confusing between the meanings of spontaneous and saturation. We will discuss this fine point in the next paragraph.

[I.3] More complexe arrangements, non-colinear like spiraling, exist like in the case of Cr.

[I.4] Similarly to antiferromagnetism, more complex arrangements may be found.

$1\,\mathrm{mm}^2$ a single wiring has 1000 turns/m. The equivalent magnetization would be $10^3\,\mathrm{A/m}$, which is three orders of magnitude smaller than M_s of usual ferromagnetic materials. Thus a significant induction may easily be obtained from the stray field of a permanent magnet, of the order of $\mu_0 M_s \approx 1\,\mathrm{T}$. It is possible to reach magnitude of induction of several Teslas with wirings, however with special designs: large and thick water-cooled coils to increase the current density and total value, or use superconducting wires however requiring their use at low temperature, or use pulsed currents with high values, this time requiring small dimensions to minimize self-inductance.

Let us finally recall the relationship between induction, magnetic field and magnetization:

$$\mathbf{B} = \mu_0(\mathbf{H} + \mathbf{M}) \tag{I.6}$$

This relationship may be derived starting from Maxwell's equations, considering as two different ensembles the free electric charges, and the so-called bound electric charges plus spin magnetic moments, contributing to magnetization **M**[3]. **B** is the induction vector field described in Maxwell's equations. From the above $\mu_0\mathbf{H}$ appears as the induction (or **H** in terms of magnetic field), excluding the local contribution of magnetization. Thus, **H** is the relevant quantity whenever is considered the effect of the environment on magnetization in materials as will be discussed in the following: Zeeman energy or internal energy, mechanical torque etc. On the reverse, **B** is the relevant quantity to describe the effect of an independent system like the Lorentz force $\mathbf{F} = q\mathbf{v} \times \mathbf{B}$ acting on a free charge.

1.3 Magnetic materials under field – The hysteresis loop

Let us consider a system mechanically fixed in space, subjected to an applied magnetic field **H**. This field gives rise to a Zeeman energy, written $E_Z = -\mu_0 \mathbf{M}_s \cdot \mathbf{H}$ for a volume density, or $\mathcal{E}_Z = -\mu_0 \boldsymbol{\mu} \cdot \mathbf{H}$ for the energy of a magnetic moment. The consequence is that magnetization will tend to align itself along **H**, which shall be attained for a sufficient magnitude of **H**. This process is called a magnetization process, or magnetization reversal. The quantity considered or measured may be a moment or magnetization, the former in magnetometers and the latter in some magnetic microscopes or in the Extraordinary Hall Effect, for example. It is often displayed, in models or as the result of measurements, as a hysteresis loop, also called magnetization loop or magnetization curve. The horizontal axis is often H or $\mu_0 H$, while the y axis is the projection of the considered quantity along the direction of **H** [*e.g.*: $(\mathbf{M} \cdot \mathbf{H})/H$].

Hysteresis loops are the most straightforward and widespread characterization of magnetic materials. We will thus discuss it in some details, thereby introducing important concepts for magnetic materials and their applications. We restrict the discussion to quasistatic hysteresis loops, *i.e.* nearly at local equilibrium. Dynamic and temperature effects require a specific discussion and microscopic modeling, which will be discussed in chapter sec.III, p.104.

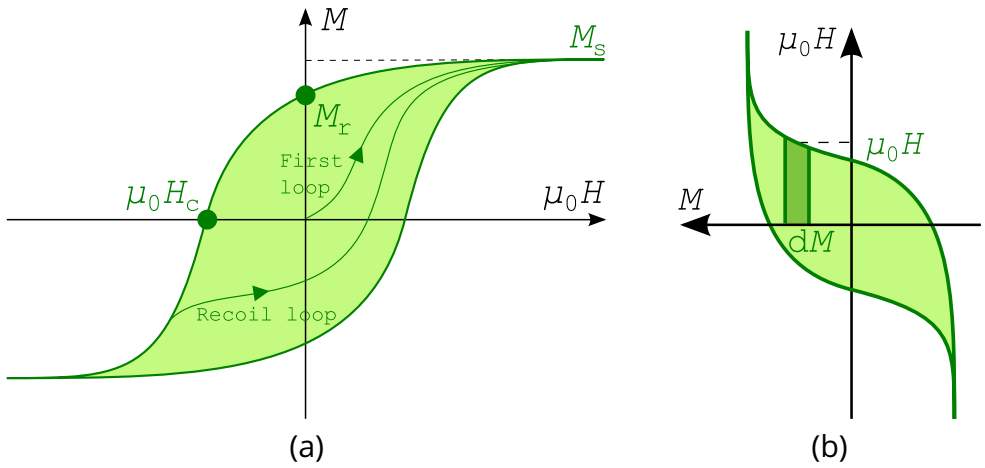

Figure I.3 – (a) **Typical hysteresis loop** illustrating the definition of coercivity H_c, saturation M_s and remanent M_r magnetization. A minor (recoil) loop as well as a first magnetization loop are shown in thinner lines (b) The losses during a hysteresis loop equal the area of the loop.

Figure I.3 shows a typical hysteresis loop. We will speak of magnetization for the sake of simplicity. However the concepts discussed more generally apply to any other quantity involved in a hysteresis loop.

- **Symmetry –** Hysteresis loops are centro-symmetric, reflecting the time-reversal symmetry of Maxwell's equations ($H \to -H$ and $M \to -M$)

Time-reversal symmetry and shifted hysteresis loops. We will see in chapter III that hysteresis loops of certain heterostructured systems may be non-centro-symmetric, due to shifts along both the field and magnetization axes. This however does not contradict the principle of time-reversal symmetry, as such hysteresis loops are minor loops. Application of a sufficiently high field (let aside the practical availability of such a high field) would yield a centro-symmetric loop.

- **'Saturation' magnetization –** Due to Zeeman energy the magnetization tends to align along the applied field when the magnitude of the latter is large, associated with a saturation of the $M(H)$ curve. For this reason one often names saturation magnetization the resulting value of magnetization. We may normalize the loop with its value towards saturation, and get a function spanning in $[-1; 1]$.

Spontaneous and saturation magnetization. Two remarks shall be made. First the 's' subscript brings some confusion between spontaneous and saturation magnetization. Both have a precise meaning in the mean-field model for magnetic ordering: the saturation magnetization is the maximum magnetization available from microscopic (local) moments, if not averaged out by thermal effects. The spontaneous magnetization is the macroscopic magnetization under zero applied field, resulting from the competition of exchange energy and thermal disorder. Saturation magnetization may also be used with an experimental meaning, that of the value of magnetization reached towards high applied magnetic field in a hysteresis loop. The knowledge of the volume of the system (if a moment is measured) or a model (in case an experiment probes indirectly magnetization) is needed to link an experimental quantity with magnetization. Intrinsic or extrinsic contributions to the absence of true saturation of hysteresis loops are also an issue.

- **Remanent magnetization –** starting from the application of an external magnetic field, we call remanent magnetization (namely, which remains) and write M_r or m_r when normalized, the value of magnetization remaining when the field is back to zero. After applying a positive (resp. negative) field, m_r is usually found positive (resp. negative)[I.5].
- **Coercive field –** We call coercive field (namely, which opposes an action, here that of an applied magnetic field) and write H_c, the magnitude of field for which the loop crosses the x axis, *i.e.* when the average magnetization projected along the direction of the field vanishes.
- **Hysteresis and metastability –** We have mentioned that the sign of remanence depends on that of the magnetic field applied previously. This feature is named hysteresis: the $M(H)$ path followed for rising field is different from the descending path. Hysteresis results from the physical notion of metastability: for a given magnitude (and direction) of magnetic field, there may exist several equilibrium states of the system. These states are often only local minima of energy, and then said to be metastable. Coercivity and remanence are two signatures of hysteresis. The number of degrees of freedom increases with the size of a system, and so may do the number of metastable states in the energy landscape. The field history describes the sequence of magnetic fields (magnitude, sign and/or direction) applied before an observation. This history is crucial to determine in which stable or metastable state the system is left[I.6]. This highlights the important role played by spatially-revolved techniques (both for microscopies and in reciprocal space) to deeply characterize the magnetic state of a system.

[I.5] See short question 3 in chap.III (see p.131) for a case of negative remanence

[I.6] The reverse is not true: it is not always possible to design a path in magnetic field liable to prepare the system in an arbitrary metastable state.

Metastability implies features displayed during first-order transitions such as relaxation (over time) based on domain-wall movement, nucleation and the importance of extrinsic features in these such as defects. This implies that the modeling and engineering of the microstructure of materials is a key to control properties such as coercivity and remanence.

- **Energy losses –** We often read the name magnetic energy, for a quantity including the Zeeman energy. This is improper from a thermodynamic point of view. The Zeeman quantity $-\mu_0 \mathbf{M} \cdot \mathbf{H}$ is the counterpart of $+PV$ for fluids thermodynamics: $\mathbf{H}$ is the vectorial intensive counterpart of pressure, and $\mathbf{M}$ is the vectorial extensive[I.7] counterpart of volume, *i.e.* a response of the system to the external stimulus. Thus, we should use the name density of magnetic enthalpy for the quantity $E_{\text{int}} - \mu_0 \mathbf{M} \cdot \mathbf{H}$, where E_{int} is the density of internal magnetic energy of the system[I.8], with analogy to $H = U + PV$. A readily-seen consequence is that the quantity $+\mu_0 \mathbf{H} \cdot \mathrm{d}\mathbf{M}$, analogous to $-P\mathrm{d}V$, is the density of work provided by the (external) operator and transferred to the system upon an infinitesimal magnetization process. Rotating the magnetization loop by 90° to consider M as the x axis, we see that the area encompassed by the hysteresis loop measures the amount of work provided to the system upon the loop, often in the form of heat (Figure I.3b).
- **Functionalities of magnetic materials –** The quantities defined above allow us to consider various types of magnetic materials, and their use for applications. Metastability and remanence are key properties for memory applications such as hard disk drives (HDDs), as its sign keeps track of the previously applied field, defining so-called up and down states. Coercivity is crucial for permanent magnets, which must remain magnetized in a well-defined direction of the body with a large remanence, giving rise to forces and torques of crucial use in motors and actuators. In practice coercivities of one or two Teslas may be reached in the best permanent-magnet materials such as $SmCo_5$, Sm_2Co_{17} and $Nd_2Fe_{14}B$. The minimization of losses in the operation of permanent magnets and magnetic memories is important, both to minimize heating and for energy efficiency. Among applications requiring small losses are transformers and magnetic shielding. To achieve this one seeks both low coercivity and low remanence, which defines so-called soft magnetic materials. These materials are also of use in magnetic field sensors based on their magnetic susceptibility, providing linearity (low hysteresis) and sensitivity (large susceptibility $\mathrm{d}M/\mathrm{d}H$). A coercivity well below $10^3\,\mathrm{A/m}$ (or 1.25 mT in terms of $\mu_0 H$) is obtained in the best soft magnetic materials, typically based on Permalloy ($Fe_{20}Ni_{80}$). On the reverse, some applications are based on losses such as induction stoves. There the magnitude of coercivity is a compromise between achieving large losses and the ability of the stove to produce large enough ac magnetic fields to

[I.7] or more precisely, the magnetic moment of the entire system $\iiint_{\mathcal{V}} \mathbf{M}_{\mathrm{s}} \mathrm{d}\mathcal{V}$.

[I.8] see part 3 for the description of contributions to E_{int}.

reverse magnetization. Finally, in almost all applications the magnitude of magnetization determines the strength of the sought effect, such as force or energy of a permanent magnet, readability for sensors and memories, energy for transformers and induction heating.

- **Partial loops –** In order to gain more information about the magnetic material than with a simple hysteresis loop, one may measure a first magnetization loop (performed on a virgin or demagnetized sample) or a minor loop (also called partial loop or recoil loop), see Figure I.3a.

Intrinsic versus extrinsic properties. One calls intrinsic those properties of a material depending only on its composition and structure, and extrinsic those properties related to microscopic phenomena related to *e.g.* microstructure (crystallographic grains and grain boundaries), sample shape etc. For example, spontaneous magnetization is an intrinsic quantity, while remanence and coercivity are extrinsic quantities.

1.4 Domains and domain walls

Hysteresis loop, described in the previous section, concerns a scalar and integrated quantity. It may thus hide details of magnetization (a vector quantity) at the microscopic level. Hysteresis loops must be seen as one out of many signatures of magnetization reversal, not a full characterization. Various processes may determine the features of hysteresis loops described above. It is a major task of micromagnetism and magnetic microscopies to unravel these microscopic processes, with a view to improve or design new materials.

For instance remanence smaller than one may result from the rotation of magnetization or from the formation of magnetic domains etc. Magnetic domains are large regions where in each the magnetization is largely uniform, while this direction may vary from one domain to another. The existence of magnetic domains was postulated by Pierre WEISS in his mean field theory of magnetism in 1907, to explain why materials known to be magnetic may display no net moment at the macroscopic scale. The first direct proof of the existence of magnetic domains came only in 1931. This is due to the Bitter technique, where nanoparticles are attracted by the loci of domain walls[6]. In 1932 Bloch proposes an analytical description of the variation of magnetization between two domains. This area of transition is called a magnetic domain wall. The basis for the energetic study of magnetic domains was proposed in 1935 by Landau and Lifshitz.

Let us discuss what may drive the occurrence of magnetic domains, whereas domain walls imply a cost in exchange and other energies, see sec.5. There exists two reasons for this occurrence, which in practice often take place simultaneously. The first reason is energetics, where the cost of creating domain walls is balanced by the decrease of dipolar energy which would be that of a body

remaining uniformly magnetized. This will be largely developed in chap.II. The second reason is magnetic history, which we have already mentioned when discussing hysteresis loops (see sec.1.3). For instance upon a partial demagnetization process up to the coercive field, domain walls may have been created, whose propagation will be frozen upon removal of the magnetic field.

Summary

Magnetic fields and magnetic materials. Following Maxwell's equations, magnetic induction **B** arises from moving charges. At each location in space **B** arises from two contributions: local spin and orbiting charges in matter, called magnetization **M**; the remainder called magnetic field **H**, arising from distant spin and moving charges (either distant magnetization, or current in a circuit, *e.g.* in a coil). Magnetization is also the volume density of magnetic moments in a magnetic material. The hysteresis loop $M(H)$ is the most common characterization of a magnetic material, underlying many processes implying magnetic domains

2 Units in Magnetism

The use of various systems of units is a source of annoyance and errors in magnetism. A good reference about units is that by F. Cardarelli[8]. Conversion tables for magnetic units may also be found in many reference books in magnetism, such as those of S. Blundell[1] and J. M. D. Coey[3]. An overview of the Système International and conventions for writing units may be downloaded from the Bureau International des Poids et Mesures (BIPM)[9]. We shall here shortly consider three aspects:

- **The units –** A system of units consists in choosing a reference set of elementary physical quantities, allowing one to measure each physical quantity with a figure relative to the reference unit. All physical quantities may then be expressed as a combination of elementary quantities; the dimension of a quantity describes this combination. For a long time many different units were used, depending on location and their field of use. Besides the multiples were not the same in all systems. The wish to standardize physical units arose during the French revolution, and the Academy of Sciences was in charge of it. In 1791 the meter was the first unit defined, at the time as the ten millionth of the distance between the equator and a pole. Strictly speaking four types of dimensions are enough to describe all physical variables. A common choice is: length L, mass M, time T, and electrical current I. This lead to the emergence of the MKSA set of units, standing for **M**eter, **K**ilogram, **S**econd, **A**mpère for the four above-mentioned quantities. The Conférences Générale des Poids et Mesures (General Conference on Weighs and Measures), an international organization, decided of the creation of the Système International d'Unités (SI).

In SI, other quantities have been progressively appended, which may in principle be defined based on MKSA, however whose independent naming is useful. The three extra SI units are thermodynamic temperature T (in Kelvin, K), luminous intensity (in candela, cd) and amount of matter (in mole, mol). The first two are linked with energy, while the latter is dimensionless. Finally, plane angle (in radian, rad) and solid angles (in steradian, sr) are called supplementary units. Another system than MKSA, of predominant use in the past, is the cgs system, standing for **C**entimeter, **G**ram, and **S**econd. At first sight this system has no explicit units for electrical current or charge, which is a weakness with respect to MKSA, *e.g.* when it comes to check the dimension homogeneity of formulas. Several sub-systems were introduced to consider electric charges or magnetic moments, such as the esu (electrostatic units), emu (electromagnetic units), or the tentatively unifying Gauss system. In practice, when converting units between MKSA and cgs in magnetism one needs to consider the cgs-Gauss unit for electrical current, the Biot (Bi), equivalent to 10 A. Other names in use for the Biot are the abampere or the emu ampere. Based on the decomposition of any physical quantity in elementary dimensions, it is straightforward to convert quantities from one to another system. For magnetic induction B 1 T is the same as 10^4 G (Gauss), for magnetic moment μ 1 $A \cdot m^2$ is equivalent to 10^3 emu and for magnetization M 1 A/m is equivalent to 10^{-3} emu/cm^3. In cgs-Gauss the unit for energy is erg, equivalent to 10^{-7} J. The issue of units would remain trivial, if restricted to converting numerical values. The real pain is that different definitions exist to relate H, M and B, as detailed below.

- **Defining magnetic field H –** In SI induction is most often defined with $B = \mu_0(H + M)$, whereas in cgs-Gauss it is defined with $B = H + 4\pi M$. The dimension of μ_0 comes out to be $L \cdot M \cdot T^{-2} \cdot I^{-2}$, thus $\mu_0 = 4\pi \times 10^{-7}\, m \cdot kg \cdot s^{-2} \cdot A^{-2}$ in SI. Using the simple numerical conversion of units one finds: $\mu_0 = 4\pi\, cm \cdot g \cdot s^{-2} \cdot Bi^{-2}$. Similar to the absence of explicit unit for electrical current, it is often argued that μ_0 does not exist in cgs. The conversion of units reveals that one may consider it in the definition of M, with a numerical value 4π. However the definition of H differs, as the same quantity is written $\mu_0 H$ in SI, and $(\mu_0/4\pi)H$ in cgs-Gauss. Thus, the conversion of magnetic field H gives rise to an extra 4π coefficient, besides powers of ten. This pitfall explains the need to use an extra unit, the œrsted, to express values for magnetic field H in cgs-Gauss. Then 1 Oe in cgs-Gauss is equivalent to $(10^3/4\pi)$ A/m[I.9] in SI. A painful consequence of the different definitions of H is that susceptibility $\chi = dM/dH$ differs by 4π between both systems, although is is a dimensionless quantity: $\chi_{cgs} = (1/4\pi)\chi_{SI}$. The same is true for demagnetizing coefficients if defined by $H_d = -NM$, with $N_{cgs} = 4\pi N_{SI}$.

[I.9] In practice, the absence of μ_0 in the cgs system often results in the use of either œrsted or Gauss to evaluate magnetic field and induction.

- **Defining magnetization M –** we often find the writing $J = \mu_0 M$ in the literature. More problematic is the (rather rare) definition to use M_s instead of $\mu_0 M_s$. It is for instance the case of the book of Stöhr and Siegmann[10], otherwise a very comprehensive book. These authors use the SI units, however define: $\mathbf{B} = \mu_0 \mathbf{H} + \mathbf{M}$. This can be viewed as a compromise between cgs and SI, however has an impact on all formulas making use of M.

Summary

M, H, B and the system of units. This section highlights that, beyond the mere conversion of numerical values, formulas depend on the definition used to link magnetization, magnetic field and induction. It is crucial to carefully check the system of units and definition used by authors before copy-pasting any formulas implying M, H or B.

3 The various types of magnetic energy

3.1 Introduction

There exists several sources of energy in magnetic systems, which we review in this section. For the sake of simplicity of vocabulary we restrict the following discussion to ferromagnetic materials, although all aspects may be extended to other types of orders. These energies will be described in the context of micromagnetism.

Micromagnetism is the name given to the investigation of the competition between these various energies, giving rise to characteristic magnetic length scales, and being the source of complexity of distributions of magnetization, which will be dealt with in chap.II. Its principles were first outlined in 1940 by William Fuller Brown, Jr[11].

Micromagnetism, be it numerical or analytical, is in most cases based on two assumptions:

- The variation of the direction of magnetic moment from (atomic) site to site is sufficiently gradual so that the discrete nature of matter may be ignored. Magnetization M and all other quantities are described in the approximation of continuous medium: they are continuous functions of the space variable $\mathbf{r}$.
- The norm M_s of the magnetization vector is constant and uniform in any homogeneous material. This norm may be that at zero or finite temperature. The latter case may be viewed as a mean-field approach.

Based on these two approximations for magnetization we often consider the unit vector $\mathbf{m}(\mathbf{r})$ to describe magnetization distributions, such that $\mathbf{M}_s(\mathbf{r}) = M_s \mathbf{m}(\mathbf{r})$.

3.2 Zeeman energy

The Zeeman energy pertains to the energy of magnetic moments in an external magnetic field. Its density is:

$$E_Z = -\mu_0 \mathbf{M} \cdot \mathbf{H} \tag{I.7}$$

E_Z tends to favor the alignement of magnetization along the applied field. As outlined above, this term should not be considered as a contribution to the internal energy of a system, however as giving rise to a magnetic enthalpy.

3.3 Magnetic anisotropy energy

The theory of magnetic ordering predicts the spontaneous occurrence of a magnetization **M**, however with no restriction on its direction in space. In a real system the internal energy depends on the direction of **M** with the underlying crystalline direction of the solid. This arises from the combined effect of crystal-field effects (coupling electron orbitals with the lattice) and spin-orbit effects (coupling orbital with spin moments).

This internal energy is called magnetocrystalline anisotropy energy, whose density will be written E_{mc} in these notes. One also often find the acronym MAE in the literature, for Magnetic Anisotropy Energy. The consequence of E_{mc} is the tendency for magnetization to align itself along certain axes (or in certain planes) of a solid, called easy directions. On the reverse, directions with a maximum of energy are called hard axes (or planes). Magnetic anisotropy is at the origin of coercivity, although the quantitative link between the two notions is complex, and will be introduced in chap.II.

The most general case may be described by a function $E_{mc} = Kf(\theta, \varphi)$, where f is a dimensionless function. In principle any set of angular functions complying with the symmetry of the crystal lattice considered may be used as a basis to express f and thus E_{mc}. Whereas the orbital functions $Y_{l,m}$ of use in atomic physics may be suitable, in practice one uses simple trigonometric functions. Odd terms do not arise in magnetocrystalline anisotropy because of time-reversal symmetry. Group theory can be used to highlight the terms arising depending on the symmetry of the lattice.

For a cubic material one finds:

$$E_{mc,cub} = K_{1c}s + K_{2c}p + K_{3c}p^2 + \dots \tag{I.8}$$

with $s = \alpha_1^2\alpha_2^2 + \alpha_2^2\alpha_3^2 + \alpha_3^2\alpha_1^2$ and $p = \alpha_1^2\alpha_2^2\alpha_3^2$, α_i being the cosines of the magnetization direction with the three axes. For hexagonal symmetry

$$E_{mc,hex} = K_1 \sin^2\theta + K_2 \sin^4\theta + \dots \tag{I.9}$$

where θ is the (polar) angle between **M** and the c axis. Here we dropped the azimuthal dependence because it is of sixth order, and that in practice the

magnitude of anisotropy constants decreases sharply with its order. Thus for an hexagonal material the magnetocrystalline anisotropy is essentially uniaxial.

Group theory predicts the form of these formulas, however not the numerical values, which are material dependent. For example for Fe $K_{1c} = 48\,\mathrm{kJ/m^3}$ so that the $< 001 >$ directions (resp. $< 111 >$) are easy (resp. hard) axes of magnetization, while for Ni $K_{1c} = -5\,\mathrm{kJ/m^3}$ so that $< 001 >$ (resp. $< 111 >$) are hard (resp. easy) axes of magnetization. In Co $K_1 = 410\,\mathrm{kJ/m^3}$ and the c axis of the hexagon is the sole easy axis of magnetization.

In many cases one often considers solely a second-order uniaxial energy:

$$E_{mc} = K_u \sin^2 \theta \tag{I.10}$$

It is indeed the leading term around the easy axis direction in all above-mentioned cases. We will see in sec.4 that it is also a form arising in the case of magnetostatic energy. It is therefore of particular relevance. Notice that it is the most simple trigonometric function compatible with time-reversal symmetry and giving rise to two energy minima, this liable to give rise to hysteresis. It is therefore sufficient for grasping the main physics yet with simple formulas in modeling. The strength of anisotropy may be expressed in terms of energy through K_u, or in field units through the so-called anisotropy field $H_a = 2K_u/\mu_0 M_s$. The meaning and usefulness of this field value will be detailed in chap.III for quasistatic magnetization reversal, and in chap.IV for precessional motion.

Hard versus soft magnetic materials. Materials with low magnetic anisotropy energy are called soft magnetic materials, while materials with large magnetic anisotropy energy are called hard magnetic materials. The historical ground for these names dates back to the beginning of the twentieth century where steel was the main source of magnetic material. Mechanically softer materials were noticed to have a coercivity lower than that of mechanically harder materials.

Sources of magnetic anisotropy. One should also consider magnetoelastic anisotropy energy, written E_{mel}. This is the magnetic energy associated with strain (deformation) of a material, either compressive, extensive or shear. E_{mel} may be viewed as the derivative of E_{mc} with respect to strain. In micromagnetism the anisotropy energy is described phenomenologically, ignoring all microscopic details. Thus we may consider the sum of E_{mc} and E_{mel}, written for instance E_a or E_K, a standing for anisotropy and K for an anisotropy constant.

3.4 Exchange energy

Exchange energy between neighboring sites may be written as:

$$\mathcal{E}_{12} = -J\mathbf{S}_1 \cdot \mathbf{S}_2 \tag{I.11}$$

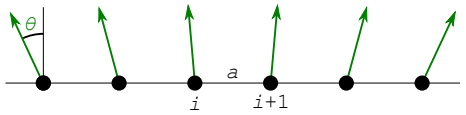

Figure I.4 – Exchange energy. Expansion of exchange with θ to link discrete exchange to continuous theory.

J is positive for ferromagnetism, and tends to favor uniform magnetization. Let us outline the link with continous theory used in micromagnetism. We consider the textbook case of a (one-dimensional) chain of XY classical spins, *i.e.* whose direction of magnetization may be described by a single angle θ_i (Figure I.4). The hypothesis of gradual variation of θ_i from site to site legitimates the expansion:

$$\begin{aligned} \mathcal{E}_{12} &= -JS^2\cos(\delta\theta) \\ &= -JS^2\left[1-\frac{(\delta\theta)^2}{2}\right] \\ &= \text{Cte} + \frac{JS^2a^2}{2}\left(\frac{\mathrm{d}\theta}{\mathrm{d}x}\right)^2 \end{aligned} \tag{I.12}$$

This equation may be generalized to a three dimensional system and moments allowed to point in any direction in space. Upon normalization with a^3 to express a density of energy, and forgetting about numerical factors related to the symmetry and number of nearest neighbors, one reaches:

$$E_{\text{ex}} = A\,(\boldsymbol{\nabla}\mathbf{m})^2\,. \tag{I.13}$$

$\mathbf{m}(\mathbf{r})$ is the unit vector field describing the magnetization distribution. The writing $(\boldsymbol{\nabla}\mathbf{m})^2$ is a shortcut for $\sum_i\sum_j(\partial m_i/\partial x_j)^2$, linked to Eq.(I.12). A is called the exchange stiffness, such as $A \approx (JS^2/2a)$. It is then clear that the unit for A is J/m, which we find also in Eq.(I.13). The order of magnitude of A for common magnetic materials such as Fe, Co and Ni is 10^{-11} J/m.

3.5 Magnetostatic energy

Magnetostatic energy, also called dipolar energy and written E_{d}, is the mutual Zeeman-type energy arising between all moments of a magnetic body through their stray field (itself called magnetostatic field or dipolar field and written H_{d}). When considering as a system an infinitesimal moment $\delta\mu = \mathbf{M}\delta V$ the Zeeman energy provides the definition for enthalpy. However when considering the entire magnetic body as both the source of all magnetic field (dipolar field $\mathbf{H}_{\text{d}}$) and that of moments, this term contributes to the internal energy. The volume density of dipolar energy may be written:

$$E_{\text{d}} = -\frac{1}{2}\mu_0\mathbf{M}.\mathbf{H}_{\text{d}}. \tag{I.14}$$

The $1/2$ prefactor results from the fact that the Zeeman interaction between two elementary moments is a mutual energy, which shall not be counted twice upon integration over the entire system (see also sec.4). Also, as dipolar fields arise in a linear fashion from magnetization, dipolar energy scales with the so-called dipolar constant $K_d = \frac{1}{2}\mu_0 M_s^2$.

Dipolar energy is the most difficult contribution to handle in micromagnetism. Indeed, due to its non-local character it may be expressed analytically in only a very restricted number of simple situations. Its numerical evaluation is also very costly in computation time as all moments interact with all other moments; this contributes much to the practical limits of numerical simulation. Finally, due to the non-uniformity in direction and magnitude of the magnetic field created by a magnetic dipole, magnetostatic energy is a major source of the occurrence of non-uniform magnetization configurations in bulk as well as nanostructured materials, especially magnetic domains. For all these reasons we dwell a bit on this term in the following section.

3.6 Characteristic quantities

In the previous paragraphs we introduced the various sources of magnetic energy, and discussed the resulting tendencies on magnetization configurations one by one. When several energies are involved, balances must be found and the physics is more complex. This is the realm of micromagnetism, the investigation of the arrangement of the magnetization vector field and magnetization dynamics. It is a major branch of nanomagnetism, and will be largely covered in chap.II.

It is a general situation in physics that when two or more effects compete, characteristic quantities emerge such as energy or length scales, and also dimensionless number. Here these will be built upon combination of three quantities with different units: exchange stiffness A, magnetization M_s and applied field H, and an anisotropy constant K such as K_u. Characteristic length scales are of special importance in nanomagnetism, determining the size below which specific phenomena occur. Here we only make two preliminary remarks; more will be discovered and discussed in the next chapter, ending with an overview.

Let us assume that in a problem only magnetic exchange and anisotropy compete. A and K_u are expressed respectively in J/m and J/m^3. The only way to combine these quantities to express a length scale, which we expect to arise in the problem, is $\Delta_u = \sqrt{A/K_u}$. We will call Δ_u the anisotropy exchange length[12] or Bloch parameter as often found in the literature. This is a direct measure of the width of a domain wall where magnetization rotates (limited by exchange) between two domains whose direction is set by K_u.

In a problem where exchange and dipolar energy compete, the two quantities at play are A and $K_d = (1/2)\mu_0 M_s^2$. In that case we may expect the occurrence of the length scale $\Delta_d = \sqrt{A/K_d} = \sqrt{2A/\mu_0 M_s^2}$, which we will call dipolar exchange

length[6] or exchange length as more often found in the literature.

In usual magnetic materials Δ_u ranges from roughly one nanometer in the case of hard magnetic materials (high anisotropy), to several hundreds of nanometers in the case of soft magnetic materials (low anisotropy). Δ_d is of the order of $10\,\mathrm{nm}$.

Summary

The various types of magnetic energy. Magnetization in a magnetic material is described by the theory called micromagnetism, where magnetization **M** is a continuous variable in space, with constant modulus. When at equilibrium, the distribution of **M** in a piece of material reflects the balance between several energies: exchange which tends to maintain magnetization uniform; magnetic anisotropy energy which tends to direct magnetization along certain crystallographic directions or in certain planes; Zeeman and dipolar energy which tend to align magnetization along the local magnetic field, be it of external nature or arise from distant moments in the material. Characteristic length scales emerge from the competition between different energies, against which the size of a system can be checked to determine the magnetization distribution likely to occur.

4 Handling dipolar interactions

4.1 Simple views on dipolar interactions

To grasp the general consequences of H_d let us first consider the interaction between two pinpoint magnetic dipoles $\boldsymbol{\mu}_1$ and $\boldsymbol{\mu}_2$, split by vector **r**. Their mutual energy reads (see sec.I.5):

$$\mathcal{E}_d = -\frac{\mu_0}{4\pi r^3}\left[3\frac{(\boldsymbol{\mu}_1\cdot\mathbf{r})(\boldsymbol{\mu}_2\cdot\mathbf{r})}{r^2} - \boldsymbol{\mu}_1\cdot\boldsymbol{\mu}_2\right] \tag{I.15}$$

We assume both moments to have a given direction **z**, however with no constraint on their sign, either positive or negative. Let us determine their preferred respective orientation, either parallel or antiparallel depending on their locii, that of $\boldsymbol{\mu}_2$ being determined by vector **r** and the polar angle θ with respect to z (Figure I.5). Equation I.15 then reads:

$$\mathcal{E}_{12} = \frac{\mu_0\mu_1\mu_2}{4\pi r^3}(1-3\cos^2\theta) \tag{I.16}$$

The ground state configuration being the one minimizing the energy, we see that parallel alignment is favored if $\cos^2\theta > 1/3$, that is within a cone of half-angle $\theta = 54.74^\circ$, while antiparallel alignment is favored for intermediate angles (Figure I.5).

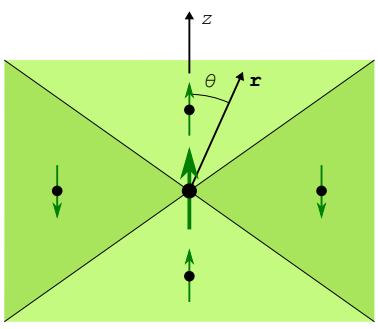

Figure I.5 – Simple view on dipolar energy. Interaction

Thus, under the effect of dipolar interactions two moments roughly placed along their easy axis tend to align parallel, while they tend to align antiparallel when placed next to each other. These rules rely on angles and not the length scale, and are thus identical at the macroscopic and microscopic scales. The example is that of permanent magnets, which are correctly approached by Ising spins.

The occurrence of a large part of space where antiparallel alignement is favored (outside the cone) makes us feel why bulk samples may be split in large blocks with different (*e.g.* antiparallel) directions of magnetization. These are magnetic domains. Beyond these hand-waving arguments, the quantitative consideration of dipolar energy is outlined below in the framework of a continuous medium.

4.2 Various ways to handle magnetostatics

The total magnetostatic energy of a system with magnetization distribution $\mathbf{M}(\mathbf{r})$ reads :

$$\mathcal{E}_d = -\frac{\mu_0}{2} \iiint_{\mathcal{V}} \mathbf{M}.\mathbf{H}_d \, d\mathcal{V}. \tag{I.17}$$

$\mathcal{V}$ is the volume of the magnetic system considered. The pre-factor $\frac{1}{2}$ results from the need not to count twice the mutual energy of each set of two elementary dipoles taken together. The decomposition of a macroscopic body in elementary magnetic moments and performing a three-dimensional integral is not a practical solution to evaluate $\mathcal{E}_d$. It is often better to proceed similarly to electrostatics, with $\mathrm{div}\,\mathbf{E} = \rho/\epsilon_0$ being replaced by $\mathrm{div}\,\mathbf{H}_d = -\mathrm{div}\,\mathbf{M}$ (derived from the definition of $\mathbf{B}$, and Maxwell's equation $\mathrm{div}\,\mathbf{B} = 0$). Within this analogy, $\rho = -\mathrm{div}\,\mathbf{M}$ are called magnetic volume charges. A little algebra shows that the singularity of $\mathrm{div}\,\mathbf{M}$ that may arise at the border of magnetized bodies (M_s going abruptly from a finite value to zero on either side of the surface of the body) can be lifted by introducing the concept of surface charges $\sigma = \mathbf{M}.\hat{\boldsymbol{n}}$. $\hat{\boldsymbol{n}}$ is the normal vector to the surface of the magnetic body, oriented towards the outside. This analogy is relevant because $\mathbf{H}_d$ has a zero curl and thus derives from a potential $\mathbf{H}_d = -\mathbf{grad}\,\phi_d$, with:

$$\phi_d(\mathbf{r}) = \iiint_{\mathcal{V}} \frac{\rho(\mathbf{u})}{4\pi|\mathbf{r}-\mathbf{u}|} \, d\mathcal{V}_\mathbf{u} + \oiint_{\partial\mathcal{V}} \frac{\sigma(\mathbf{u})}{4\pi|\mathbf{r}-\mathbf{u}|} \, d\mathcal{S}_\mathbf{u} \tag{I.18}$$

Concerning the field, one then has:

$$\mathbf{H}_d(\mathbf{r}) = \iiint_{\mathcal{V}} \frac{\rho(\mathbf{u})\,(\mathbf{r}-\mathbf{u})}{4\pi|\mathbf{r}-\mathbf{u}|^3} d\mathcal{V}_\mathbf{u} + \oiint_{\partial\mathcal{V}} \frac{\sigma(\mathbf{u})\,(\mathbf{r}-\mathbf{u})}{4\pi|\mathbf{r}-\mathbf{u}|^3} d\mathcal{S}_\mathbf{u} \tag{I.19}$$

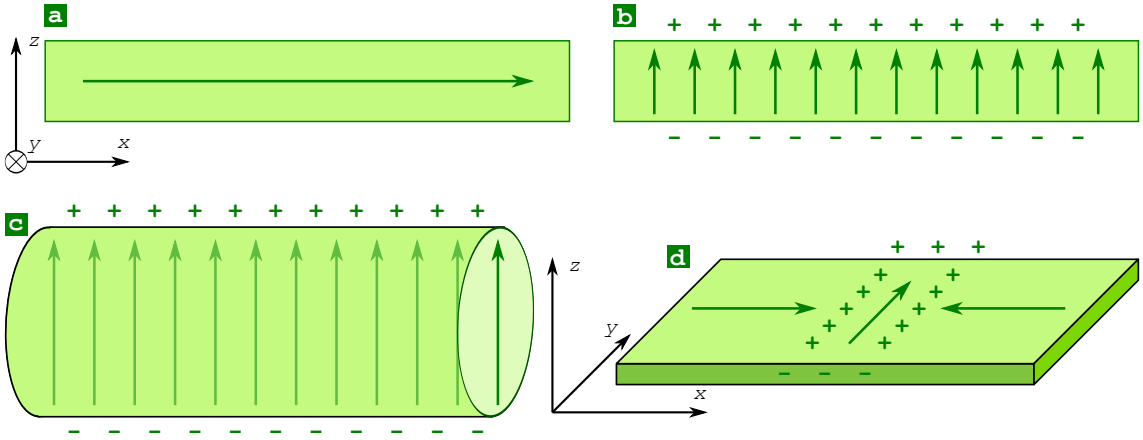

Figure I.6 – Magnetic charges. Magnetization and magnetic charges in simple cases: (a) An infinite thin film with in-plane magnetization (cross-sectional view) (b) An infinite thin film with out-of-plane magnetization (cross-sectional view) (c) A cylinder of infinite length with uniform axial magnetization (d) A strip with infinite length and a head-to-head domain wall.

In Eq.(I.18), the integral of the first term on the right hand side is performed over the volume of the system, except at its very boundary where the singularity was considered above and is taken into account as surface charges. So, in principle the volume of integration should be written $\mathcal{V}$
$d\mathcal{S}$. However, for the simplicity of notations, we write it $\mathcal{V}$.

Simple distributions of magnetization and the associated magnetic charges are displayed on Figure I.6. Equation I.17 may then be worked out, integrating in parts:

$$\mathcal{E}_d = \frac{1}{2}\mu_o \iiint_{\text{Space}} \mathbf{M}.\mathbf{grad}\,\phi_d \, d\mathcal{V} \tag{I.20}$$

$$= \frac{1}{2}\mu_o \iiint_{\text{Space}} M_i(\partial\phi_d/\partial x_i) \, d\mathcal{V} \tag{I.21}$$

$$= \left[\frac{1}{2}\mu_o\phi_d M_i\right]_{-\infty}^{\infty} - \frac{1}{2}\mu_o \iiint_{\text{Space}} (\partial M_i/\partial x_i)\phi_d \, d\mathcal{V} \tag{I.22}$$

$$\tag{I.23}$$

The first term cancels for a finite size system considered in the infinite space, and one finds a very practical formulation:

$$\mathcal{E}_d = \frac{1}{2}\mu_o \left(\iiint_{\mathcal{V}} \rho\phi_d \, d\mathcal{V} + \oiint_{\partial\mathcal{V}} \sigma\phi_d \, d\mathcal{S} \right). \tag{I.24}$$

Another equivalent formulation may be demonstrated:

$$\mathcal{E}_d = \frac{1}{2}\mu_0 \iiint_{\text{Space}} H_d^2 \, d\mathcal{V} \tag{I.25}$$

where integration if performed over the entire space. From the latter we infer that $\mathcal{E}_d$ is always positive or zero. Equation I.24 shows that if dipolar energy alone is considered, its effect is to promote configurations of magnetization free of volume and surface magnetic charges. Such configurations are thus ground states (possibly degenerate) in the case where dipolar energy alone is involved.

- The tendency to cancel surface magnetic charges implies a very general rule for soft magnetic materials: their magnetization tends to remain parallel to the edges and surfaces of the system.
- The name dipolar field is a synonym for magnetostatic field. It refers to all magnetic fields created by a distribution of magnetization or magnetic moments in space. The name stray field refers to that part of dipolar field, occurring outside the body responsible for this field. The name demagnetizing field refers to that part of dipolar field, occurring inside the body source of this field; the explanation for this name will be given later on.

The term dipolar brings some confusion between two notions. The first notion is dipolar (field or energy) in the general sense of magnetostatic. The name dipolar stems from the fact that to compute total magnetostatic quantities of a magnetic body, whatever its complexity, one way is to decompose it into elementary magnetic dipoles and perform an integration; the resulting calculated quantities are then exact. The second notion is magnetic fields or energies arising from idealized pinpoint magnetic dipoles, and obeying Eq.(I.15). When using the name dipolar to refer to the interactions between two bodies, one may think either that we compute the exact magnetostatic energy based on the integration of elementary dipoles, or that we replace the two finite-size bodies with pinpoint dipoles for the sake of simplicity, yielding on the reverse an approach evaluation. In that latter case one may add extra terms, called multipolar, to improve the accuracy of the approximation. **To avoid confusion one should stress explicitly the approximation in the latter case, for instance mentioning the use of a point dipole approximation**.

4.3 Demagnetizing factors

Demagnetizing factors (or coefficients) are a simple concept providing figures for the magnetostatic field inside a body, and the associated magnetostatic energy.

When Eq.(I.19) is applied to uniform magnetization, only the surface contribution remains:

$$\mathbf{H}_\mathrm{d}(\mathbf{r}) = M_\mathrm{s} \oiint_{\partial\mathcal{V}} \frac{(\mathbf{r}-\mathbf{u})}{4\pi|\mathbf{r}-\mathbf{u}|^3}\, m_i n_i(\mathbf{u})\, \mathrm{d}\mathcal{S}_\mathbf{u} \tag{I.26}$$

with $\mathbf{M} \equiv M_\mathrm{s}\mathbf{m}$, $\mathbf{m} = m_i\mathbf{u}_i$ and $\mathbf{n} = n_i\hat{\boldsymbol{\imath}}$, with Einstein's summation notation. $\hat{\boldsymbol{n}}$ is the local normal to the surface, oriented towards the outside of the body. Upon integration over the entire volume, one gets the average value of the dipolar field inside the system:

$$\begin{aligned} \langle \mathbf{H}_\mathrm{d} \rangle &= -M_\mathrm{s}\overline{\overline{\mathbf{N}}}\cdot\mathbf{m} \\ &= -M_\mathrm{s}\, m_i N_{ij}\, \hat{\boldsymbol{\imath}} \end{aligned} \tag{I.27}$$

In these formula, $\overline{\overline{\mathbf{N}}}$ is a 3×3 matrix with coefficients:

$$N_{ij} = -\frac{1}{\mathcal{V}} \iiint_{\mathcal{V}} \mathrm{d}\mathcal{V}_\mathbf{r} \oiint_{\partial\mathcal{V}} \frac{n_i(\mathbf{u})\cdot\,(\mathbf{r}-\mathbf{u})\big|_j}{4\pi|\mathbf{r}-\mathbf{u}|^3}\, \mathrm{d}\mathcal{S}_\mathbf{u} \tag{I.28}$$

in which $(\mathbf{r}-\mathbf{u})\big|_j$ is the j^{th} component of $(\mathbf{r}-\mathbf{u})$. $\overline{\overline{\mathbf{N}}}$ is called the demagnetizing matrix. It may be shown that $\overline{\overline{\mathbf{N}}}$ is symmetric and positive, and thus can be diagonalized. The set of *xyz* axes upon diagonalization are called the main or major axes. The new coefficients N_{ii} of the diagonal matrix are called the demagnetizing coefficients and will be written N_i hereafter as a shortcut. Along these axes one now has:

$$\langle \mathbf{H}_{\mathrm{d},i} \rangle = -N_i\mathbf{M}. \tag{I.29}$$

This highlights a simple interpretation of demagnetizing coefficients. First, they are called demagnetizing as they are positive, so that on the average the internal magnetostatic field is indeed opposite to magnetization. Second, each coefficient is a direct measure of the strength of the demagnetizing field along the considered direction.

The same concepts can be applied to dipolar energy. As magnetization is assumed to be uniform, from Eq.(I.17) it is straightforward that the density of demagnetizing energy is directly connected to the average demagnetizing field through $E_\mathrm{d} = -(\mu_0/2)\,\langle \mathbf{H}_\mathrm{d} \rangle \cdot \mathbf{M}$, so that in the end:

$$\begin{aligned} E_\mathrm{d} &= K_\mathrm{d}\ {}^\mathrm{t}\mathbf{m}\cdot\overline{\overline{\mathbf{N}}}\cdot\mathbf{m} \\ &= m_i m_j\, N_{ij}\, K_\mathrm{d} \end{aligned} \tag{I.30}$$

with $K_\mathrm{d} = \frac{1}{2}\mu_0 M_\mathrm{s}^2$. Again, when one considers the main axes of the system (in which $\overline{\overline{\mathbf{N}}}$ is diagonal), this boils down to:

$$E_\mathrm{d} = m_i^2 N_i K_\mathrm{d} \tag{I.31}$$

Table I.3 – Demagnetizing factors. Cases of practical use

Case	Demagnetizing factor	Note
Slab	$N_x = 1$	Normal along x
Sphere	$N_x = 1/3$	Along any direction
Cylinder, disk cross-section	$N_x = 1/2$	Along transverse directions
General ellipsoid	$N_x = \frac{1}{2}abc \int_0^\infty \left[(a^2+\eta)\sqrt{(a^2+\eta)(b^2+\eta)(c^2+\eta)}\right]^{-1} \mathrm{d}\eta$	
Prolate revolution ellipsoid	$N_x = \frac{\alpha^2}{1-\alpha^2}\left[\frac{1}{\sqrt{1-\alpha^2}} \operatorname{arg\,sinh}\left(\frac{\sqrt{1-\alpha^2}}{\alpha}\right) - 1\right]$	$\alpha = c/a < 1$
Oblate revolution ellipsoid	$N_x = \frac{\alpha^2}{\alpha^2-1}\left[1 - \frac{1}{\sqrt{\alpha^2-1}} \arcsin\left(\frac{\sqrt{\alpha^2-1}}{\alpha}\right)\right]$	$\alpha = c/a > 1$
Cylinder with elliptical section	$N_x = 0$, $N_y = c/(b+c)$ and $N_z = b/(b+c)$	Axis along x
Prism	Analytical however long formula	See: [6] or [15]

Based on this, a common use of demagnetization coefficients is to estimate the difference of energy along different directions. Let us consider the simple case of magnetization confined in the xy plane. $m_x^2 + m_y^2 = 1$, so that the above equation becomes, dropping a constant term,

$$E_\mathrm{d} = (N_i - N_j)K_\mathrm{d} \cos^2\theta \tag{I.32}$$

with $\cos\theta = m_x$. In this example, dipolar energy takes the form of a second-order uniaxial anisotropy. More generally, from Eq.(I.30) it is clear that $\overline{\overline{\mathbf{N}}}$ yields a quadratic form for the energy even in the most general case, so that only second-order anisotropies can arise from dipolar energy, at least for perfectly uniform samples[I.10].

The handwaving consideration of the distribution of surface charges shows that the dipolar energy should be lower when magnetization is aligned parallel to a long dimension of the system. This translates into lower values of the demagnetizing coefficients along such directions. Besides, it can be shown that $\mathrm{Tr}(\overline{\overline{\mathbf{N}}}) = 1$, so that $N_x + N_y + N_z = 1$. For example, for an infinitely-long cylinder with axis along $\hat{\boldsymbol{z}}$, $N_z = 0$ because there are no magnetic charges for $\mathbf{M}$ directed along $\hat{\boldsymbol{z}}$; $N_x = N_y = 1/2$ because x and y transverse directions are equivalent, and the sum of al three coefficients is 1. Similarly, all N_i's equal $1/3$ for a sphere. For a thin film (also called slab), $N_x = N_y = 0$ and $N_z = 1$. Analytical formulas or expansions for N_i's may be found for other shapes, such as revolution ellipsoids[13], prisms[14, 15] (Figure I.7), cylinders of revolution of finite length[16, 17], infinite cylinders with a triangular cross-section[18], tetrahedrons[19, 20], torii[21]. Some formulas are gathered in Table I.3. For other geometries micromagnetic codes or Fourier-space computations[20] may be used.

[I.10] see sec.4.4 for effects due to non-uniformities.

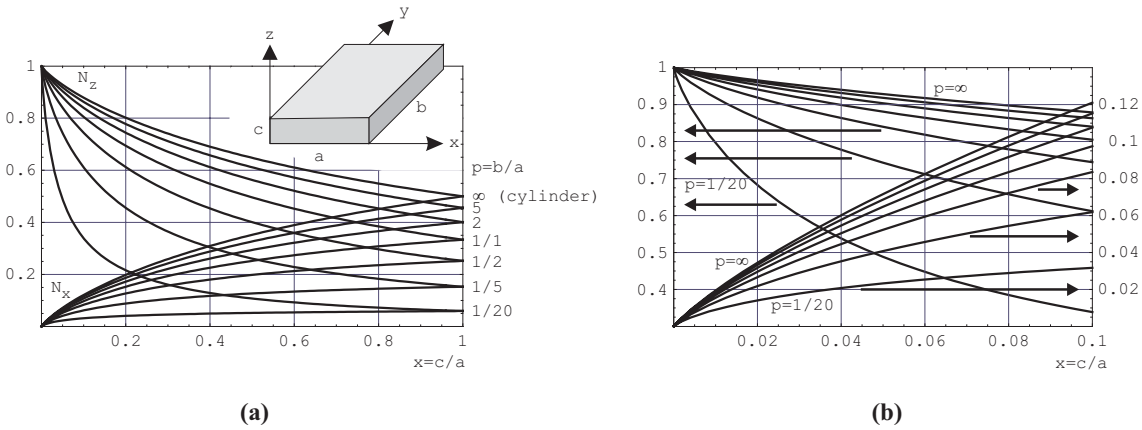

(a) (b)

Figure I.7 – Demagnetizing factors. Numerical evaluation for prisms. (a) is the full plot, while (b) is en enlargement for flat prisms.

Demagnetizing factors for an arbitrary shape?. While all the above is true for bodies with an arbitrary shape, not even necessarily connected, a special subset of bodies is worth considering: that of shapes embodied by a polynomial surface of degree at most two. To these belong slabs, ellipsoids and cylinders with an ellipsoidal cross-section. In that very special case it may be shown within the non-trivial theory of integration in space[22] that Eq.(I.29) is then true locally: in the case of uniform magnetization, $\mathbf{H}_\mathrm{d}$ is uniform and equal to $-N_i\mathbf{M}$ when $\mathbf{M}$ is aligned parallel to one of the major directions. This may allow the torque on magnetization to be uniformly equal to zero, and thus ensures the self-consistency of the assumption of uniform magnetization. This makes the application of demagnetizing factors of somewhat higher reliability than for bodies with an arbitrary shape. Notice, however, that self-consistency does not necessarily imply that the uniform state is stable and a ground state.

Caution needed for the applicability of demagnetizing factors. Demagnetizing factors are derived based on the assumption of uniform magnetization. While this assumption allows demagnetizing factors to be defined and calculated analytically or numerically, care should be taken when applying these to practical cases, where magnetization configurations may not be uniform.

Summary

The various types of magnetic energy. Magnetostatic or equivalently-called dipolar interactions, are complex to evaluate as they are long ranged, and involve all couples of any two infinitesimal moments in a system. While dipolar energy can be expressed conceptually in several equivalent integral forms, only in some very

special cases can these be integrated analytically. This is the case of the concept of demagnetizing factors, describing the situation of uniform magnetization, and predicting the value of the internal demagnetizing field in a tensor form. Due to this rather restrictive hypothesis, care need to be taken when applying these.

5 The Bloch domain wall

The existence of magnetic domains was suggested by Pierre WEISS in his mean field theory of Magnetism in 1907. Magnetic domains were postulated to explain why large bodies made of a ferromagnetic materials could display no net magnetic moment under zero external magnetic field. Their existence was confirmed only in 1931 with a Bitter technique, based on magnetic nanoparticles decorating the locii of domain walls because these particles are attracted by the local gradient of magnetic field[6]. This example highlights the importance of magnetic microscopy in the progress of micromagnetism. In 1932 Bloch provides an analytical solution in a simple case to describe the region of transition between two magnetic domains, which is named a magnetic domain wall. At this stage we do not discuss the origin of magnetic domains, however focus on the model of a domain wall.

The Bloch model is one-dimensional, *i.e.* considers a chain of spins. The idea is to describe the transition between two three-dimensional domains (volumes) in the form of a two-dimensional object with translational invariance in the plane of the domain wall. It is assumed that magnetization remains in the plane of the domain wall, a configuration associated with zero volume charges $-\mathrm{div}\,\mathbf{M}$ and thus associated zero dipolar energy. The only energies at play are then the exchange energy, and the magnetic anisotropy energy which is assumed to be uniaxial and of second order: $E_K(x) = K_u \sin^2\theta$. Under these assumptions the density of magnetic energy reads:

$$E(x) = K_u \sin^2\theta + A\left(\mathrm{d}\theta/\mathrm{d}x\right)^2 \tag{I.33}$$

where x is the position along the chain of spins. The case thus consists in exhibiting the magnetic configuration which minimizes the total energy

$$\mathcal{E} = \int_{-\infty}^{+\infty} [E_K(x) + E_{ex}(x)]\mathrm{d}x. \tag{I.34}$$

while fulfilling boundary conditions compatible for a 180° domain wall: $\theta(-\infty) = 0$ and $\theta(+\infty) = \pi$.

Wall energy per unit surface. The unit for the wall energy in Eq.(I.34) is clearly an energy per unit area, expressed in J/m^2. This makes sense as a domain wall is a two-dimensional object. To calculate the total energy of a wall in a real system, for instance across a wire, one needs to integrate Eq.(I.34) over the domain wall area, to get an energy in joules.

5.1 Simple variational model

This paragraph proposes an approximate solution for a domain wall, however appealing for its simplicity and ability to highlight the physics at play, and a reasonable numerical result. We consider the following model for a domain wall of width ℓ: $\theta = 0$ for $x < -\ell/2$, $\theta = \pi(x/\ell + 1/2)$ for $x \in [-\ell/2; \ell/2]$ and $\theta = \pi$ for $x > \ell/2$. In a variational approach we search for the value ℓ_{var} which minimizes Eq.(I.34), after integration: $\mathcal{E} = K_u\ell/2 + A\pi^2/\ell$. The minimization yields $\ell_{\text{var}} = \pi\sqrt{2}\sqrt{A/K_u}$ and $\mathcal{E}_{\text{var}} = \pi\sqrt{2}\sqrt{AK_u}$ is the associated energy.

How to 'read' the domain wall width. Letting aside the factor $\pi\sqrt{2}$ a simple variational model highlights the relevance of the Bloch parameter Δ_u defined previously. How may we read this formula? Exchange only would tend to enlarge the domain wall, hence its occurrence at the numerator. To the reverse, the anisotropy energy gives rise to a cost of energy in the core of the domain wall. This tends to decrease its width, explaining its occurrence at the denominator.

5.2 Exact model

The exact profile of a Bloch domain wall may be derived using the principle of functional minimization to find the function θ minimizing $\mathcal{E}$. It may be shown that the principle of minimization is equivalent to the so-called Euler equation:

$$\frac{\partial E}{\partial \theta} = \frac{\mathrm{d}}{\mathrm{d}x}\left[\frac{\partial E}{\partial(\frac{\mathrm{d}\theta}{\mathrm{d}x})}\right] \tag{I.35}$$

Considering a magnetic system described by Eq.(I.34) one finds:

$$\frac{\mathrm{d}E_K}{\mathrm{d}\theta} = \frac{\mathrm{d}}{\mathrm{d}x}\left(2A\frac{\mathrm{d}\theta}{\mathrm{d}x}\right) \tag{I.36}$$

$$= 2A\frac{\mathrm{d}^2\theta}{\mathrm{d}x^2} \tag{I.37}$$

Upon multiplying both parts by $\mathrm{d}\theta/\mathrm{d}x$ and integration, this reads:

$$\begin{aligned} E_K(x) - E_K(a) &= A\left[\frac{\mathrm{d}\theta(x)}{\mathrm{d}x}\right]^2 - A\left[\frac{\mathrm{d}\theta(a)}{\mathrm{d}x}\right]^2 \\ &= E_{\mathrm{ex}}(x) - E_{\mathrm{ex}}(a) \end{aligned} \tag{I.38}$$

a is the origin of integration, here chosen as the center of the domain wall. Considering two semi-infinite domains with equal local density of energy, E is stationary (minimum) in both domains, and by convention may be chosen zero with no loss of generality. Equation I.38 applied to $\pm\infty$ shows that $E_K(a) = E_{\mathrm{ex}}(a)$, and finally:

$$\forall x \quad E_K(x) = E_{\mathrm{ex}}(x) \tag{I.39}$$

We hereby reach a general and very important feature of a domain wall separating two semi-infinite domains under zero applied field: the local density of anisotropy and exchange energy are equally parted at any location of the system. The equal parting of energy considerably eases the integration to get the areal density of the domain wall[I.11]:

$$\begin{aligned} \mathcal{E} &= 2\int_{-\infty}^{+\infty} A\left(\mathrm{d}\theta/\mathrm{d}x\right)^2 \mathrm{d}x \\ &= 2\int_{-\infty}^{+\infty} E_K(x)\,\mathrm{d}x \\ &= 2\int_{-\infty}^{+\infty} \sqrt{AE_K(x)}\,(\mathrm{d}\theta/\mathrm{d}x)\,\mathrm{d}x \\ &= 2\int_{\theta(-\infty)}^{\theta(+\infty)} \sqrt{AE_K(\theta)}\,\mathrm{d}\theta \end{aligned} \tag{I.40}$$

The energy of the domain wall may thus be expressed from the angular dependence of the energy alone, without requiring solving the profile of the domain wall, which may be interesting to avoid calculations or when the latter cannot be solved.

Let us come back to the textbook case of the functional I.33. After some algebra one finds for the exact solution:

$$\theta_{\mathrm{ex}}(x) = 2\arctan\left[\exp(x/\Delta_{\mathrm{u}})\right] \tag{I.41}$$

$$\mathcal{E}_{\mathrm{ex}} = 4\sqrt{AK_{\mathrm{u}}}. \tag{I.42}$$

$\Delta_{\mathrm{u}} = \sqrt{A/K_{\mathrm{u}}}$ is of course confirmed to be a natural measure for the width W of a domain wall. The exact solution along with that of the variational model are displayed on Figure I.8. Despite its crudeness, the latter is rather good, for both the wall profile and its energy: the true factor afore $\sqrt{AK_{\mathrm{u}}}$ equals 4 against $\pi\sqrt{2} \approx 4.44$ in the variational model. It is trivial to notice that $\mathcal{E}_{\mathrm{var}} > \mathcal{E}_{\mathrm{ex}}$, as the energy of a test function may only be larger than the energy of the minimum functional.

[I.11] We set arbitrarily $\mathrm{d}\theta/\mathrm{d}x > 0$ without loss of generality, using the symmetry $x \to -x$.

It shall be noticed that the equal parting of energy is retained in the variational model, however only in its global form, not locally.

5.3 Defining the width of a domain wall

Several definitions for the width W of a domain wall have been proposed (see *e.g.* Ref.[6], p.219). One may classify all possible definitions in mainly two categories.

The first type of definitions are based on the intercept of the asymptotes of the domains, with some related to the domain wall. It was introduced and discussed in detail by Lilley, to be applied to any kind functional of anisotropy, beyond the simple case of uniaxial with second order[23]. Lilley considered the domain wall described by the function of angle $\theta(x)$. In the case of uniaxial anisotropy of second order this yields $W_L = \pi\sqrt{A/K_u} = \pi\Delta_u$ for the exact solution, and $W_{L,lin} = \ell_{variational} = \sqrt{2}\pi\Delta_u$ for the linear variational model. A variation in this type of definition consists in using the asymptotes of the curve $\cos\theta(x)$, instead of that of $\theta(x)$. One then finds $W_m = 2\sqrt{A/K_u}$, both in the exact and variational models[6]. In the notation here m stands for the component of magnetization in the domains. Definitions using asymptotes are more robust against the detailed shape of the anisotropy function or experimental noise, than definitions based on a threshold, named W_t[24].

Beware of notations. The wall width is sometimes written δ, instead of W. Also, some call Δ_u the domain wall width. To avoid any confusion it is advised to keep the name Bloch parameter for the latter quantity, or the anisotropy exchange length (sec.3.6).

A second type of definitions are based on the integral of a function, instead of its asymptote(s). This was introduced by Jakubovics[24], with the argument that it would be less sensitive to the detailed shape of the anisotropy function, compared to W_L and W_m. In the case of the analysis of experimental data, an integral

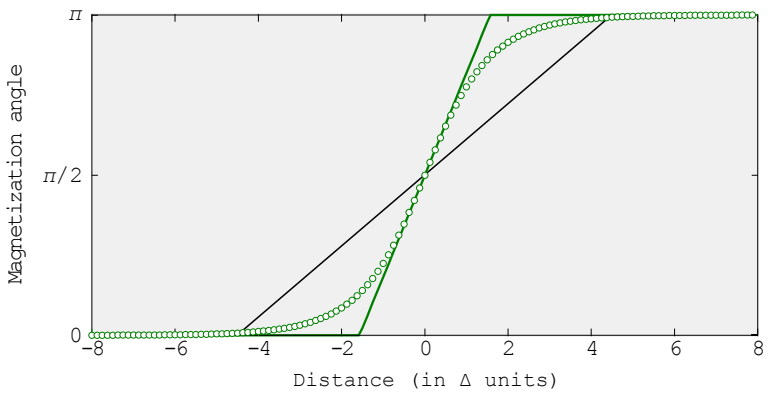

Figure I.8 – Domain wall profile. Exact solution for the profile of the Bloch domain wall (green dots), along with its asymptote (green line). The lowest-energy solution of the linear variational model is displayed as a black line.

function is also less sensitive to noise than an asymptote defined at one point. Following Jakubovics'paper[I.12] one may define the quantity: $W_J = \int_{-\infty}^{+\infty} \sin^2\theta(x)dx$, where J stands for Jakubovics. A variation of this definition is $W_F = \int_{-\infty}^{+\infty} \sin\theta(x)dx$. In the latter definition F stands for the flux of magnetization $m = \sin\theta$. In the present case of a uniaxial anisotropy of second order one finds $W_F = W_L$ and $W_J = W_m$. Yet another integral definition is the one proposed by Thiele: $W_T = 2/\int_{-\infty}^{+\infty} |\frac{dm}{dx}|^2 dx$[25]. It has been argued to be of special relevance for precessional domain wall motion (see chap.IV), or domain-wall magnetoresistance[26].

Independent from the choice of asymptote versus integral computation, definitions based on a component of magnetization ($\sin\theta$) may be more suited for the analysis of domain walls investigated by magnetic microscopies probing the projection of magnetization in a given direction.

Domain walls other than π angle. The use of cos and sin functions in the definitions W_m and W_F is dependent on the starting and ending angles of the domain wall, here 0 and π. For other choices or domain walls with angle differing from 180°, these definitions shall be modified.

Summary

The Bloch domain wall. The properties of domain walls can be calculated exactly in simple cases, for example when only magnetocrystalline energy competes with exchange energy. This is the case of Bloch walls in which magnetization rotates in the plane of the domain wall, creating a charge-free wall associated with no dipolar energy. The wall width then scales like $\sqrt{A/K}$ and its energy like $\sqrt{AK}$. The prefactors depend on the wall angle (180° or different), the type of anisotropy (uniaxial of second order, or different), as well as the exact definition of wall width.

6 Magnetometry and magnetic imaging

There exist many techniques to probe magnetic materials. Due to the small amounts to be probed, and the need to understand magnetization configurations, high sensitivity and/or microscopies are of particular interest for nanomagnetism. There exists no such thing as a universal characterization technique, that would be superior to all others. Each of them has its advantages and disadvantages in terms of versatility, space and time resolution, chemical sensitivity etc. The combination of several such techniques is often beneficial to gain the full understanding of a system.

Here a quick and non-exhaustive look is proposed over some techniques that

[I.12] In the original paper from Jakubovic[24] the definition of the width is twice larger than the present one

are useful in nanomagnetism. This is a mere descriptive overview. In-depth reviews may be found elsewhere[6, 27–29].

6.1 Extraction and vibrating magnetometers

Magnetometers are instruments capable of measuring the moment of a sample as a function of various parameters, such as an applied field to deliver a magnetization loop.

Magnetometers are based on the measurement of the stray field arising from the total moment of a sample. Their various implementations differ by the principle of detection of the magnetic field. Two widespread techniques are electromotive force through pick-up coils, and Josephson junctions in the so-called SQUID (Superconducting QUantum Interference Device). Most magnetometers are based on extraction and vibration schemes: the sample is set in oscillatory motion along an axis, so that its stray field arising at the probing element varies over time, allowing a better precision using lock-in techniques, and the rejection of some artifacts. The motion may be slow to moderate for SQUID (a fraction of, to several Hz), or at a few tens of Hz for inductive techniques (so-called vibrating sample magnetometers, VSM). Thus, magnetometers cannot probe high-frequency magnetization processes. Variations exist such as torque magnetometers, of particular interest for determining magnetic anisotropy.

Magnetometers measure the integrated moment of a sample; they are not a microscopy technique. Samples need in general to be one centimeter or smaller in size. This ensures that they fit the cavity where the magnetic field is produced, and also remain of moderate size against the pick-up coils so that the point dipole approximation is valid and measurements are quantitative. Modern magnetometers achieve a sensibility in the range $10^{-8} - 10^{-11}\,\mathrm{A \cdot m^2}$, which means one or much smaller than one atomic layer of Fe, Co or Ni on a surface of the order of $1\,\mathrm{cm^2}$. Nevertheless contributions arising from the sample holder, substrates or impurities, may limit the absolute precision of the measurements.

A hysteresis loop is obtained in a couple of seconds to several tens of minutes depending on the sensitivity and the number of points required. The external field is produced by resistive or superconducting coils. A common environmental condition is variable temperature (Figure I.9). Pb. 6 considers the vibrating sample magnetometer.

Magnetometers are one of the first techniques to have been developed in the history of magnetism, and have been largely used to characterize materials to determine their ordering state and temperature, their magnetization and magnetic anisotropy. Magnetometers remain very important for material development.

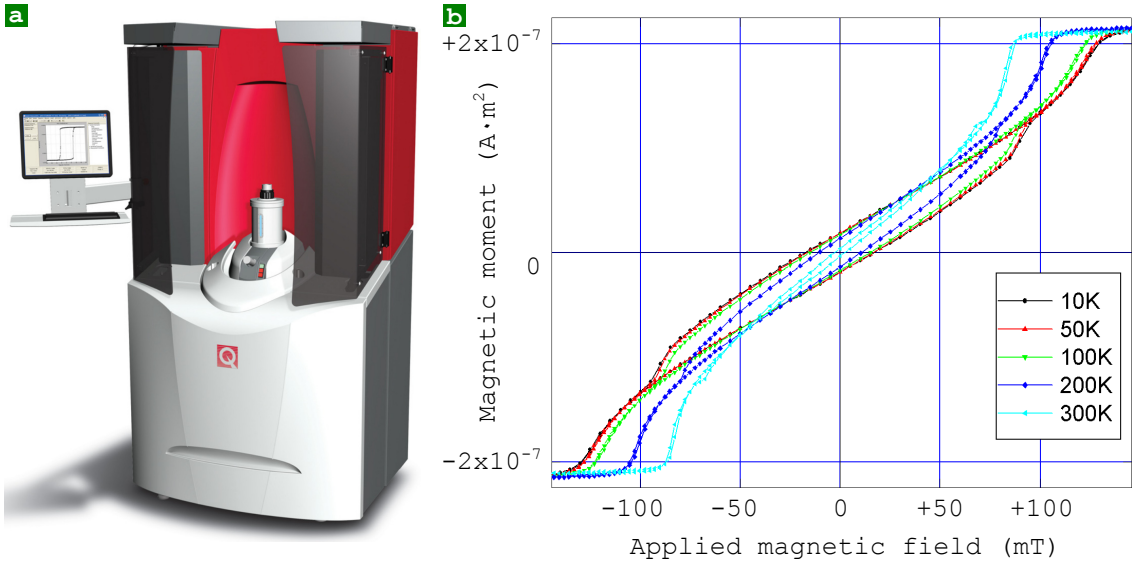

Figure I.9 – Magnetometry. (a) Artist view of a VSM-Squid magnetometer from the company Quantum Design. (b) Hysteresis loops performed at various temperatures of an epitaxial film Mo\Fe(2 nm)\Mo with a (110) base plane for the epitaxy. The field was applied a few degrees from the hard axis, itself defined by a combination of second order and fourth order contributions.

6.2 Faraday and Kerr effects

Faraday and Kerr methods measure changes of the polarization of light upon transmission into or reflection from (respectively) a magnetic sample; these are called magneto-optical effects. Kerr is often labeled as MOKE, for Magneto-Optical Kerr Effect. These methods allow indirectly to gather information about the magnetization state of a sample.

Magnetization is not probed directly, although monitoring changes of the polarization of light versus *e.g.* applied field allow to determine the shape of *e.g.* hysteresis loops. Magnetic order is related to unfilled electronic shells, with split states or band splitting of the order of an electron volt. Thus light, especially in the visible range, is sensitive to magnetism through spin-dependent transition between these states and bands. There are two microscopic effects. The first one is birefringence, which is the delay of propagation of light depending on its polarization, here in relation with the magnetization direction. Birefringence occurs both in insulating and conductive materials. The second effect is dichroism, which is the difference of absorption / reflection depending on the polarization of light and the magnetization of the material.

Faraday is usually implemented with light impinging on the sample at normal incidence. Kerr may be implemented at normal incidence (so-called polar MOKE), or tilted incidence. The polarization of the incident light may be linear, circular or modulated over time for more complex measurements. Depending on the setup one may measure the change of intensity, the ellipticity or the rotation of the light. They may arise from birefringence and/or dichroism, again depending on the setup. MOKE is very sensitive due to the low penetration depth of light

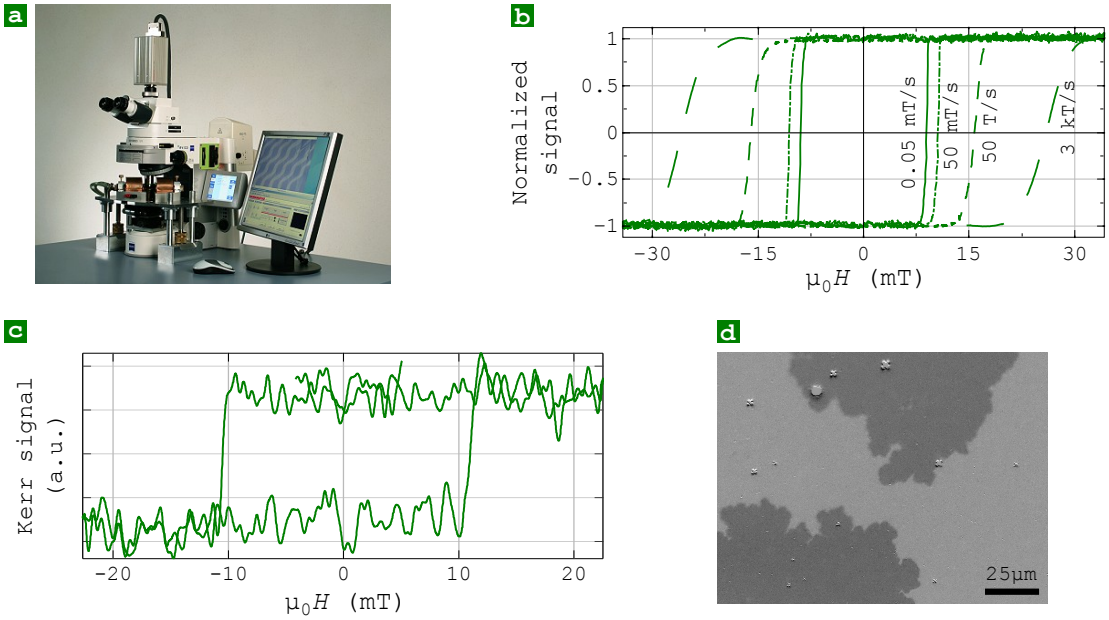

Figure I.10 – Magneto-optical techniques. (a) A Kerr microscope from the evico magnetics company, equipped with an electromagnet to allow for in-field measurements. (b) Hysteresis loops (averaged over thousands of loops) of a thin Co film for various ramping rates of the applied field (Courtesy J. Vogel) (c) Hysteresis loop (averaged over thousands of loops) of a single nano-object, a magnetic nanotube of diameter 350 nm (focused Kerr setup. Courtesy M. Staňo). (d) Static domain pattern with a ramified shape, obtained using Kerr microscopy. Sample: Au/Co/graphene ultrathin film with perpendicular anisotropy.

in metals, so that the sensibility can be better than one atomic layer. In the Faraday geometry thick samples may be measured, while in MOKE in on metals the probing depth does not exceed 10 nm.

Magneto-optical effects allow the combination of various environmental conditions, such as magnetic field, temperature, pressure, embedded in other measurement setup such as electric probers. They are also compatible with time-resolved measurements, either averaged or in a stroboscopic mode. Finally, all this may be averaged over a large spot of light, or in a focus spot for nano-object measurement, or in an optical microscope to directly deliver magnetic images. The spatial resolution is limited to the wavelength of light, or slightly below if an objective with large numerical aperture is used, or with lenses immersed in high-index transparent oils (Figure I.10).

6.3 X-ray Magnetic Dichroism techniques

6.3.A X-RAY MAGNETIC CIRCULAR DICHROISM

Dichroism exploits the dependence of the absorption of X-ray photons, in relation with the direction of moments in the material, thus allowing to measure the latter in an indirect way[30]. X-ray dichroism is non-negligible only when the energy of photons is tuned to equal certain electronic transitions, where the final

states are those of the partly-filled shells responsible for magnetism. Based on the spin imbalance of free states, and selection rules for absorbtion based on Fermi golden rule and involving the electronic orbital momentum and the photon polarization, the probability of absorbtion depends on the polarization of the X-ray photon. X-ray magnetism circular dichroism (XMCD) is the imbalance between left and right circularly-polarized beams. It is only an indirect measurement of the component of magnetization parallel to the beam direction, although analytical selection rules or simulations allow to extract it, and besides with an indication of both the spin and the orbital contributions. Magnetic dichroism is element sensitive, due to the addressing of an electronic transition of a given element. It is often implemented in the soft X-ray range, considering L transitions in 3d materials (from *p* states to the *d* band), and M transitions for rare earth (from *p* states to *f* states). The need to control X-ray energy requires the use of synchrotron radiation.

The amount of absorption can be detected directly (transmission geometry), or indirectly through fluorescence or photo-emitted electrons (total electron yield) involved in de-excitation. In the soft X-ray range the latter two have a probing depth limited by the mean free path of X-rays (a few tens to a hundred of nanometers) and/or of the collected photons (a few to tens of nanometers), or the mean free path of electrons (a few nanometers). Thus, it cannot probe bulk samples, and is neither sensitive to only one atomic plane. It is therefore very suitable to investigate thin films. In practice one often sets the energy of photons at an absorption edge, proceeds to two countings with opposite helicities, and computes the dichroic ratio $(I_+ - I_-)/(I_+ + I_-)$.

XMCD is often implemented under vacuum because soft X-rays are strongly absorbed in air, and also when the detection involves the collection of electrons. It can be combined with magnetic field, variable temperature, time-resolved measurements based on stroboscopic methods and the temporal structure of the orbiting particles in the synchrotron ring in well-defined packets. Used with a white beam it is a magnetometry technique. Implemented with electron optics or a small beam it provides a microscopy approach, as detailed in the next two paragraphs.

X-ray magnetic linear dichroism (XMCD) also exists. It results from the directional selection of certains orbitals based on electric dipole selection rules. When magnetism has an orbital character XMLD allows to probe the direction of magnetization, however not the pointing direction. It is a technique which allows to probe domains of various orientations in certain antiferromagnetic materials.

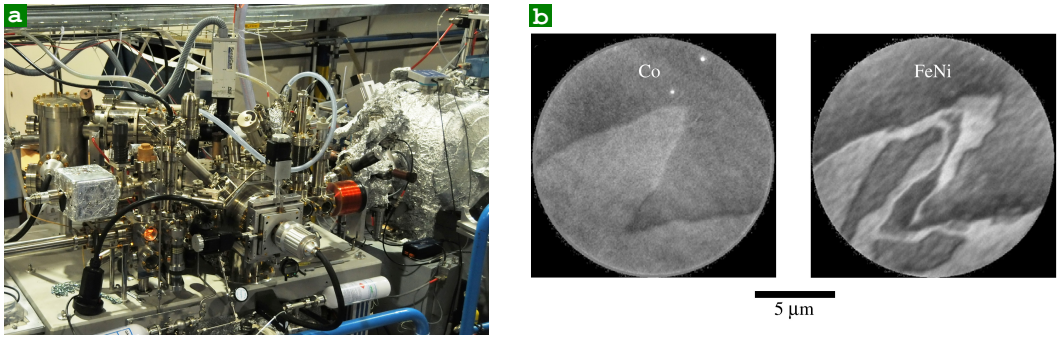

Figure I.11 – Photo-Emission Electron Microscopy. (a) PEEM-LEEM instrument installed at the Nanospectroscopy beamline in Elettra synchrotron, Italy. The sample and the entire imaging column are enclosed in ultra-high vacuum chambers. The beamline with the X-ray optics coming from the synchrotron start at the right of the image, extending twenty meters. (b) Illustration of the elemental resolution: imaging magnetic domains at the Co and Fe edges at the same location of a Al[3 nm]\$Fe_{20}Ni_{80}$[4 nm]\$Al_2O_3$[2.6 nm]\Co[7 nm] thin film with in-plane uniaxial magnetic anisotropy[33], a stack that can be used as a magnetic tunnel junction. $Fe_{20}Ni_{80}$ is the top layer and Co is the buried layer.

X-ray magnetic dichroism can also be implemented with hard X-rays, for example at the K edges of 3d elements. The magnitude of dichroism is much less than at the L edges, however it is better suited when very thick samples must be probed, because of the larger mean free path of photons at these energies.

6.3.B XMCD PHOTO-EMISSION ELECTRON MICROSCOPY

This technique collects the electrons photo-emitted following the dichroic absorption of X-rays, so again it is a synchrotron-based technique. An image is built thanks to a complex electron column developed for the Low-Energy Electron Microscope (LEEM). Electrons are accelerated into the column, and are converted to an image on a fluorescent screen at the end of the column[31, 32]. XMCD-PEEM has the same features as total electron yield XMCD: probing depth of a few nanometers, elemental resolution, possible combination with time resolution. However, it is very difficult to image under applied fields larger than a few mT, because low-energy electrons are very sensitive to these.

As the imaging column is perpendicular to the sample surface, the incidence of the X-ray beam is tilted for geometric reasons. Thus, what is probed is a combination of an in-plane and the out-of-plane components of magnetization. There now exist rotatable sample holders, which allow to separate the two in-plane components, acquiring two successive images. The spatial resolution in the best instruments and under optimum conditions is of the order of 25 nm.

XMCD-PEEM is very important in nanomagnetism and spintronics, making use of multilayered architectures, which can be probed separately if they consist of different materials, thanks to the elemental resolution.

6.3.c XMCD TRANSMISSION X-RAY MICROSCOPY

Transmission X-ray Microscopy (TXM) is yet another technique based on dichroism[34]. As the name suggests, this technique was introduced as a transmission technique. The imaging capability is brought by Fresnel lenses[I.13] positioned before and after the sample. There are two implementations, each with spatial resolution around $20\,\mathrm{nm}$. In the Scanning mode (STXM) the first Fresnel lens focuses the beam to a spot determining the resolution, while the second Fresnel collimates the transmitted beam to collect it on a photodiode. In the regular TXM mode the first Fresnel lens condenses the beam to define the full field of view, while the second lens acts as an objective to make the gather in the far field. STXM is better suited to perform local hysteresis loops because of the high local intensity, while regular TXM is considered better suited for imaging because it prevents artifacts arising from the scanning, such as drift-related.

(S)TXM offers more versatility for the sample environment than PEEM, because it is a photon-in photon-out technique; it is fully compatible with magnetic field, and needs to be implemented in secondary vacuum only, not ultra-high vacuum like LEEM. However, a constraint is the transmission geometry, requiring to work on samples thinned like for transmission electron microscopy, or deposited on thin X-ray transparent membranes such as silicon nitride. Note that this condition is being lifted, with the emergence of instruments where the detection scheme is fluorescence or total electron yield[35].

6.4 Scanning probe microscopies

These techniques are based on the local measurement of a property, performed thanks to a local probe. The measurement spot is then scanned in a two-dimensional fashion to construct an image. We consider the three such microscopies with magnetic capabilities, which have a large use and impact in nanomagnetism (Figure I.12).

[I.13] Fresnel lenses are made of successful ring-shaped strips of an X-ray absorbing material. The strips have a width and are located at the locus of what would be the scattering pattern of a small aperture. Following Babinet's reciprocal theorem, a collimated beam of X-rays shone on it focuses part of the beam in the focal plane.

6.4.a MAGNETIC FORCE MICROSCOPY

Magnetic Force Microscopy (MFM) is a technique mapping the stray field emanating from a sample, whose analysis allows one to infer the distribution of magnetization inside the sample.

MFM is derived from Atomic Force Microscopy. Along with Kerr microscopy, it is the most popular magnetic microscopy technique owing to its combination of moderate cost, reasonable spatial resolution (routinely $25 - 50\,\mathrm{nm}$) and versatility. Many reviews are available for both AFM[36] and MFM[27, 28].

AFM and MFM probe forces between a sample and a sharp tip. The tip is non-magnetic in the former case, and coated with a few tens of nanometers of magnetic material in the latter case. The forces are estimated through their impact on the displacement or oscillation of a soft cantilever holding the tip, usually monitoring the deflection of a laser reflected at the backside of the cantilever. The most common working scheme of MFM is an ac technique: while the cantilever is mechanically excited close to its resonance frequency f_0 (or more conveniently written as the angular velocity $\omega_0 = 2\pi f_0$), the phase undergoes a shift proportional to the vertical gradient of the (vertical) force $\partial F/\partial z$ felt by the tip: $\Delta\varphi = -(Q/k)\partial F/\partial z$. In practice magnetic images are gathered using a so-called two-pass technique: each line of a scan is first conducted in the tapping mode with strong hard-sphere repulsive forces probing mostly topography (so-called first pass), then a second pass is conducted flying at constant height (called the lift height) above the sample based on the information gathered during the first pass (Figure I.12). Forces such as Van der Waals are assumed to be constant during the second pass, and the forces measured are then ascribed to long-range forces such as magnetic.

The difficult point with MFM is the interpretation of the images, and the possible mutual interaction between tip and sample. A basic discussion of MFM is proposed in the Problems section, p.61. A summary of the expected signal measured is provided in Table I.4.

Table I.4 – Simple models for MFM tips. Expected MFM signal with respect to the vertical component $H_{d,z}$ of the stray field in static (cantilever deflection) and dynamic (frequency shift during the second pass) modes versus the model for the MFM tip.

Tip model	Static response	Dynamic response
Monopole	$H_{d,z}$	$\partial H_{d,z}/\partial z$
Dipole	$\partial H_{d,z}/\partial z$	$\partial^2 H_{d,z}/\partial z^2$

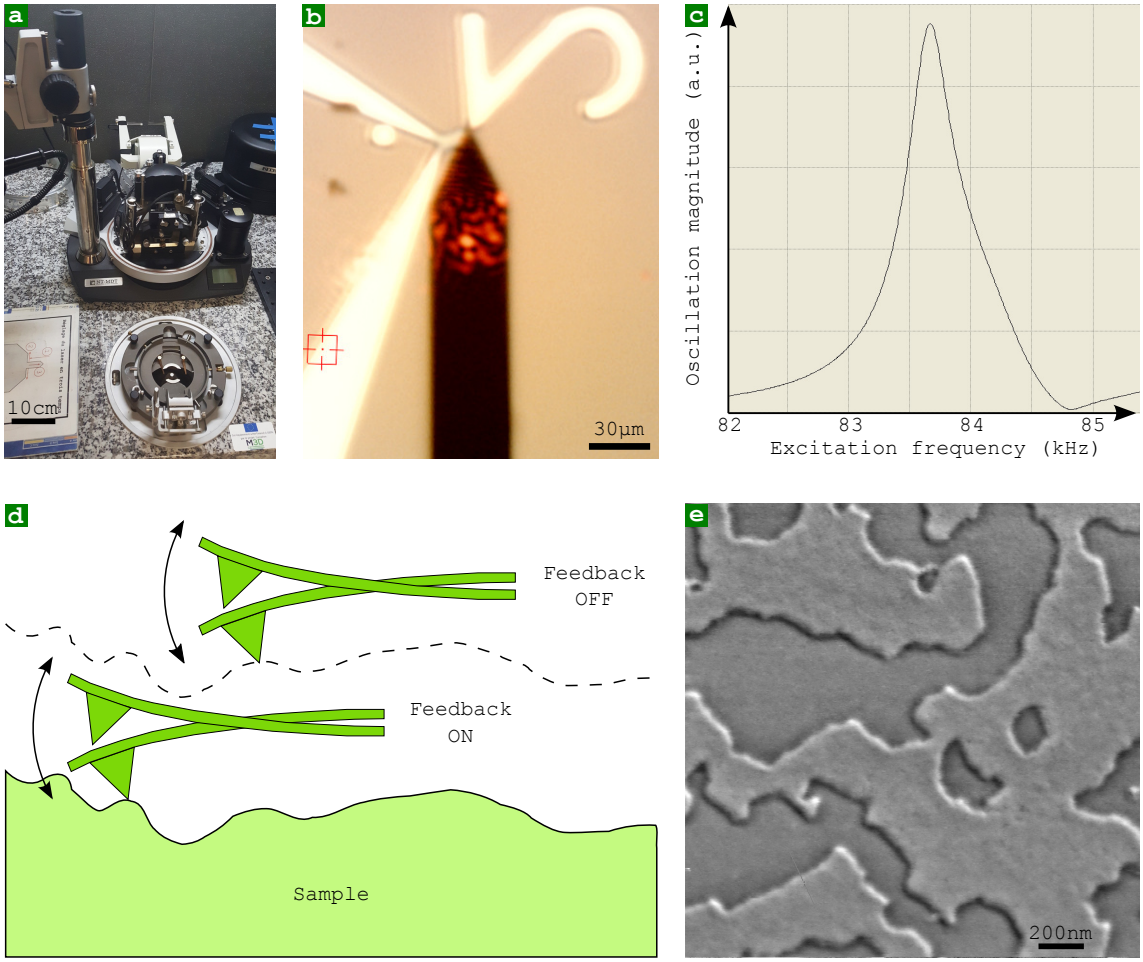

Figure I.12 – Magnetic Force Microscopy (MFM). (a) View of an NT-MDT AFM/MFM instrument, with built-in in-plane 200 mT magnetic field (magnetic circuit at the top part of the picture), and home-made stage for out-of-plane 1.1 T magnetic field (bottom of the image). (b) Optical top-view of the cantilever (dark part, laser focused close to its end) while imaging a patterned structure. (c) Typical resonance curve of a cantilever used for MFM. (d) Scheme for the two-pass MFM procedure. (e) 2×2 µm MFM domain pattern of a 4 nm-thick epitaxial FePt(001) film with perpendicular magnetization (sample courtesy: A. MARTY).

6.4.B SPIN-POLARIZED SCANNING TUNNELING MICROSCOPY

Spin-polarized Scanning Tunneling Microscopy (sp-STM) is a unique technique able to resolve the magnetic state at a surface, down to single atoms and molecules (Figure I.13).

Sp-STM is the magnetic implementation of the Scanning Tunneling Microscope (STM). STM was invented by Binnig and Rohrer in 1982, who were awarded the Nobel prize in 1986, recognizing the giant leap it enabled for the exploration of matter at surfaces at the atomic scale. STM exploits the tunnel current flowing between a sharp tip and the surface to investigate. It is therefore restricted to imaging metals or semiconductors. Keys for sensitivity and spatial resolution are the exponential variation of this current with tip-sample distance, and the small distance itself, of the order of one nanometer.

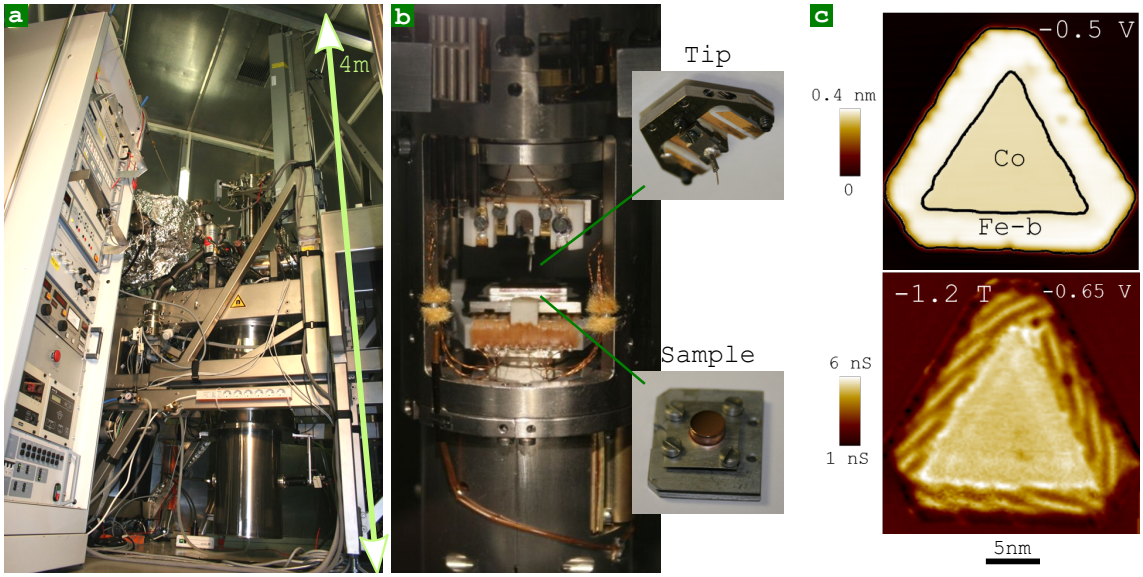

Figure I.13 – Spin-polarized Scanning Tunneling Microscopy (sp-STM). (a) Set-up allowing sp-STM, operating under ultra-high vacuum, at cryogenic temperature (7 K) and variable field (up to 8 T), installed at the Max-Planck Institut für Mikrostruckturphysik in Halle, Germany. The entire instrument is mounted on damped supports in a shielded room to allow for the lowest perturbations to achieve the highest sensitivity. (b) Close-up view of the tip and sample parts, with typical size a couple of centimeters. (c) Example of topographic (top) and magnetic (bottom) images of a self-assembled thin-film patch deposited on a Cu(111) surface, made of a core of Co atomic bilayer (ferromagnetic), surrounded by a bilayer Fe brim (with a helix spin structure)[39]. Courtesy: D. SANDER.

spSTM consists of capping an STM tip with magnetic material[37]. The tunnel current is sensitive to the respective orientations of tip and sample, so that a tip magnetized in a given direction allows through scanning to derive a magnetic map of the sample surface. It took close to an extra fifteen years after the invention of the STM, to get a working spSTM[38]. The reason is that magnetic imaging relies on fine spectroscopic analysis, requiring very sensitive and stable instruments, work at cryogenic temperatures to avoid spin excitations at the sample of tip location, and the need to develop tips with well-controlled magnetization.

The experimental constraints are severe, as detailed above, and the versatility in terms of samples is moderate, as only single-crystalline samples grown and investigated under ultra-high vacuum are eligible. Despite this, spSTM has allowed key discoveries in nanomagnetism, thanks to its unique ability to resolve the magnetic state of individual atoms and molecules. Breakthrough includes the discovery of antiferromagnetic face-centered cubic iron, and peculiar periodic spin textures such as cycloids and skyrmions[40]. The technique has also been extended to manipulation, *e.g.* injection of spin-polarized current to switch magnetization (chap.**??**), or inducing a magnetic phase transition with an electric field[41].

6.4.c NV-CENTER MICROSCOPY

NV-center microscopy allows to measure quantitatively one component of the stray field of a sample with an extreme sensitivity, down to single electron spins[42].

The principle relies on a defect introduced on purpose in the structure of diamond, consisting of a pair of a nitrogen atom and a vacancy. This combined center is quantum in nature. It has a triplet state $S = 1$ with a splitting of the states $m_s = 0$ and $m_s = \pm 1$, which can be measured resonantly with a gigahertz wave. The resonance peak is narrow and well-defined by the NV center. The measurement can be performed at room temperature thanks to the low level of decoherence in the diamond matrix. When the NV center is subject to a magnetic field the degeneracy of the states $m_s = \pm 1$ is lifted, splitting the resonance peak. The measurement of the splitting is a direct quantitative measure of the component of magnetic field along a quantized direction set by the orientation of the diamond material embedding the NV center. Scanning above a magnetic sample thus allows to measure a map of its stray field with high accuracy and quantitatively.

In practice, single defects in diamond nanoparticles are required, to be put at the apex of an atomic force microscope for the combined magnetic and topographic imaging. Although is suffers from the restriction to rather low fields and more complexity than MFM, it has emerged as a very important technique in recent years. It was used for example to resolve the internal structure of domain walls in ultrathin films, discriminating Bloch walls from Néel walls (see chap.II). It is compatible with variable temperature, and with magnetization dynamics as long as the frequency is much lower than the monitored microwave resonance.

6.5 Electron microscopies

Electrons are particles with both a spin and a charge, which can each be exploited for magnetic imaging. Three main techniques exist, as described below.

6.5.a LORENTZ MICROSCOPY AND HOLOGRAPHY

Lorentz microscopy, and holography, are implemented in transmission electron microscopes. They deliver quantitative maps of in-plane induction related to thin samples and integrated along the beam path (including magnetization and dipolar field), with a spatial resolution down to a few nanometers. Two different principles are exploited.

In Lorentz microscopy one uses the Lorentz force, responsible for the deflection of the electron beam. A way to recover information about induction is to use an off-centered aperture in the image plane to select only those electrons with a given deflection, reflecting a given in-plane component of induction; this

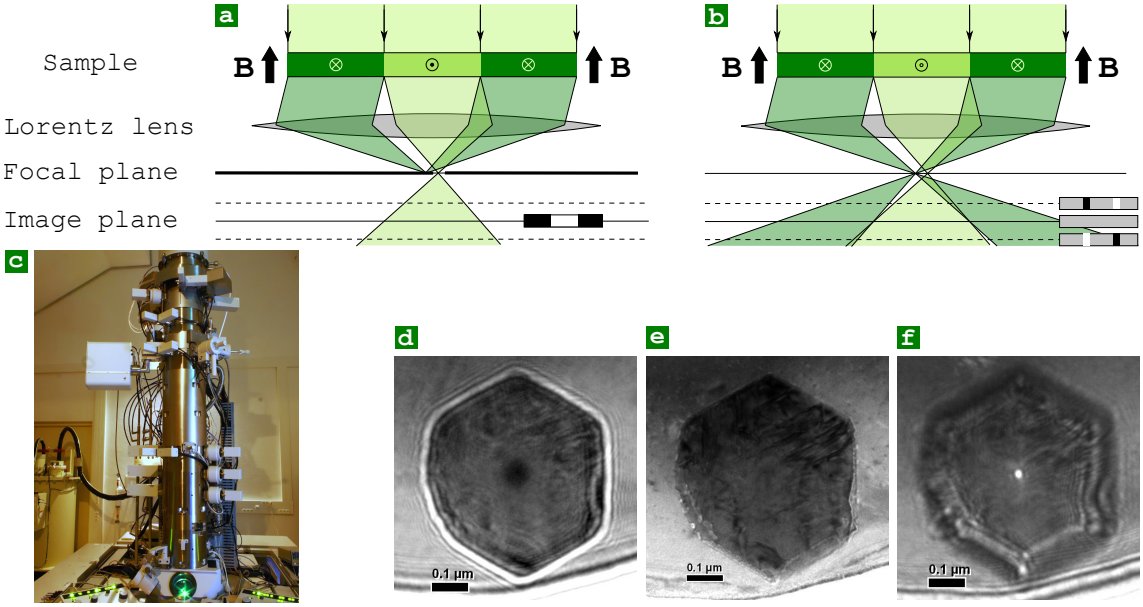

Figure I.14 – Lorentz Microscopy. Schematics for the (a) Foucault mode and (b) Fresnel mode. (c) $I^2$2TEM (Hitachi) microscope installed at CEMES laboratory, Toulouse, specially designed for in-situ and interferometry measurements of micromagnetism at the nanoscale. Images of a flux-closure Co(0001) self-assembled dot in the Fresnel mode, (d) under-focussed, (e) in focus, (f) over-focussed[43].

highlights domains, and combining several images with different positions of the aperture a 2D map of induction can be reconstructed. Another way does not use an aperture, but images made in slightly over- under-focused conditions, in which case electron beams from neighboring domains with opposite magnetization either overlap or split; this reveals domain walls, and reconstructions algorithms allow to reconstruct the 2D map of in-plane induction (Figure I.14).

In electron holography one uses the phase shift of the electrons, related to the magnetic vector potential **A** projected and again integrated along the electron path. As detectors are not sensitive to the phase of electrons, a special design needs to be used: the beam having passed through the sample is recombined with a reference beam to produce an interference pattern, from which the phase shift through the sample can be extracted.

Both techniques have the constraint of thin sample, however they provide several key advantages: they are quantitative; magnetic field can be applied from zero up to several tesla; variable-temperature sample holders are available; their spatial resolution is currently the highest among all microscopies, apart from sp-STM. Developments are under way such as combination with GHz excitations and pump-probe measurements for time resolution, or also vectorial tomography (reconstruction of a 3D map of magnetization from a series of images measured at different tilt angles of a sample)[44].

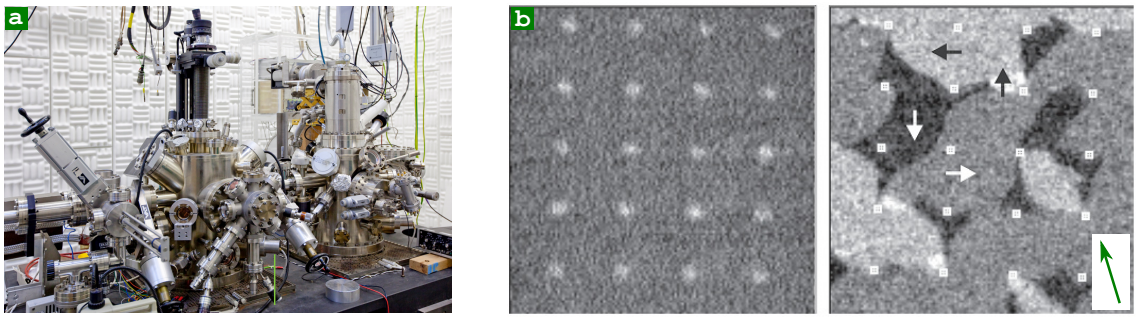

Figure I.15 – Scanning Electron Microscopy with Polarization Analysis, or spin-SEM. (a) Overview of the spin-SEM setup at the IBM research laboratories in Zürich (courtesy R. Allenspach). The Mott detector is located in a separate room, not seen here. (b) Illustration of the magnetic domain pattern imaged by SEMPA (right) of a thin Co film deposited on a Cu(001) crystal and displaying a regular array of holes, in a so-called antidot fashion (left, topographic view, the bright areas highlighting the places where Co is missing)[45]. This system has a fourfold magneto-crystalline anisotropy, and thus may display domains aligned along four directions. The direction of sensitivity to the magnetization direction is indicated with the arrow in the inset. Each image is $18 \times 18\,\mu m$.

6.5.B SCANNING ELECTRON MICROSCOPY WITH POLARIZATION ANALYSIS (SEMPA)

SEMPA is a powerful however not so widespread technique. It is based on a Scanning Electron Microscope (SEM) and delivers 3D vectorial maps of surface magnetization. It is also called spin-SEM[45].

As for SEM, a focused beam of non-spin-polarized electrons is scanned at the surface of a sample; the difference with SEM lies in the fact that the electrons arrive at the sample with nearly zero kinetic energy, so that it is mostly the material electrons close to the Fermi level (responsible for ferromagnetism) that matter. Although the beam is not spin-polarized as a whole, each individual electron has a spin. The probability of absorption and reflection of an electron on a ferromagnetic surface depends on its spin quantized along the direction of magnetization of the sample, as the latter has a different number of occupied and empty states in the two channels. As a consequence the reflected beam is highly spin-polarized. The analysis of this polarization as a function of the position of the beam on the sample, allows to make a map of magnetization (Figure I.15).

The standard technique to analyze the polarization of electrons is a Mott detector, based on the asymmetric scattering of electrons arriving at relativistic energies on high spin-orbit-element surface such as tungsten, which are measured simultaneously with a several-quadrant detector. The weak point of the technique is the low efficiency of detection, of the order of 10^{-4}. This raises concerns of signal-to-noise ratio, which is what in practice limits the spatial resolution to a few tens of nanometers. The strength of the technique is that the use of detectors differently located in space reveal several component of magnetization. Thus, a complete vectorial map of magnetization can be reconstructed. The depth probed on the magnetic sample is a few atomic layers at most.

The technique can be combined with variable temperature. Application of magnetic field is more complex because of the deflection of electrons, however small coils of millimeter size implemented in the proximity of the sample have been demonstrated to allow imaging in field up to 100 mT[46]. The development of novel detectors with increased efficiency could revive this technique[47].

6.5.c SPIN-POLARIZED LOW-ENERGY ELECTRON MICROSCOPY (SPLEEM)

The characteristics of SPLEEM are very similar to those of SEMPA, in that it provides vectorial maps of surface magnetization.

SPLEEM is based on the LEEM microscope, described in the PEEM paragraph (sec.6.3.b). The magnetic working principle is opposite to that of SEMPA. Indeed, the beam of electrons sent to the sample is highly spin-polarized, being produced by optical pumping of a GaAs cathod with circularly-polarized light[48, 49]. Reflection at the sample surface is again spin-dependent, so that beams with opposite spin values and identical intensity, are reflected as beams with two very different intensities. Their difference is a direct probe of the magnetic state of the surface. Manipulation of the spin state of the incoming beam also provides the ability to measure vectorial maps. Note also that SPLEEM is a full-field imaging, unlike SEM. Combined with the high spin polarization of the incoming beam, this makes it a technique easier to use than SEMPA. Nevertheless, only a handful of such instruments exist worldwide, especially due to the complexity of the spin gun producing spin-polarized electrons at will.

SPLEEM has an ultimate resolution of the order of 10 nm, and probes a couple of atomic layers. It is compatible with variable temperature, however as in PEEM virtually no magnetic fields can be applied.

Summary

Magnetometry and magnetic imaging. Besides magnetometry, the emphasis has been put here on magnetic microscopy, which plays a key role in nanomagnetism. There is no universal and best technique, each having its advantages and drawbacks. Criteria include spatial resolution, physical quantity probed, sensitivity, quantitative or not, conditions that can be applied such as field or temperature, time resolution, elemental sensitivity. The combination of several types of microscopies is sometimes required to get the full picture of a situation.

Problems for Chapter I

Problem 1: Self-testing

1. What is the scaling law for the long-range stray field arising from a magnetic dipole?
2. Provide the definition and unit for a magnetic moment, and for magnetization. How are they linked one with the other?
3. Which are the only three elements ferromagnetic at room temperature?
4. Provide the definition for coercive field and for remanence.
5. Name the four main contributions to the magnetic energy of a system.
6. Provide the name and equation for a measure of the volume density of magnetostatic energy in a given material.
7. What is the definition of stray field and demagnetizing field?
8. What is the definition of a demagnetizing coefficient?
9. What is a Bloch domain wall? Why is it considered as the domain wall of lowest energy in a bulk ferromagnetic material?
10. Provide equations for the width and energy of a Bloch domain wall

Problem 2: Short questions

1. See Table I.1. Write the mutual energy as a function of distance between two magnetic charges Q, and that between two magnetic dipoles with magnitude μ, aligned along their separation vector. Discuss the difference in power law.
2. Provide the expressions for the dipolar exchange length Δ_d, the anisotropy exchange length Δ_u and the anisotropy field $H_a = 2K/\mu_0 M_s$ in the cgs system (see problem on units for a detailed analysis).
3. Draw the equivalent magnetic charges and the magnetic fields resulting from the distribution of magnetization in the four cases shown on Figure I.16.

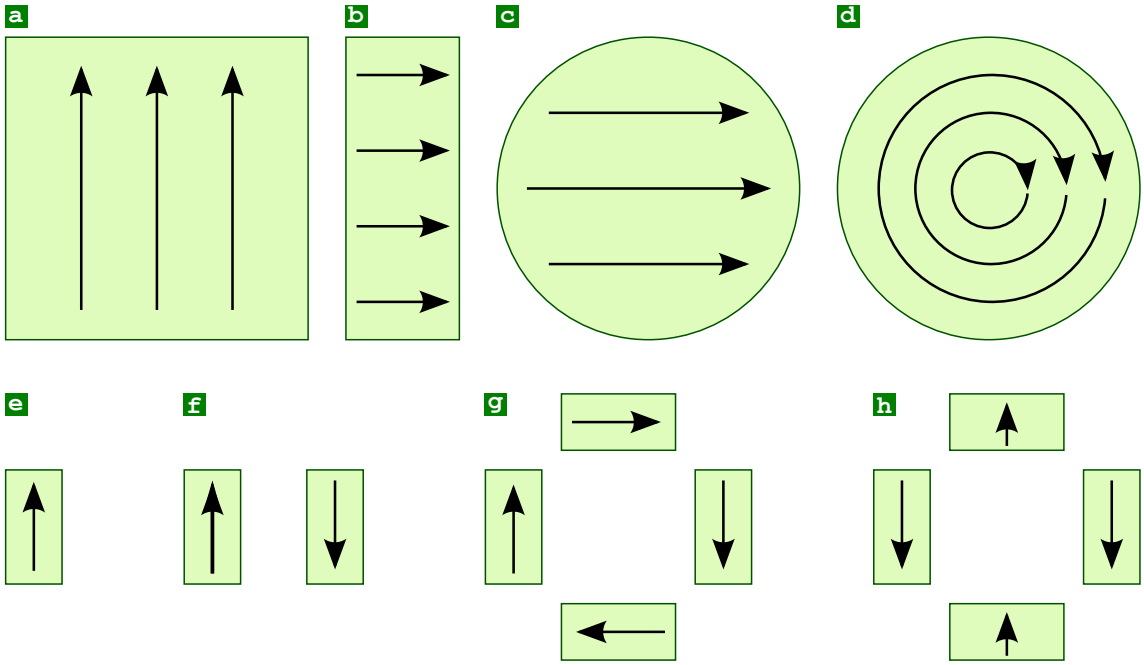

Figure I.16 – Magnetic charges, demagnetizing and stray fields (a) cross-section of a uniformly-magnetized cube (b) side view of a perpendicularly-magnetized thin film with infinite lateral dimensions (c) Cross-section of a cylinder magnetized along a transverse direction (d) Top view of a thin and flat element with very large lateral dimensions. (e-h) various sets of permanent magnets.

4. Demagnetizing coefficients. Provide the main directions for the following geometries (make a sketch and label all three axes in each case): sphere, cube, thin film, cylinder of infinite length, cylinder of finite length, thin flat element with a circular shape, thin flat element with a rectangular shape, thin flat element with a triangular shape. In each case provide figures for all three demagnetizing coefficients, if available exactly, or inequalities bounding them.
5. Provide the proof for the domain wall width formula given in sec.5.3: W_L, W_m, W_J, W_F and W_T, both for the variational linear model, and the exact profile [Eq.(I.41)].

Problem 3: Demagnetizing coefficients of composite materials

This problem considers the estimation of the demagnetizing matrix $\overline{\overline{\mathbf{N}}}$ for composite materials, a situation at first sight more complex than considered in the main text, however conceptually covered by the concept thereby developed. Let us recall this definition for a uniformly-magnetized body: $< \mathbf{H}_d >= -\overline{\overline{\mathbf{N}}} \cdot \mathbf{M}$.

1. Consider a body with magnetization of modulus M_s, in which there exists an empty cavity. Let us call $\overline{\overline{\mathbf{N}}}_c$ the demagnetizing matrix of a particle which would have the shape of the cavity. Sketch the distribution of magnetic charges around the cavity for a given direction of magnetization, and provide an expression for the dipolar field $\mathbf{H}_{d,c}$ inside the cavity. This situation is known as the Lorentz cavity. The effect of the outer shape of the body shall for the moment not be considered, *e.g.* such as in the case of a slab (thin film) with in-plane magnetization.
2. We now consider a body made of a dilute assembly of magnetic particles in a non-magnetic matrix, with porosity p defined as the fraction of volume occupied by the particles. When one focuses on a given particle, the dipolar field arising from all other particles may be calculated in a mean field approach, coming from a body carrying magnetization with modulus pM_s. Let us call again $\overline{\overline{\mathbf{N}}}_c$ the shape of the cavity of neighbors surrounding the particle. Provide an expression for $\mathbf{H}_{d,c}$ felt at the nanoparticle locus, as arising from this cavity effect.
3. Still for the body made of a dilute assembly of magnetic particles in a non-magnetic matrix, consider now the superposition of all three effects: the Lorentz cavity, the outer shape of the body with demagnetizing matrix $\overline{\overline{\mathbf{N}}}_b$, the shape of each particle with demagnetizing matrix $\overline{\overline{\mathbf{N}}}_p$, the latter assumed to all share the same tensor with no angular distribution of the axes. Express the dipolar field $\mathbf{H}_d$ felt inside each nanoparticle, and derive an expression for $\overline{\overline{\mathbf{N}}}$ defined as $< \mathbf{H}_d >= -\overline{\overline{\mathbf{N}}} \cdot \mathbf{M}$. Check that it fulfills $\mathrm{Tr}\, \overline{\overline{\mathbf{N}}} = 1$.
4. Apply the above calculations in the following cases. For each case draw a sketch, name the main axes, calculate the demagnetizing coefficients along all three directions, and comment on the limiting cases $p \to 0$ and $p \to 1$. Provide an expression for the angular variation of the density of dipolar energy E_d, and calculate the value of p for which the system behaves isotropically.
   (a) Spherical particles in a spherical body; the Lorentz cavity shall be assumed to be spherical.
   (b) Spherical particles in a slab (thin film). Discuss what proper choice shall be made for the shape of the Lorentz cavity, in the case of slab thickness much larger than the inter-particle distance.
   (c) Close-to-infinitely-long cylinders packed in a thin-film body, with their axis perpendicular to the film. Discuss what proper choice shall be made for the shape of the Lorentz cavity, in the case where the film thickness is much larger than the inter-cylinder distance.

Problem 4: More about units

Here we derive the dimensions for physical quantities of use in magnetism, and their conversions between cgs-Gauss and SI.

4.1. Notations

We use the following notations:

- X is a physical quantity, such as force in $F = mg$. It may be written **X** for vectors.
- $\dim X$ is the dimension of X expressed in terms of powers of fundamental dimensions, here length (L), mass (M), time (T) and electrical current (I). For example, dimensions of speed and electrical charges read: $\dim v = \mathsf{L}\cdot\mathsf{T}^{-1}$ and $\dim q = \mathsf{I}\cdot\mathsf{T}$. As a shortcut we will use here a vector matrix to summarize the dimension of quantities, with components the powers of fundamental dimensions; it will be written $[X]$ for the dimension of X. The above examples now read $[v] = [\mathsf{L}] - [\mathsf{T}] = [1\ 0\ -1\ 0]$ and $[q] = [\mathsf{I}] + [\mathsf{T}] = [0\ 0\ 1\ 1]$. We use shortcuts [L], [M], [T] and [I] for the four fundamental dimensions.
- In a system of units α (*e.g.* SI or cgs-Gauss) a physical quantity is evaluated numerically based on the unit physical quantities: $X = X_\alpha \langle X\rangle_\alpha$. X_α is a number, while $\langle X\rangle_\alpha$ is the standard (*i.e.*, used as unit) for the physical quantity in the system considered. For example $\langle L\rangle_{\mathsf{SI}}$ is a length of one meter, while $\langle L\rangle_{\mathsf{cgs}}$ is a length of one centimeter: $\langle L\rangle_{\mathsf{SI}} = 100\langle L\rangle_{\mathsf{cgs}}$. For derived dimensions we use the matrix notation. For example the unit quantity for speed in system α would be written $\langle 10{-}10\rangle_\alpha$.

4.2. Expressing dimensions

- Based on laws for mechanics, find dimensions for force F, energy $\mathcal{E}$ and power $\mathcal{P}$, and their volume density E and P.
- Based on the above, find dimensions for electric field **E**, voltage U, resistance R, resistivity ρ, permittivity ϵ_0.
- Find dimensions for magnetic moments $\boldsymbol{\mu}$, magnetic field and magnetization **H** and **M**, induction **B** and flux ϕ, and permeability μ_0.

4.3. Conversions

Physics does not depend on the choice for a system of units, so doesn't any physical quantity X. The conversions between its numerical values X_α and X_β in two such systems is readily obtained from the relationship between $\langle X\rangle_\alpha$ and $\langle X\rangle_\beta$. In the cgs-Gauss system, the unit for length, mass and time are centimeter, gram and second. The electric current may also be considered as existing and named

Biot or abampère, equivalent to 10 A. Thus we have the following conversion relationships: $\langle L\rangle_{\text{SI}} = 10^2\langle L\rangle_{\text{cgs}}$. Similarly we have $\langle M\rangle_{\text{SI}} = 10^3\langle M\rangle_{\text{cgs}}$, $\langle T\rangle_{\text{SI}} = \langle T\rangle_{\text{cgs}}$ and $\langle I\rangle_{\text{SI}} = 10^{-1}\langle I\rangle_{\text{cgs}}$.

In practice conversion can be formally written the following way: $X = X_\alpha\langle X\rangle_\alpha = X_\beta\langle X\rangle_\beta$. Let us consider length l as a example. $l = l_{\text{SI}}\langle L\rangle_{\text{SI}} = l_{\text{cgs}}\langle L\rangle_{\text{cgs}}$. From the above we readily have: $l_{\text{SI}} = (1/100)l_{\text{cgs}}$. Thus the numerical value for the length of an olympic swimming pool is 5000 in cgs, and 50 in SI. For derived units (combination of elementary units), $\langle X\rangle_\alpha$ is decomposed in elementary units in both systems, whose relationship is known. For example for speed: $\langle v\rangle_\alpha = \langle L\rangle_\alpha\langle T\rangle_\alpha^{-1}$.

Exhibit the conversion factor for these various quantities, of use for magnetism:

- Force **F**, energy $\mathcal{E}$, energy per unit area E_s, energy per unit volume E. The units for force and energy in the cgs-Gauss system are called dyne and erg, respectively.
- Express the conversion for magnetic induction B and magnetization M, whose units in cgs-Gauss are called gauss and emu/cm^3, respectively. Express related quantities such as magnetic flux ϕ and magnetic moment μ.
- Let us recall that magnetic field is defined in SI with $B = \mu_0(H + M)$, whereas in cgs-Gauss with $B = H + 4\pi M$, with the unit called œrsted. Express the conversion for μ_0 and comment. Then express the conversion for magnetic field H.
- Discuss the cases of magnetic susceptibility and demagnetizing coefficients. In SI these are defined by $\chi = \mathrm{d}M/\mathrm{d}H$ and $H_{\text{d}} = -NM$. What should be their definition in the cgs-Gauss system so that these dimensionless quantities have the same numerical value in both systems? Notice that definitions sometimes used in the cgs-Gauss system are: $H_{\text{d}} = -4\pi NM$ and $H_{\text{d}} = -DM$.

Problem 5: More about the Bloch domain wall

The purpose of this problem is to go deeper in the mathematics describing the textbook case of the Bloch domain wall discussed in sec.5. The first section is mainly mathematics and may be skipped if desired.

5.1. Euler-Lagrange equation

We will seek to exhibit a magnetization configuration that minimizes an energy density integrated over an entire system. Finding the minimum of a continuous quantity integrated over space is a common problem solved through Euler-Lagrange equation, which we will deal with in a textbook one-dimensional framework here. Let us consider a microscopic variable defined as $E(\theta, \mathrm{d}\theta/\mathrm{d}x)$, where x is the spatial coordinate and θ a quantity defined at each point. In the

case of micromagnetism we will have:

$$E\left[\theta(x), \frac{\mathrm{d}\theta}{\mathrm{d}x}(x)\right] = A\left[\frac{\mathrm{d}\theta}{\mathrm{d}x}(x)\right]^2 + E_\mathrm{a}[\theta(x)] \tag{I.43}$$

When applied to micromagnetism $E_\mathrm{a}(\theta)$ may contain anisotropy, Zeeman and dipolar terms (the latter taken as local through the hypothesis of demagnetizing coefficients or other approximations). We define the integrated quantity:

$$\mathcal{E}[\theta] = \int_{x_A}^{x_B} E\left[\theta(x), \frac{\mathrm{d}\theta}{\mathrm{d}x}(x)\right] \mathrm{d}x + \mathcal{E}_A\left[\theta(x_A)\right] + \mathcal{E}_B\left[\theta(x_B)\right]. \tag{I.44}$$

A and B are the boundaries of the system, while $\mathcal{E}_A(\theta)$ and $\mathcal{E}_B(\theta)$ are surface energy terms. These may stem from, *e.g.*, surface magnetic anisotropy, or the Dzyaloshinskii-Moriya interaction. Let us now consider an infinitesimal function variation $\delta\theta(x)$ for θ. Show that extrema of $\mathcal{E}$ are determined by the following local relationships:

$$\frac{\partial E}{\partial \theta} - \frac{\mathrm{d}}{\mathrm{d}x}\left(\frac{\partial E}{\partial \frac{\mathrm{d}\theta}{\mathrm{d}x}}\right) \equiv 0 \tag{I.45}$$

$$\frac{\mathrm{d}\mathcal{E}_A}{\mathrm{d}\theta} - \left.\frac{\partial E}{\partial \frac{\mathrm{d}\theta}{\mathrm{d}x}}\right|_A = 0 \tag{I.46}$$

$$\frac{\mathrm{d}\mathcal{E}_B}{\mathrm{d}\theta} + \left.\frac{\partial E}{\partial \frac{\mathrm{d}\theta}{\mathrm{d}x}}\right|_B = 0 \tag{I.47}$$

Note that equations Eq.(I.46) and Eq.(I.47) differ in sign because a surface quantity should be defined with respect to the unit vector normal to the surface, with a unique convention for the sense, such as the outwards normal. Here the abscissa x is outwards for point B however inwards at point A. An alternative microscopic explanation would be that for a given sign of $\mathrm{d}\theta/\mathrm{d}x$ the exchange torque exerted on a moment to the right (at point B) is opposite to that exerted to the left (at point A), whereas the torque exerted by a surface anisotropy energy solely depends on θ.

5.2. Micromagnetic Euler equation

Apply the above equations to the case of micromagnetism [Eq.(I.43)]. Starting from Eq.(I.45) exhibit a differential equation linking $E_\mathrm{a}(\theta)$ with $\mathrm{d}\theta/\mathrm{d}x$. Equations I.46-I.47 are called Brown equations. $\mathcal{E}_A(\theta)$ and $\mathcal{E}_B(\theta)$ may be surface magnetic anisotropy, for instance. Discuss the microscopic meaning of these equations. Comment the special case of free boundary conditions (all bulk and surface energy terms vanish at A and B), in terms of energy partition. Show that $\mathcal{E}$ can be expressed as:

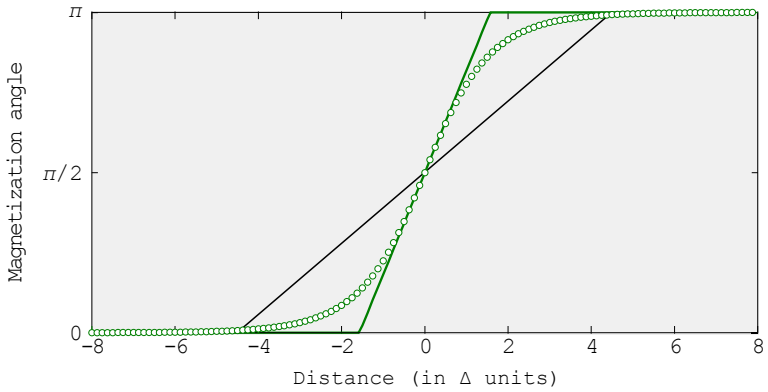

Figure I.17 – Bloch domain wall profile: the exact solution (green dots) versus the asymptotic profile (red line). The solution with linear ersatz is shown as a dark line.

$$\mathcal{E}[\theta] = 2\int_{\theta(x_A)}^{\theta(x_B)} \sqrt{AE_a(\theta)}\,\mathrm{d}\theta \tag{I.48}$$

5.3. The Bloch domain wall

Let us assume the following free boundary conditions, mimicking two extended domains with opposite magnetization vectors separated by a domain wall whose profile we propose to derive here: $\theta(-\infty) = 0$ and $\theta(+\infty) = \pi$. We will assume the simplest form of magnetic anisotropy, uniaxial of second order: $E(\theta) = K_u \sin^2\theta$.

Based on a dimensional analysis give approximate expressions for both the domain wall width δ and the domain wall energy $\mathcal{E}$. What are the SI units for $\mathcal{E}$? Discuss the form of these quantities in relation with the meaning and effects of exchange and anisotropy.

By integrating the equations exhibited in the previous section, derive now the exact profile of the domain wall:

$$\theta(x) = 2\arctan\left(\exp\frac{x}{\Delta_u}\right) \tag{I.49}$$

and its total energy $\mathcal{E}$. $\Delta_u = \sqrt{A/K_u}$ is the anisotropy exchange length.

The most common way to define the Bloch domain wall width δ_{Bl} is by replacing the exact $\theta(x)$ by its linear asymptotes (red line on Figure I.17). Derive δ_{Bl} as a function of Δ_u.

Let us stress several issues:

- The model of the Bloch wall was named after D. Bloch who published this model in 1932[50].

- As often in physics we have seen in this simple example that a dimensional analysis yields a good insight into a micromagnetic situation. It is always worthwhile starting with such an analysis before undertaking complex analytical or numerical approaches, which especially for the latter may hide the physics at play.
- We have exhibited here a characteristic length scale in magnetism. Other length scales may occur, depending on the energy terms in balance. The physics at play will often depend on the dimensions of your system with respect to the length scales relevant in your case. Starting with such an analysis is also wise.
- When the system has a finite size the anisotropy and exchange energy do not cancel at the boundaries. The integration of Euler's equations is more tedious, involving elliptical functions.

Problem 6: Extraction and vibration magnetometer

6.1. Preamble

Here we consider the principle of extraction magnetometry, either in full quasi-dc extraction operation, or in the vibration mode (Vibrating Sample Magnetometer, VSM). Their purpose is to estimate the magnetic moment held by a sample, possibly as a function of field, temperature, time etc. The general principle is to move a sample along the axis of a coil of radius R. This induces a change over time of the flux in the coil, arising from the sample, which may be measured thanks to the induced electromotive force (EMF)[I.14]. In a so-called extraction magnetometer the sample is moved sufficiently away from end to the other along the axis so as to nearly cancel the flux, resulting in an absolute measurement of the flux. In a vibrating sample magnetometer the sample vibrates along the axis at several tens of hertz close to the coil, inducing a large EMF and opening the use of a lock-in technique to further reducing the noise, however the full extraction curve is not measured, resulting in higher sensitivity to artefacts, as will be discussed below.

6.2. Flux in a single coil

Based on the Biot and Savart formula, express as a vector the induction $B(z)$ arising along the axis of a circular coil of radius R with electrical current I. Below is reminded the Biot and Savart formula expressing at an arbitrary location M in space the infinitesimal induction δB arising from a current I on an infinitesimal

[I.14] An alternative and very sensitive device for measuring the flux through a coil is SQUID: Superconducting Quantum Interference Device.

element δl at location P :

$$\delta B = \frac{\mu_0 I \delta \mathbf{l}(P) \times \mathbf{PM}}{4\pi PM^3} \tag{I.50}$$

For reaching a high sensitivity the coil is wound several time, $N \gg 1$. In the following we will assume $N = 1000$ for numerics. We will assume here that the location of all loops is the same. Based on the reciprocity theorem for induction, derive the magnetic flux $\Phi(z)$ in the series of coils, arising from a pinpoint magnetic moment μ located on the axis of the coil. $\Phi(z)$ will be expressed as $\Phi(z) = Kf(z)$, with $f(z)$ a dimensionless function. Draw a schematics of $f(z)$

Numerics: what is the uniform magnetic induction that would be required to create a flux in these coils, equivalent to that of a square piece of thin film of iron of lateral size 1 cm and thickness 1 nm (reminder: the magnetization of iron is $\approx 1.73 \times 10^6$ A/m). Comment with respect to the magnitude of the earth magnetic field.

6.3. Vibrating in a single coil

The sample is now moved periodically along the axis of the coil, around the location z_0: $z(t) = z_0 + \Delta z \cos(\omega t)$. Based on a first-order expansion in $\Delta z/z_0$, derive the EMF $e(t)$ induced in the coil. Draw a schematics of this curve. At which position is found the maximum of magnitude for $e(t)$?

Numerics: calculate the magnitude of $e(t)$ arising from the iron thin film mentioned above with a frequency of 30 Hz and $\Delta z = 1$ mm. Comment about this value.

6.4. Noise in the signal

Owing to a mechanical coupling the coils for measurement vibrate with angular frequency ω in the supposedly static induction B applied to magnetize the sample. Let us assume that due the coils' imperfections or finite size this induction displays an inhomogeneity ΔB at the spatial scale for vibration of the sample. Derive the EMF induced in the measuring coils due to this inhomogeneity.

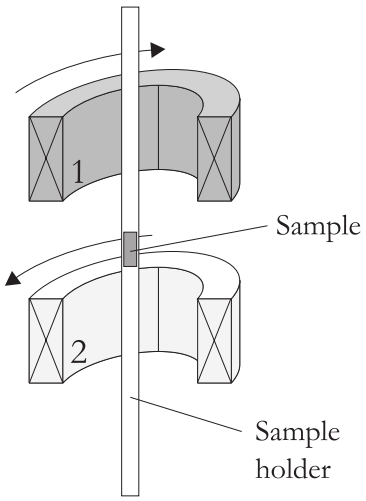

Figure I.18 – Coil compensation in magnetometers. Geometry for two coils winded in opposite directions

Numerics: vibration of magnitude 1 μm in an induction of strength 1 T, with a relative change of 10^{-3} over a distance of 5 mm. Comment the value.

6.5. Winding in opposition

The above noise can be reduced by using two coils with same axis, measured in series however wound in opposite senses (Figure I.18). The measured EMF is then $e_{tot}(t) = e_2(t) - e_1(t)$, and the sample is vibrated at equal distance from the two coils, at the position z_0 such that the signal is maximum (see above). Why is the above noise significantly reduced? Comment this setup with respect to the

Helmoltz geometry for two coils.

Problem 7: Magnetic force microscopy

This problem is an extension of the short paragraph about magnetic force microscopy in this chapter. This paragraph should be read first, before addressing this problem.

7.1. The mechanical oscillator

The dynamics of the AFM cantilever is modeled by a mechanical oscillator:

$$m\frac{\mathrm{d}^2z}{\mathrm{d}t^2} + \Gamma\frac{\mathrm{d}z}{\mathrm{d}t} + k(z - z_0) = F(z,t) \tag{I.51}$$

$F(z,t)$ is a force arising from either the operator or from the tip-sample interaction, and z_0 is the equilibrium position without applied force. m, Γ and k are the oscillator mass, damping and stiffness, respectively. We use the notation $\omega_0 = \sqrt{k/m}$ and $Q = \sqrt{km}/\Gamma$, the latter being called the quality factor.

Rewrite Eq.(I.51) with the use of ω_0 and Q. The cantilever is excited by the operator with $F(t) = F_{\mathrm{exc}}e^{j\omega t}$. Provide the transfer function $H = z/F$, the gain $G = |H|$ and phase shift $\varphi = \arg(H)$, as well as the following quantities, at resonance: angular velocity ω_r, magnitude z_r and phase φ_r. For the case $Q \gg 1$ calculate the magnitude at resonance, and the full-width at half maximum (FWHM) $\Delta\omega_\mathrm{r}$ of the resonance peak. Comment.

7.2. AFM in the static and dynamic modes

The cantilever is brought in the vicinity of the surface, inducing a non-zero force $F(z)$ between the tip and sample, adding up to the sinusoidal from the operator. For the sake of simplicity we will model the variations of F using a simple affine function: $F(z) = F(z_0) + (z - z_0)\partial F/\partial z$.

Calculate the new position at equilibrium z_{eq}. Rewrite Eq.(I.51) in this case, and in the case $Q \gg 1$ the normalized change of resonance angular velocity $\delta\omega_\mathrm{r}/\omega_0$. In most cases the cantilever is excited at a constant frequency ω_{exc} and the force gradient is monitored through the change of phase $\Delta\varphi$. Show that $\Delta\varphi = -(Q/k)\partial F/\partial z$.

7.3. Modeling forces

We assume here that the magnetization configurations of both the tip and the sample are not influenced one by another. The vertical component of the force applied by the sample on the tip is $F = -\partial\mathcal{E}/\partial z$, where $\mathcal{E}$ is the mutual energy. The tip may be modeled either by a magnetic dipole $\boldsymbol{\mu}$, or by a magnetic monopole

q) (in practice tips may be modeled by a linear combination of both components). For both models express to which *z* derivative of the vertical component of the sample stray field $H_{\mathrm{d},z}$ are proportional the deflection in the static AFM mode, and the frequency shift in the dynamic AFM mode.

Numerical evaluation – A typical MFM cantilever has $Q = 1000$ and $k = 4\,\mathrm{N/m}$. Modeling both the tip and samples by a magnetic dipole made of Co with a diameter $25\,\mathrm{nm}$, and assuming a probing distance of $50\,\mathrm{nm}$, provide a crude estimate of the frequency shift expected. Comment.

Chapter II

Magnetism and magnetic domains in low dimensions

Overview

In the previous chapter we have recalled basic knowledge about magnetic materials. However, both their microscopic and micromagnetic properties depend on the dimension and size of the system considered, because of geometrical reasons or related to characteristic length scales to be compared to the system's dimensions. This chapter covers the impact of dimensionality and dimensions on all aspects which matter in nanomagnetism: magnetic ordering, magnetic anisotropy, domains and domain walls. While thin films are a textbook case of reduction of dimensionality easy to consider due to the translational symmetry, we also progressively cover the case of nanostructures. This chapter is concerned with static properties only. The impact of dimensionality on magnetization reversal, dynamics and spintronics are to be found in the following chapters.

1 Magnetic ordering in low dimensions

1.1 Ordering temperature

The main feature of a ferromagnetic body is spontaneous ordering below a critical temperature T_C, called Curie temperature. It was Weiss who first proposed a mean-field approach to describe the ordering. In this theory it is postulated that the local moments feel an internal magnetic field

$$\mathbf{H}_i = n_W \mathbf{M}_s + \mathbf{H} \tag{II.1}$$

where $\mathbf{H}$ is the external field, and $n_W\mathbf{M}_s$ is the co-called *molecular field*. This is a phenomenological representation of magnetic exchange, whose quantum-mechanical origin was not known at the time. A semi-classical description allows to link the Heisenberg hamiltonian $\hat{\mathbf{H}} = -2\sum_{i>j} J_{i,j}\hat{\mathbf{S}}_i.\hat{\mathbf{S}}_j$ with n_W:

$$2ZJ_{i,j} = \mu_0 n_W n g_J^2 {\mu_B}^2 \tag{II.2}$$

where Z is the number of nearest neighbors, n the volume density of sites, each holding a dimensionless spin S bounded between $-J$ and $+J$, associated with total magnetic moment $\mu_J = g_J J \mu_B$[II.1]. Based on the site susceptibility related to the Brillouin function $\mathcal{B}_J$, the expected ordering temperature may be expressed as:

$$T_C = \frac{2ZJ_{i,j}J(J+1)}{3k_B} \tag{II.3}$$

The expected Curie temperature is therefore proportional to Z. Let us now draw trends for the Curie temperature in low dimensions. To do this we consider a thin film as a model system, and extend the mean-field approach to averaging the number of nearest neighbors over the entire system. For a film with N layers of sites with magnetic moments we get: $Z_N = Z + 2(Z_s - Z)/N$ where Z_s is the number of nearest neighbors of each of the two surface/ interface layers (Figure II.1a). As $Z_s < Z$ we immediately see based on Eq.(II.3) that the ordering temperature should be reduced. The decrease follows the law $T_C(t) = T_C(\infty) - \Delta T_C(t)$ with a $\Delta T_C \sim 1/t$, with t the film thickness. Our hand-waving considerations are confirmed by a more rigorous layer-dependent mean-field theory[51]. Going beyond mean-field, one may find other critical exponents λ for $T_C \sim t^{-\lambda}$.

As a rule of thumb, following Eq.(II.3) T_C should be decreased to half the bulk ordering temperature for N equaling one or two atomic layers. Figure II.1b-c shows the $M_s(T)$ variation and the Curie temperature measured for several types of ultrathin films, where the latter prediction appears largely valid, although the scaling law is best fitted with $\lambda = 1.27 \pm 0.20$.

Finally, the $M_s(T)$ law again depends on the model used (dimensionality, type

[II.1] Beware of this local possible confusion between the exchange constant J, and the total angular momentum J.

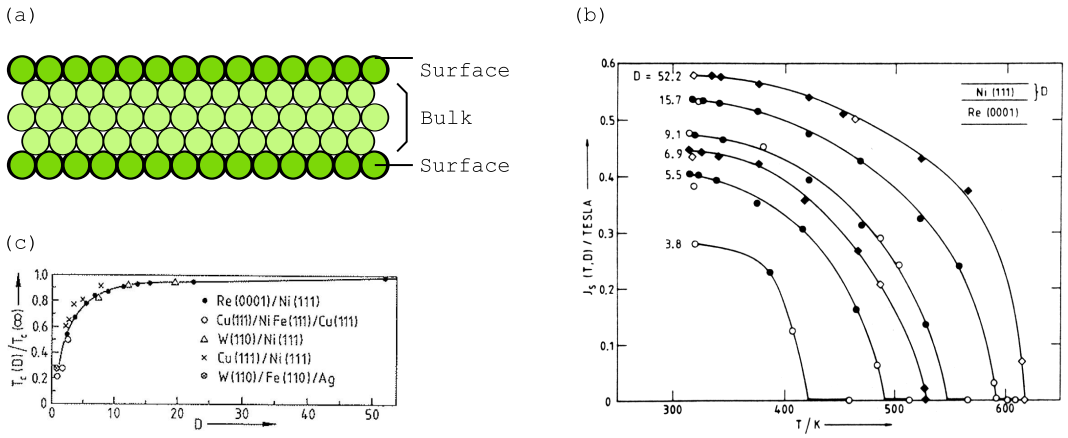

Figure II.1 – Magnetic ordering in low dimensions, here with $N = 5$ atomic layers. (a) Counting the reduced average number of nearest neighbors in a thin film with N atomic layers. Example of an experimental determination of (b) the temperature dependence of magnetization and (c) the Curie temperature in various ultrathin film materials[52].

of moment, ordering model), and so do critical exponents in both limits of $T \to 0^+$ and $T \to T_C^-$. In the low temperature range the decay is dominated by spin waves and follows a Bloch law:

$$M_s(T) = M_s(T = 0\,\mathrm{K})[1 - b_N T^{3/2}] \tag{II.4}$$

whereas mean-field theory predicts an exponentially-weak decay. b_N is the spin-wave parameters, which again happens to be thickness-dependent and well fitted with a $1/t$ law[52]. The case of a truly two-dimensional system should clearly be treated on a different footing due to the absence of out-of-plane excitations. While Onsager derived an expression for the finite Curie temperature in a 2D array of Ising spins[53], the Mermin and Wagner theorem states that long-range ordering is not expected to occur at finite temperature for a 2D array of Heisenberg spins; the divergence of susceptibility is found only for $T \to 0\,\mathrm{K}$. This problem has long excited experimentalists, with no report of absence of ferromagnetism in any experimental 2d system. The reason is that an energy gap is opened in the spin-wave spectrum as soon as magnetic anisotropy sets in, of magnetocrystalline origin[54] or even simply magnetostatic[55].

Promotion of magnetic ordering in low dimensions. Said in a hand-waving fashion, any source of anisotropy mimics Ising spins at sufficiently low temperature, going in the direction of the Onsager solution.

In one dimension thermal fluctuations have an even stronger impact, leading to absence of ordering at any finite temperature even for Ising spins. Thus the correlation length is not expected to diverge until truly zero temperature. Experimental results pertaining to such systems are available and indeed points at the existence of finite-size spin blocks[56].

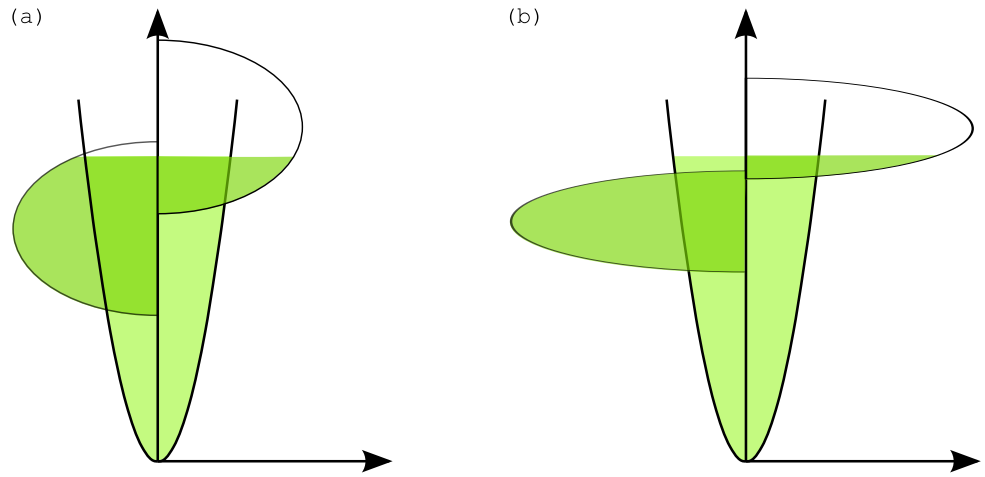

Figure II.2 – Band ferromagnetism at interfaces. Schematics of the effect of band narrowing on Stoner criterion and the magnitude of the magnetic moment.

1.2 Ground-state magnetic moment

Here we discuss the magnitude of the ground-state spontaneous magnetization at zero temperature. The case of itinerant magnetism in 3*d* metals is particularly well documented, and the general trend is physically interesting. Let us consider the case of a free-standing layer, *i.e.* with no supporting nor capping material. Due to the loss of coordination at both surfaces, 3*d* bands are expected to narrow (Figure II.2). As the total number of electrons is conserved this should help satisfying Stoner criterium $1 - I\rho(\epsilon_F) < 0$ where I is the exchange integral and $\rho(\epsilon_F)$ the density of electrons for each spin channel. This in turn should enhance the imbalance of the number of occupied states in both spin channels, and thus magnetization. This trend may be understood as moving towards free electron magnetism where Hund's rules apply and orbital momentum is not quenched, hence giving rise to a larger magnetic moment per atom. In most systems this trend is confirmed through *ab initio* calculations and observed experimentally[52]. Exceptions (reduction of moment with respect to the bulk) may be explained by phenomena whose consequences are more difficult to predict such as epitaxial or surface strain, dislocations, hybridization and charge transfer with an interfacial material, quantum-size effects.... Mainly the latter play a role in more localized magnetism, leading to effects more difficult to predict.

Thin films are easy to model and simulate thanks to translational invariance. However low-dimensional effects arise equally in other systems such as clusters. The magnetic moment per atom has been measured to be clearly enhanced in these, evidenced in-flight with Stern-Gerlach experiments or capped with sensitive techniques such as XMCD[57]. The Stoner criterium may even be fulfilled in clusters, while it is not in the bulk form. A famous case is Rhodium[58, 59].

Summary

Magnetic ordering in low dimensions. We have reviewed the basics of ferromagnetic ordering in low dimensions for itinerant magnetism. The general trend is that of two competing effects. The zero-temperature ground state displays a moment generally larger than that of the bulk, due to band narrowing. An opposite trend, which is the one of highest importance, is the enhanced *decay* of magnetization with temperature. At finite temperature both effects compete, requiring care in the analysis of measurements.

2 Magnetic anisotropy in low dimensions

We first consider magnetostatic anisotropy, long-ranged and related to the outer shape of a system. We then consider the magnetic anisotropy of microscopic origin, arising from spin-orbit and the crystal electric field. These are magnetocrystalline and magnetoelastic anisotropies, which were introduced in sec.3. We consider thin films as a model system, however those concepts apply to all low-dimensional systems, however in a more complex manner.

2.1 Dipolar anisotropy

In sec.4.3 we introduced the concept of demagnetizing factors. These were calculated on the assumption that the system under consideration is uniformly magnetized. Although this may be questionable in some cases even under applied field, in the present section we will rely on these factors for a first discussion. In this framework we have seen [Eq.(I.30)] that the dipolar contribution to magnetic anisotropy reads, after proper diagonalization defining the so-called main directions of anisotropy: $E_\mathrm{d} = K_\mathrm{d} N_i m_i^2$, and the internal so-called demagnetizing field reads $\mathbf{H}_\mathrm{d} = -N_i M_\mathrm{s} m_i \hat{\boldsymbol{\imath}}$, where i runs over all three main directions, and $N_x + N_y + N_z = 1$.

For thin films $N_x = N_y = 0$ along the two in-plane directions, resulting in zero demagnetizing field and demagnetizing energy. N_z=1, resulting in $E_\mathrm{d} = K_\mathrm{d}$ and $\mathbf{H}_\mathrm{d} = -M_\mathrm{s}\hat{\boldsymbol{z}}$ for perpendicular magnetization. The resulting demagnetizing induction $\mu_0 M_\mathrm{s}$ is of the order of one tesla for common materials (Table I.2).

In-plane magnetization for thin films. Unless the material displays a very large microscopic energy, or a very strong field is applied perpendicular to the plane, the magnetization of a thin film lies preferentially in-the-plane.

For cases other than films, however of reduced dimension in at least one direction, we will speak of nanostructures. The demagnetizing factors are all

three non-zero, and again if no microscopic energy or applied field applies, the magnetization will have a tendency to point along the direction with the lowest demagnetizing factors.

Let us add a fine point often subject to controversy, however of great importance for domains and magnetization reversal in nanostructures: the range of dipolar interactions. Dipolar interactions are commonly described as long-ranged. This is so because the stray field from a magnetic dipolar decays with distance like $1/r^3$. Thus, an upper bound for the stray field at a given location is of type $\int (1/r^3) 4\pi r^2 \mathrm{d}r$, summing over the entire system magnitudes instead of vectors. This diverges logarithmically (however converges if vectors are considered instead of magnitudes), revealing the long range of dipolar fields. More precisely, it is straightforward to show that what matters is the solid angle under which a surface density of charges is seen, not its distance. Let us now consider a flat system, for instance an element patterned out of a thin film with lithography. The upper bound becomes $\int (1/r^3) 2\pi r \mathrm{d}r$, which converges to a finite value with a radius of convergence scaling with the sample thickness. In other words:

Range of dipolar interactions. Dipolar energy is short-ranged in two dimensions. This can be understood in a hand-waving manner as most of stray fields escape in the third dimension, not contributing to the self energy $-(1/2)\mu_0 \mathbf{M}_s \cdot \mathbf{H}_d$. This implies that stray- and demagnetizing fields are often highly non-homogeneous, with important consequences on both magnetization patterns and magnetization reversal processes. For the same reason, the concept of demagnetizing factors and energy shall be used with great care in such cases.

Ellipses versus ellipsoids. Elements with two flat surfaces (made out of a thin film) and with a circular or elliptical shape are not ellipsoids. Their demagnetizing field is therefore highly non-uniform, as for all flat elements.

2.2 Projection of magnetocrystalline anisotropy due to dipolar energy

One consequence of magnetostatic energy is to favor the alignement of magnetization in directions with small demagnetizing coefficients. If magnetostatic energy prevails over magnetocrystalline anisotropy energy, the magnetization will tend to lie in certain planes or directions imposed by the former, while the latter will play a role only through its projection in these planes or directions. Let us consider the example of a cubic material; its magnetocrystalline anisotropy is described by Eq.(I.8), whose magnitude is measured through the parameter K_{1c}. If

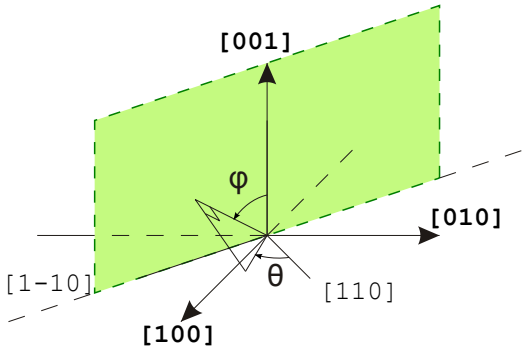

Figure II.3 – Crystal directions for the (110) **texture**. Definition of axes for a cubic crystal projected along the (110) plane.

K_{1c} is much smaller than K_d then the direction of magnetization will be imposed by the latter, for instance in-the-plane for a thin film (sec.4.3). As an example, let us consider a cubic crystal cut along a (110) plane as shown on Figure II.3, with (θ, φ) spherical coordinates. θ is measured with respect to the axis perpendicular to the plane, while φ is the in-plane angle. When restricted to $\theta = 90°$, Eq.(I.8) reads:

$$E_{mc,cub} = K_{1c} \sin^2 \varphi + (-\frac{3}{4} K_{1c} + \frac{1}{4} K_{2c} + K_{3c}) \sin^4 \varphi + \dots \quad \text{(II.5)}$$

Then, the effective anisotropy in the plane becomes uniaxial.

Symmetry and reduction of dimensionality. We illustrated a feature of symmetries with application to many fields in physics, such as bulk versus surface crystallography: considering a function defined in a space with d dimensions and displaying certains symmetries, its projection or restriction into a sub-space of dimension lower than d does not necessarily preserve or restrict the initial symmetry, even if the sub-space is an element of symmetry of the initial function.

2.3 Interface magnetic anisotropy

The local environment of atoms differs at both surfaces of a thin film with respect to the bulk one. In 1954 L. NÉEL suggested that this breaking of symmetry induced by the loss of translational invariance along the normal to the film, should result in an additional term to magnetic anisotropy. This was well before technology enabled to produce films so thin and well characterized that experiments could suggest the effect. This additional term is called surface magnetic anisotropy, or interface magnetic anisotropy, or also Néel magnetic anisotropy[II.2].

[II.2] In principle interface is appropriate to describe a thin magnetic film in contact with another material while surface is appropriate to describe a free surface (in contact with vacuum). This latter case is in principle restricted to fundamental investigations performed *in situ* in UHV, where a surface may remain free of contaminant for some time. In practice, both terms are often used

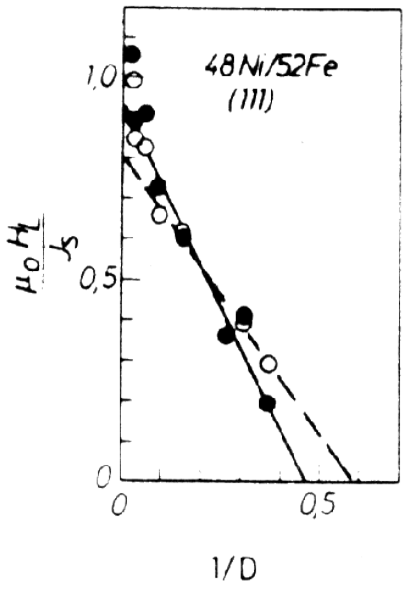

Figure II.4 – Perpendicular anisotropy. A historical example of $1/t$ plot for evaluating interfacial anisotropy[60].

As for magnetocrystalline anisotropy, interface anisotropy may favor an easy direction or an easy plane, and be decomposed in angular terms with various orders. As it applies only once per each interface, its effects becomes vanishingly small at large thickness. In practice it is observed that its effect becomes negligible beyond a few nanometers. One speaks of ultra thin films in this range smaller than characteristic length scales, where magnetization is obviously allowed to vary along the thickness. At a given lateral position its magnetization[II.3] may be described as a single vector, the so-called macrospin, on which apply both surface and bulk magnetic anisotropy. As a simple example let us assume that both terms are uniaxial along the same axis, with two identical surfaces. The resulting anisotropy then reads $K_v t + 2K_s$ with K_v and K_s the volume and surface contributions. The effective density of energy thus reads:

$$K_{\text{eff}} = K_v + \frac{2K_s}{t} \tag{II.6}$$

Following this, the usual way to estimate K_s in theory and experiments is to plot K_{eff} versus $1/t$. The intercept with the y axis should yield the bulk anisotropy, while the slope should yield K_s (Figure II.4). Interfacial anisotropies between various types of materials have thus been tabulated[52, 61] (Table II.1). K_s indeed depends on the material, may be of different sign, and is of the order of $0.1\,\text{mJ}\cdot m^{-2}$. However, consider these numbers as indications. We will indeed see in the following the complexity of the underlying physics, which induces a subtle dependence on slight variations of the material structure, interfaces, stress etc.

In its 1954 model Néel proposed the estimation of an order of magnitude for K_s values, based on the phenomenological analogy between removing the atoms to create an interface, and pulling them away infinitesimally. K_s was then linked with magneto-elastic constants of the material, with surprisingly good agreement on the order of magnitude, although the exact value and even the sign may be wrong. The so-called *pair model* of Néel aims at describing the direction and material-dependence of surface anisotropy by counting the bounds between a surface atom and the neighbors, and associate them with a uniaxial angular function.

Theory can also be used to evaluate K_s values. Letting aside *ab initio* calculations, for 3*d* metals tight binding links magnetocrystalline anisotropy with the

interchangeably

[II.3] More precisely its moment per unit area, thus expressed in amperes

Table II.1 – Tabulated indications of values of interfacial anisotropy K_s (mJ/m²)[61].

	Co	Fe	Ni
Ag	0.22 ± 0.07	0.4 ± 0.1	-0.1
Au	0.5 ± 0.1	0.6 ± 0.2	
Cu	0.15 ± 0.05	0.4 ± 0.2	-0.2 ± 0.1
Gr	0.15		
Ir	0.8		
Pd	0.5 ± 0.8	0.2 ± 0.1	0.35 ± 0.1
Ru	$-.45 \pm 0.05$		
W	-0.45 ± 0.15	-1.9	

anisotropy or the orbital magnetic moment. For a uniaxial anisotropy the energy per magnetic atom is:

$$\kappa = \alpha \frac{\xi}{4\mu_B} \Delta\mu_L. \tag{II.7}$$

ξ is the spin-orbit coupling, defined by contribution $-\xi \hat{\mathbf{S}}.\hat{\mathbf{L}}$ to the Hamiltonian. $\Delta\mu_L$ is the difference of orbital magnetic moment between hard and easy directions, and α is a factor close to unity and only weakly related with the details of the band structure.

In bulk 3*d* metals the orbital momentum is nearly fully quenched because crystal electric field energy dominates over spin-orbit, and eigen functions in a cubic symmetry should have nearly zero orbital momentum. Thus $\Delta\mu_L$ are very weak, typically of the order of $10^{-4}\,\mu_B$/atom, yielding $K \approx 10^4\,\mathrm{J/m^3}$. At both surfaces and interfaces this anisotropy is enhanced close to $0.1\,\mu_B$/atom, inducing an anisotropy of energy of the order of 1 meV per surface atom, which lies close to $1\,\mathrm{mJ/m^2}$. The link between surface magnetic anisotropy and $\Delta\mu_L$ has been checked experimentally and by *ab initio* calculations to be essentially valid. Some experiments hint at a quantitative link between bulk and surface magnetic anisotropy[62], however the universality of this link remains speculative.

The most dramatic consequence of surface magnetic anisotropy, with also of technological use, arises when K_s favors the alignement of magnetization along the normal to a thin film : $E_s = K_s \cos^2(\theta)$ with $K_s < 0$ and θ the angle between magnetization and the normal to the film. If K_{eff}, defined in Eq.(II.6), is negative and becomes greater in absolute value than K_d for a realistic critical value of thickness t_c, magnetization will point spontaneously along the normal to the film. This is perpendicular magnetic anisotropy (PMA). For a long time the most efficient interfaces to promote PMA combined 3*d* elements for the ferromagnet, and a heavy element to bring in spin-orbit. Prototypical examples are Co/Au, Co/Pt and Co/Pd. t_c is of the order of $2\,\mathrm{nm}$ or less. Recently even larger contributions to perpendicular anisotropy, and thus larger critical thicknesses (up to $3.5\,\mathrm{nm}$), have been reported at the interface between 3d metals and oxides, with the prototypical case of Co/MgO. If films thicker than this are needed with

perpendicular magnetization, a route is the fabrication of multilayers[61].

Perpendicular magnetization for technology. Perpendicular magnetization has become very important for storage applications, such as hard-disk drives (introduced in 2005 in shipped products), and the emerging solid-state magnetic random access memories (MRAM). First, it allows to define a unique direction of easy axis, unlike the case of anisotropy for planar magnetization, relying on textured materials with planar-isotropic grains, or elements of elongated shape however with an unavoidable lithography-related spread of orientation. This reduces the distribution of properties, which is crucial for the proper functioning of a device. Second, it allows to increase the strength of anisotropy, which provides the energy barrier promoting the long-term conservation of information. The latter is particularly true for shape anisotropy , which in practice cannot exceed much 10 % of M_S in planar flat elements.

2.4 Magnetoelastic anisotropy

The concept of magnetic surface anisotropy has been presented above as a textbook case. In fact it is not the single source of modification of magnetic anisotropy in ultrathin films. We review here an equally important source, magnetoelastic anisotropy.

In the bulk form strain may be obtained through stress applied by an external user. Strain is always present in thin films to some extent even at rest. This is due to the effect of the supporting material (and to some smaller extent the capping material), which having a lattice parameter and possibly symmetry different from that of the overgrown magnetic material, stresses the latter. Stress may also appear upon cooling (resp. warming up) thin films fabricated at high (resp. low) temperature. This results in a strain field in the magnetic film, generally not uniform, which gives rise to a magnetoelastic contribution to the total MAE.

Strain and stress. One should not confuse strain with stress. The former is the deformation, the latter is the force per area, related to the strain.

To first order magnetoelastic anisotropy is proportional to the matrix elements of strain. Group theory predicts the type of coupling terms[63], not their strength. In thin films there clearly exists an asymmetry between out-of-plane and in-plane directions: stress is applied in the latter, while along the former the film is free to relax. This results in a uniaxial magnetoelastic contribution.

Let us understand the qualitative effect of magnetoelasticity in thin films using a simple model. We consider the epitaxial growth of a film material (lattice parameter a_f) on a substrate (lattice parameter a_s), the latter being assumed

to be rigid. The lattice misfit is defined as $\eta = (a_f - a_s)/a_s$. During growth the deposited material will tend to relax its strain $\epsilon = (a - a_f)/a_f$ through, *e.g.*, the introduction of interfacial dislocations. We further assume that the linear energy cost per dislocation k does not depend on the density of dislocations, and that each dislocation allows the coincidence of $N+1$ atoms of the film with N substrate atoms (resp., the reverse), which corresponds to negative (resp. positive) η. Working in a continuum model, the density of mechanical energy of the system is :

$$E_{mec} = \frac{1}{2}C\epsilon^2 + \frac{k}{ta_f}|\eta + \epsilon - \epsilon^2| \tag{II.8}$$

where t is the film thickness and C an elastic constant. The equilibrium value for a is found through minimization of this equation with the constraint $|\epsilon| < |\eta|$:

- Below the critical thickness $t_c = k/(a_s C|\eta|)$ the introduction of dislocations is unfavorable, and $a = a_s$. The layer is said to be pseudomorph. As a rule of thumb, $t_c \approx 1\,\text{nm}$ for $\eta \approx 2-5\,\%$. This value is however dependent on the crystal symmetry, growth temperature and technique of deposition.
- Above t_c dislocations are created and allow to reduce strain like: $|\epsilon(t)| = k/(a_s C t)$.

What we have described so far is a structural model, proposed in 1967 by Jesser[64]. In 1989 Chappert et Bruno applied this model to magneto-elasticity[65]. They considered linear magneto-elastic terms[II.4]. As a simple case, let us assume that all deformations may be expressed in terms of ϵ, so that $E_{mel} = B\epsilon$ with B a coupling constant. Based on the structural model of Jesser we derive: $K_{mel} = kB/(a_s C t)$. Beyond the pseudomorphic regime we therefore expect a dependence of K_{mel} with $1/t$, thus exactly like for a contribution of magnetic interface anisotropy. In most cases magneto-elasticity and surface anisotropy are intermingled in thin films; it is almost impossible experimentally and conceptually to disentangle them. Nevertheless, it remains common to designate as *surface anisotropy* the total effective contribution revealed as a $1/t$ variation of the density of magnetic anisotropy.

2.4.a ANISOTROPY RESULTING FROM THE SYNTHESIS PROCESS

Following the above, it might be expected that beyond a few nanometers of thickness, the anisotropy of thin films is similar to that of bulk. While this is often the case, there are cases of persistence for large thickness of a magnetic anisotropy different from the bulk one.

A first reason is that the Jesser model considers the minimum of energy. In practice this minimum may not be reached perfectly due to the energy barriers required to create dislocations, and it is often the case that thin films retain a fraction of percent of strain. The exact value strongly depends on the couple

[II.4] It was recently shown that non-linear effects may be important in thin films[66]. This fact had not been reported in bulk materials, where plastic deformation sets in well before strain values large enough for non-linearities may be reached

of materials, the orientation of the grains, the conditions and technique of deposition.

A second reason for the persistence of deviations from bulk anisotropy is the often fine microstructure induced by the growth method. The microstructure may take the form of grains separated by grain boundaries, incorporation of foreign atoms (like Ar during sputtering growth), an anisotropic orientation of atomic bounds etc. This effect has dramatic consequences for materials with large magnetostriction such as 3d-4f compounds, which can be tailored to display perpendicular anisotropy for fairly thick films. It is also possible to tailor a uniaxial anisotropy between two in-plane directions, through deposition under an applied field like for Permalloy ($Ni_{80}Fe_{20}$), or deposition with oblique incidence or on a trenched surface. Another elegant technique to tailor the anisotropy of thin films is irradiation with ion of medium energy. This irradiation may be done during growth or post-growth. When the irradiation energy is suitably chosen, the ions may either favor the mixing of atoms or their segregation, depending on the thermodynamics trend for random alloying or phase ordering. Irradiating thin films with perpendicular anisotropy, the former leads to a decrease of anisotropy, while the latter can lead to an increase[67]. Irradiation may be combined with masks to deliver films with patterned anisotropy, however no changes in topography[68].

Summary

Magnetic anisotropy in low dimensions. Contributions to anisotropy of magnetic energy in thin films include magnetostatic, magnetocrystalline, interfacial and magnetoelastic energies. For very thin films the latter two often dominate in the nanometer range of thickness, opening the way to beating dipolar anisotropy to display perpendicular magnetization.

3 Domains and domain walls in thin films

3.1 Bloch versus Néel domain walls

In sec.5 and problem sec.5 we considered a textbook case of domain-wall: the Bloch domain wall, resulting from the competition of exchange energy against magnetocrystalline anisotropy. A translational invariance along both directions perpendicular to the domain wall was assumed, so that the problem boiled down to a unidimensional equation that can be solved.

Translational invariance makes sense in the bulk, where domain walls may extend laterally on distances much longer than their width. This hypothesis becomes questionable in thin films, where the core of a Bloch domain wall, displaying perpendicular magnetization, induces the appearance of magnetic

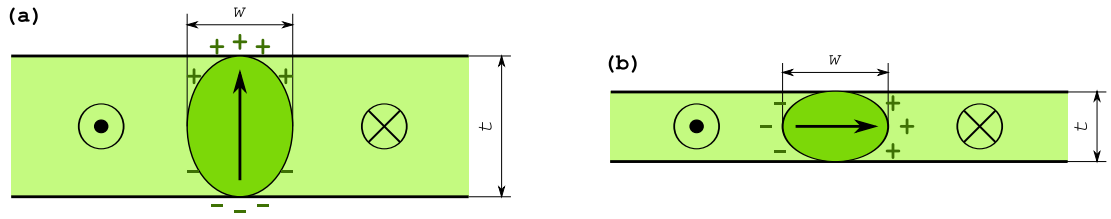

Figure II.5 – Schematics for (a) a Bloch domain wall and (b) a Néel domain wall.

charges at both surfaces of the thin film (Figure II.5a).

L. NÉEL was first in addressing this issue and providing a rule-of-thumb prediction for a cross-over in the nature of domain walls in thin films[69]. In a thin film of thickness t he considered a domain wall of bulk width $w \approx \Delta_u$, such as determined from exchange and anisotropy energies. He took into account the finite size effect along the normal to the film, modeling the domain wall as a cylinder of perpendicular magnetization with an elliptical cross-section of axes $w \times t$ (Figure II.5). For a Bloch domain wall the resulting density of magnetostatic energy is of the order of $K_d \; w/(w+t)$, based on demagnetizing coefficients (Table I.3). When $t < w$ it becomes more favorable for magnetization in the core of the domain wall to turn in-the-plane, for which the density of magnetostatic energy is $K_d \; t/(w+t)$ (Figure II.5b). This configuration where magnetization turns in-the-plane, *i.e.* perpendicular to the domain wall, is called a Néel wall.

In the above model the core of the domain wall was assumed to be rigid and uniformly magnetized. Besides, its energy was calculated crudely, and is not suitable for soft magnetic materials where magnetostatic energy dominates magnetic anisotropy so that no natural width of the domain wall exists. The phase diagram of Bloch versus Néel wall can then be refined using micromagnetic simulations. These show in the case of soft magnetic material that Néel walls become stable for thickness below $7\Delta_d$ (already below $15-20\Delta_d$ for cross-tie walls, see next paragraph)*e.g.* for $50\,\mathrm{nm}$ for Permalloy and $20\,\mathrm{nm}$ for Fe[70].

Micromagnetic simulations also revealed a phase diagram more complex than merely Bloch versus Néel walls (Figure II.6a). Going towards large thicknesses domain walls undergo a breaking of symmetry with respect to a vertical plane; they are named asymmetric Néel wall and asymmetric Bloch wall, and were first proposed in 1969 through both micromagnetic simulation[71] and an ersatz model[72]. Let us examine the detail of the asymmetric Bloch wall, of higher practical interest (Figure II.6b). Close to the surface the magnetization turns in-the-plane; this may be understood from the necessity to eliminate surface magnetic charges to decrease magnetostatic energy, or in other words to achieve a flux-closure state. The surface profile of magnetization is similar to that of a Néel wall, later motivating the name of Néel cap to designate this area of flux-closure[73]. Notice that the center of the Néel cap is displaced from the vertical of the core of the Bloch wall, explaining the name asymmetric for this domain wall. This asymmetry arises so as to reduce now volume magnetic charges, balancing $\partial m_x/\partial x$ with $\partial m_z/\partial z$ terms in the divergence of $\mathbf{M}$. Close to the transition from

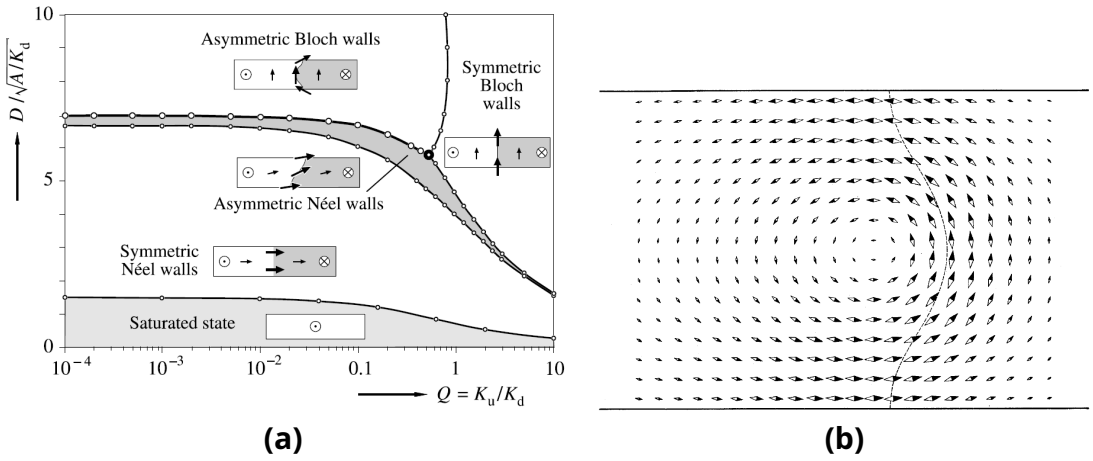

Figure II.6 – (a) **phase diagram of domain walls in thin films**, calculated for practical reasons in a strip of finite width[70]. Along the *y* axis *D* stands for *Dicke* in German, so thickness *t* here (b) one of the first success of micromagnetic simulation, predicting the existence of the asymmetric Bloch domain wall[71].

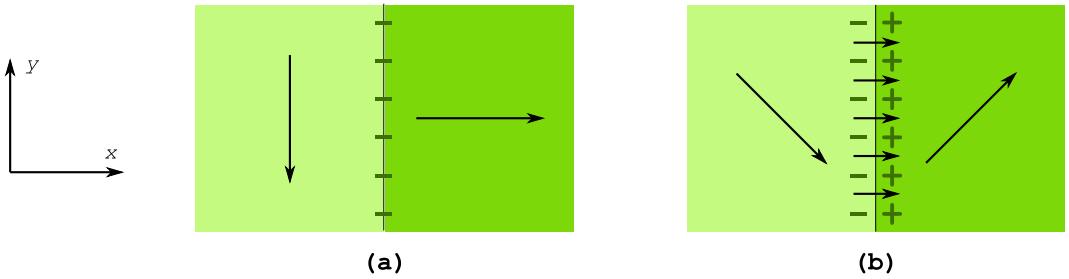

Figure II.7 – **Wall angle and magnetostatic charges**. (a) A wall that would not bisect the direction of magnetization in the neighboring domains would bear a net charge (b) A wall bisecting the magnetization directions in neighboring domains is associated with a dipolar line.

Bloch to Néel the cross-section of the asymmetric Bloch wall looks similar to a vortex, so that the name vortex wall is sometimes used.

3.2 Domain wall angle

We define as wall angle θ, the angle between the direction of magnetization in two neighboring domains. The properties of a domain wall as a function of its angle depend on parameters such as film thickness *t*, anisotropy strength and symmetry. Here we restrict the discussion to rather soft magnetic materials in rather thin films, so that most of the energy of a domain wall is of magnetostatic plus exchange origin.

The density of volume charges in an extended domain wall is $-\partial M_x/\partial x$, where *x* is the coordinate along the in-plane axis perpendicular to the domain wall (Figure II.7). Generally a wall is induced to bisect the direction of magnetization of the two neighboring domains, so that it bears no net magnetic charge and thus does not contribute significantly to magnetostatic energy through a long-range

$1/r$ decay of stray field (Figure II.7). Following Néel, we model the core of the domain wall with a cylinder of elliptical cross-section, and estimate its energy through the suitable demagnetizing coefficient.

We first consider a Néel wall. The total quantity of charge in each half of the elliptical cylinder scales with $1 - \cos(\theta/2)$, which can be replaced with $\theta^2/8$ with a reasonable accuracy even for not so small angles. As dipolar energy scales with the square of charges, and assuming that the domain wall width does not depend significantly on the wall angle, we come to the conclusion that the energy of a Néel domain wall varies like θ^4.

We now consider a Bloch wall. Volume charges can be avoided if m_x is uniform and equal to $\cos(\theta/2)$ from one domain to the other, through the domain wall. This means that, apart from the case $\theta = 180°$, the core of such a wall has both in-plane and out-of-plane components, the latter equal to $\sqrt{1 - \cos^2(\theta/2)} = \sin(\theta/2)$. Thus the magnetostatic energy of a Bloch wall scales like $\sin^2(\theta/2) \sim \theta^2$, again neglecting any change in the domain wall width, and the thickness dependence of the demagnetizing field inside de domain wall.

Wall energy versus angle. The energy of a domain wall depends on its angle θ. In thin films domain walls are of Néel type with an energy varying like θ^4, much faster than that of a Bloch wall in thicker films, varying like θ^2.

3.3 Composite domain walls

Dramatic consequences result from the convex variation of domain wall energy with angle outlined above. To set ideas, the cost per unit length of a 90° Néel wall is less than 10 % that of a 180° Néel wall. This means that a 180° Néel wall may be unstable and be replaced by walls of smaller angle, even if this implies an increase of the total length of domain wall. This is confirmed experimentally with the occurrence of composite domain walls.

One type of composite domain wall is the so-called cross-tie (Figure II.8a-b). It can be checked that each wall fulfills the rule that its direction is bisecting that of magnetization in the neighboring domains. Cross-tie domain walls occur only in soft magnetic material, because the extended domain with different orientations shall not come at the expense of an anisotropy energy. Notice also that as the energy of a Bloch wall scales like θ^2 whereas that of a Néel scales like θ^4 (see previous paragraph), 180° Bloch walls are replaced with cross-tie walls for a thickness larger than that predicted by the Néel model for the cross-over between Bloch and Néel.

Another type of composite wall is the zig-zag domain wall. Although domain walls tend to bisect the direction of neighboring domains, it may happen due to the history of application of field and nucleation of reversed domains, that two

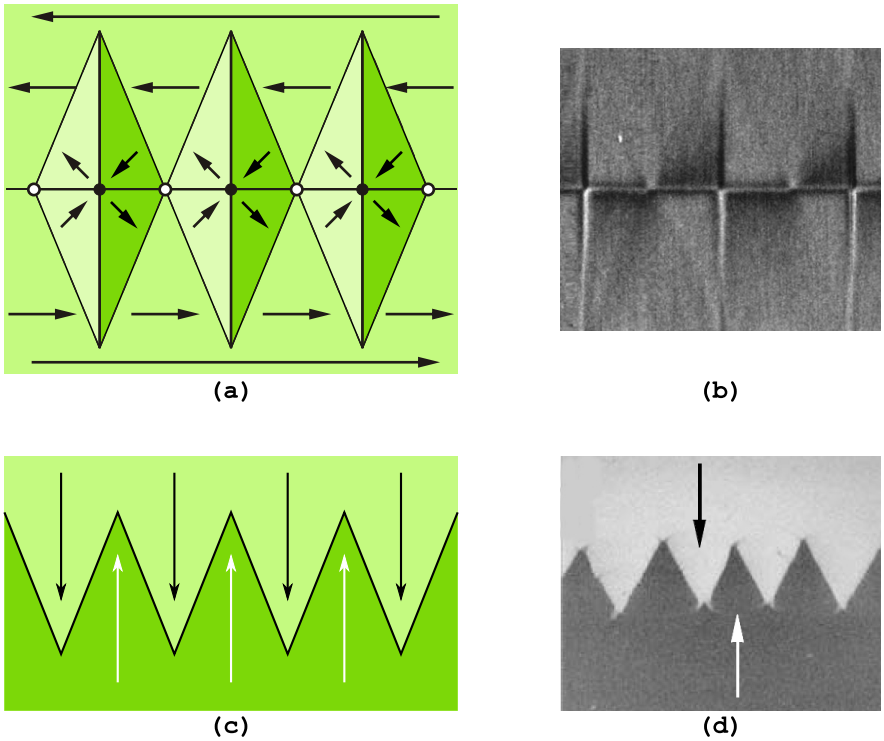

Figure II.8 – Composite domain walls in thin films. (a-b) Schematics and MFM image (13 × 15 μm)[74] of a cross-tie wall. On the schematics open and full dots stand for vortices and antivortices, respectively (c-d) schematics and Kerr image(350 × 450 μm)[6] of a zig-zag wall.

domains face each other and are each stabilized, *e.g.* by a uniaxial anisotropy or a gradient of external field with opposite signs. A 180° wall is unstable as the net magnetostatic charge carried would be M_s, the largest possible value. In this case the domain wall breaks into short segments connected in a zig-zag line (Figure II.8c-d). Along the segments of the walls have a tendency to turn 180° to be free of volume charges, implying some continuous rotation of magnetization in the dihedron formed by two consecutive segments. The angle of the zig-zag is determined by a complex balance between the reduction of magnetostatic energy due to the net charge, versus the increase of energy through the wall length, and anisotropy and exchange energy in the domains.

3.4 Vortices and antivortex

The inspection of Figure II.8a reveals the existence of loci where, from symmetry and continuity arguments, the direction of magnetization may be in no direction in the plane. These were called Bloch lines, consisting of a cylinder of perpendicular magnetization separating two Néel walls with opposite directions of in-plane magnetization. The direction of perpendicular magnetization in a Bloch line is called the polarity, and summarized by the variable $p = \pm 1$. Bloch lines also occur inside Bloch walls, separating parts of the wall core with opposite directions of perpendicular magnetization. Thus Bloch lines are the one-dimensional analo-

gous domain walls, separating two objects of dimensionality larger by one unit. In Bloch lines exchange and dipolar energy compete, yielding a diameter scaling with Δ_d, of the order of $10\,\mathrm{nm}$ in usual materials.

For the present case of in-plane magnetization, it is useful to introduce the concept of winding number defined like:

$$n = \frac{1}{2\pi} \oint \nabla\theta \cdot \mathrm{d}\boldsymbol{\ell} \tag{II.9}$$

Integration is performed along a path encircling the Bloch line, and θ is the angle between the in-plane component of magnetization and a reference in-plane direction. In short, the winding number is the total number magnetization rotates along a circular contour. Applied to the cross-tie wall, this highlights alternating Bloch lines with $n = 1$ and $n = -1$ (resp. open and full dots on Figure II.8a). A line such as the former is also called a vortex and such as the latter an anti-vortex. Notice that through the transformation of a translation-invariant Néel wall with no Bloch line into a cross-tie wall, the total winding number is thus conserved. This is a topological property, also called the topological number, which will be further discussed in the framework of nanostructures (see sec.4).

We also introduce the circulation[II.5] number:

$$c = -\frac{\hat{\boldsymbol{z}}}{2\pi} \cdot \oint (\hat{\boldsymbol{t}} \cdot \nabla)\mathbf{m} \times \mathrm{d}\boldsymbol{\ell} \tag{II.10}$$

or equally written:

$$c = \frac{1}{2\pi} \oint (\boldsymbol{\nabla} \times \mathbf{m}) \cdot \hat{\boldsymbol{z}}\, \mathrm{d}\boldsymbol{\ell} \tag{II.11}$$

where $\hat{\boldsymbol{z}}$ is the (arbitrary) normal to the plane defining the chirality and $\hat{\boldsymbol{t}}$ the unit vector tangent to the integration path. In short, in practice in the case $n = 1$ (vortices), the circulation is the sense of rotation of magnetization, either positive or negative. So, vortices may have circulation ± 1, for anticlockwise and clockwise circulation, respectively. On Figure II.8a) vortices have $c = +1$.

One also defines a so-called skymrion winding number, to characterize chiral magnetic bubbles that may occur in the presence of the Dzyaloshinskii-Moriya interaction (sec.5):

$$w = \frac{1}{4\pi} \iint \mathbf{m} \cdot \left(\frac{\partial \mathbf{m}}{\partial x} \times \frac{\partial \mathbf{m}}{\partial y} \right) \mathrm{d}x\mathrm{d}y. \tag{II.12}$$

Integration is performed over an area this time, and (x, y) are in-plane cartesian coordinate. w is also called topological charge. The absolute value of w counts how times magnetization maps all possible 4π directions in space, while its sign indicate the clockwise or anticlockwise in-plane winding around its core, like for

[II.5] Some authors use the name *chirality number*.

the winding number n. Skyrmions (see skyrmions) give rise to $w = +1$, while antiskyrmions give rise to $w = -1$. The skyrmion winding number is more suitable for magnetization textures over a surface, however with the direction of magnetization continuously mapping all three directions.

Topological numbers. The topology of micromagnetic Bloch lines is fully characterized by three numbers: polarity p, winding number n and circulation c. The product pc is also called the chirality. An antivortex has zero circulation and is therefore non-chiral, while vortices have $c = \pm 1$ depending on the direction of rotation of magnetization, either clockwise or anticlockwise.

Winding versus skyrmion winding numbers. Care should be taken to properly define which winding number is being used. Indeed, when applied to a vortex in the case of planar magnetization, one finds n=1 and w=1/2 although both are called winding numbers or topological charge.

Bloch points. There exists also a zero-dimensional object, the Bloch point, separating two parts of a Bloch line with opposite polarities. For topological (continuity) reasons, at the center of the Bloch point the magnitude of magnetization vanishes, making it a very peculiar object[75].

3.5 Films with an out-of-plane anisotropy

Here we consider thin films with a microscopic contribution to the magnetic anisotropy energy, favoring the direction perpendicular to the plane. Most depends on the quality factor $Q = K_u/K_d$ and film thickness t. For $Q < 1$ uniform in-plane magnetization is a (meta)stable state however with large energy, while uniform out-of-plane magnetization is not a (meta)stable state. For $Q > 1$ the situation is reversed. In all cases a balance between anisotropy energy and shape anisotropy needs to be found, the best compromise being through non-uniform states. The competition of all four energy terms leads to a rich phase diagram, see Ref.6 for a comprehensive theoretical and experimental review. A schematic classification with no applied field is presented below, and summarized in Table II.2.

In the case of large thickness (see table and below for numbers), in all cases the state of lowest energy is one of alternating up-and-down domains, with a period $2W$ (Figure II.9a). This pattern is called strong stripe domains. This situation was first examined by Kittel[76], and later refined by several authors.

Table II.2 – Perpendicular anisotropy. Summary of the magnetization state of films with an out-of-plane contribution to magnetic anisotropy. t and W are the film thickness and the optimum domain width, respectively.

	$Q < 1$	$Q > 1$
$t > t_c$	Weak to strong stripe domains with increasing t. $W \sim t^{1/2}$ and then $W \sim t^{2/3}$ upon branching	Strong stripe domains. $W \sim t^{1/2}$ and then $W \sim t^{2/3}$ upon branching. May be hindered by hysteresis.
t_c	Second order transition (no hysteresis in the case of purely uniaxial anisotropy) from uniform in-the-plane to weak stripes	A minimum value for W is reached.
$t < t_c$	Uniform in-plane magnetization	Perpendicular domains with diverging W, however quickly masked by hysteresis.

The alternance cancels surface charges on the average, keeping magnetostatic energy at a low level. Magnetic anisotropy is also kept at a low level as most of magnetization lies along an easy direction. The remaining costs in energy arise first from the vertical domain walls (of Bloch type with in-plane magnetization to avoid volume charges), second from flux-closure slabs close to the surface with a complex mixture of anisotropy, dipolar and wall energy. Minimization of this energy yields straightforwardly an optimum value for W scaling like $\sqrt{t}$, more precisely like $\sqrt{t\sqrt{AK_u}/K_d}$ for $Q \gtrsim 1$ (Figure II.9a) and like $\sqrt{t\sqrt{A/K_u}}$ for $Q \lesssim 1$ (Figure II.9b). At quite large thicknesses[6], typically hundreds of nanometers or micrometers, this law is modified due to branching of domains close to the surface (Figure II.9c). Branching decreases the energy of closure domains, while saving wall energy in the bulk of the film. We then have $W \sim t^{2/3}$.

For decreasing thickness we shall consider separately two cases. For $Q > 1$ there exists a critical minimum domain width $W_c \approx 15\sqrt{AK_u}/K_d$, which is reached for $t_c \approx W_c/2$. Below this thickness flux-closure between neighboring domains becomes largely ineffective due to the flat shape of the domains, thereby leading to a sharp increase of W, with ultimately a divergence for $t \to 0$ (Figure II.9d). For $Q < 1$ the magnetization in the domains progressively turns in-the-plane, with a second-order transition towards a uniform in-plane magnetization around $t = 2\pi\Delta_u$. This pattern is called weak stripe domains due to the low angle modulation of direction of magnetization in neighboring domains. Close to the transition the situation is very simple to describe: the deviations from uniformity are sinusoidal in space to first order, and one finds $W \approx t$.

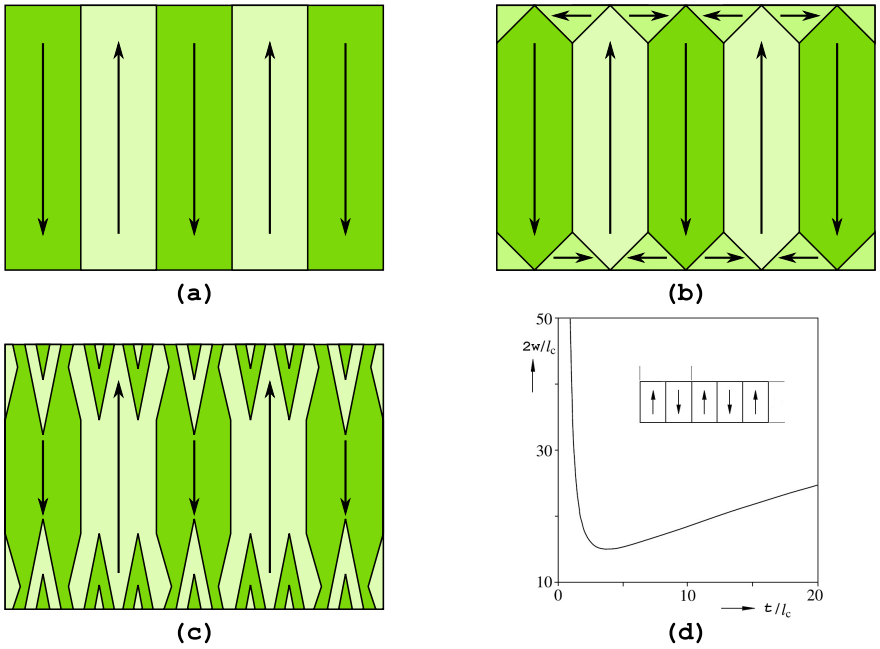

Figure II.9 – Stripe domains. Sketches of cross-sections of films with perpendicular magnetization, for (a) open domains (initial Kittel's model), (b) perfect flux-closure domains and (c) domain branching. (d) predicted width of domain W with film thickness t, from ref.6. On the latter figure, on the y axis $l_c = 2\sqrt{AK_u}/K_d$.

Hysteresis and stripe domains. In the above, notice that the state with lowest energy may not be reached for $Q > 1$, as the uniform state perpendicular to the plane is (meta)stable. Thus strong stripe domains may not occur even at large thickness, for very coercive materials. Below t_c the energy gain resulting from the creation of domains is very weak, so that the divergence of W is often hidden again behind coercive effects.

Summary

Domains and domain walls in thin films. The features of domain walls are different in thin films, compared to the bulk. This is mostly related to the need to reduce dipolar energy, arising because of the loss of translational invariance along the normal to the film. The thickness of the film has a strong impact, and often approximations are required to describe the physics analytically.

4 Domains and domain walls in nanostructures

In this section we examine the effect of reducing the lateral dimensions of nanostructures, from large to small nanostructures. We consider first the domains, followed by special cases of domain walls.

4.1 Domains in nanostructures with in-plane magnetization

We consider a piece of a thin film of soft magnetic material, quite extended however of finite lateral dimensions. Under zero applied field these assumptions allow us to describe the arrangement of magnetization as an in-plane vector field **m** of norm unity, and neglect the energy inside and between domain walls. Under these conditions Van den Berg proposed a geometrical construction to exhibit a magnetization distribution with zero dipolar energy[77, 78]. As dipolar energy is necessary zero or positive, this distribution is a ground state.

Zero dipolar energy can be achieved by canceling magnetic charges. Absence of surface charges $\mathbf{M} \cdot \hat{\boldsymbol{n}}$ requires that magnetization remains parallel to the edge of the nanostructure (Figure II.10); this is a boundary condition. At any point P at the border, let us consider the cartesian coordinates (x, y) with $\hat{\boldsymbol{x}}$ and $\hat{\boldsymbol{y}}$ respectively tangent and inward normal to the boundary. The density of volume charges reads $\partial m_x/\partial x + \partial m_y/\partial y$. As **m** lies along $\hat{\boldsymbol{x}}$, $\partial m_x/\partial x = 0$. Thus cancelation of volume charges is achieved if $\partial m_y/\partial y = 0$; this is the differential equation to be solved. As $m_y = 0$ at the boundary, absence of volume charges is fulfilled by keeping **m** normal to the radius originating from P.

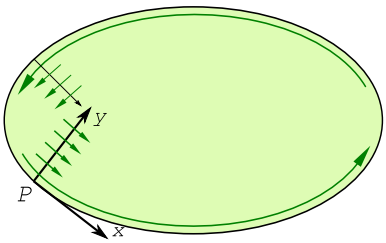

Figure II.10 – The theory of flux-closure patterns. The principle for building a magnetizaiton configuration free of dipolar fields.

Radii originating from different points at the boundary may intersect, each propagating inwards magnetization with a different direction, in which case highlighting the locus of a domain wall. It can be demonstrated that domain walls in the nanostructure are at the loci of the centers of all circles inscribed inside the boundary at two or more points. This geometrical construction satisfies that any domain wall is bisecting the direction of magnetization in the neighboring domains, a requirement pointed out in sec.3.2. Figure II.11a-b shows examples of the Van den Berg's construction. A mechanical analogy of this construction is sand piles, where lines of equal height stand for flux lines.

Higher-order Van den Berg constructions. Divide a nanostructure in two or more parts, apply the construction to each of them before bringing all parts back together: a higher order ground state is found with zero dipolar energy. An infinity of such states exists. In experiments such states may be prepared through special (de)magnetization procedures. High order states may also not be stable in a real sample, because the wall width and energy neglected in the model will become prohibitively large. Notice also that the construction may still be used in the case of a weak in-plane magnetic anisotropy in the sample, however suitably dividing the sample into several parts with lines parallel to the easy axis of magnetization (Figure II.11)c.

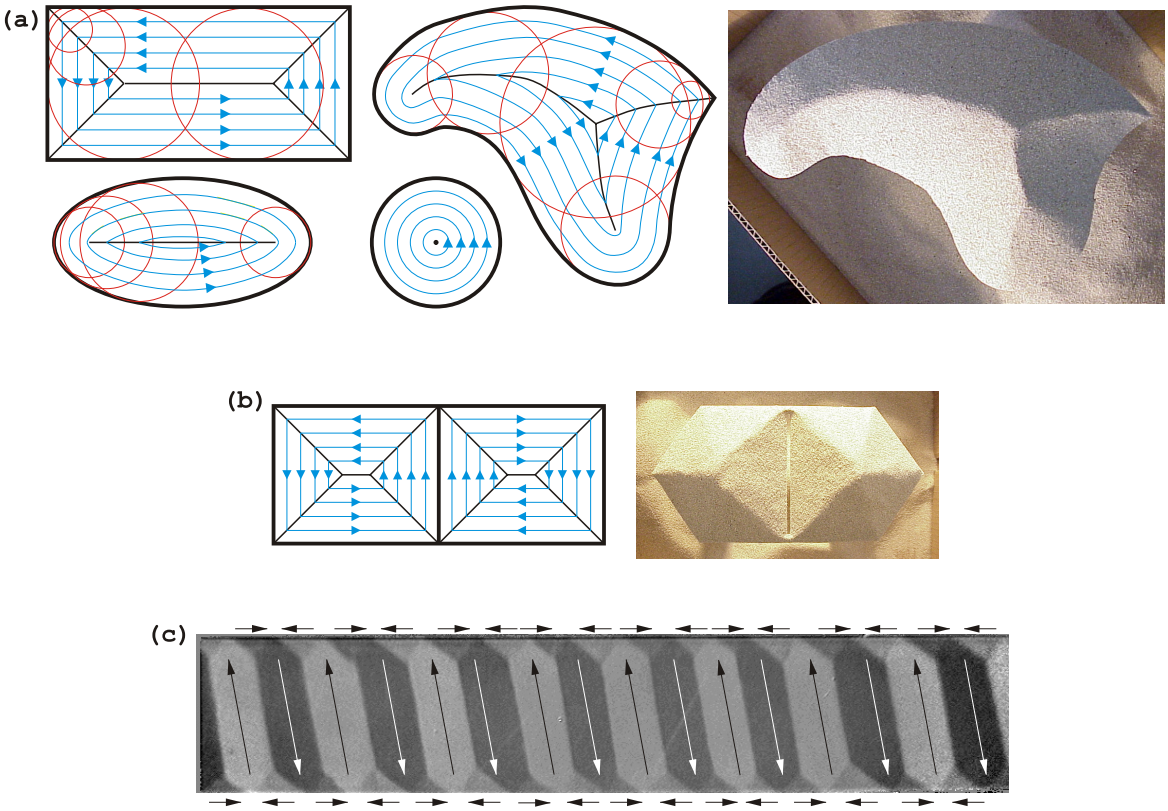

Figure II.11 – Examples of the geometrical construction of Van den Berg. (a) first order construction, along with a sand pile analogue (b) higher-order construction, along with a sand pile analogue (c) Kerr microscopy of an experimental realization of a high order pattern from a strip with an in-plane axis of anisotropy (sample courtesy: B. Viala, CEA-LETI).

4.2 Domains in nanostructures with out-of-plane magnetization

Although to a lesser extent than for in-plane magnetization, domains of perpendicularly-magnetized material are influenced by lateral finite-size effects. This is obviously the case for weak-stripe domains, as a significant part of magnetization lies in-the-plane, calling for effects similar to those highlighted in the previous paragraph. Strong stripe domains may also be influenced in a flat nanostructure. Two arguments may be put forward: the local demagnetizing field is smaller close to an edge, with respect to the core of a nanostructure; this would favor uniform magnetization close to an edge, and thus local alignement of the stripes along this edge. Another argument is that a stripe with opposite magnetization is 'missing' beyond the border, removing a stabilizing effect on the stripe at the border; this would call for orienting stripes perpendicular to the border to better compensate surface charges. It seems that in some experiments the stripes display a tendency to align either parallel or perpendicular to the

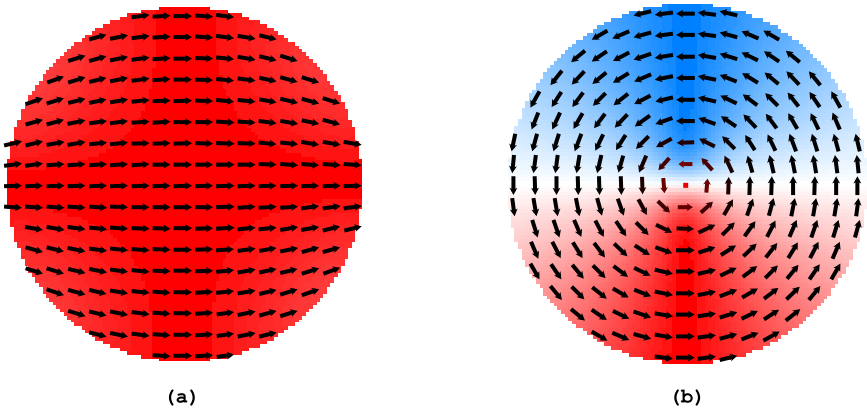

Figure II.12 – The vortex state. Magnetization states of a disk of permalloy with diameter $100\,\mathrm{nm}$ and thickness $10\,\mathrm{nm}$. The background color codes the y component of magnetization. Arrows stand for the magnetization vector. (a) near single-domain and (b) vortex states. These (and later) simulations were done using the freeware OOMMF[81, 82].

border, in the same sample[79]. For thick films it seems that alignement of the stripes parallel to the border is favored[80].

4.3 The critical single-domain size

In the above we considered domains in large samples. We now examine down to which size domains may be expected in nanostructures, called the critical single-domain size.

Let us consider a rather compact nanostructure, *i.e.* with all three demagnetizing coefficient N close to $1/3$, and lateral size ℓ. If uniformly magnetized, its total energy is $\mathcal{E}_{SD} = NK_d\,\ell^3$. We now have to discuss separately the cases of hard versus soft magnetic materials.

In hard magnetic materials domain walls are narrow and with an areal energy density γ_W determined from materials properties. If split in two domains to close its magnetic flux, the energy of such a nanostructure is $\mathcal{E}_D \approx \epsilon_d NK_d\ell^3 + \gamma_W\ell^2$ with ϵ_D expressing the residual dipolar energy remaining despite the flux closure. $\gamma_W = 4\sqrt{AK_u}$ in the case of uniaxial anisotropy. Equating $\mathcal{E}_{SD}$ and $\mathcal{E}_D$ yields the critical single-domain size $\ell_{SD} = \gamma_W/[N(1-\epsilon_d)K_d]$ below which the single-domain state is expected, while above which splitting into two or more domains is expected. $\ell_{SD} \approx \gamma_W/NK_d \approx \sqrt{AK_u}/K_d$. ℓ_{SD} is of the order of one hundred nanometers for permanent magnet materials.

In soft magnetic materials a flux-closure state often takes the form of a collective magnetization distribution, implying a gradual rotation of magnetization as seen in Van den Berg's constructions (sec.4.1). The relevant quantities are then exchange and dipolar energy, so that the critical single-domain size is expected to scale with the dipolar exchange length Δ_d. Numerical simulation provides the numerical factor, $\ell_{SD} \approx 7\Delta_d$ for cubes and $\ell_{SD} \approx 4\Delta_d$ for spheres[6, p.156].

Estimating the critical single domain dimensions for non-compact nanostructures (*i.e.* with lengths quite different along the three directions) requires specific models. An important case is the transition from single-domain to the vortex state in a disk of diameter w and thickness t (Figure II.12). $\mathcal{E}_{SD} \approx NK_d tw^2$ with $N \approx t/w$ the in-plane demagnetizing coefficient. As a crude estimate the (lower bound for the) energy $\mathcal{E}_D$ of the flux-closure state is the exchange plus dipolar energy of the core, around $10\Delta_d^2 tK_d$. Equating both we find the scaling law $wt \approx 10\Delta_d^2$ for the critical dimensions. Numerical simulation provides an excellent agreement with the scaling law, however refines the numerics: $wt \approx 20\Delta_d^2$[83].

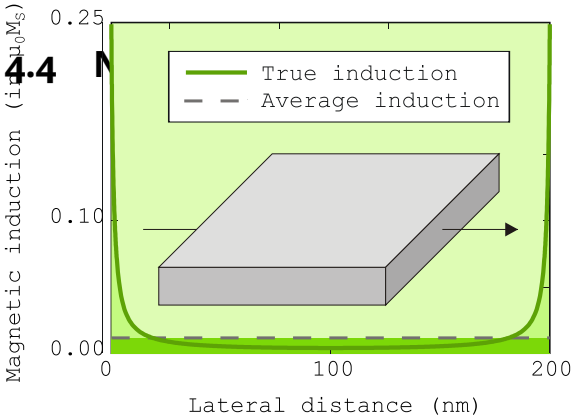

Figure II.13 – Illustration of the short range of interactions in 2D. Demagnetizing field in a strip magnetized uniformly across the width, of width 200 nm and thickness 2.5 nm

4.4 N

In the previous paragraph we discussed the scaling laws for dimensions, below which a nanostructure does not display domains. Here we notice that such nanostructures are often not perfectly uniformly-magnetized. We discuss the origins and the consequences of this effect.

When deriving the theory of demagnetization coefficients in sec.4.3, we noticed that the self-consistence of the hypothesis of uniform magnetization may be satisfied only in the case of homogenous internal field. In turn, this may be achieved only in ellipsoids, infinite cylinders with elliptical cross-section, and slabs with infinite lateral dimensions. Many samples do not display such shapes, in particular flat structures made by combining deposition and lithography. Figure II.13 shows the demagnetizing field in a flat strip assumed magnetized uniformly across its width. The field is highly non-homogeneous: it is very intense close to the edges, mathematically going towards $M_s/2$; and very weak in the center, below its average value $-NM_s$[II.6]. This is a practical example of the statement found in sec.2.1, about the short range of dipolar fields for a two-dimensional nanostructure.

Due to the high value of demagnetizing field close to the edges, magnetization undergoes a strong torque and the system cannot remain uniformly magnetized, at least in the absence of an external field. The resulting areas are called end domains, with a tendency of magnetization to turn parallel to the edge to reduce edges charges and instead spread them in the volume. Although no real domains develop, this is a reminiscence of the Van den Berg construction. In the case of elongated elements, so-called 'S' and 'C' states arise, named after the shape

[II.6] The analytical derivation of which is proposed in problem sec.3.

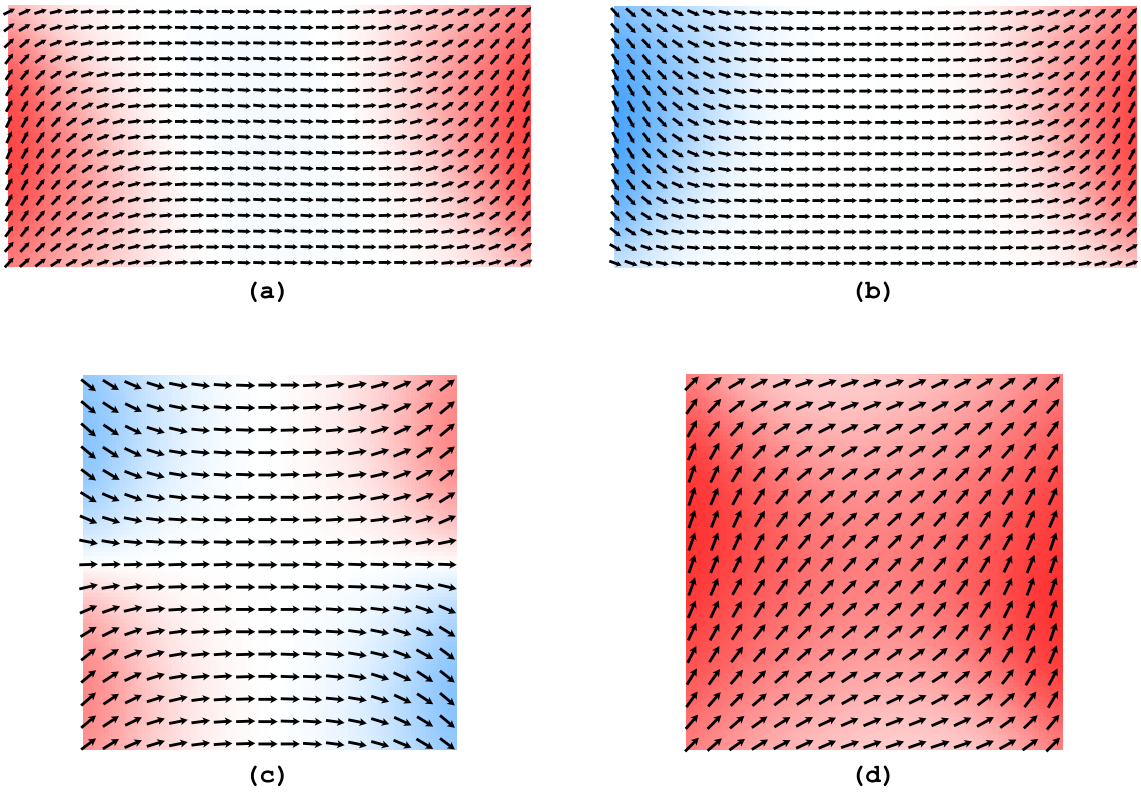

Figure II.14 – Near-single-domain states in rectangles of dimensions $2\,00 \times 10010$ nm and squares of dimensions $1\,00 \times 10010$ nm. (a) S state (b) C state (c) flower state (d) leaf state.

of the flux lines, and reflecting the almost independence of end domain when sufficiently apart one from another (Figure II.14a-b).

Non-uniform magnetization configurations may persist down to very small size, especially close to corners where demagnetizing fields diverge in the mathematical limit[84, 85]. This leads to the phenomenon of configurational anisotropy, described both analytically and computationnally[86–88]: certain directions for the average moment have an energy lower than others, arising from the orientation-dependent decrease of dipolar energy (at the expense of exchange) made possible by the non-uniformity of magnetization. This effect adds up to the quadratic demagnetizing tensor, and may display symmetries forbidden by the latter, in relation with the shape of the element: order 3, 4, 5 etc (Figure II.14c-d).

4.5 Domain walls in strips and wires

We consider nanostructures elongated in one direction, which we will call wires when the sample dimensions are similar along the other two directions, and strips when one of them is much smaller than the other. The latter is the case for most samples made by lithography, while the former is the case for samples made *e.g.* by electrodeposition in cylindrical pores[89]. We restrict the discussion

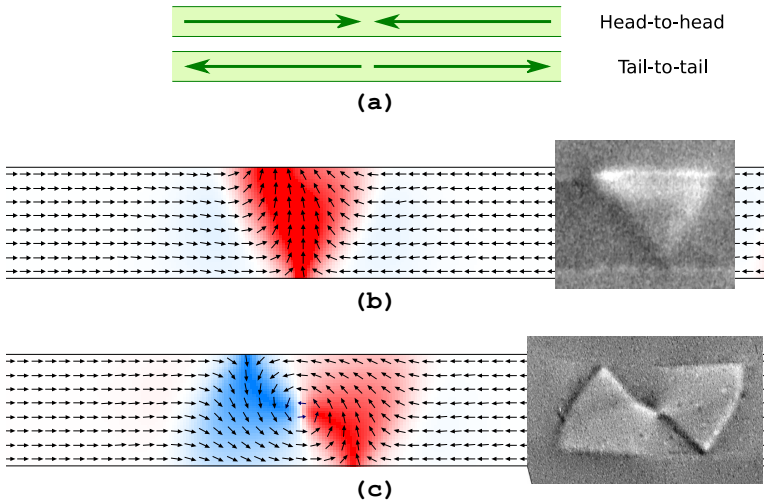

Figure II.15 – Head-to-head domain walls in strips. (a) Schematic of head-to-head and tail-to-tail walls. (b) simulated and MFM transverse wall (c) simulated and MFM vortex wall. (top views).

to those strips and wires where no magnetocrystalline anisotropy is present, so that shape anisotropy forces magnetization to lie along the axis. Domain walls may be found in long objects, called head-to-head or tail-to-tail depending on the orientation of magnetization in the two segments (Figure II.15a).

Micromagnetic simulation predicts the existence of two main types of domain walls for strips: either the vortex wall (VW) or the transverse wall (TW) (Figure II.15b-c). The lowest energy is for the latter for $tw < 61\Delta_d^2$, while the vortex domain wall prevails at large thickness or width. Although this scaling law is similar to that of the single-domain-versus-vortex phase diagram for disks however with a larger coefficient (sec.4.3), its origin is slightly different. It was indeed noticed that most of the energy in both the VW and TW are of dipolar origin[90], resulting from charges of the head-to-head or tail-to-tail. These charges are spread over the entire volume of the domain wall. Using integration of H_d^2 over space to estimate dipolar energy, and noticing that the surface of the TW is roughly twice as large as that of the VW and the decay with height of H_d is roughly w, the tw scaling law is again derived. Although both transverse and vortex domain walls are observed experimentally (Figure II.15b-c), the range of metastability is large so that it is not possible to derive an experimental energetic phase diagram. TW may for instance be prepared far in the metastability area through preparation with a magnetic field transverse to the strip. For the largest thickness and especially width TW turn asymmetric (ATW) through a second-order transition.

Summary

Domains and domain walls in nanostructures. The ground state of large nanostructure may involve domain walls to achieve a non-uniform distribution of magnetization, so as to decrease dipolar energy. This takes the form of flux-closure

domains described by the van den Berg construction for in-plane magnetization, and stripes and bubbles for out-of-plane magnetization. When the system size is decreased these are not more favorable, and the ground state is an essentially-uniform-magnetized state. Domain walls may exist in strips, with an inner structure dependent on the material parameters and geometry of the strip cross-section.

5 An overview of characteristic quantities

In the course of this chapter we met many characteristic quantities: lengths, energies, dimensionless ratios etc. Here we make a short summary of them.

5.1 Energy scales

- $K_d = (1/2)\mu_0 M_s^2$ is called the dipolar constant. It is a measure of the maximum density of dipolar energy that can arise in a volume, *i.e.* for demagnetizing coefficient $N = 1$.
- $4\sqrt{AK_u}$ is the energy of a Bloch wall per unit area.

5.2 Length scales

- **Exchange and anisotropy**. In a situation where only magnetic exchange and anisotropy compete, the two relevant quantities in energy are A and K_u, expressed respectively in J/m and J/m^3. The typical case is that of a Bloch domain wall (sec.5). The resulting length scale is $\Delta_u = \sqrt{A/K_u}$. We call Δ_u the anisotropy exchange length[12] or Bloch parameter, a name often found in the literature. The latter is more often used, however the former makes more sense, see the note below. Notice that Δ_u is sometimes called the Bloch wall width, which however brings some confusion as several definitions may be used for this, see sec.5.
- **Exchange and dipolar**. When exchange and dipolar energy compete, the two quantities at play are A and K_d. This is the case in the vortex core (sec.3.4). The resulting length scale is $\Delta_d = \sqrt{A/K_d} = \sqrt{2A/\mu_0 M_s^2}$, which we call dipolar exchange length[6] or exchange length as more often found in the literature, see again the note below.
- **Exchange, anisotropy and dipolar**. $\ell_{SD} \approx \sqrt{AK_u}/K_d$ is the critical domain size of a compact nanostructure made of a quite hard magnetic material. It emerges out of the comparison of two energies, one per unit volume, the other one per unit surface. It is relevant in other situations, such as hard stripe domains for films with perpendicular magnetocrystalline anisotropy. Notice that ℓ_{SD} may be written $\Delta_d\sqrt{Q}$ or $\Delta_u Q$.
- **Other cases**. In more complex situations other length scales may arise, taking into account an applied magnetic field, dimensionless quantities

such as the ratio of geometric features etc. For example the pinning of a domain wall on a defect gives rise to the length scale $\sqrt{A/\mu_0 M_s H}$ for a soft magnetic material, or $\sqrt{2A/\sqrt{K_u \mu_0 M_s H}}$ for a material with significant magnetic anisotropy.

Exchange lengths. The name exchange length has historical grounds however is not well suited. Indeed exchange plays an equal role in both Δ_u and Δ_d. It is more relevant to name Δ_u the anisotropy exchange length, and Δ_d the dipolar exchange length. We use the subscripts u (for uniaxial) and d (for dipolar) to account for this, as suggested in Hubert's book[6]. It would also be consistent to call $\Delta_H = \sqrt{A/\mu_0 M_s H}$ the field exchange length.

5.3 Dimensionless ratios

- A quantity of interest in the quality factor $Q = K_u/K_d$, which describes the competition between uniaxial anisotropy and dipolar energy. Q largely determines the occurrence and type of domains in thin films with an out-of-plane magnetocrystalline anisotropy.

Summary

An overview of characteristic quantities. The distribution of magnetization often results from the balance of the various energies involved in a system. Dimensional analysis can be used to show that characteristic quantities emerge out of this competition: length, energy, dimensionless ratios. Consideration of these quantities allow to predict qualitatively the behavior in a given situation, and its scaling law with material parameters and system dimensions, without having to perform any calculation.

Problems for Chapter II

Problem 1: Self-testing

1. How does the ordering temperature vary with the thickness t of an ultrathin film?
2. Why is the magnetic moment per atom changed at the surface of a magnetic film?
3. What can you say about the direction of magnetization for a thin film made of a soft magnetic material
4. Describe what a Bloch wall and a Néel wall are, and when one or the other occurs.
5. What is a cross-tie wall? In which case and why does it occurs?
6. What is the critical single-domain size? What is the order of magnitude of this length for a sphere made of a soft magnetic material?
7. Describe the principle and hypothesis of the geometrical van den Berg construction.
8. Comment on the range of magnetostatic interactions in a bulk magnetic material, and in a thin film.

Problem 2: Short questions

1. Consider a cubic material with first-order magnetocrystalline anisotropy constant $K_{1,\mathrm{cub}}$ much weaker than K_d, in the form of a thin film with surface normal (001).
   - Express the resulting in-plane magnetic anisotropy $E(\theta)$ with θ the in-plane angle of magnetization with an easy axis, assuming that magnetization lies purely in-the-plane. Comment.
   - Find exactly the easy directions of magnetization.

   For both items consider both cases of positive and negative $K_{1,\mathrm{cub}}$, and comment.

2. Explain shortly what is in general the trend for the Curie temperature and magnetic anisotropy in ultra-thin films.
3. Figure II.16 displays the top view of flat elements made of a soft ferromagnetic material, with a lateral size very large compared to any magnetic length scale. Explain shortly the physical reasons and the resulting rules allowing one to predict the distribution of magnetization in such elements. For each of the elements, sketch the local direction of magnetization, and possibly the locus of domain walls.

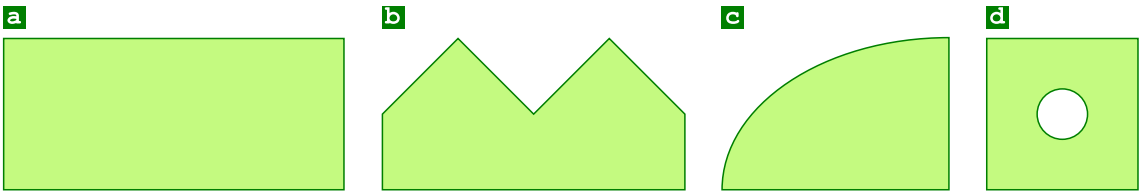

Figure II.16 – Distributions of magnetization

4. Draw a sketch of the expected contrast in the magnetic microscopy of domain walls. Consider four types of domain walls: perpendicular anisotropy with Bloch wall; in-plane anisotropy with Bloch wall and Néel caps, 180° Néel wall and 90° Néel wall. Consider four techniques: XMCD-PEEM, Lorentz, MFM, polar Kerr. The sketches may be presented as an array for clarity.
5. Explain why a Bloch wall with Néel caps in a film with perpendicular magnetization has only one internal degree of freedom, whereas Bloch walls in films with in-plane magnetization have two.
6. Derive with simple arguments the scaling law $W \sim t^{1/2}$ for the period of strong stripe domains (p.80). This may be done in the limit $W \ll t$ with suitable approximations to estimate the order of magnitude of the magnetostatic and domain wall energies involved for one period W of the pattern, and minimizing the proper quantity considering W as a variational parameter.
7. The Co layer displayed in Figure I.11b has in-plane magnetization, with an in-plane easy axis of magnetization. Sketch its direction based on the observation of the domain walls. Comment on the type of these domain walls.

Problem 3: Demagnetizing field in a strip

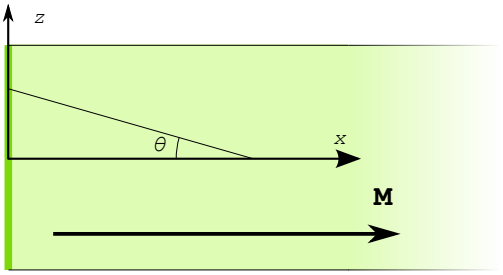

Figure II.17 – Geometry. The left side of the strip considered. The edge hold-

Here we derive the analytical formula for the in-plane demagnetizing field in a flat and infinitely-long strip magnetized in-the-plane, a case that was shortly dis-

cussed in sec.4.4. We call t and w its thickness and width, respectively. We assume magnetization to be homogeneous and along the transverse direction.

3.1. Deriving the field

Express the stray field H_d arising from a line holding the magnetic charge per unit length λ. As a first step, we consider only $H_{d,x}(x)$, the x component of the demagnetizing field calculated at mid-height of the strip, arising from the charges on one of its edges. Write an integral form for this function. Show that it reads, upon integration:

$$H_{d,x}(x) = \frac{M_s}{2}\left[1 - \frac{2}{\pi}\arctan\left(\frac{2x}{t}\right)\right] \tag{II.13}$$

3.2. Numerical evaluation and plotting

Derive the limits and first derivative for Eq.(II.13) for $x \to 0$ and $x \to \infty$, and comment. Provide a hand-drawn qualitative plot of this function. Without performing more calculation, discuss how it compares in magnitude with the z average over the thickness, *i.e.* $\langle H_{d,x,z}\rangle(x)$? What is the (x,z) average of the latter over the entire cross-section of the strip?

Problem 4: Three-dimensional micromagnetics: a magnetic nanotube

In this problem we consider some aspects of micromagnetics in the 3D space, with issues of curvature and topology. We illustrate this with a nanotube with length L (along z), inner radius ρ_1 and outer radius ρ_2. We describe magnetization with cylindrical coordinates (Figure II.18). In cylindrical coordinates, the volume density of exchange energy reads:

$$E_{ex} = A\left[\left(\frac{\partial m_\rho}{\partial z}\right)^2 + \left(\frac{\partial m_\theta}{\partial z}\right)^2 + \left(\frac{\partial m_z}{\partial z}\right)^2 + \left(\frac{\partial m_\rho}{\partial \rho}\right)^2 + \left(\frac{\partial m_\theta}{\partial \rho}\right)^2 + \left(\frac{\partial m_z}{\partial \rho}\right)^2 + \frac{1}{\rho^2}\left(m_\theta^2 + m_\rho^2\right)\right] \tag{II.14}$$

4.1. Uniform magnetization

As a first approximation, we consider that magnetization is uniform in the tube, *i.e.* m_x, m_y and m_z are uniform.

- For $L = \infty$, give the demagnetizing coefficients of the tube along x, y, z. Describe the state of lowest energy.
- Describe the state (or states) of lowest energy for $\rho_2 = 2\rho_1$ and $L \ll \rho_1$.

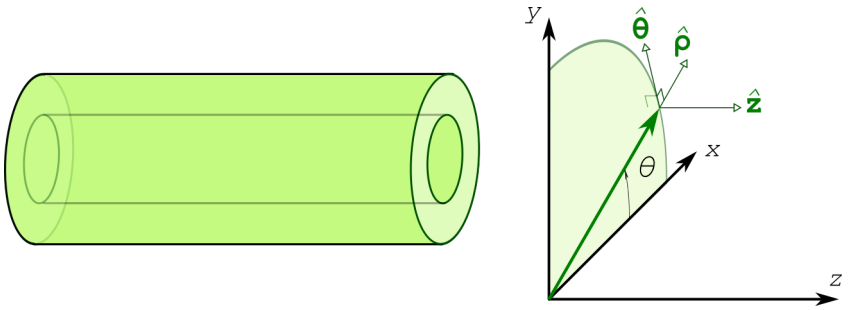

Figure II.18 – Magnetic nanotube described with cylindrical coordinates

4.2. Cylindrical symmetry

We now consider situations with, simultaneously, a cylindrical and translational symmetry for magnetization, meaning that m_ρ, m_θ and m_z are uniform. We name radial, azimuthal and longitudinal the directions along $\hat{\boldsymbol{\rho}}$, $\hat{\boldsymbol{\theta}}$ and $\hat{\boldsymbol{z}}$.

- Draw a sketch of magnetization for each of these situations: $m_\rho \equiv 1$; $m_\theta \equiv 1$ and $m_z \equiv 1$.
- Write Eq.(II.14) in the present case, and discuss the formula. What is the reason of the remaining terms in the equation? Calculate the exchange energy $\mathcal{E}_{\text{ex}}$ per unit length of the tube in the three cases. Using a linear expansion, propose a simplified expression in the case of thin-walled tubes, *i.e.* for $\Delta\rho = \rho_2 - \rho_1 \ll \rho_2$. Discuss what are the states of highest and lowest energy in the case of a soft magnetic material, within the cases: $m_\rho \equiv 1$, $m_\theta \equiv 1$ and $m_z \equiv 1$.
- Let us now consider a material with magnetocrystalline anisotropy with volume density $E_{\text{mc}} = -Km_\theta^2$, with $K > 0$. If E_{mc} only is considered, describe the state of lowest energy. Calculate the magnetocrystalline energy $\mathcal{E}_{\text{mc}}$ per unit length of the tube. When both E_{ex} and E_{mc} are considered and thus $\mathcal{E}_{\text{ex}}$ and $\mathcal{E}_{\text{mc}}$ compete, discuss the state of lowest energy. We will restrict the discussion to the case of thin-walled tubes. Discuss the specific length arising from this competition. If the case where azimuthal magnetization is favored, discuss what happens in the limit of a magnetic wire ($\rho_1 \to 0$).

4.3. Domain walls

We consider a domain wall centered at $z = 0$, separating two semi-infinite domains extending towards $-\infty$ and $+\infty$, respectively. We restrict the cas to cylindrical symmetry, and consider a thin-walled tube with radius ρ and thickness $t = \rho_2 - \rho_1$. We will make an analogy between the nanotube and a thin film, or more precisely a strip of width $2\pi\rho$ and thickness t, which would be obtained by unrolling the tube.

4.3.a. LONGITUDINAL MAGNETIZATION

We assume that $m_z \equiv \pm 1$ are the ground state domains. In analogy with a

strip, how would you name a domain wall between the two domains? Make an unrolled sketch of the domain walls which may arise.

This system is subject to a longitudinal magnetic field **H**, *i.e.* applied along $\hat{z}$. With your knowledge of the domain wall dynamics in a strip, describe qualitatively what is expected for the wall velocity as a function of strength of the applied field.

4.3.B. AZIMUTHAL MAGNETIZATION

We assume that $m_\theta \equiv \pm 1$ are the ground state domains. In analogy with a thin film, what are the two kinds of domain walls that may arise? Make an unrolled sketch. Can you move such domain walls with an external magnetic field? Now, consider that the ferromagnetic tube surrounds a non-magnetic metallic core. What is the consequence of passing an electric current through and metallic core?

4.3.C. RADIAL MAGNETIZATION

We assume that $m_\rho \equiv \pm 1$ are the ground state domains. Such a state was not predicted in sec.5.3. In analogy with a thin film, how would you name such domains? Discuss how you could think of favoring this orientation of magnetization, based on your knowledge of magnetic material science. What are the two kinds of domain walls that may arise? Make an unrolled sketch.

Problem 5: The Dzyaloshinskii-Moriya interaction and chiral magnetic structures

In this problem we consider the consequences of a peculiar exchange interaction, the Dzyaloshinskii-Moriya interaction (DMI), occurring only at atomic sites lacking space inversion symmetry. This may occur either in bulk materials with a suitable lattice structure, or at the interface between two materials.

5.1. Defining and handling the Dzyaloshinskii-Moriya interaction

The DMI interaction may be expressed the following way, for one bound (Figure II.19):

$$\epsilon_{\mathrm{DMI}} = -\mathbf{d}_{ij} \cdot (\hat{\boldsymbol{S}}_i \times \hat{\boldsymbol{S}}_j) \tag{II.15}$$

In this equation $\hat{\boldsymbol{S}}_i$ and $\hat{\boldsymbol{S}}_j$ are unit vectors standing for atomic moments at sites i and j, ϵ_{DMI} is expressed in Joules, and $\mathbf{d}_{ij}$ is called the DMI vector. This vector is specific to the bound considered, and when arising from an interface it may be written:

$$\mathbf{d}_{ij} = d_{ij}(\mathbf{n} \times \hat{\boldsymbol{r}}_{ij}). \tag{II.16}$$

$\hat{\boldsymbol{r}}_{ij}$ is the unit vector from atomic site i to atomic site j, and $\mathbf{n}$ is the outward normal

to the magnetic surface, here taken along $\hat{\boldsymbol{x}}$. Angles are such that a positive value around $\hat{\boldsymbol{y}}$ means counter-clock-wise rotation on Figure II.19.

1. When in competition with conventional exchange $\epsilon_{\text{ex}} = -J_{ij}(\hat{\mathbf{S}}_i \cdot \hat{\mathbf{S}}_j)$, discuss qualitatively the consequence of the DMI interaction (no calculation required). What is the sign of d_{ij} consistent with the gradual change of angle displayed on Figure II.19?
2. For the sake of simplicity we consider a square lattice of atomic sites in the (y, z) plane, with nearest-neighbor distance a along the y and z directions, and DMI restricted to these four nearest neighbors. $\mathbf{d}_{ij}$ is thus identical in strength for all bounds. d_{ij} will be written d in the following. When the change of angle between sites i and j is small, expand the vector product of Eq.(II.15) using the operator $\mathbf{r}_{ij} \cdot \boldsymbol{\nabla}$. Show that, normalized to one atomic site, the DMI energy may be written:

$$\epsilon_{\text{DMI}} = da \left[\hat{\boldsymbol{y}} \cdot \left(\mathbf{m} \times \frac{\partial \mathbf{m}}{\partial z} \right) - \hat{\boldsymbol{z}} \cdot \left(\mathbf{m} \times \frac{\partial \mathbf{m}}{\partial y} \right) \right] \tag{II.17}$$

3. We introduce the DMI energy per unit surface $E^{\text{S}}_{\text{DMI}} = \epsilon_{\text{DMI}}/a^2$, and its normalization per unit volume $E^{\text{V}}_{\text{DMI}} = \epsilon_{\text{DMI}}/(a^2 t)$ when dealing with an ultrathin film of thickness t. Define the surface and volume quantities D_{S} and D_{V}, such as for example:

$$E^{\text{V}}_{\text{DMI}} = D_{\text{V}} \left[\hat{\boldsymbol{y}} \cdot \left(\mathbf{m} \times \frac{\partial \mathbf{m}}{\partial z} \right) - \hat{\boldsymbol{z}} \cdot \left(\mathbf{m} \times \frac{\partial \mathbf{m}}{\partial y} \right) \right] \tag{II.18}$$

   Discuss their units. Express again Eq.(II.17), in terms of energy per unit volume. Simplify this expression when a variation of magnetization is expected only along z. Write it first in terms of components of $\mathbf{m}$, then in terms of the angle φ, showing that $E_{\text{DMI}} = D_{\text{V}}\, \mathrm{d}\varphi/\mathrm{d}z$.

5.2. Micromagnetic consequences of the Dzyaloshinskii-Moriya interaction

We consider the combination of exchange, DMI and anisotropy energies, expressed in energy per unit volume:

$$E(\mathbf{r}) = A \left(\frac{\mathrm{d}\varphi}{\mathrm{d}z} \right)^2 + D_{\text{V}} \left(\frac{\mathrm{d}\varphi}{\mathrm{d}z} \right) + K \sin^2 \varphi \tag{II.19}$$

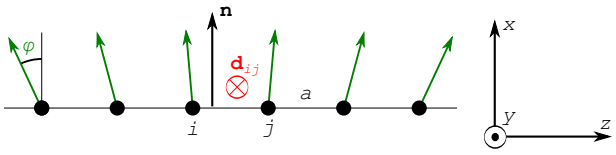

Figure II.19 – Notations for the Dzyaloshinskii-Moriya interaction

Note that the variation of magnetization drawn on Figure II.19 is the geometry for a Néel wall.

1. Discuss the units of A, D_V and K. Which are the various characteristic length scales that may arise due to the competition of these terms? Which are the various domain wall energies that may arise?
2. Searching for the equilibrium shape of a domain wall we consider the functional energy:

$$\mathcal{E}[\mathbf{m}] = \int_{-\infty}^{+\infty} E\left[\mathbf{m}(\mathbf{r}), \frac{\mathrm{d}\mathbf{m}}{\mathrm{d}z}(\mathbf{r})\right] \mathrm{d}z \tag{II.20}$$

   It is reminded that this energy is minimized under the Euler-Lagrange condition:

$$\frac{\partial E}{\partial \varphi} = \frac{\mathrm{d}}{\mathrm{d}z}\left[\frac{\partial E}{\partial\left(\frac{\mathrm{d}\varphi}{\mathrm{d}z}\right)}\right] \tag{II.21}$$

   We will search for a solution with extended boundary conditions $\varphi(-\infty) = \epsilon\pi$ and $\varphi(+\infty) = 0$, with $\epsilon = \pm 1$. The sign of ϵ is related to the chirality of the wall, which you will comment a priori. Apply the Euler-Lagrange equation and comment on the influence of D_V on the shape of the domain wall. Remembering that the energy per unit surface of a conventional domain wall is $4\sqrt{AK}$, show that the energy of the domain wall when the DMI interaction is present is: $\sigma_W = 4\sqrt{AK} - \epsilon\pi D_V$. Discuss.
3. We define the quantity $D_{cyc} = 4\sqrt{AK}/\pi$. What is the unit of this quantity? Express D_{cyc} in terms of the anisotropy exchange length. For $D > D_{cyc}$ we have $\sigma_W < 0$, which means that domain walls may be nucleated spontaneously, forming a periodic cycloid. Considering the energy per unit volume of the cycloid, calculate its period L in the simple case where the magnetic anisotropy K may be neglected, so that $\mathrm{d}\varphi/\mathrm{d}z$ is a constant. We introduce the variable $\xi = 2A/|D_V|$ to express L. How could ξ be named?
4. In the above we considered that the domain wall is of Néel type, as depicted in Figure II.19. However, it is known that a Néel wall implies a cost of dipolar energy, compared to a Bloch wall. A domain wall may be written, in a general fashion: $m_y = \sin\Phi \sin\varphi$, $m_z = \cos\Phi \sin\varphi$ and $m_x = \cos\varphi$. Draw a sketch for such a general wall. Which are the values of Φ for a Néel or a Bloch wall? Express again E_{DMI} for an arbitrary value of $\cos\Phi$. Derive again the energy of a domain wall, as a function of Φ. If we neglect the dipolar cost of a Néel wall compared to a Bloch wall, what is the most favorable wall in the presence of the DMI?
5. We write K_N the extra cost per unit volume of dipolar energy of the Néel wall, compared to the Bloch wall. Using the arguments of Néel to estimate this dipolar cost of Néel walls based on the demagnetizing coefficient of a cylinder, express the extra cost for an arbitrary angle Φ. Then, remembering the equipartition of exchange and anisotropy energy occurring in walls of

second order, and assuming that the profile of the wall is still determined by exchange and anisotropy solely, show that the energy of a general wall may be written: $\sigma_W = 2\Delta K_N \cos^2\Phi - \epsilon\pi D_V \cos\Phi$, where Δ is the anisotropy exchange length. Discuss the type and energy of a wall occurring naturally depending on the value of D_V. We introduce the critical parameter $|D_c| = 4\Delta K_N/\pi$.

6. Finally, we consider an external field **H** applied along $\hat{\boldsymbol{y}}$. Again assuming that the profile of the domain wall is still determined by A and K, calculate σ_Z, the contribution of the Zeeman energy to the wall. Show that the effect of the DMI is similar to an applied field H_{DMI} applied along y, and provide the formula for this equivalent field. Determine the type and energy of the wall as a function of H.

Chapter III

Magnetization reversal

Overview

The previous two chapters have led to the understanding of the arrangement of magnetization in low-dimension system. We are now ready in this chapter to address processes of magnetization reversal, *i.e.* the effect of an applied magnetic field on the overall direction and local arrangement of magnetization. We restrict the discussion to quasistatic effects, including thermally-assisted processes. We leave aside precessional magnetization dynamics, to be examined in chap.IV, as well as magnetization processes induced by spin-polarized currents, to be covered in the last chapter. Systems will be discussed from the smallest to the largest, meaning single-domain to potentially with non-uniform magnetization, so with increasing complexity. The former are more prone for analytical modeling, while the latter are tackled with approximations and dedicated modeling.

1 Macrospins - The case of uniform magnetization

The determination of the energy landscape is crucial for describing hysteretic phenomena, however difficult or impossible in practice in extended systems due to the large number of degrees of freedom. Only simple problems may be tackled analytically. Coherent rotation of magnetization is one of the oldest and a useful starting point for more complex theories. It describes systems with essentially uniform magnetization, which in practice applies reasonably only to those systems with dimensions smaller than all magnetic length scales (nanoparticles).

1.1 The Stoner-Wohlfarth model

The model of coherent rotation was proposed by Stoner and Wohlfarth in 1948 to describe the angular dependence of magnetization reversal[91, 92, the latter being a reprint of the former], and developed in parallel by Néel to describe thermally-activated processes. Many developments were made later, including clever graphical interpretations[93] and generalization to three dimensions[94].

The model is based on the hypothesis of uniform magnetization, reducing the problem to solely one or two angular degrees of freedom. This hypothesis is very restrictive and may be reasonably applicable only to very small particles. For large systems it is not suitable as is, with for example an experimental coercivity being much smaller than the one predicted. Nevertheless, the concept introduced for uniform magnetization bears some generality (*e.g.* exponents, angular dependence), and may be applied to extended systems with some care, *e.g.* to describe nucleation volumes (sec.3).

We consider a system with volume V, total uniaxial anisotropy energy $\mathcal{K} = K_u V$, magnetic moment $\mathcal{M} = M_s V$. Its magnetic energy reads:

$$\mathcal{E} = \mathcal{K} \sin^2\theta - \mu_0 \mathcal{M} H \cos(\theta - \theta_H). \tag{III.1}$$

θ refers to the direction of magnetization with respect to the lattice, $\theta = 0$ being the initial state along an easy axis. θ_H is the angle between the applied field and this initial direction of magnetization. For simplicity here we consider only the case $\theta_H = \pi$, thus a positive H is applied to promote magnetization reversal. We use dimensionless variables $e = \mathcal{E}/\mathcal{K}$, $H_a = 2K_u/\mu_0 M_s$ and $h = H/H_a$. H_a is called the anisotropy field. The equilibrium positions are determined by solving $de/d\theta = 0$. The stability of these positions (stable or unstable) are determined by the sign of $d^2e/d\theta^2$ (respectively positive or negative).

Table III.1 – Stoner-Wohlfarth model calculations. Summary of the anisotropy of energy and its derivatives, for the external field applied along an easy axis [$\theta_H = \pi$, see Eq.(III.1)].

	e	$de/d\theta$	$d^2e/d\theta^2$
	$\sin^2\theta + 2h\cos\theta$	$2\sin\theta(\cos\theta - h)$	$4\cos^2\theta - 2h\cos\theta - 2$
$\theta_+ = 0$		0	$2(1-h)$
$\theta_- = \pi$		0	$2(1+h)$
$\theta_b = \arccos(h)$		0	$-2(1-h^2)$

The anisotropy field. Whereas dimensional analysis shows that $K/\mu_0 M_s$ it the characteristic quantity emerging when anisotropy and Zeeman energies compete, the general definition of the anisotropy field is $\mathbf{H}_a = -\partial E_{mc}/\partial\mu_0\mathbf{M}$, and H_a implicitly refers to its magnitude along the easy axis of magnetization. It reads $2K/\mu_0 M_s$ for the case of uniaxial anisotropy of second order, however have different expressions for other cases.

The formulas for e, its angular derivatives, and their values for extrema of e, are gathered in Table III.1; $h = 1$ is clearly a threshold value. Thanks to the symmetry of the case considered, we may assume $\theta \in [0 - \pi]$ without loss of generality. While $\theta_+ = 0$ and $\theta_- = \pi$ are always equilibrium positions, for $h < 1$ an extra equilibrium position θ_b exists. In that case $\theta_\pm$ equilibrium positions are stable, while θ_b is an unstable position, associated with an energy barrier preventing magnetization reversal from the metastable θ_+ towards the most stable θ_- (Figure III.1a). The energy barrier is:

$$\Delta e = (1-h)^2 \tag{III.2}$$

$$\Delta\mathcal{E} = \mathcal{K}(1 - H/H_a)^2 \tag{III.3}$$

For $h > 1$ only θ_+ and θ_- remain as equilibrium positions, respectively unstable and stable. An abrupt switching of magnetization occurs for $h_{sw} = 1$, as revealed consistently by many signatures: $\Delta e \to 0$, $\theta_b \to \theta_+$ before vanishing, and θ_+ changes from a stable to an unstable equilibrium position. The resulting hysteresis loop is square, with remanence exactly one, and coercive field equaling the anisotropy field.

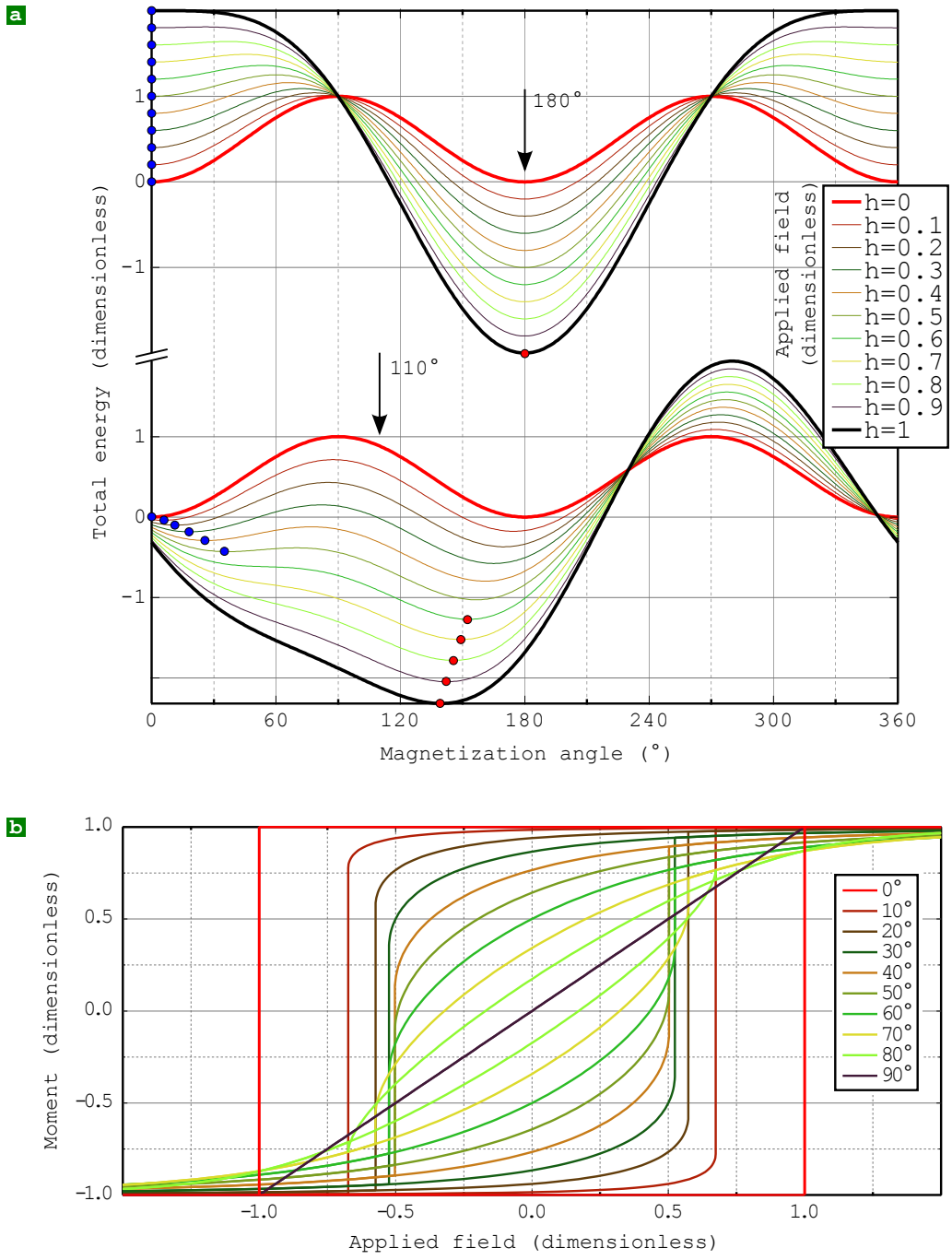

Figure III.1 – (a) **Energetics and hysteresis loops for the macrospin**. Energy profiles for increasing values of applied field, of a macrospin with uniaxial anisotropy of second order. Profile are drawn for both easy axis ($\theta_H = 180°$, top) and intermediate angle ($\theta_H = 110°$, bottom). For the latter, the series of profiles are slightly shifted vertically for clarity. The initial (resp. final) minima are marked with blue (resp. red) dots. (b) Hysteresis loops for various angles of applied field θ_H. Equal values for angles symmetric with respect to 45° are clearly evidenced.

- **The vocabulary of magnetization reversal**. Several words may be found to describe magnetization reversal, such as reversal, switching, coercivity. Their meaning is slightly different, and their use should depend on the case considered. Switching, used in the above, refers to the abrupt change of direction of magnetization, reflecting the existence of two distinct minima in an energy landscape. It is a notion best suited to small systems in nanomagnetism, such a single-domain, characterized by a limited number of degrees of freedom. Coercivity is defined as $\mathbf{M} \cdot \mathbf{H} = 0$, referring to states in which a system is half-way reversed. It is best suited as a statistical value to characterize large systems, such as for material science, where individual degrees of freedom (*e.g.* single-domain grains) cannot be distinguished. Notice that no special event may occur around coercivity for single particle, *e.g.* when the field is applied closer to the hard than easy axis (Figure III.1b). Reversal has the broader meaning of magnetization changing of orientation along a given direction, generally that of an applied field. The microscopic origin of the reversal may be diverse, such as switching for a nanoparticule, domain wall motion, continuous rotation of magnetization. Coercivity characterizes a half-way reversed system.

- **Critical exponents for energy barriers**. In most cases, even idealized, $\Delta\mathcal{E}$ is not a polynomial with h and an expansion is used: $\Delta\mathcal{E} \sim (1-h)^{\alpha}$. $\alpha = 1.5$ in many cases, such as whenever the field is applied in a direction which is not an axis of symmetry for a macrospin, or for the one-dimensional model of a domain-wall motion hindered by local defects (sec.4).

The calculation of the switching field may be generalized to an arbitrary value of θ_H. Although the calculation is somewhat tedious, the result is simple:

$$h_{sw}(\theta_H) = \frac{1}{\left(\sin^{2/3}\theta_H + \cos^{2/3}\theta_H\right)^{3/2}} \tag{III.4}$$

The angular variation of the switching field is plotted in both polar and cartesian coordinates in Figure III.2. The former is known as the Stoner-Wohlfarth astroid[III.1], although the plot and associated geometrical interpretations were proposed only later by Slonczewski[93]. The resulting hysteresis loops are displayed in Figure III.1b. They evolve from perfectly square for the external field applied exactly along the easy axis direction ($\theta_H = 0°$), to fully reversible with no remanence nor coercivity for the field applied exactly along a hard axis direction ($\theta_H = 90°$).

[III.1] The mathematical name for this curve

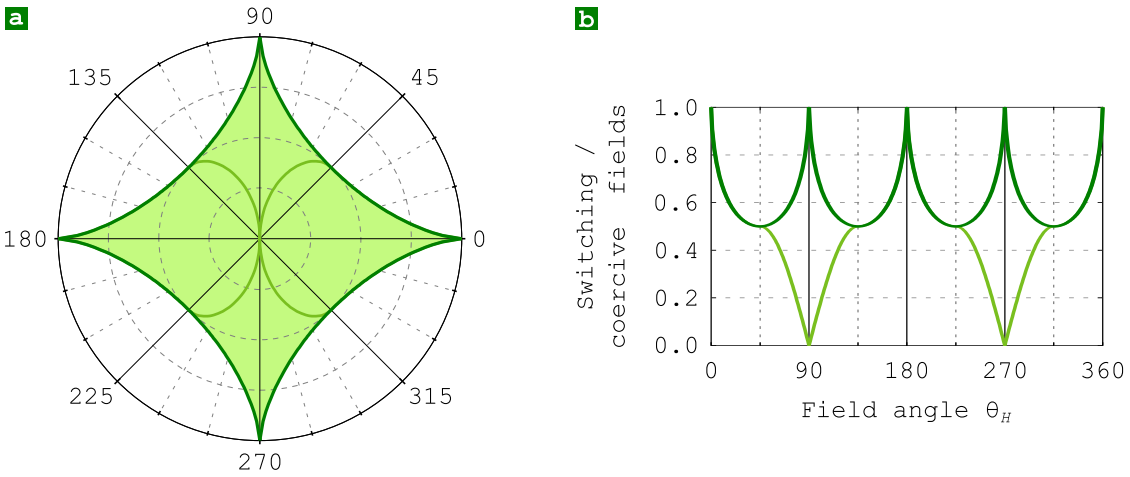

Figure III.2 – Stoner-Wohlfarth switching . (a) Polar and (b) cartesian plots of the switching field h_{sw} and coercive field h_c as a function of the angle θ_H of applied field. The former is known as the Stoner-Wohlfarth astroid.

Limitations of the Stoner-Wohlfarth model. In the framework of the model of coherent rotation, the maximum switching field equals the anisotropy field (1) and is reached for $\theta_H \equiv 0[\pi/2]$, while the minimum switching field is 1/2 and is reached for $\theta_H \equiv \pi/4[\pi/4]$. We will see in sec.3 that in most systems the model of coherent rotation is not relevant, and coercivity may be much smaller than the anisotropy field.

Fourfold symmetry of the astroid. It is at first sight surprising that the Stoner-Wohlfarth astroid has a fourfold symmetry, while the anisotropy of energy is twofold (uniaxial). The reason is linked with the above discussion about the meaning of switching and coercive fields, in the sense that the switching field is only one signature of magnetization reversal. While h_{sw} has the same value for two angles symmetric with respect to $\pi/4$, the magnitude of the jump is larger close to the easy axis, compared to close to the hard axis. This magnitude in terms of $\mathbf{m} \cdot \mathbf{h}$ ranges from 2 along the easy axis, to zero in the limit of the hard axis. The angular variation of coercivity, another signature of magnetization reversal, displays the expected twofold symmetry: $h_c(\theta_H) = \frac{1}{2}|\sin(2\theta_H)|$ (Figure III.2).

1.2 Dynamic coercivity: effects of temperature and waiting time

In the previous section we considered that a switching event occurs when the associated energy barrier vanishes; this is a zero-temperature view. At finite

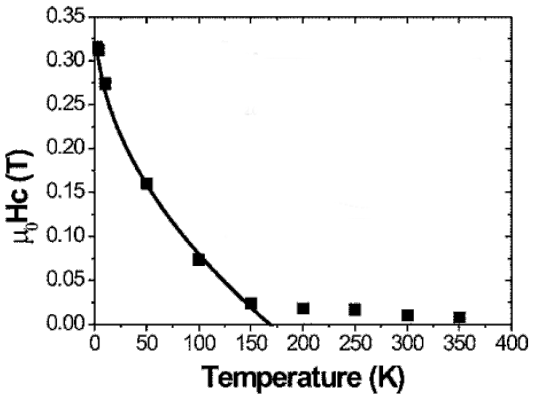

Figure III.3 – Experimental variation of coercive field with temperature in a low-dimensional system[95]. The fit follows Eq.(III.5)

temperature thermal energy may help overcome an energy barrier of finite height, an effect which we address here.

The effect of thermal energy is often described with a Boltzmann law: the probability to overcome a barrier $\Delta\mathcal{E}$ is $\exp(-\Delta\mathcal{E}/k_B T)$ during a time characteristic of magnetization dynamics, a so-called attempt time τ_0. It follows that the probability p of not having switched obeys $\mathrm{d}p/\mathrm{d}t = -p[\exp(-\Delta\mathcal{E}/k_B T)]/\tau_0$, and thus $p(t) = p_0 \exp(-t/\tau_m)$ with $\tau_m = \tau_0 \exp(\Delta\mathcal{E}/k_B T)$. chap.IV provides some ground for an order of magnitude for most magnetic systems: $\tau_0 \simeq 10^{-10}$ s.

Attempt time. The meaning of the attempt time τ_0 is the typical time involved in magnetization dynamics. $1/\tau_0$ is called the attempt frequency.

In the framework of the Stoner-Wohlfarth model, $\Delta\mathcal{E}$ follows Eq.(III.3). Let us express this effect the other way round: for a duration of observation τ (*e.g.* for a measuring technique requiring this averaging time), the field for which the probability for magnetization switching reaches 50 %, which by definition is the coercive field, may be expressed as:

$$H_c(T) = H_c(0\,\mathrm{K})\left[1 - \sqrt{\frac{k_B T}{\mathcal{K}}\ln(\tau/\tau_0)}\right] \qquad \text{(III.5)}$$

While this equation may be applied to various cases, in the framework of the Stoner-Wohlfarth model we have $H_c(0\,\mathrm{K}) = H_a$ and $\mathcal{K} = KV$. Figure III.3 shows an experimental example of an $H_c(T)$ plot, along with a fit with Eq.(III.5). Notice that when $\alpha \neq 2$ this law is modified.

Effects of temperature versus waiting time. The logarithmic function varies extremely slowly, so that while variations of temperature have a direct impact on the coercivity, changes of time scales must be of orders of magnitude to have a similar impact.

- **Extrapolating coercive field at zero temperature**. $H_c(T)$ is a function decreasing monotonously with temperature. Notice that the variation is ever sharper close to zero temperature, with a diverging derivative. This highlights that a measurement at a somewhat low temperature to estimate the limiting value $H_c(0)$ may not be adequate, yielding an underestimation of its value. Applying a scaling law of $H_c(T)$ versus $\sqrt{T}$ over a range of accessible low temperatures, is more suitable.
- **Approximations**. Eq.(III.5) neglects the thermal variation of magnetization and of anisotropy coefficients, which may be readily taken into account in a mean field approach by feeding *a priori* known $M_s(T)$ and $K(T)$ curves. Another annoying effect is deviations from the idealized Stoner-Wohlfarth case, responsible for an energy barrier lower than KV. The discrepancy is likely to be temperature-dependent, so that the latter effect cannot be corrected *a priori*.

Eq.(III.5) shows that there exists a temperature at which coercivity vanishes. It is called the blocking temperature T_B, as below this temperature the total moment of the system does not fluctuate under the time of observation; it is the blocked state. Above T_B the moment fluctuates spontaneously, so that the average moment vector is zero; this is the superparamagnetic regime, studied in more detail in the next section.

From Eq.(III.5) T_B is defined as:

$$\mathcal{K} = k_B T_B \ln\left(\frac{\tau}{\tau_0}\right) \tag{III.6}$$

Notice that the value of T_B is not unique; it depends on the time scale it is defined: the shorter the time scale, the higher the blocking temperature. For $\tau \approx 1\,s$ one finds $\ln(\tau/\tau_0) \approx 25$, so that the above law is often found written $\mathcal{K} \approx 25 k_B T_B$ in the literature. In data storage the retention time should be years, which is of the order of 10^{10} s, so that the numerical factor is then close to 50. As the energy barrier is proportional to the volume for coherent rotation, the larger the anisotropy, the smaller the diameter up to which the particle is superparamagnetic. Critical diameters of superparamagnetism for various materials are in the range from a few to a few tens of nanometers, as summarized in Table I.2.

1.3 The superparamagnetic regime

Here we analyze the behavior under applied field of a superparamagnetic system described by a macrospin of moment $\mathcal{M} = M_s V$. We make use of reduced moments m_i to refer to the component of the macrospin along a given direction ($m = 1$).

We first consider the case of no magnetic anisotropy. Let us use the partition function of statistical physics defined as $\mathcal{E}$: $Z = \sum \exp(-\beta \mathcal{E}_i)$ from the probability of occupancy of states i with energy $\mathcal{E}_i$; i sums over all possible states. As $\mathcal{E}$ contains the term $-\mu_0 \mathcal{M}_z H$ (H being applied along the z direction), the average moment along the direction z of the applied field may be computed like:

$$\langle m_z \rangle = \frac{1}{\mathcal{M}\beta\mu_0 Z}\frac{\partial Z}{\partial H}. \tag{III.7}$$

Integration on all possible orientations of magnetization in space reads:

$$Z = \int_0^\pi \sin\theta \, \exp\left(\beta\mu_0 \mathcal{M} H \cos\theta\right) \, \mathrm{d}\theta \tag{III.8}$$

Simple algebra then yields $\langle m_z \rangle = \mathcal{L}(x)$ with $x = \beta\mu_0\mathcal{M}H$ and $\mathcal{L}(x) = \coth x - 1/x$ is the Langevin function (Figure III.4b).

The situation is different in the case of magnetic anisotropy. A textbook case is a system with a large uniaxial anisotropy ($\mathcal{K} \gg k_B T$), and magnetic field applied along the easy axis. In that case only rare events drive magnetization away from the easy axis and lead to switching its direction. We may thus consider that the system is essentially either in the up or in the down state at most times. An approximate partition function then simply reads $Z = 2\cosh x$ and $\langle m_z \rangle = \mathcal{B}_{1/2}(x)$. $\mathcal{B}_{1/2} = \tanh$ is the Brillouin 1/2 function also describing the susceptibility of an Ising spin $S = 1/2$, except that here the spin moment is replaced by the macrospin moment $\mathcal{M}$. The proof for this handwaving argument, and the transition from the Brillouin 1/2 to the Langevin function may be found elsewhere[96]. This highlights the origin of the name superparamagnetism: its phenomenology is similar to that of paramagnetism, however implying macrospins instead of individual electron or atomic spins.

The analysis of the $m(H)$ curve of a macrospin in the superparamagnetic regime informs one about the magnitude of its magnetic moment, as saturation is reached for $x \approx 1$. Similar to the case of paramagnetism, $m(H/T)$ curves are expected to superimpose, which is a check of the validity of the method in a given context. Instead of fitting the entire curve the analysis is often restricted to the zero-field susceptibility χ. A quantitative analysis requires however the careful choice of the model best fitted to describe a situation, as to first order expansion $\mathcal{L}(x) \sim x/3$ while $\mathcal{B}_{1/2}(x) \sim x$. It shall be noted that anisotropy may be neglected only when $k_B T$ becomes comparable with $\mathcal{K}$. Using the Langevin model in a case when it is the Brillouin 1/2 that is relevant, yields to a threefold overestimation

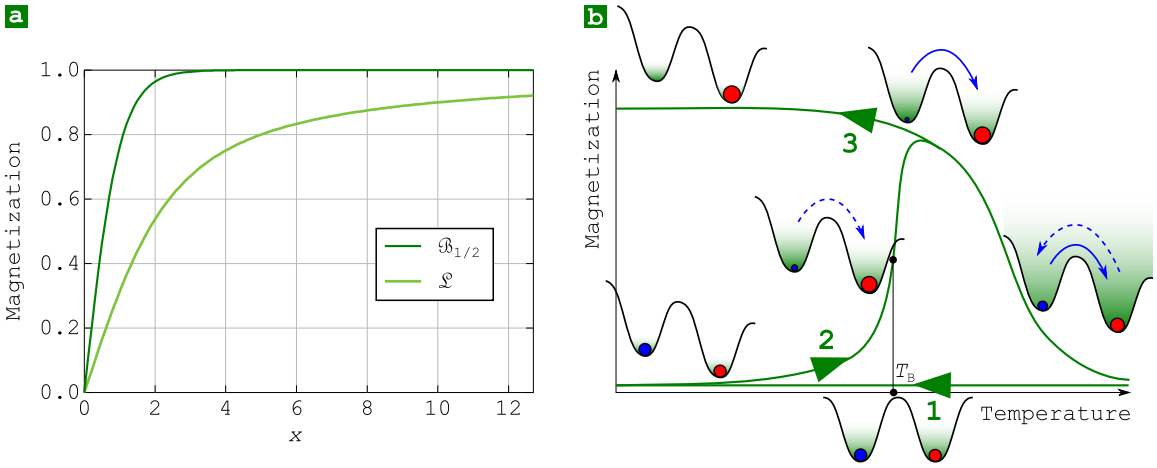

Figure III.4 – (a) **Langevin $\mathcal{L}$ and Brillouin one-half $\mathcal{B}_{1/2}$ functions**. (b) The three-steps zero-field-cooled / field-cooled procedure for an assembly of particles. On the energy landscapes the red (resp. blue) dots illustrate magnetization parallel (resp. antiparallel) to the applied field. The green shade illustrates the states accessible through thermal excitations.

of the moment. For a reliable analysis $1/\chi$ is often plotted versus T, expecting a linear variation whose slope is inversely proportional to the magnitude of the magnetic moment. In the usual case of the study of an assemble of particle, a shift of the $1/\chi$ line towards positive (resp. negative) field values is indicative of ferromagnetic (resp. antiferromagnetic) coupling between the particles, similarly to the Curie-Weiss law.

Rule of thumb. $\mathcal{B}_{1/2}$ tends to saturate for $x \approx 1$. As $k_B \approx 1.38 \times 10^{-23}\,m^2 \cdot kg \cdot s^{-2}$ and $\mu_B \approx 9.27 \times 10^{-24}\,A \cdot m^2$, as a rule of thumb we shall remember that an induction $\mu_0 H = 1\,T$ is required for polarizing a magnetic moment of $1\,\mu_B$ at $T = 1\,K$. At room temperature 300 T would be required to significantly polarize atomic moments; this is the order of magnitude of the conceptual molecular field describing magnetic ordering with sizable Curie temperature.

Beware of the model used. For the anisotropic case we considered here only the textbook case of the magnetic field applied along the direction of easy axis. In the case of an assembly of anisotropic particles with an isotropic distribution of easy axis, the resulting magnetization curve lies very close to a Langevin function. In real cases distributions may arise (of particle moment and anisotropy). Introducing more parameters for describing superparamagnetic curves will always yield a better fit from the mathematical sense, however care should be taken about the independence of the effect of the various parameters introduced, and also on the reliability of the fitting if the values of parameters depend on faint features of the magnetization curve.

Figure III.4b illustrates a routine procedure for characterizing the transition from the blocked to the superparamagnetic state of an assembly of particles: the zero-field-cool / field-cooled curves. The first step is driving the system down in temperature through the superparamagnetic transition. This is done under zero applied field, so that at any temperature the average moment is zero. The second step consists in raising the temperature back to above the superparamagnetic transition (zero-field-cooled part). This is done under an applied field of moderate magnitude, *i.e.* much smaller than the anisotropy field so that the two energy minima still exist and are simply imbalanced in energy. When thermal fluctuations become sufficient the energy barrier may be crossed and the population of the two minima obeys the Boltzmann law, yielding an average moment scaling like $1/T$, see above the $\mathcal{B}$ functions. In the third step the temperature is lowered again, while keeping the moderate applied field (field-cooled curve). Upon crossing the superparamagnetic temperature the system freezes with magnetization mostly aligned along the field, yielding a high average moment. On these curves the splitting between steps 2 and 3 allows one to identify the blocking temperature. When there exists a distribution of blocking temperatures in an assembly, it is reasonable to define the blocking temperature as half-way up the field-cooled magnetization curve (Figure III.4b).

Parameters influencing FC/ZFC curves. The exact shape of FC/ZFC depends on the strength of the applied field, especially the value and field for the maximum of the ZFC part. So does it also in relation with magnetic anisotropy, its strength and angular distributions, inter-particles interactions etc[97, 98]. Thus, some care needs to be taken when interpreting the values extracted from ZFC-FC curves.

Superparamagnetic or non-magnetic? There is often an argument how to differentiate or even define the superparamagnetic regime from the loss of magnetic order. From a theoretical perspective a particle may be called magnetically-ordered when the magnetic correlation length exceeds the size of a particle. For compact nanoparticles of diameter at least $5-10\,\mathrm{nm}$ this should happen not far below the bulk ordering temperature, which may be very large compared to the blocking temperature. From a practical point of view the susceptibility should scale like $\mathcal{M}/T$ in the superparamagnetic regime, and sharply drop to m_{at}/T above the ordering temperature, with m_{at} the value of individual moments at the atomic scale.

1.4 What do we learn from dynamic coercivity and superparamagnetism?

In the previous three subsections we considered the magnetization reversal of macrospins with increasing thermal energy, neglected in the Stoner-Wohlfarth model (probed by low-temperature measurements), up to the superparamagnetic regime. To schematize, we may learn a different information from experiments performed in each regime. Here is a possible way to combine these informations. This of course is an idealized procedure, and should be applied and output taken with care. Pitfalls may come from non-perfectly uniform magnetization, non-uniaxial anisotropy, distributions of various types in the assemblies measured, inter-particle interactions etc.

1. The superparamagnetic regime is primarily sensitive to the *moment* $\mathcal{M}$ of the particle. Thus, if M_s is known and a suitable model for fitting is chosen, then information about the particle volume V may be extracted.
2. Second, the thermal decay of coercivity and the blocking temperature (sec.1.2) involves $\mathcal{K} = KV$, so that based on the value of V estimated previously, information about the volume density of anisotropy K may be extracted.
3. Third, the extrapolation of coercivity down to low temperature provides some information about the intrinsic process of magnetization switching. For a truly single-domain nanometer-sized particle the Stoner-Wohlfarth model should apply and coercivity reflect the volume density of anisotropy, to be compared to the value estimated in the second step. Deviations may reflect discrepancies in the analysis, or a magnetization process deviating from coherent rotation as will be discussed in the next section.

1.5 Ensembles of grains

Some features of the magnetization reversal of isolated single-domain grains were presented in the previous paragraphs. Some consequences may be drawn for systems consisting of assemblies of individual grains, neglecting inter-grain interactions of any type. Of easy access and modeling are the remanence m_r and the internal energy at saturation E_K, derived from the area above the remagnetizing curve. Both depend on the dimensionality of the distribution of easy axis. Assuming uniaxial magnetic anisotropy with constant K for simplicity, we consider three common cases:

- The polycrystalline case, *i.e.* with an isotropic distribution of easy axis in space. This may correspond to particles diluted in a matrix, or a polycristalline bulk material. We then find: $m_r^{3D} = 1/2$ and $E_K^{3D} = 2K/3$.
- The polytextured case. By this we mean a shared axis with no distribution for the hard axis, while the easy axis is evenly distributed in the plane perpendicular to this axis. This would be the case of Fe(110) grains grown

on a surface, the easy axis lying along the in-plane [001] direction. When the field is applied in-the-plane we find: $m_r^{2D} = 2/\pi \approx 0.64$ and $E_K^{2D} = K/2$.

- The textured case, where all grains share the same direction of easy axis. This would be the case for oriented powders, or *e.g.* (0001) hcp Co grains on a surface. When the field is applied along this axis we find the case of a single grain: $m_r^{1D} = 1$ and $E_K^{1D} = 0$.

Remanence, texture and interactions. The comparison of experimental findings with the expected figure for m_r is often used as an indication for interactions, positive (*e.g.* through direct exchange between neighboring grains) if the experimental value exceeds the expectation, negative it it lies below. Systems with coupled grains will be considered in more detail in the following section.

Concerning anisotropy, notice that in the first two cases the measure of E_K provides an indication of K. In all cases, the sum of areas above the loops for all three main axes equals $2K$.

Summary

Macrospins. The model of uniform magnetization (also called macrospins) in magnetization reversal is interesting because it can be solved analytically, however it must be handled with care in large systems, in which non-uniform magnetization distributions may play the leading role in magnetization reversal. Among the quantities predicted is the switching field, which is reduced at elevated temperature due to thermal excitations. Sufficiently-small magnetic grains may even switch spontaneously above a given temperature, called the blocking temperature. This phenomenon is called superparamagnetism.

2 Magnetization reversal in nanostructures

When the dimensions of a system reach or go beyond some magnetic length scale, the hypothesis of uniform magnetization is in most cases no more reliable. Internal degrees of freedom show up and change the properties of magnetization switching, as they already do for the static configurations as seen in the previous chapter. Below we progressively release the constraint of uniform magnetization, going from the simplest to the more complex nanostructures.

2.1 Near single domains

It was stressed in sec.I.4.3 that the demagnetizing field may be homogenous and collinear to magnetization only in uniformly-magnetized bodies such as cylinders,

ellipsoids and slabs. Thus for all other shapes spatially-dependent torques act on magnetization, making the hypothesis of strictly uniform magnetization not possible self-consistently. This gives rise to the occurrence of near-single-domain configurations and configurational anisotropy, discussed in sec.II.4.4. This additional contribution to the angular variation of magnetic anisotropy, composed of magnetostatic and exchange energy, induces deviations from the Stoner-Wohlfarth model and Slonczewski's astroid and rounding of magnetization curves (non-full remanence). In a small system with no uniaxial anisotropy of neither shape nor magnetocrystalline origin, configurational anisotropy determines easy directions of anisotropy and leads to a finite coercivity, whereas zero coercivity would result from macrospin considerations. Micromagnetic simulation or advanced micromagnetic modeling are required to quantify these effects[86].

When the particle size increases, it may happen that while the zero-field magnetization configuration is single-domain or near-single-domain, magnetization reversal involves a static (under constant negative field) or dynamic state with significant deviations from uniform magnetization. This has early been suspected as one of the possible reasons of the often-found discrepancy between the large values of coercive field predicted by the Stoner-Wohlfarth model, and experiments. This discrepancy is now referred to as the Brown paradox. For the moment we still restrict the discussion to finite-size systems and let aside the case of extended bodies in which magnetization reversal is often triggered at structural inhomogeneities and defects, to be discussed in sec.3.1.

The first model for non-uniform magnetization switching in systems with nevertheless small dimensions was proposed concomitantly by Brown[99] and Frei *et al.* [100][III.2]. This new mode is called curling, and consists of a radius-dependent orthoradial (azimuthal) tilting of magnetization around the initial direction of magnetization, itself being along an easy and high-symmetry axis. This breaks the initial symmetry of the system and gives rise to some vorticity or curling (Figure III.5). This reversal mode is still highly symmetric and described by one single linear functional degree of freedom. For this reason we will call it a collective magnetization switching.

A scaling law for the range of relevance of curling is easily derived, in a way similar to the one describing the critical size for single domain (sec.4.3) however now implying an applied field. We consider a system with uniaxial anisotropy of second order K_u, demagnetizing coefficients N_u along the easy axis and $N_\perp$ in the transverse directions. R is the half dimension across the hard direction, *e.g.* the radius for a cylinder. Under the constraint of uniform magnetization the average density of magnetic energy varies quadratically with the magnetization angle, from $K_d N_u$ along the easy axis to $K_u + K_d N_\perp$ in the hard plane. We assume $K_u + K_d(N_\perp - N_u) > 0$, defining the easy axis along $\mathbf{u}$. Compared to coherent rotation, the configuration shown in Figure III.5 may allow to decrease significantly

[III.2]The former manuscript came first by a few month, while the latter has a more detailed presentation and set the notations for later use by the community

the magnetostatic energy $K_d N_\perp$ of the transient state in the hard plane. This is achieved at the cost of exchange energy with density of the order of $A(\pi/2R)^2$. Translating this into fields, it is therefore expected that the switching field behaves like

$$H_{curl} = H_a - M_s\left(N_u - \frac{k}{\rho^2}\right) \tag{III.9}$$

where k is a dimensionless number and $\rho = \frac{R}{\Delta_d}$. Detailed calculations[100] confirm this law and provide a figure for k, for example 3.393 for the infinite cylinder and 4.367 for the sphere. In the calculation exchange and magnetostatic anisotropy are estimated, both contributing to k. As the switching field for coherent rotation is $H_a - M_s(N_u - N_\perp)$, the crossover from coherent rotation for low radius to curling for large radius occurs at $\rho_c = \sqrt{k/N_\perp}$.

The dipolar exchange length appears again as the relevant length scale, as the problem is that of the competition between exchange stiffness and magnetostatic energy.

Curling in SI and cgs. Erroneous numerical factors for k in Eq.(III.9) are sometimes found in the literature, due to the conversion to SI units from the cgs-Gauss system used in the initial calculations by Frei[100]. Following the latter the ρ^{-2} dependance in Eq.(III.9) is often written S^{-2} with $S = R/R_0$, $R_0 = \sqrt{A/M_s^2}$ in cgs-Gauss. Correct formulas in SI units may be found in section 3.5.4 of Hubert's book[6].

Let us take simple examples. For a cylinder of soft magnetic material $H_a = 0$, $N_u = 0$ and $N_\perp = 1/2$. Coherent rotation allows magnetization switching at field $H_{cr} = M_s/2$, curling may start for $H_{curl} = kM_s(\Delta_d/R)^2$. Thus coherent rotation will be the expected switching mechanism for R smaller than the critical radius $R_c = \sqrt{2k}\Delta_d = 2.6\Delta_d$, and curling will be the expected mechanism for larger dimensions. If magnetocrystalline anisotropy is non-zero these fields become $H_{cr} = H_a + M_s/2$ and $H_{curl} = H_a + kM_s(\Delta_d/R)^2$, thus leaving the critical radius unchanged. For a sphere we have $H_{cr} = H_a$ and $H_{curl} = H_a - M_s\left[1/3 - k(\Delta_d/R)^2\right]$, with a critical radius $R_c = \sqrt{3k}\Delta_d = 3.619\Delta_d$.

Calculations for curling can be extended as a function of the angle θ_H of applied field with respect of the main axis of the sample[101, 102]. Expressing the source of magnetic anisotropy as originating from longitudinal N_u and transverse $N_\perp$ demagnetizing coefficients, one finds:

$$H_{curl}(\theta_H) = -M_s \frac{(N_u - k/\rho^2)(N_\perp - k/\rho^2)}{\sqrt{(N_u - k/\rho^2)^2 \sin^2\theta_H + (N_\perp - k/\rho^2)^2 \cos^2\theta_H}} \tag{III.10}$$

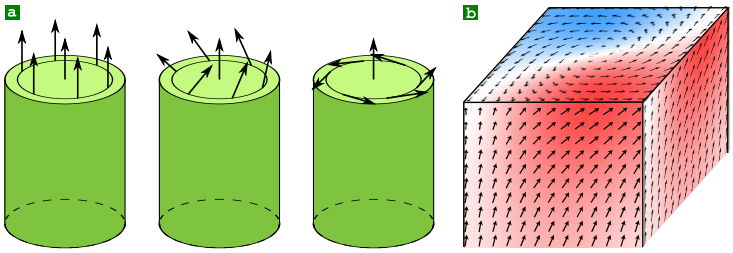

Figure III.5 – (a) **Schematics for the curling mechanism** in a cylinder, from uniformly-magnetized (left) to full curling (right). (b) Simulation of curling close to the end of a cylinder with a square cross-section. On each surface the color codes a transverse component of magnetization.

Nucleation or full switching?. Analytical calculations for curling modes require the linearization of equations. Thus what is in principle predicted is the nucleation field in the sense of linear theory, *i.e.* the onset of deviation from uniform magnetization (this should not be confused with nucleation in the sense of the switching of a small volume of material). This does not warranty that full reversal will follow. Numerical solving shows that it coincides with the coercive field for direction of the applied field close to the easy axis, while for angles close to the hard axis the coercive field is distinct and larger than H_n.

We learned above that the (minimum) critical size for a collective non-uniform mode of magnetization switching to occur is about a few times the dipolar exchange length. Still increasing the dimensions of a system, up to what point do collective modes survive in practice? Indeed we have seen in chapter chap.II that nanostructures of dimensions much larger than the dipolar exchange length may remain essentially uniformly magnetized in their remanent state, for instance for large magnetocrystalline anisotropy, or for flat elements even made of a rather soft magnetic material. In these cases, even if collective modes may lower the energy barrier compared to coherent reversal, the energy barrier is still of the same order of magnitude as the anisotropy energy. In such cases a more efficient way to reverse magnetization is incoherent modes, *i.e.* the local nucleation of a small reversed volume that then quickly expands and propagates the reversal to the entire system. The energy involved is then only that contained in the domain wall separating the already reversed from the yet unreversed domains. Such modes are of particular relevance for systems with high anisotropy such as materials for permanent magnets, strongly non-uniform demagnetizing field such as for very flat elements, or with defects locally lowering the nucleation field. An unambiguous proof that systems near-single-domain in the remanent state may be reversed incoherently is a variation of coercivity much faster than predicted by Eq.(III.5), indicative that the volume involved in nucleation is much smaller than the volume of the entire system. We will come back to this when describing extended systems (sec.3).

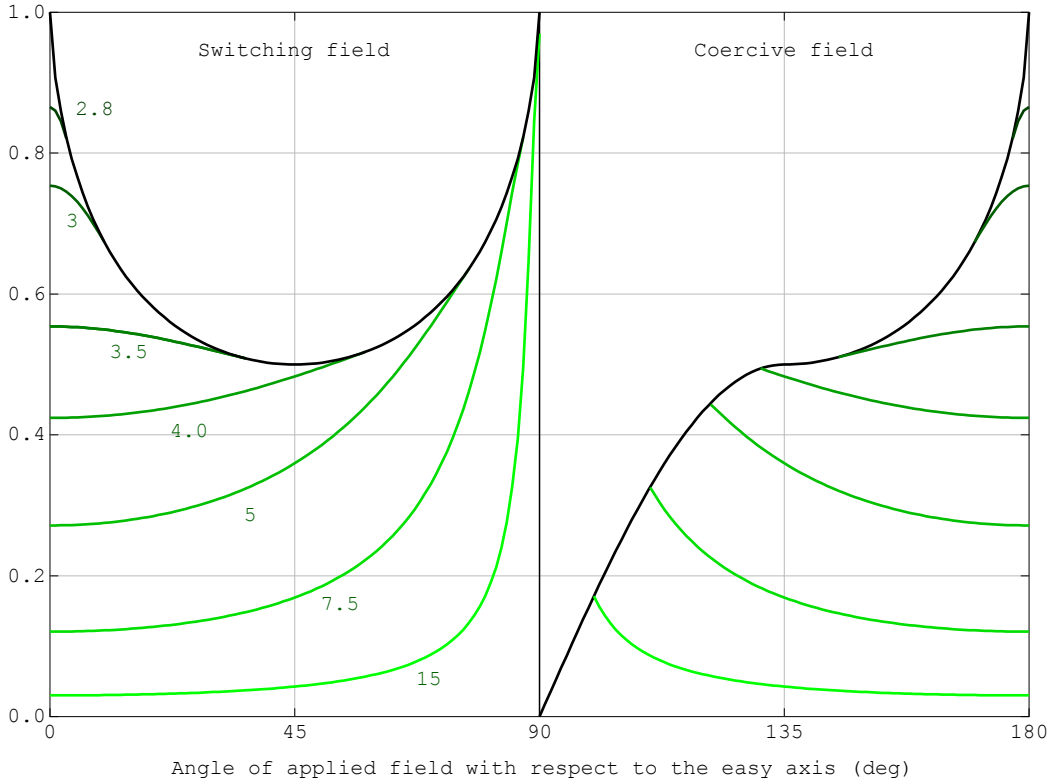

Figure III.6 – Curling model for magnetization reversal in the textbook case of an infinitely-long cylinder made of a soft magnetic material: dimensionless switching field (left) and coercive field (right) versus the angle of applied field θ_H with respect to the easy axis of magnetization. Curves for various values $\rho = R/\Delta_d$ are shown (see figures on the plot), along with those of coherent rotation (Figure III.2b). The reversal mechanism to be expected is the one with the lowest value. Thus below the critical value $\rho_c \approx 2.8$ the mechanism for switching is curling close to the easy axis direction, while it remains coherent rotation close to the hard axis.

Let us give an example of incoherent magnetization reversal. In the previous chapter we saw that extended and flat elements with in-plane magnetization may curl their magnetization close to edges, where demagnetizing field are the largest[III.3] (Figure II.13). It is obviously these areas that are more prone to reversal, triggering an incoherent process for magnetization reversal (Figure III.7). Suitable approximations enable simple models to be developed. For instance it was noticed the switching field of elongated and flat elements scales like $M_s(t/w)$[103], with width w, thickness t, magnetization M_s . This can be understood as the end domain of the S- or C-state being the locus of nucleation, with an energy barrier to overcome scaling like the lateral demagnetizing coefficient of the dot, itself to first order scaling with t/w: $H_c \approx H_{c,0} + 0.25 M_s t/w$. In this formula $H_{c,0}$ relates to the pinning of the thin-film material itself. Thus, engineering the geometry of the end of a stripe is a mean to control the nucleation field, to a certain extent. For example, nucleation occurs at a smaller applied field for tapered ends than for

[III.3] Now that we have seen curling states, let us note that these edge states are sometimes called edge curling walls[6]

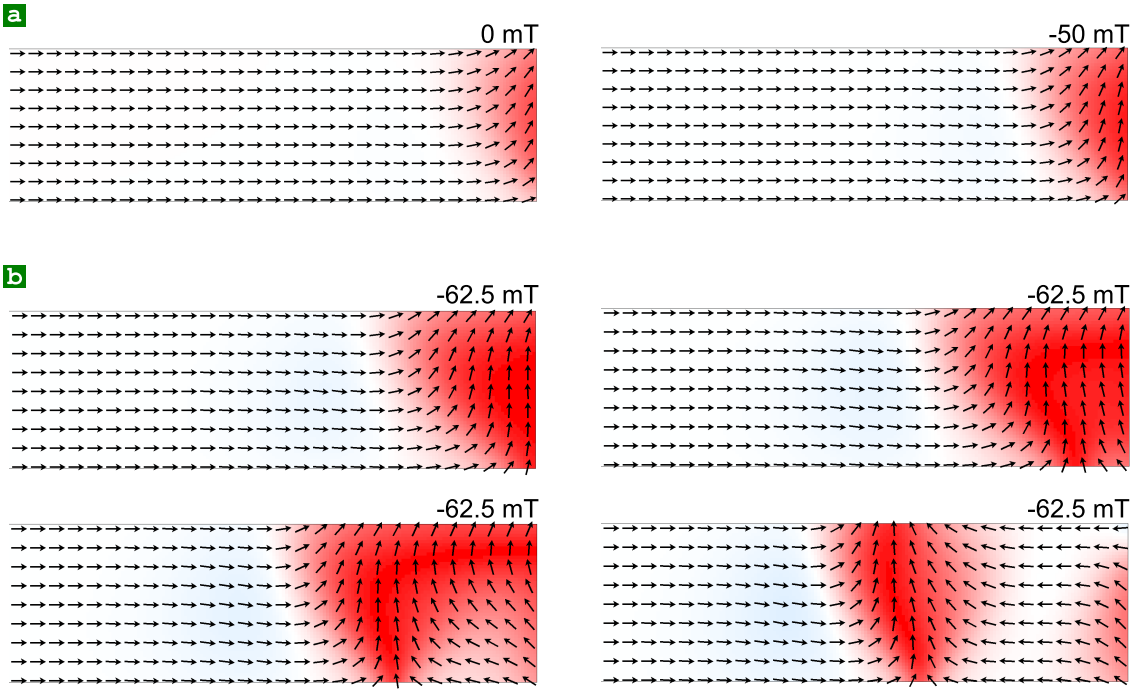

Figure III.7 – Incoherent magnetization reversal in a strip of Permalloy with width $100\,\text{nm}$ and thickness $10\,\text{nm}$, through growth of a nucleation volume, followed by propagation of a domain wall.(a) Magnetization states at equilibrium (b) Snapshots under a fixed field, of magnitude larger than the nucleation field. The value of applied induction field is indicated above each map. The simulations were run with damping parameter $\alpha = 1$ to get simple magnetization configurations, however in real samples α is much smaller than 1. This will be discussed in chap.IV.

arrow-shaped ends[104].

The above scaling law for the nucleation field in strips[103] was derived experimentally at room temperature. Both thermal activation and edge roughness[103, 105] contribute to reduce the nucleation, compared to an ideal system as considered in most micromagnetic simulations.

Summary

In this section we have seen that upon increasing size, the mode of magnetization switching is expected to evolve from coherent, to non-coherent however collective, to finally incoherent (nucleation-propagation).

2.2 Large elements of soft magnetic material

When further increasing its dimensions, a system may contain domain walls to close its flux and thus reduce magnetostatic energy. This is a flux-closure state.

We restrict the discussion here to flat element made of soft magnetic material, for which the number and locus of the domain walls are expected to result from energy minimization. The Van den Berg solutions described in sec.4.1 were extended by Bryant and Suhl[106, 107] when an external field is applied. The model is that of a perfectly soft material with infinite susceptibility, leading to the perfect expulsion of magnetic field (applied plus dipolar), with div $\mathbf{M} = 0$ and zero edge charges. This leads to the description of magnetization as $\mathbf{M} = \mathbf{curl}\,\mathbf{A}$ where $\mathbf{A}$ is a vector potential; magnetization lines happen to be lines of isovalues for A. Unfortunately there is no more a geometrical construction for describing the magnetization state, and the solution shall only be obtained from examining boundary conditions at the lateral edges of the element. Figure III.8a shows an example of the evolution of such flux-closure elements under magnetic field.

Later, more elaborate (numerical) theories were proposed, lifting the constraint of full expulsion of magnetic field[108–110], and considering edge charges. This in principle allows one to fully describe the magnetization curve $M(H)$ of a soft element of large dimensions. Some features of magnetization curves may however be discussed without the need to resolve in detail the magnetization configuration at any field step. We noticed in sec.1.3 that the Zeeman term contributes in principle to a magnetic enthalpy, not an internal energy. In this thermodynamic framework and under quasistatic variation of the applied field, the work provided to the system upon rising the external field is stored as internal energy:

$$E_{\text{int}}(H = \infty) - E_{\text{int}}(H = 0) = \mu_0 M_s V \int_0^1 \mathbf{H} \cdot \mathrm{d}\mathbf{m} \qquad \text{(III.11)}$$

Thus, assuming that a near single-domain state is reached at high field, and neglecting the energy of the remanent state, the area above the magnetization curve equals the demagnetizing energy in the direction considered NK_d. Contrary to the case of a macrospin, and due to the non-uniformity of demagnetizing fields, the $M(H)$ curve is not a straight line with slope $1/N$, but a concave curve with initial susceptibility larger than $1/N$ (Figure III.8c).

Eq.(III.11) holds for infinitely-soft materials only, where the system always resides in a state of minimum energy, with no hysteresis. In the case of hysteresis, implying jumps between local minima of different energy, part of the work provided is lost for the magnetic system and contributes to heating.

The above considerations remain valid in the presence of anisotropy of a microscopic energy such as magnetocrystalline, as long as hysteresis is negligible. In that case both demagnetization energy and anisotropy energy contribute to the area above the curve.

We also neglected the energy of the remanent state that may contain domain walls and vortices, which we know have a finite energy (sec.I.5). As the energy of a vortex is constant and that of a domain wall is linear with its length, their

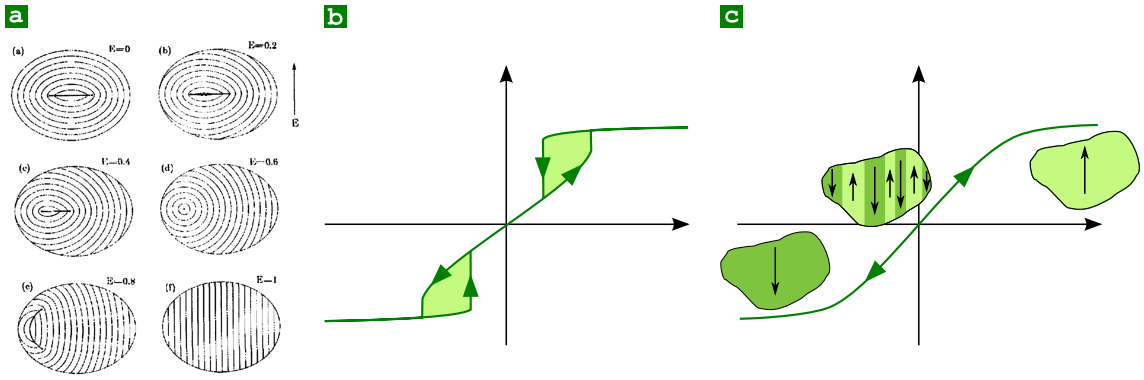

Figure III.8 – Hysteresis loop of flux-closure systems. (a) Numerical solution of a magnetization process in an extended soft element with a flux-closure and one domain wall[106] (b) Hysteresis loop of a soft element of moderate size, for which some hysteresis remains around nucleation / annihilation events of vortices and domain walls (c) Hysteresis loop of a soft element of extended dimensions.

contribution to the average energy (normalized with its area $\sim L^2$) is indeed negligible for large size L of a nanostructure. When the dipolar exchange length is not negligible before L then a sizeable change of moment occurs upon nucleation and annihilation of vortices and domain walls, often associated with hysteresis (Figure III.8b). Besides these objects contribute to a non-zero remanent energy, reducing the area above the magnetization curve[111]. Its measurement is an elegant way to estimate the energy of a micromagnetic state with flux closure, a quantity that cannot be measured directly.

2.3 Motion of domain walls in one-dimensional elements

A domain wall is a two-dimensional object in a bulk system, and takes asymptotically the form of a one-dimensional object in an extended thin film with decreasing thickness. Still decreasing dimensionality, a domain wall may be viewed as a point (a zero-dimensional object) in an essentially one-dimensional system, either a strip or a wire, if the details of its internal structure are ignored (sec.II.4.5). This situation provides the simple example of domain-wall motion, to start with a qualitative feeling. Various models suited to describe magnetization reversal in extended systems in the presence of pinning will be described in sec.3.

Over the past fifteen years studies have been thriving on the motion of domain walls in strips made by lithography. The motion has been set under the stimulus of either magnetic field or spin-polarized current. As this motion implies precessional dynamics, we will study it in detail in chap.IV. Here we provide a quasistatic description of domain wall motion under a quasistatic applied magnetic field.

A domain wall in a one-dimensional system may be modeled as an object moving in a one-dimensional energy landscape, whose examples of microscopic basis will be discussed in the next paragraph. Local minima in the energy

landscape imply trapping or pinning of domain walls. A magnetic field applied in the direction of one of the domains on either side of the wall, applies a pressure on the wall. We call propagation field the magnetic field for which the pressure becomes larger than the pinning force, setting the domain wall in motion. In a quasistatic picture, the domain wall will move until a large enough pinning site is reached.

The microscopic origin for an energy landscape and thus for pinning, may come from the material or from the edges of the track. The former may result from defects such as grains and grain boundaries, affecting exchange, anisotropy and/or magnetization. The latter may come from spatial variations of the strip/wire width or thickness (roughness). Of special focus is edge roughness induced by lithography, either residual[112] or done intentionally[113]. As a general rule the strength of this pinning increases with decreasing strip width, as the source of pinning arises just once at either edge, while the Zeeman pressure scales with the strip width. When roughness is large one may better describe it as a modulation of strip width, either a constriction (local decrease of cross-section) or protrusion (local increase of cross-section). As the total energy of a wall increases with the cross-section of the one-dimensional object, a constriction is expected to act as a potential well, whereas a protrusion is expected to act as an energy barrier.

Investigating domain wall motion in a strip requires a means to create single domain walls. A common way to create domain walls in strips with in-plane magnetization is to design curbed areas along the wires, then apply and remove a large magnetic field along the radius of the curb (Figure III.9a); this was proposed independently by two groups[114, 115]. Upon application of a field larger than the lateral demagnetizing field of the strip, the magnetization becomes essentially oriented along the applied field. When the field is reduced the magnetization progressively rotates back along the local direction of the strip, to decrease magnetostatic energy. The sense of rotation is opposite on either side of the curb, resulting in a head-to-head or tail-to-tail domain wall at remanence. Another common way to create a domain wall is to connect a pad at an end of the strip, whose existing domain walls may serve as a reservoir for injection[116, 117] (Figure III.9b). For a material with in-plane magnetization it is often designed to have a flux-closure pattern to permanently host one or more domain walls. For a material with out-of-plane magnetization the pad is designed with large dimensions, so that the probability to include defects promoting nucleation is high. Yet another way is to pattern a crossed metallic strip run by an electric current to create a local Œrsted field, locally reversing magnetization[118]. This route is again effective for both in-plane and out-of-plane magnetization.

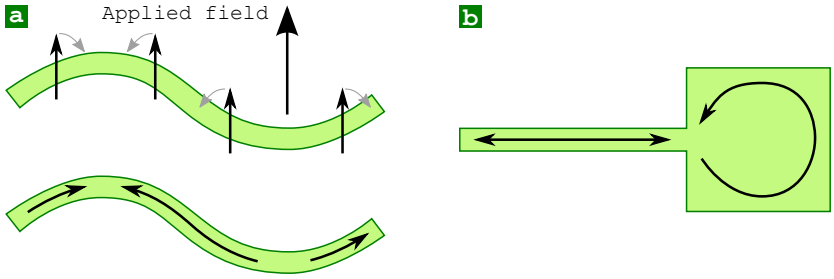

Figure III.9 – (a) **Strategies for the controlled nucleation of domain walls in strips with in-plane magnetization**. Creation of domain walls in a curbed strip upon application (top) and removal (bottom) of a magnetic field along the radius of the curbs. This scheme is valid only for in-plane magnetization (b) Injection of a domain wall in a strip from a reservoir. This scheme is valid both for in-plane (as shown) and out-of-plane magnetization.

2.4 Magnetization processes inside domain walls and vortices

Domain walls define the boundary of domains, and as such have a dimensionality lower by one unit to that of domains. Let us now consider domain walls and vortices as structures in themselves, whose magnetic texture is described by internal degrees of freedom. For example, the core of a magnetic vortex or that of a Bloch domain wall in a film with in-plane magnetization may be pointing either up or down. A Bloch domain wall has also a second degree of freedom: its chirality, or in other words the transverse orientation of its top versus bottom Néel caps (sec.II.3). A Néel wall also has one degree of freedom: its chirality (related to the sign of the transverse magnetization in the core of the domain wall), clockwise or anticlockwise. Can one switch the magnetization underlying these degrees of freedom, in a way similar to the switching of magnetization in a strip or wire?

Although theories had been developed long ago for switching such degrees of freedom[6, 119], their practical realization in extended thin films is problematic, as applied fields induce domain wall and vortex motion. It has only been more recently that such processes could be evidenced when vortices and domain walls are trapped in flux-closure dots, so that their location is not affected by external fields.

Let us first consider the edge curling domain found at the edge of a flat and extended element. Applying a magnetic field along the edge may allow to switch the direction of this edge domain, through the propagation of a localized volume of magnetization pointed perpendicular to the edge[120–122]. The core of magnetic vortex is also a one-dimensional object. Its switching with a magnetic field applied along the core was demonstrated for vortices trapped at the center of micron-sized circular dots[123]. This magnetization process requires the nucleation and propagation of a zero-dimensional object, the Bloch point[75]. Topological constraints (the boundary conditions) indeed require that the magnitude of magnetization be zero at some location during the course

of magnetization reversal. Notice that this process is poorly reproduced by micromagnetic simulations[124], because its characteristic length scale is close to the atomic size. Yet another one-dimensional magnetization texture is the Néel caps found at surfaces of a Bloch domain wall, as discussed in sec.II.3.1. Switching of Néel caps is also possible, by application of a magnetic field in the direction transverse to the wall, *i.e.* parallel to the magnetization in the Néel cap[125]. This process does not require a Bloch point, however is achieved through the motion of a surface vortex.

Summary

Magnetization reversal in nanostructures. As soon as the size of a system is larger than a few times the smallest characteristic length scale, magnetization reversal occurs in a non-uniform fashion, even if at rest the system is mostly uniformly-magnetized. Reversal modes may include curling for small systems with a uniaxial symmetry, and other collective modes *e.g.* for large structures made of a soft magentic material with in-plane magnetization.

3 Magnetization reversal in extended systems

We consider now systems with macroscopic lateral dimensions, with in mind mostly the case of thin films. It is then impractical to describe all domains and domain walls in detail. Magnetization switching must be described by statistical means, and understood on the basis of effective models. We introduce the concepts of nucleation and propagation, and magnetic aftereffects, which are standard concepts in magnetic materials science.

3.1 Description of the question at stake

In sec.1 we introduced the Stoner-Wohlfarth model, describing magnetization reversal of single-domain systems. The model predicts an angular dependence of the coercive field scaling with the anisotropy field, be it of magnetocrystalline or shape origin. Experiments show that in most cases the coercive field of extended systems is much lower than these predictions, sometimes by one to two orders of magnitude. This discrepancy is known as the Brown paradox, and was an early issue of micromagnetism.

In the previous section (sec.2) we discussed that releasing the constraint of uniform magnetization reduces the energy along the pathways for magnetization reversal. This is analogous to the consideration of static cases in chap.II, for which releasing this constraint allows in most cases to reduce the energy of a system at rest. Non-uniform reversal modes are then favored, with a coercive field smaller than predicted by the Stoner-Wohlfarth model. In both cases, static

configurations and reversal pathways, most examples of non-uniform configurations discussed so far resulted from the magnetic anisotropy, size and overall shape of the system. Such ingredients and their related consequences are named intrinsic. Figure III.7 provides an example of intrinsic nucleation of magnetization reversal. However a real system has nearly always defects in its structure: grains and grain boundaries, inclusion of other phases, variations of composition or crystal ordering, roughness (of special relevance for low-dimensional systems)[III.4]. Such ingredients and their consequences on magnetization reversal are named extrinsic.

In practice both intrinsic and extrinsic phenomena affect magnetization reversal. However the number of defects increases with system size, so that in general the larger the systems, the more extrinsic effects tend to determine magnetization reversal. Depending on the phenomena involved the reversal may take several forms such as continuous rotation of magnetization inside domains, successive switching of individual grains or small nuclei, propagation of domain walls etc. Due to the large number of degrees of freedom involved in extended systems, these phenomena may be described only macroscopically and phenomenologically. It is the role of models to extract signatures of the underlying phenomena, from experimental statistical or averaged quantities. It is necessary to identify these microscopic phenomena in order to control them and tailor the macroscopic properties of a material.

In the following we first examine simple examples of pinning models, to highlight the physics of extrinsic magnetization processes. Then we discuss the effect of temperature, helping to overcome energy barriers against pinning or nucleation, and introduce the concepts of activation volumes and magnetic aftereffects. Finally we come back to practical cases of models, applied to deriving energy barriers and laws for aftereffects. We will show how the various types of physics at play at the microscopic scale may be inferred through their temperature- or waiting time dependence.

3.2 Zero-temperature views

Some of the earliest models for extrinsic coercivity are based on the propagation of a domain wall in a heterogeneous medium. In 1932 Bloch provided a calculation for the width and the energy of a domain wall[50]. Becker had already stressed that inhomogeneities of strain must induce variations of the strength and direction of the easy axis of magnetization due to magnetostriction, and the same year as Bloch he proposed that this is a source of pinning for domain walls[126]. In 1937 Kondorski quantified this effect, making a link between coercivity and a one-dimensional energy landscape arising from strain[127]. This is known as the Becker or the Kondorski model. Here we keep from this early work only

[III.4] We briefly mentioned it and took it into account phenomenologically in the previous section, in the Kondorski model, see sec.2.3

the simple picture of a one-dimensional energy landscape $\mathcal{U}(x)$ (Figure III.10). We remain at the phenomenological level, so that $\mathcal{U}(x)$ may reflect a variety of situations such as defects affecting anisotropy or exchange, the lateral size of a system such as width in a strip, diameter in a wire[128], thickness in a film etc. Important to notice as an approximation is that the domain wall is considered as pinpoint in this model. The link between the energy landscape and the propagation field is the focus of problem 4. In short, for an applied field favoring motion of the domain wall along $+x$, the field needed to achieve propagation is:

$$H_p = \frac{1}{2\mu_0 M_s}\frac{d\mathcal{U}}{dx} \tag{III.12}$$

The propagation field is thus determined by the steepest rising slope of $\mathcal{U}(x)$, as illustrated on Figure III.10a-b. Let us consider the simple case of a flat landscape with a local variation. A maximum of $\mathcal{U}$ gives rise to an energy barrier. This hinders the propagation of the domain wall, however does not prevent its going backwards if the field is reversed (Figure III.10c). To the contrary, a minimum of $\mathcal{U}$ is a potential well into which a domain wall is trapped (Figure III.10d). Once there it is prevented to move in either direction, unless a field of sufficient magnitude is applied, a so-called depinning field. In practice one expects a distribution of local propagation fields, unless the source of defects is well controlled and reproducible from one place to another. A gaussian distribution of defects is then expected to induce a propagation increasing logarithmically with the length of the segment considered[128]

The reading of the Kondorski formula is the following: for propagation to occur, the increase of internal energy must be compensated by the energy provided by the operator through the Zeeman term. The factor 2 accounts for the fact that upon a change of position δx, a volume with initially down magnetization is converted into an up domain, associated with a difference of energy $2\mu_0 M_s H$.

Eq.(III.12) may be extended to the case of an external field applied at an angle θ with magnetization in the two domains. For a 180° domain wall M_s is simply replaced with $M_s \cos\theta$, provided that the magnitude of the applied field is small compared to the anisotropy field; in other words: the magnetization in the domains remains essentially fixed along the direction of easy axis. If these propagation fields control magnetization reversal, then one expects the coercive field to vary like $1/\cos\theta$. Notice then the minimum and rather flat variation close to the easy axis of magnetization. When measured experimentally, this is considered as a signature of a propagation phenomenon. The $\cos\theta$ may also be viewed as related to the susceptibility of the core of the domain wall, making an angle θ with the applied field. The similarity with the curling model for large system radius (Figure III.6) is understandable as in this case the orthoradial component of magnetization, which appears spontaneously to reduce magnetostatic energy,

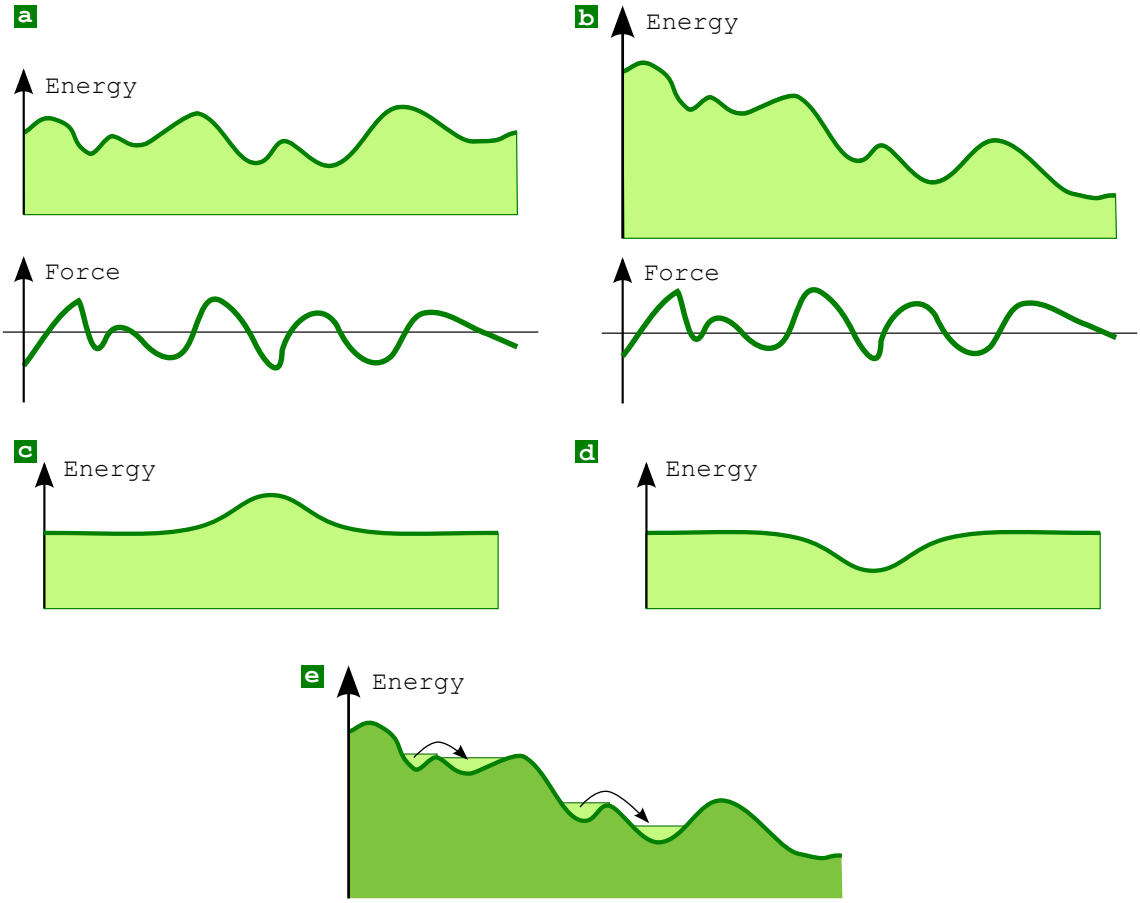

Figure III.10 – One-dimensional model for domain-wall motion. (a) Energy and the associated force under zero magnetic field (b) Similar plots with a magnetic field added (c-d) An energy barrier and an energy well (e) The energy landscape depicted in b in the presence of thermal energy. The lighter green areas show the states reachable through thermal excitations, and arrows indicate energy barriers that may be crossed.

has the same orientation as the core of a domain would have, with susceptibility proportional to $\cos\theta$.

When the scale of the spatial variation of the properties of a material is comparable or larger than the domain wall width, the Kondorski model may readily be applied with $\mathcal{U}(x) \approx 4\sqrt{A(x)K(x)}$ (see sec.I.5), or any other type of formula for the domain wall energy if applicable. However, when the spatial variation of a property becomes significant at the scale of a domain wall, then its impact on the micromagnetic arrangement of the wall must be studied to derive $\mathcal{U}(x)$. In this case x is, *e.g.*, the center of mass of the domain wall. Let us provide an example, proposed by A. Aharoni[129]. This author considers a uniaxial anisotropy of second order varying in space $K(x)$ with simple shapes (Figure III.11).

The first case considered is that of a soft inclusion in the material: $K = 0$ for $|x| \leq d$, and $K = K_0$ elsewhere. This inclusion induces a potential well for the domain wall, centered at $x = 0$. In the limit $d \ll \Delta_u$ the depinning field scales with $H_a d/\Delta_u$ (see problem 4). The meaning of this law is straightforward: when

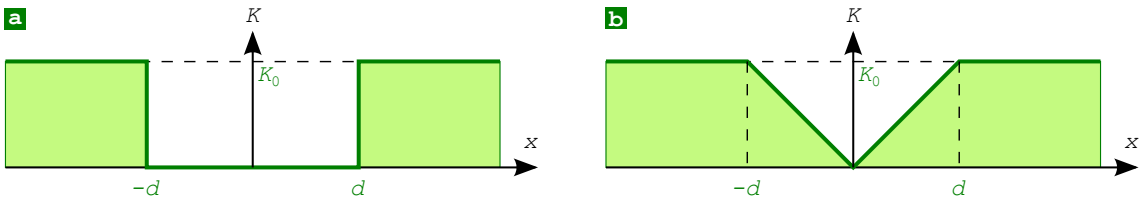

Figure III.11 – Simple models of defects favoring local nucleation, or the pinning of domain walls.

the domain wall overlaps the defect no anisotropy energy is paid over a length d, resulting in a potential well of the order of $K_0 d$. If moving by Δ_u the domain wall leaves the defect, yielding a gradient of energy scaling with $K_0 d/\Delta_u$. The scaling law is then derived easily from Eq.(III.12). If no domain wall pre-exists, the defect allows to nucleate one at a field lower than the anisotropy field of the non-defective phase. As the defect is only a perturbation to the main phase, the nucleation volume may be viewed as an entity subject to coherent switching. The angular law for nucleation events is thus expected to show some similarity with the Stoner-Wohlfarth law, *i.e.* displaying a maximum for the field applied close to the easy axis of magnetization. Now consider the limit $d \gg \Delta_u$. At the scale of micromagnetism, it is as if two extended materials exist: one soft, one hard. Thus, a reversed domain may be created under a low applied field $H_n \ll H_a$ in the soft material, like in any extended system made of a soft magnetic material. Once the reversed domain is nucleated, a domain wall will be located at each boundary with the hard magnetic material, requiring a larger value of applied field to allow its propagation into the hard phase. Simple arguments considering energies and length scales as above, show that the propagation field scales with H_a, while the exact calculation provides: $H_p = H_a/4$[129, 130].

The second case considered is a linear variation of $K(x)$. The nucleation or propagation fields may then both be as small as desired, by choosing a small gradient of energy, in other words a large d. This model was revived recently by the proposal of the use of grains for hard disk drive media with a spatially graded anisotropy. These allow to decrease the switching field thanks to the moderate gradient of energy, while preventing spontaneous magnetization switching thanks to the height of the energy barrier still related to K_0[131].

Angular dependance of coercivity as a probe of the reversal mechanism. In the series of examples above we illustrated the concepts of nucleation and propagation phenomena, used to describe magnetization reversal in extended materials. The examination of the angular variation of coercivity is a mean widely used to determine which is the phenomenon limiting magnetization reversal. In practice the situation may be less clear, as there is no strict border between the two phenomena.

Switching versus coercive fields. Remember that the Stoner-Wohlfarth model predicts the switching field, which coincides with the coercive field only for $|\theta \leq \pi/4|$. Thus, for the analysis of the angular variation of magnetization reversal over a large range to determine whether nucleation or propagation is the best description for magnetization reversal, what needs to be measured is the switching field, related to irreversible events only. One way to do this is apply a negative field of given magnitude, then measure the resulting magnetization when back to remanence. This eliminates irrelevant processes from the measurement, such as the reversible rotation of magnetization in domains.

3.3 Activation volume

In part sec.1.1 we derived an expression for the energy barrier of a macrospin, involving the product KV [Eq.(III.3)]. Here we introduce a similar concept for the phenomenological description of extended systems. Right above we discussed that in extended systems magnetization reversal may be determined by local processes such as nucleation, pinning and propagation of domain walls. Thus, the energy barrier preventing magnetization reversal concerns a volume much smaller than its total volume V. We shall name it an activation volume and write it V_a. In Eq.(III.3) V shall thus be replaced with V_a. Note that the name and writing nucleation volume V_n is also often used, however it introduces some confusion with the nucleation and propagation processes, as here we aim at describing any type of thermally-activated magnetization process. We will thus stick to the name activation.

Besides, due to extrinsic or intrinsic deviations from the macrospin situation, switching will occur before H reaches H_a. We shall therefore replace the latter with a parameter $H_{c,0}$, the coercive field in the limit of zero temperature. Also, the magnetization process may involve energies other than magnetocrystalline, such as exchange energy. While detailed models take this into account, for the sake of simplicity we will keep K here. Finally, the power law may be different from a square law, depending on the situation and thus its modeling. In the end we generalize Eq.(III.3) with the expression:

$$\Delta\mathcal{E} = KV_a \left(1 - \frac{H}{H_{c,0}}\right)^{\alpha} \tag{III.13}$$

where α is an exponent *a priori* not equal to 2. This expression determines the time and temperature dependence of magnetization processes as in sec.1.2. A

similar analysis yields the following relationship:

$$\alpha \ln\left[1 - \frac{H_c(T)}{H_{c,0}}\right] = \ln\left[\frac{k_B T \ln(\tau/\tau_0)}{K V_a}\right] \tag{III.14}$$

Experimentally, plotting $\ln(1 - H/H_{c,0})$ versus $\ln T$ or $\ln(\ln \tau)$ allows to extract numbers for α and V_a. In practice V_a is of the order of δ^3 with δ the domain wall width. The plots and notably the value of α, compared to various models for magnetization reversal, provide hints for the processes at play in determining coercivity. It may thus be used to compare various samples and improve their properties. However several possible biases must be present:

- The anisotropy coefficients are temperature-dependent. Not only the real $K(T)$ function should be used in Eq.(III.14), but deriving this equation in practical cases shows that a correction should also be included along side in $H_{c,0}$.
- The determination of $H_{c,0}$ is required for these plots, although measurements can never be performed at strictly zero temperature. As the variation of coercivity is expected (and confirmed) to increase at low temperature (Figure III.3), extrapolation from a series of measurements at several temperatures is required.
- Magnetization processes may vary with temperature, affecting this formula. For example α may be obtained as an expansion in models, so that depending on the temperature range and thus height of the barrier probed the effective α will vary.

In the next paragraph we give a few simple examples of energy barriers.

The time or temperature dependence of coercivity may be analyzed to provide indications of the microscopic mechanisms determining magnetization reversal.

3.4 Practical cases and models

A one-dimensional energy landscape may be described locally with the following expansion:

$$\epsilon = ax + bx^2 + cx^3 + dx^4 + \dots \tag{III.15}$$

Here dimensionless variables are used. x is the internal degree of freedom describing the state of the system, and a to d are coefficients depending on the applied field h. The latter are assumed to display no specific feature such as singularities, and may thus be expanded linearly at any location. This expression may describe many situations, where x stands for the location of a domain wall, direction of magnetization: in a macrospin, a domain wall or nucleation volume. Besides, it is suitable to describe magnetization reversal as well as moderate

deviations from uniform magnetization, such as edge domains, curling structures etc.

We consider the above expression to describe a system in a local energy minimum at x_m, being metastable however not the lowest energy state. We aim at determining the field-dependent energy barrier preventing magnetization switching. Only results are provided here; more details can be found in problem... A thorough discussion can be found in Ref.[2]. Notice that in general x_m depends on h. To go further it is useful to consider the symmetry around the local energy minimum. For symmetric and non-symmetric barriers it is always possible to rewrite Eq.(III.15) in the respective forms:

$$\epsilon = \tilde{b}\tilde{x}^2 + \tilde{d}\tilde{x}^4 + \dots \quad \text{(III.16)}$$

$$\epsilon = 2(\tilde{a}\tilde{x} + \tilde{c}\tilde{x}^3) + \dots \quad \text{(III.17)}$$

$\tilde{x} = x - x_0$ where $x_0(h) = x_m(h)$ for a symmetric barrier (in general x_m is independent from h), and $x_0(h)$ is the locus of the inflexion point on the side of lowest energy barrier for asymmetric barriers. We end up in purely even and odd functions. In the even situation an irreversible event is described by $\tilde{d} < 0$ and $\tilde{b}$ changing sign from positive to negative (Figure III.12a). The energy barrier is then characterized by $\alpha = 2$. This situation boils down to the Landau functional describing phase transitions, and describes for example magnetization switching of a macrospin with magnetic field applied exactly along an easy axis of magnetization [Eq.(III.1)]; x is in that case θ, the direction of magnetization. In the odd case an irreversible event is characterized by arvitrary $\tilde{c}$ and $\tilde{a}$ changing sign from initially opposite to the same sign as $\tilde{c}$ (Figure III.12b). The energy barrier is then characterized by $\alpha = 1.5$. This situation is that found in the Becker-Kondorski model, where x is the locus of the domain wall. It is also the case of magnetization switching of a macrospin with the magnetic field applied away from an easy axis of anisotropy. With this in mind, it is clear that the odd case is the general situation, while the even case is an exception. It can be checked mathematically that the transformation from Eq.(III.15) to Eq.(III.17) is in general always possible, while transformation to Eq.(III.16) requires special relationships between the coefficients. Thus the barrier exponent $\alpha = 1.5$ is the most common case[132]. The above examples are simplified pictures of nucleation and propagation events in extended systems.

When one tries to describe in more detail or more realistically real nucleation and propagation events, the resulting models may not be described by a polynomial function such as Eq.(III.15) with barriers canceling around symmetric or asymmetric energy wells. Laws for energy barriers scaling with $H^{-\mu}$ may be derived in some cases, as detailed below.

An example of such a model for nucleation is the droplet model, topic for problem 5. This model gets its name from the analogy with supercooled in hydrodynamics, where the temperature driving force for vaporization is contained by the cost of surface energy required to create a bubble of gas in the liquid. Let

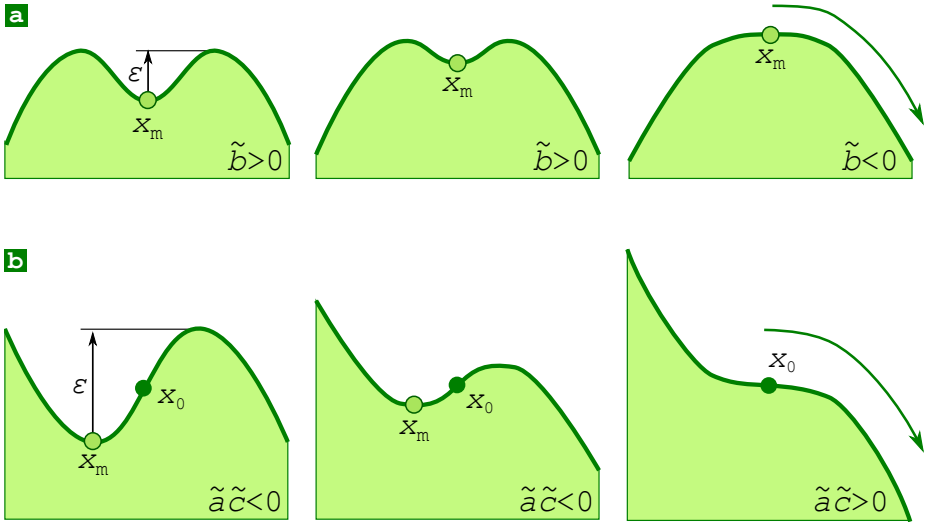

Figure III.12 – Evolution of symmetric and antisymmetric energy barriers up to switching.

us consider the case of a thin film, initially uniformly magnetized. The picture for a nucleation bubble consists of a circular domain with reversed magnetization, separated from the rest of the film by a domain wall. If one considers a bubble large enough so that the domain wall can be identified clearly, the energy of a bubble with radius R reads:

$$\mathcal{E}(R) = \left(2\pi R\Gamma_w - 2\pi R^2\mu_0 M_s H\right) t. \tag{III.18}$$

The first term is the cost for the domain wall with energy per unit area Γ_w, while the second is the gain in Zeeman energy inside the bubble. No bubble ($R = 0$) is a local minimum due to the linear cost in wall energy, *i.e.* it is a metastable solution, while above a critical radius the quadratic gain in Zeeman energy drives the expansion of the bubble. These two limiting cases are bounded by an energy maximum for a critical radius R_c, *i.e.* spotting an unstable equilibrium situation whose crossing means nucleation. The associated energy barrier is readily calculated as $\Delta\mathcal{E} = \pi\Gamma_w^2 t/(2\mu_0 M_s H)$. The energy barrier does not vanish for any finite value of applied field, so that no barrier exponent may be defined. The use of the Arrhenius law yields the temperature dependance of the nucleation field: $H_n(T) = (\pi/2)(t\Gamma_w^2)/[\mu_0 M_s k_B T \ln(\tau/\tau_0)]$. As expected the nucleation field decreases with increasing temperature. Other droplet models can be developed for specific geometries of finite-size systems, such as at the edge of a finite-size platelet[133] or strip[134, 135]. Other variational parameters may be used besides the bubble radius, such as to describe a non-circular shape, however its main features remain qualitatively valid. Note that if in the above we assume $\Gamma_w \sim \sqrt{AK}$ and the wall width scales like $\Delta_u = \sqrt{A/K}$, then $\Delta\mathcal{E} \sim t\Delta_d^2 K$. The later can be understood in terms of an activation volume, scaling like $t\Delta_d^2$ (thickness times the minimum area of a domain wall).

Validity of droplet models. Droplet models may be suited for a high temperature regime, however they fail at low temperature where the nucleation volume shrinks and thus the picture of a well-defined domain wall is not valid. A micromagnetic model must instead be used.

As regards propagation, a one-dimensional picture may not be sufficient to describe a domain wall. Random-pinning models have been proven experimentally to be quite successful for describing a two-dimensional energy landscape within which a domain wall may meander to find its way at the lowest cost of energy. The theory weighs the cost in elastic energy (length of the domain wall) with the trend for the wall to meander through randomly-distributed places of low local energy. Its derivation is rather complex and makes use of microscopic parameters such as energy and length scales characterizing the energy landscape, and predicts that $\mu = 1/4$[136]. At finite temperature and under an applied magnetic field the domain wall resides essentially at rest for some time in a given configuration, before a burst of thermal energy allows it to cross an energy barrier. It then propagates over a certain distance before it is again blocked until another activation event may allow its further progress. This way of propagation with discrete jumps is called the creep regime and is a common feature of thin films with a non-negligible distribution of defects or spatial fluctuations of magnetic anisotropy, and subject to a magnetic field of moderate magnitude. The creep regime is a possible microscopic mechanism for the long-recognized Barkhausen jumps measured macroscopically. Investigation of this regime informs us about the local fluctuations in the film.

Similar to the simplest picture of the Becker-Kondorski model, domain walls may propagate continuously even through distributed pinning sites if a magnetic field of sufficient magnitude is applied. This is the so-called flow regime, whose nature is intrinsically precessional and will thus be described in the next chapter.

Summary

Magnetization reversal in extended systems. Magnetization reversal occurs generally by the nucleation of one or several small volumes with reversed magnetization, followed by propagation of domain walls reversing the remaining of the system. Both phenomena are thermally-activated, and can be described by models to extract microscopic information about the material and the defects or geometric features involved.

Problems for Chapter III

Problem 1: Self-testing

1. What is the difference between the concepts of switching field and coercive field?
2. In the Stoner-Wohlfarth model, for which directions of the applied magnetic field the switching field is the smallest? The largest? What are the values?
3. How does the blocking temperature vary with the volume of a magnetic system?
4. What is the Langevin function, and in which case is it applied to a magnetic system?
5. What can be learned from the remanence of an assembly of small grains?
6. What is curling in micromagnetism?
7. A magnetic system is nearly uniformly-magnetized at rest. Do this imply that magnetization reversal proceed following the Stoner-Wohlfarth model?
8. Describe the principle of the Becker-Kondorski model for domain-wall propagation.
9. What is the typical dimensions of a nucleation volume?
10. What is the scaling law describing the height of an energy barrier preventing reversal, against the applied field? Comment on the critical exponent.

Problem 2: Short questions

1. Give a realistic example of a magnetically-uniaxial system whose coercivity H_c is larger than its anisotropy field H_a (the latter taking into account both magnetocristalline and shape anisotropy for uniform magnetization).
2. Look closely at the switching field on the Stoner-Wohlfarth curve for θ_H = 80°, Figure III.1b. You will notice that $\mathrm{d}m/\mathrm{d}H < 0$ at the jump. DIscuss whether this violates a law of conservation of energy.
3. It was mentioned in chap.I (see p.17) that the remanence of a magnetic

system is in general positive. Give an example of a magnetic system displaying a negative remanence (hint: consider a system made of two sub-systems with different coercivities and moments, and coupled through an interaction, *e.g.* of dipolar origin). A negative remanence implies that the up and down curves forming the hysteresis loop cross each-other. Discuss whether or not this violates the conservation of energy based on the argument of the area encompassed inside a hysteresis loop (Figure I.3).

4. We consider a uniformly-magnetized system with uniaxial magneto-crystalline anisotropy of volume density K, volume V and zero applied field. The effect of thermal energy is taken into account with the Arrhenius law for the waiting time to overcome an energy barrier $\Delta\mathcal{E}$: $\tau = \tau_0 \exp \Delta\mathcal{E}/k_B T$. $k_B \approx 1.38 \times 10^{-23}$ S.I. is the Boltzmann constant, and $\tau_0 \approx 100$ ps. Express the height of the barrier required so that the system has not switched after a given time τ at a given temperature. To set numbers, we consider a material with $K = 7 \times 10^4$ J/m^3 at the temperature 500 K. Provide an estimate of the minimum length a of the edge of a cube of such material, so that magnetization has remained stable over three years. For the numerical estimate, you may use this approximation: $\ln(10^8) \approx 18$.
5. Derive the formulas for remanence m_r and remagnetization energy E_K for the various cases of texture provided in sec.1.5.
6. Read the seminal paper of Frei about magnetization curling[100] and convert the values of nucleation and coercive fields in the SI system.
7. If a system is mostly uniformly-magnetized at rest (under zero of constant applied field), does this mean that the process for magnetization reversal is uniform? Comment.

Problem 3: Herzer model for coercivity in nanocrystalline materials

The purpose of this problem is to outline trends for the coercivity of magnetic materials made of exchange-coupled nanograins. In the entire problem we assume that magnetostatic energy may be neglected. This is known as Herzer's model[137, 138].

3.1. The material

We consider a magnetic material with a uniaxial magnetic anisotropy with magnitude per unit volume K_g, spontaneous magnetization M_s and exchange stiffness A. Based on dimensional analysis provide an expression for the domain wall width and its areal density of energy. We will write $\Delta_g = \sqrt{A/K_g}$ the anisotropy

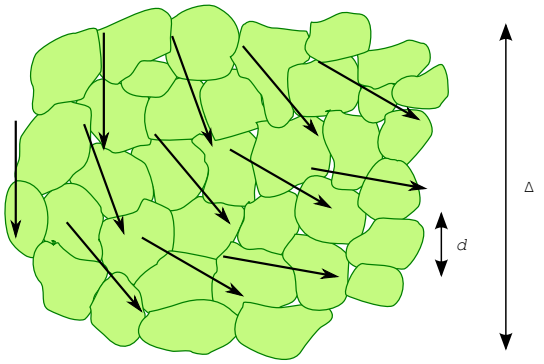

Figure III.13 – Effective anisotropy averaged over many grains. The magnitude of anisotropy is averaged over a large number of grains N_{3D} within a domain wall.

exchange length of the material.

3.2. Averaging anisotropy

We consider grains of typical size d arranged in a polycristalline fashion, *i.e.* with a random distribution of easy axis in space. Each grain is coupled with its neighbors through ferromagnetic exchange.

Let us first consider two neighboring grains only. Based on simple scaling laws, show for which range of values of d magnetization is expected to be essentially uniform over the two grains, and on the contrary for which range the direction of magnetization may vary significantly over the two grains. In the following we consider the first situation.

Let us write Δ_{3D} the domain wall parameter in such a material, and consider first a bulk material (three-dimensional). Δ_{3D} is the length over which the direction of magnetization may not vary significantly in any of the three directions. Thus the effective anisotropy energy K_{3D} in this volume will be that averaged over the (large) number of grains N_{3D} in the volume: $K_{3D} = K_g/\sqrt{N_{3D}}$ (Figure III.13). Based on the fact that $\Delta_{3D} \approx \sqrt{A/K_{3D}}$, provide an expression for both Δ_{3D} and K_{3D}. Explain how one may infer a scaling law for the variation of coercive field with grain size d in such a material.

3.3. Dimensionality effects

Generalize the above calculation for a two-dimensional (Δ_{2D} and K_{2D}) and one-dimensional (Δ_{1D} and K_{1D}) material. Comment.

3.4. Numerical evaluation

We consider a material with anisotropy induction $\mu_0 H_a = 10\,\mathrm{mT}$, spontaneous magnetization $M_s = 8 \times 10^5\,\mathrm{A/m}$, exchange stiffness $A = 10^{-11}\,\mathrm{J/m}$ and grain size

$d = 10\,\mathrm{nm}$. Provide estimates for Δ_g, Δ_{3D} and K_{3D}. Comment.

Problem 4: A model of pinning - Kondorski's law for coercivity

In an extended system magnetization reversal often proceeds through nucleation of small reversed domains, followed by their inflation through motion of domain walls. Domain wall motion may however be hampered by local heterogeneities in the material. This sets a finite value of applied field necessary for the propagation, thus for magnetization reversal and coercive field. It is the purpose of this problem to make the link between material inhomogeneities and coercivity.

4.1. Energy landscape and propagation field

We consider a domain wall in a one-dimensional framework, as for deriving the profile of the Bloch domain wall, see Pb. 5. Let us assume that the material inhomogeneities create an energy landscape $\mathcal{U}(x)$ for the domain wall, where x refers to the location of the wall, *e.g.* its center. Energies are expressed in $\mathrm{J/m^2}$, related to the translational invariance in the two directions perpendicular to x. Assuming that an applied field does not change significantly the profile of the domain wall, and hence its internal energy $\mathcal{U}(x)$, consider the extra term of the Zeeman energy to derive a condition defining the propagation field. The magnetic is applied along the direction of magnetization in the domains.

4.2. An example of energy landscape

Starting from a homogeneous material let us model a local defect in the form of a magnetically softer (*i.e.* anisotropy constant $K - \Delta K$ with $\Delta K > 0$) insertion of width $\delta\ell$, located at position $x = 0$. Discuss what approach should be followed if one wished to derive exactly the profile of the domain wall, especially the boundary conditions at the edges of the defect. Past these considerations, to handle simple algebra we make the assumption of a rigid domain wall, *i.e.* Eq.(I.41) still holds:

$$\theta(u) = 2\arctan\left(\exp\frac{u-x}{\Delta_u}\right) \tag{III.19}$$

where x is the locus of the center of the domain wall. We also assume that the defect is a perturbation, in the sense that $\delta\ell \ll \Delta_u$.

Under these conditions, show that the energy of the domain wall with center at location x reads:

$$\mathcal{U}(x) = 4\sqrt{AK}\left[1 - \frac{1}{4}\frac{\delta\ell}{\Delta_u}\frac{\Delta K}{K}\frac{1}{\cosh^2(x/\Delta_u)}\right] \tag{III.20}$$

Draw a schematic graph of $\mathcal{U}(x)$ and display the characteristic length or energy scales.

4.3. The propagation field

An external field is then applied along the easy axis of magnetization, ie parallel (resp. antiparallel) to magnetization in the domains. Show that the propagation field of the domain wall over the defect reads:

$$H_p = H_a \frac{\Delta K}{K} \frac{\delta \ell}{\Delta_u} \frac{1}{3\sqrt{3}}. \tag{III.21}$$

where $H_a = 2K/\mu_0 M_s$ is the so-called anisotropy field. How is this law modified when the field is now applied with an angle θ_H with respect to the easy axis direction in the domains? To do this, assume that $H \ll H_a$

Notice:

- The $1/\cos\theta_H$ dependence of coercivity is often considered as a signature a weak-pinning mechanism, a law known as the Kondorski model[127].
- This model had been initially published in 1939 by Becker and Döring[139], and is summarized *e.g.* in the book of Skomski: *Simple models of Magnetism*[5].
- While coercivity requires a high anisotropy, the latter is not a sufficient condition to have a high coercivity. To achieve this one must prevent magnetization reversal that can be initiated on defects (structural or geometric) and switch the entire magnetization by propagation of a domain wall. In a shorthand classification one distinguishes coercivity made possible by hindering nucleation, or hindering the propagation of domain walls. In reality both phenomena are often intermixed. Here we modeled an example of pinning.
- Simple micromagnetic models of nucleation on defects[129] were the first to be exhibited to tentatively explain the so-called Brown paradox, *i.e.* the fact that values of experimental values of coercivity in most samples are smaller or much smaller than the values predicted by the ideal model of coherent rotation[91].

Problem 5: Droplet model for nucleation

Here we are concerned with a simple model of nucleation of a reversed domain in a material with magnetization M_s and exchange stiffness A. Starting from a uniformly-magnetized domain, we assume that a so-called bubble of radius R of reversed magnetization is nucleated thanks to a thermal fluctuation. We examine whether the bubble expands or collapses, subject to an external field applied antiparallel to the initial direction of magnetization. Let us write Γ_W the

energy per unit area of the domain wall between the non-reversed domain and the interior of the bubble. For numerical evaluation we will consider $K = 10^6\,\mathrm{J/m^3}$ and $A = 10^{-11}\,\mathrm{A/m}$. We recall: $k_B = 1.38 \times 10^{-23}\,\mathrm{m^2 \cdot kg \cdot s^{-2}}$.

5.1. Three-dimensional case

We consider a bulk material, so the bubble is a sphere.

1. Based on crude geometrical approximations, write the total energy of the bubble $\mathcal{E}(R)$, taking into account the wall energy and the Zeeman energy. Find the stable and unstable positions for $\mathcal{E}(R)$, the latter defining the critical radius R_c that you shall write. Make a sketch for $\mathcal{E}$. Describe the evolution of the bubble depending on the value of its radius.
2. Calculate the energy barrier $\Delta\mathcal{E} = \mathcal{E}(R_c) - \mathcal{E}(0)$ to be overcome so that nucleation is successful and leads to the propagation of the domain wall on a long scale in the domain.
3. Assume an Arrhenius law for overcoming the barrier by thermal fluctuations: the mean waiting time is $\tau = \tau_0 \exp(\Delta\mathcal{E}/k_B T)$. From this, calculate the expected thermal variation of the coercive field $H_c(T)$ for a given waiting time τ.
4. We now assume $\Gamma_W = \sqrt{AK}$, and a domain wall width $\delta = \sqrt{A/K}$. Explain why the model may be valid only if $R_c \gtrapprox \delta$. Write what condition this sets on H. Calculate the coercive field at this cross-over. Comment.
5. Rewrite $H_c(T)$ using A and K, and provide a rough numerical evaluation for the cross-over temperature based on $\ln(\tau/\tau_0) = 25$.

5.2. Two-dimensional case

We consider now a film with thickness t, so that the bubble is a disk with thickness t and radius R.

1. Calculate again the energy barrier and the critical radius.
2. Calculate the temperature dependence of the coercive field, and the cross-over temperature. Provide a numerical evaluation for the cross-over temperature for $t = 1\,\mathrm{nm}$. Comment about the coercive field expected at room temperature.

5.3. One-dimensional case

We consider now consider a wire with a cross-section with area S, so that the bubble is a segment of wire with length $2R$.

1. Explain why the previous calculations cannot be extended to one dimension as is. Explain why you may write as an approximation, instead: $\Delta\mathcal{E} = (8\sqrt{AK} - 4\mu_0 M_s H\sqrt{A/K})S$.
2. Derive $H_c(T)$ from the above expression.

3. Show that the system becomes superparamagnetic, and provide an expression for the blocking temperature T_B. Make a numerical evaluation for section $S = 10^{-18}$ m^2.

Chapter IV

Precessional dynamics of magnetization

Overview

In the previous chapters we have considered the arrangement of magnetization at rest, then its quasistatic evolution with time. At typically the nanosecond time scale a crossover occurs, below which the time evolution of magnetization is mostly governed by precession around the local effective magnetic field. The resulting phenomena are drastically different, and request specific consideration. In this chapter we review the physics of spin precession, and then examine a few cases of precessional dynamics in nanomagnetism: ferromagnetic resonance, precessional switching of magnetization, and domain wall motion.

1 Ferromagnetic resonance and Landau-Lifshitz-Gilbert equation

Only simple features of precession of magnetization are described in the following, meant as an introduction to the topic. More detailed and rigorous coverage may be found elsewhere, *e.g.* in the book of D. D. Stancil and A. Prabhakar[140].

1.1 Precession

Precession of magnetization around a magnetic field is the direct consequence of the angular momentum underlying magnetic moments. Let us first consider a magnetic moment $\boldsymbol{\mu}$ of purely orbital nature (*i.e.*, no contribution from spins), modeled in a classical fashion with a circular loop of current: $\boldsymbol{\mu} = \mathbf{S}I$. $\mathbf{S}$ is the vector area normal to the loop of current, and I is the current flowing in the loop. It is readily shown that

$$\boldsymbol{\mu} = \frac{e}{2m}\boldsymbol{\ell} \tag{IV.1}$$

where e is the charge of the charge carrier, m its mass and $\boldsymbol{\ell} = \mathbf{r} \times \mathbf{p}$ its angular momentum. $\gamma = e/2m$ is called the gyromagnetic ratio. Note that γ is negative for electrons, which thus have angular momentum and magnetic moment pointing along opposite directions. Classical mechanics states that the time evolution of the angular momentum obeys $\dot{\boldsymbol{\ell}} = \boldsymbol{\Gamma}$ with $\boldsymbol{\Gamma}$ the mechanical torque, here of magnetic origin and equal to $\mu_0\boldsymbol{\mu} \times \mathbf{H}$. From this we derive the time evolution for the magnetic moment:

$$\dot{\boldsymbol{\mu}} = \mu_0\gamma\boldsymbol{\mu} \times \mathbf{H} \tag{IV.2}$$

The gyromagnetic ratio γ (and γ_0) is negative for an electron, due to its negative charge. Thus, in most works the choice has been made to write γ as a positive quantity, and insert the minus sign in the equation. Other works consider γ as negative. To avoid ambiguity, here we write $-|\gamma|$ in place of γ, restricting the discussion to $\gamma < 0$. This means that $|\gamma|$ should be replaced with $-|\gamma|$ in case a material with positive gyromagnetic ratio is considered, *e.g.* with a band structure such that magnetism is related to holes.

Expression Eq.(IV.2) remains valid for magnetic moments with both orbital and spin contributions to the angular momentum, introducing the Landé factor in the gyromagnetic ratio: $\gamma = ge/2m$ ($g = 1$ for orbital magnetic moments, $g \approx 2$ for spin magnetic moments). In the following we use the notation $\gamma_0 = \mu_0\gamma$ for the sake of concision. Again, note that $\gamma_0 < 0$ for electrons, while some authors define it as positive, requiring a minus sign in Eq.(IV.2). Eq.(IV.2) is straightforward to solve in the case of a constant magnetic field $\mathbf{H}$:

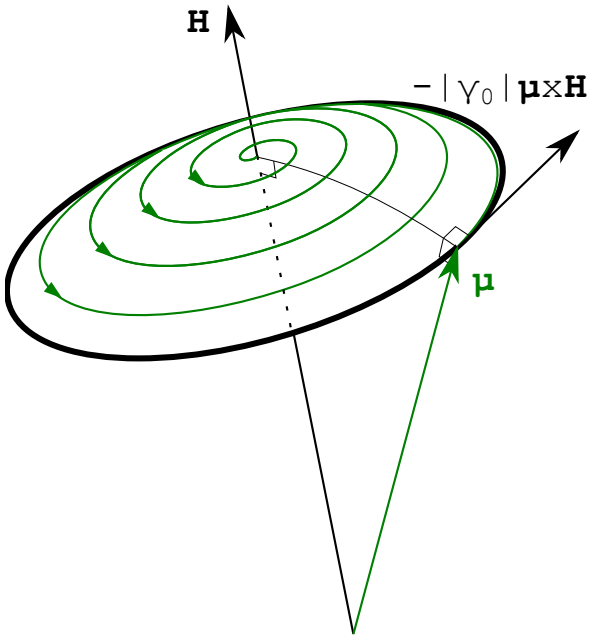

Figure IV.1 – Precession of a magnetic moment μ around a magnetic field. The thick line is the energy-conservative trajectory, while the thinner one along with arrows indicates the trajectory of magnetization when damping is considered.

$$\begin{pmatrix} \dot{\mu}_x \\ \dot{\mu}_y \\ \dot{\mu}_z \end{pmatrix} = -\mu_0|\gamma| \begin{pmatrix} \mu_x \\ \mu_y \\ \mu_z \end{pmatrix} \times \begin{pmatrix} 0 \\ 0 \\ H_0 \end{pmatrix} \tag{IV.3}$$

$$= -\mu_0|\gamma| \begin{pmatrix} \mu_y \\ -\mu_x \\ 0 \end{pmatrix} H_0 \tag{IV.4}$$

Let us write $\mathbf{H} = H_0\hat{\boldsymbol{z}}$ with $H_0 > 0$, $\boldsymbol{\mu} = \mu_i\hat{\boldsymbol{i}}$ using Einstein's compact notation, and introduce the complex number $Z = \mu_x + i\mu_y$. From Eq.(IV.3) it follows that μ_z is constant and $\dot{Z}(t) = i\omega_0 Z$, with $\omega_0 = |\gamma_0|H_0$. We have readily $Z = Z_0 e^{i\omega_0 t}$: the moment is precessing around the applied field with the angular frequency ω_0 (Figure IV.1).

- $|\gamma|/2\pi$ is often expressed in frequency per tesla. $|\gamma|/2\pi \approx 14$ GHz/T for orbital moments, and $|\gamma|/2\pi \approx 28$ GHz/T for spin moments.
- The precession angular frequency ω_0 does not depend on the angle between the moment and the magnetic field.
- The trajectory of the moment is energy conservative, as its projection along the applied field remains constant. This is an obvious consequence of the fact that the Lorentz force, at the base of Eq.(IV.2), is energy conservative.

1.2 Ferromagnetic resonance

When normalized per unit volume Eq.(IV.2) converts to magnetization:

$$\dot{\mathbf{m}} = -|\gamma_0|\mathbf{m} \times \mathbf{H} \tag{IV.5}$$

The possibility to drive precession of magnetization at a specific frequency in ferromagnetic bodies was discovered by Griffiths in 1946[141]; this is called ferromagnetic resonance (FMR). The discrepancy between the observed angular frequency with that expected from the above was soon solved by Kittel[142]. It is these arguments that we describe below.

In practice, a constant magnetic field is applied to align magnetization along a given direction, while precession is driven by a sinusoidal field of much small magnitude applied along a transverse direction. Precession is usually monitored through the losses of the transverse oscillatory field driving precession. The difference with the previous part comes from the fact that in matter not only the external field will be felt by magnetization, but also all fields deriving from the local density of internal energy E_{tot}. Formally, $\mathbf{H}$ must thus be replaced with an effective field defined as

$$\mu_0 \mathbf{H}_{\text{eff}} = -\frac{\delta E_{\text{tot}}}{\delta \mathbf{M}} \tag{IV.6}$$

It is clear that the above generalization is consistent with the torque provided by the external field, and derived from the Zeeman energy. New terms in matter are the magnetostatic field $\mathbf{H}_{\text{d}}$, and those microscopic terms associated *e.g.* with magnetocrystalline or exchange energies, introduced in sec.I.3.

Exchange and anisotropy fields are written $\mathbf{H}_{\text{ex}} = (2A/\mu_0 M_s)\Delta\mathbf{m}$ and $\mathbf{H}_K = (K/\mu_0 M_s)\nabla_{\mathbf{m}} f_K(\mathbf{m})$, with f the dimensionless anisotropy function (see Pb. 3).

Detailed discussion of ferromagnetic resonance in an arbitrary landscape of total energy may be found elsewhere[143–145]. In the following we restrict the discussion to the prototypical case of uniform magnetization in a soft magnetic material, and consider only the magnetostatic fields in addition to the applied field. We assume that the demagnetizing field is uniform and may be expressed based on demagnetizing coefficients. Finally, only small angle precession around $\hat{\boldsymbol{z}}$ is considered as is the case in most ferromagnetic resonance experiments. This permits to derive simple formulas through Taylor expansions, while in general the

angular frequency of motion depends on its amplitude. Eq.(IV.5) is rewritten:

$$\dot{\mathbf{m}} = -|\gamma_0| \begin{pmatrix} m_x \\ m_y \\ m_z \end{pmatrix} \times \begin{pmatrix} -N_x m_x M_s \\ -N_y m_y M_s \\ H_0 - N_z m_z M_s \end{pmatrix}. \tag{IV.7}$$

Although this set of equations can again be solved elegantly using a complex variable Z defined from a linear combination of m_x and m_y, let us use another method. Eq.(IV.7) is first expanded:

$$\begin{pmatrix} \dot{m}_x \\ \dot{m}_y \\ \dot{m}_z \end{pmatrix} = -|\gamma_0| \begin{pmatrix} m_y(H_0 - N_z m_z M_s) + m_z N_y m_y M_s \\ -m_z N_x m_x M_s - m_x(H_0 - N_z m_z M_s) \\ -m_x N_y m_y M_s + m_y N_x m_x M_s \end{pmatrix}. \tag{IV.8}$$

$\dot{m}_z$ is of second order with respect to the small transverse components m_x and m_y. We can thus assume that $m_z(t) \equiv 1$ and the above equations become:

$$\begin{pmatrix} \dot{m}_x \\ \dot{m}_y \\ \dot{m}_z \end{pmatrix} = -|\gamma_0| \begin{pmatrix} m_y \left[H_0 + (N_y - N_z)M_s\right] \\ -m_x \left[H_0 + (N_x - N_z)M_s\right] \\ 0 \end{pmatrix} \tag{IV.9}$$

Then, differentiating the first line and replacing $\dot{m}_x$ with the second one, one gets:

$$\ddot{\mathbf{m}} = -\gamma_0^2 \left[H_0 + (N_y - N_z)M_s)\right] \cdot \left[H_0 + (N_x - N_z)M_s)\right] \mathbf{m} \tag{IV.10}$$

Thus $m_x(t) = m_{x,0} \cos(\omega_0 t)$ and $m_y(t) = m_{y,0} \sin(\omega_0 t)$, with the following relationships:

$$\omega_0 = |\gamma_0| \sqrt{\left[H_0 + (N_x - N_z)M_s\right] \cdot \left[H_0 + (N_y - N_z)M_s\right]} \tag{IV.11}$$

$$m_{x,0} \sqrt{H_0 + (N_x - N_z)M_s} = m_{y,0} \sqrt{H_0 + (N_y - N_z)M_s} \tag{IV.12}$$

The motion is thus an elliptical precession with angular frequency ω_0. Note that the previous case of an isolated moment is retrieved for N_i's all zero. It is also valid for a sphere of soft magnetic material, with all N_i equal to $1/3$. Of special interest to discuss are the cases of a thin film, with a static field applied along either the normal to the film, or along an in-plane direction.

Let us first discuss the case of an out-of-plane static field. The axes are chosen such that $N_z = 1$ is associated with the perpendicular direction, while for in-plane directions $N_x = N_y = 0$. The above equations become:

$$\omega_0 = |\gamma_0|(H_0 - M_s) \tag{IV.13}$$

$$m_{x,0} = m_{y,0} \tag{IV.14}$$

This case is straightforward: the trajectories are circular and the angular velocity is constant. Note that precession occurs only when the applied field exceeds the magnitude of magnetization (Figure IV.2b). For $H_0 \to M_s$ the precession frequency

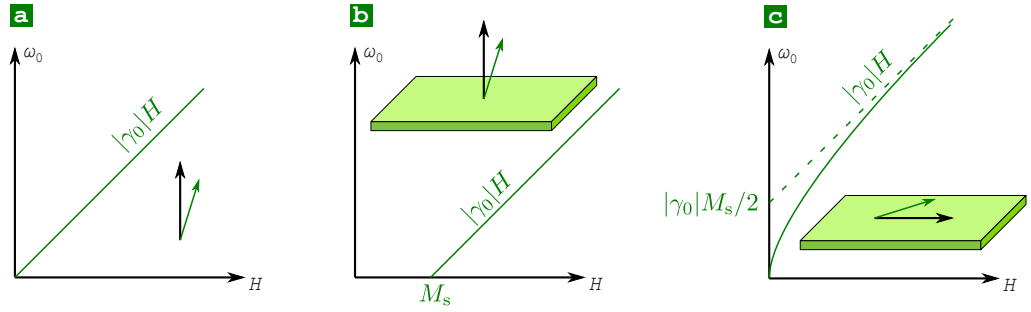

Figure IV.2 – Dispersion curves of ferromagnetic resonance in simples cases: (a) single moment in an external field (b) thin film, field normal to the surface (c) thin film, field in-plane.

vanishes, as the internal field around which precession occurs goes to zero. This is called a soft mode.

Let us now discuss the case of an in-plane static field. We simply rotate the axes: $N_x = 1$ is associated with the perpendicular direction, while for in-plane directions $N_y = N_z = 0$. The above equations become:

$$\omega_0 = -|\gamma_0|\sqrt{H_0(H_0 + M_s)} \quad \text{(IV.15)}$$

$$m_{x,0}\sqrt{H_0 + M_s} = m_{y,0}\sqrt{H_0} \quad \text{(IV.16)}$$

When the applied field is small compared with magnetization Eq.(IV.16) shows that the trajectory is very anisotropic, with $m_{x,0} \ll m_{y,0}$. The need to conserve energy explains this trajectory: only a weak excursion is allowed out of the plane, because of the high cost of demagnetization energy. As a consequence the angle with the applied field is considerably reduced when m_x is maximum, so that the Zeeman energy is then very small in absolute value. Thus, with this geometry the precession periodically converts most of the Zeeman energy into demagnetizing energy and vice versa. The angular velocity reaches a maximum when the perpendicular component of magnetization m_x is maximum. The asymptotic dependences are: $\omega_0 \sim |\gamma_0|\sqrt{H_0 M_s}$ at low field, and $\omega_0 = |\gamma_0|(H_0 + \gamma_0 M_s/2)$ at high field (Figure IV.2c). The linear dependance at high field has a simple meaning: when $H_0 \gg M_s$ the situation is close to an isolated moment in a static field H_0.

Here we considered precession around a main direction of the demagnetizing tensor. This is a usual and useful situation, however it remains a specific situation. More general formulas should be used for precessional around an arbitrary direction[143, 144].

Historically, ferromagnetic resonance was monitored as a function of the applied field, because an efficient source (field enhancement in a metallic cavity) existed only at fixed excitation frequency. This corresponds to horizontal cross-sections in the graphs on Figure IV.2. Since roughly the year 2000, ferromagnetic resonance is also implemented in broad-band devices based on strip lines. This corresponds to vertical lines on Figure IV.2. The superiority of this approach is first its sensitivity because it is a local measuring device, second its ability

to monitor the response under a magnetic field of arbitrary magnitude and notably at remanence. This opened the possibility to measure resonance modes of non-uniformly-magnetized structures, whose arrangement of magnetization would not be preserved upon sweeping the field in a conventional ferromagnetic resonance setup. A drawback is the possible non-uniformity of the applied field due to the finite width of the strip line. This may require calibration and modeling to extract quantitative information[146].

FMR to measure gyromagnetic ratio and exchange stiffness. Ferromagnetic resonance is a very important technique, for its ability to measure quantities hardly accessible otherwise, such as the gyromagnetic ratio γ and exchange stiffness A (see sec.1.4). It also yields very precise measurements of magnetization and anisotropy (see Pb. 3).

1.3 Damping and Landau-Lifshitz equations

As seen above, the precession of an isolated moment in a constant applied field is energy conservative, and thus in principle goes on for ever. In condensed matter, however, magnetization at a given point is coupled to the system through the lattice (phonons), conduction electrons, and electrons on neighboring orbitals contributing to magnetization. Angular momentum and energy may be exchanged with these baths, notably decreased for the latter. This is damping, which permits that magnetization is essentially aligned along the effective field after some time. Damping mechanisms are very complex and stochastic and can only be taken into account analytically with a phenomenological term. Historically it was first introduced in 1935 in a form nowadays known as the Landau-Lifshitz (LL) equation:

$$\frac{\mathrm{d}\mathbf{m}}{\mathrm{d}t} = -|\gamma_{0,\mathrm{LL}}|\mathbf{m}\times\mathbf{H} - (\lambda/M_\mathrm{s})\mathbf{m}\times(\mathbf{m}\times\mathbf{H}). \tag{IV.17}$$

In the right part of this equation, the first term is similar to the one already discussed, and describes the energy-conservative precession. The second term was added and it is exactly perpendicular to the energy-conservative one, while preserving the norm of magnetization constant. It thus purely describes a mechanism for releasing energy. The damping term is in most cases observed to be (very) small compared to the precessional term: $\lambda/(|\gamma_0|M_\mathrm{s}) \ll 1$

In 1953, Gilbert made the analogy between damping and a viscous force for a mechanical motion, opposed to the velocity: $-\eta\mathrm{d}\mathbf{m}/\mathrm{d}t$. This leads to the now-called Landau-Lifshitz-Gilbert (LLG) equation:

$$\frac{\mathrm{d}\mathbf{m}}{\mathrm{d}t} = -|\gamma_{0,\mathrm{G}}|\mathbf{m}\times\mathbf{H} + \alpha\left(\mathbf{m}\times\frac{\mathrm{d}\mathbf{m}}{\mathrm{d}t}\right). \tag{IV.18}$$

It can be shown that the two equations are exactly equivalent mathematically, based on a suitable conversion between the parameters γ_0's, λ and α. In the limit of low damping relevant for most experimental cases, as noticed above, one finds with a second-order difference only: $\gamma_{0,G} = \gamma_{0,LL}$, which we will keep writing γ_0, and $\lambda = \alpha|\gamma_0|M_s$. Nowadays the Landau-Lifshitz-Gilbert form is of more common use, than the Landau-Lifshitz one. The condition of low damping is thus expressed as $\alpha \ll 1$. Its influence on precession may be introduced as a perturbation to the trajectories described above. In the simple case of circular precession this results to first order in a relative decrease of angle between **M** and **H** of $2\pi\alpha$ per turn (Figure IV.1). The treatment of damping of a magnetic dipole moment for ferromagnetic resonance in matter is the topic of Pb. 5.

Precession in magnetic recording. The characteristic time scale to reach equilibrium is such that $1/(\alpha\gamma \approx 1\,\mathrm{ns}\cdot\mathrm{T})$. Thus, precession of magnetization can no longer be ignored in magnetic storage devices with high data throughput, both on the media and on the head side (write as well as read head).

Fixed magnitude of M in micromagnetism. Notice that both equations thankfully preserve the norm of **M**, a hypothesis of micromagnetism. Another equation was introduced to allow one to describe mechanisms where the magnetization vector is not preserved in time or space: the Landau-Lifshitz-Bloch equation[147]. It is more suitable than the Landau-Lifshitz(-Gilbert) equation(s) to describe situations like the Bloch point (see p.80), or ultrafast (de)magnetization processes[147, 148].

1.4 Spin waves

So far we have disregarded any contribution of exchange to the effective field, which is suitable for describing uniform precession of magnetization. There also exist non-uniform modes, for which the exchange field needs to be taken into account: $\mathbf{H}_{ex} = (2A/\mu_0 M_s)\Delta\mathbf{m}$. The general theory of these modes goes beyond the purpose of these notes. Only a textbook case is covered here.

In sec.1.1 we described precession of a moment $\boldsymbol{\mu}$ around a magnetic field using the complex function $Z = Z_0 e^{j\omega t}$, standing for the components $\mu_x(t) = \mathfrak{Re}(Z)$ and $\mu_y(t) = \mathfrak{Im}(Z)$, while $\mu_z \simeq 1$. Let us extend this notation to describe modes of the form:

$$Z = Z_0 e^{j(\mathbf{k}\cdot\mathbf{r}+\omega t)} \tag{IV.19}$$

Figure IV.3 illustrates the situation of so-called transverse spin waves, with magnetization pointing along $\hat{\boldsymbol{z}}$ and **k** chosen along the transverse x direction. When

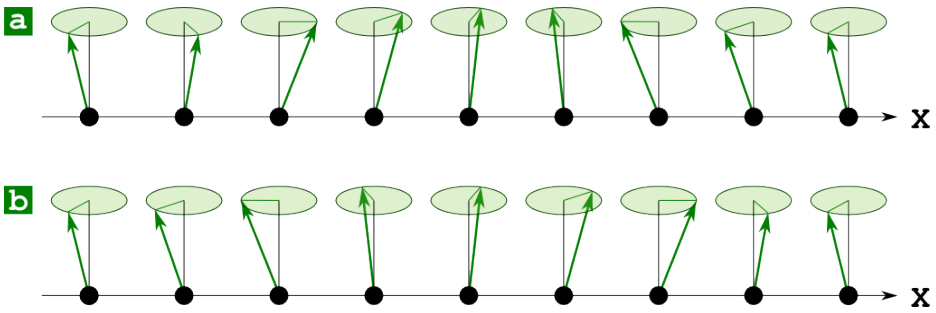

Figure IV.3 – Spin waves. Schematics for spin waves of the form $Z = Z_0 e^{i(kx+\omega t)}$ with (a) $k > 0$ (propagating towards $-\hat{\boldsymbol{x}}$) and (b) $k < 0$ (propagating towards $+\hat{\boldsymbol{x}}$).

computing the exchange field, $\Delta\mathbf{m}$ is described by $\partial^2 Z/\partial x^2 = -k^2 Z$. The LLG equation

$$\frac{\mathrm{d}\mathbf{m}}{\mathrm{d}t} = \gamma_0 \mathbf{m} \times (\mathbf{H}_0 + \mathbf{H}_{\mathrm{ex}}) \tag{IV.20}$$

is described with the complex notation:

$$\frac{\mathrm{d}Z}{\mathrm{d}t} = iZ|\gamma_0|H_0 + ik^2 Z \left(\frac{2A}{\mu_0 M_\mathrm{s}}\right)|\gamma_0|. \tag{IV.21}$$

This may be written $\mathrm{d}Z/\mathrm{d}t = i|\gamma_0|\omega_k Z$ with:

$$\omega_k = \omega_0 + k^2 \Delta_\mathrm{d}^2 \omega_M \tag{IV.22}$$

with $\omega_M = |\gamma_0|M_\mathrm{s}$, and still $\omega_0 = |\gamma_0|H_0$. This simple non-uniform mode has a larger angular frequency than the uniform mode, characterized by a quadratic variation with the wave vector $\mathbf{k}$. Forward and backward motion are here equivalent. The $\omega(k)$ dispersion curve may be measured experimentally, using *e.g.* neutron scattering. This approach is one of the rare techniques providing a direct estimate for the exchange stiffness A.

Summary

Ferromagnetic resonance and Landau-Lifshitz-Gilbert equation. Magnetization is a consequence of the angular momentum carried by the charged particles electrons, whose dynamics is governed by torques. Its motion is thereby of precessional nature. It is described by the Landau-Lifshitz-Gilbert equation, in which damping is described phenomenologically. Among the prominent phenomena are resonance et given frequencies, and propagating modes called spin waves.

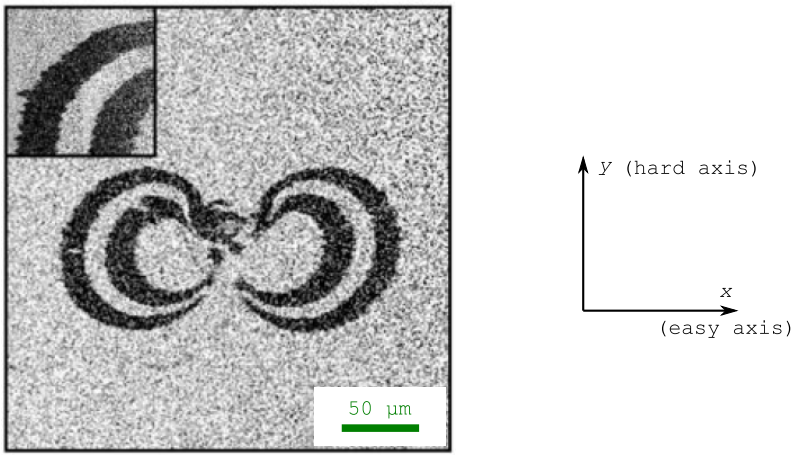

Figure IV.4 – A clever experiment to evidence precessional switching. Ring-shaped reversed domains (dark contrast) induced by precessional magnetization switching of a thin Co film initially uniformly-magnetized, with uniaxial magnetic anisotropy in-the-plane along $\hat{x}$[149].

2 Precessional switching of macrospins driven by magnetic fields

In the previous section the ground for the LLG equation was set. Simple trajectories were discussed with or without damping, especially the free precession around a constant magnetic field. Since the late 1990's precession was used in conjunction with nanosecond pulses of magnetic field, to switch magnetization through precessional (ballistic) trajectories. It can be faster and more energy-efficient for switching magnetization than quasistatic fields.

2.1 The role of shape anisotropy

In 1999 Ch. BACK *et al.* reported an experiment, which opened the field of precessional switching of magnetization[149]. They used a $\tau = 4.4$ ps-long pulse of the beam of a particule accelerator[IV.1] along the normal to a thin film with in-plane magnetization, initially prepared with uniform magnetization aligned along an easy axis. Observation of the sample after the shot showed that domains of reversed magnetization had appeared, shaped like concentric crescents around the impact (Figure IV.4). What is the physics at play, and what do we learn from this experiment?

Let us make a handwaving description, before we derive equations. The dynamics of magnetization is driven by the in-plane orthoradial Œrsted field created by the current associated to the beam of charged particles. Thanks to the cylindrical symmetry of the beam and the $1/r$ radial dependence of the strength of the Œrsted field, the physics of the effect on magnetization of a pulse of

[IV.1] SLAC: Stanford Linear Accelerator Center

magnetic field of arbitrary magnitude and orientation could be derived based on the location-dependent effect observed on the sample. While the initial direction of magnetization is along $+\hat{\boldsymbol{x}}$, let us consider the case where the Œrsted field is applied along the perpendicular direction $+\hat{\boldsymbol{y}}$, and ignore damping. Following Eq.(IV.5) $\dot{\mathbf{m}}$ is initially along $-z$ and drives magnetization towards below the plane of the film. At later stages, this gives rise to a demagnetization field along $+\hat{\boldsymbol{z}}$, which adds to the effective field. It results in a new component of $\dot{\mathbf{m}}$ aligned along $+\hat{\boldsymbol{y}}$. Very rapidly the demagnetizing field becomes the leading term in the effective field against the Œrsted field, so that the main feature of motion is the precession of magnetization around its own demagnetizing field. Another way of seeing this is a large-angle precession around the applied field. As discussed for FMR (Figure 1.2), the trajectory is very flat, due to the need to convert Zeeman energy into demagnetizing energy. The angular frequency of motion is expected to increase with the magnitude of the applied field, and thus be larger closer to the impact. The final state long after the beam has terminated, depends on the period T of precession compared with the fixed duration τ of the pulse of field. For $T = 2\tau$ the magnetization performs half a turn, meaning final alignement along $-\hat{\boldsymbol{x}}$ and thus switching. This is the most outer crescent with magnetization reversed. Further inside $T = \tau$: the magnetization makes one turn and falls back along its initial direction. Still further inside $3/2$ turns lead again to magnetization switching.

Note on Figure IV.4 that no switching occurs with the field aligned close to parallel or antiparallel to initial magnetization, because in those cases the transient torque acting on magnetization is close to zero. This and the symmetry of the pattern highlights the fundamental difference between precessional switching and quasistatic switching, in which case switching would only occur in the upper panel ($y > 0$ to get a negative H_y).

The trajectories described above can be computed exactly when damping is neglected. As an alternative to the integration of differential equations as performed in the FMR section, one can derive analytically the trajectory from the conservation of energy? While the general case involves non-standard functions, in the absence of magnetocrystalline anisotropy it simply reads $E = -\mu_0 M_s^2 h m_y + (1/2)\mu_0 M_s^2 m_z^2$. Here h is the applied field normalized with magnetization. Combined with the constraint $m_i^2 = 1$ this provides the projection of the equation of motion in all three planes. Alternatively the trajectory can be described parametrically using m_z as a parameter:

$$\begin{aligned} 2hm_y &= m_z^2 \\ m_x^2 + (m_y + h)^2 &= 1 + h^2 \\ m_x^2 + m_z^2 + m_z^4/(4h^2) &= 1 \end{aligned} \tag{IV.23}$$

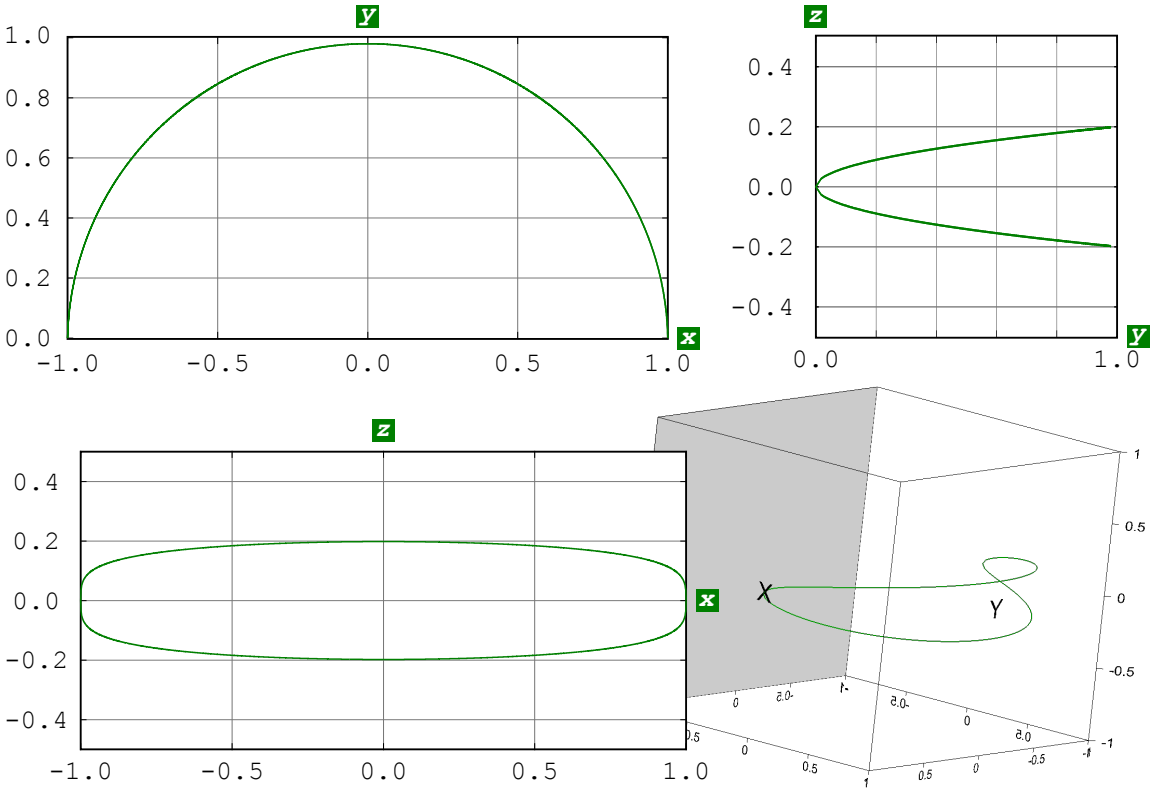

Figure IV.5 – Precessional switching of a thin film with zero in-plane anisotropy, out-of-plane demagnetizing coefficient 1, and no damping. Trajectories followed by magnetization during switching for $h = 0.04$: projection along the three main planes, and three-dimensional view.

They are plotted on Figure IV.5. We recognize the large-angle precession around the applied field, expected from the above handwaving discussion. So, the determination of trajectories from energy conservation is a powerful method, however, it does not provide the time-evolution nor the precession frequency.

2.2 Setting-in in-plane uniaxial anisotropy

The case of a thin film or flat nanostructure with a uniaxial anisotropy between two in-plane axes is directly relevant in the context of magnetization switching, and is richer in terms of physics. The detailed calculation is proposed in Pb. 2, and the resulting trajectories are plotted in Figure IV.6. We define the anisotropy field as usual as $H_K = 2K/\mu_0 M_s$, and $h_K = H_K/M_s$ for the dimensionless variable. In this case a threshold appears in terms of applied field. For $h < h_K/2$ the trajectories do not cross the plane $m_x = 0$. Switching does not occur and moderate-angle precession occurs around the combined applied and anisotropy fields, in a direction intermediate between $+\hat{\boldsymbol{x}}$ and $+\hat{\boldsymbol{y}}$. For $h > h_K/2$ the trajectory crosses the plane m_x; switching is again possible, as in the case of zero anisotropy.

It is interesting to understand why the threshold field for precessional switching is $h_K/2$, while the quasistatic switching field in the Stoner-Wohlfarth model

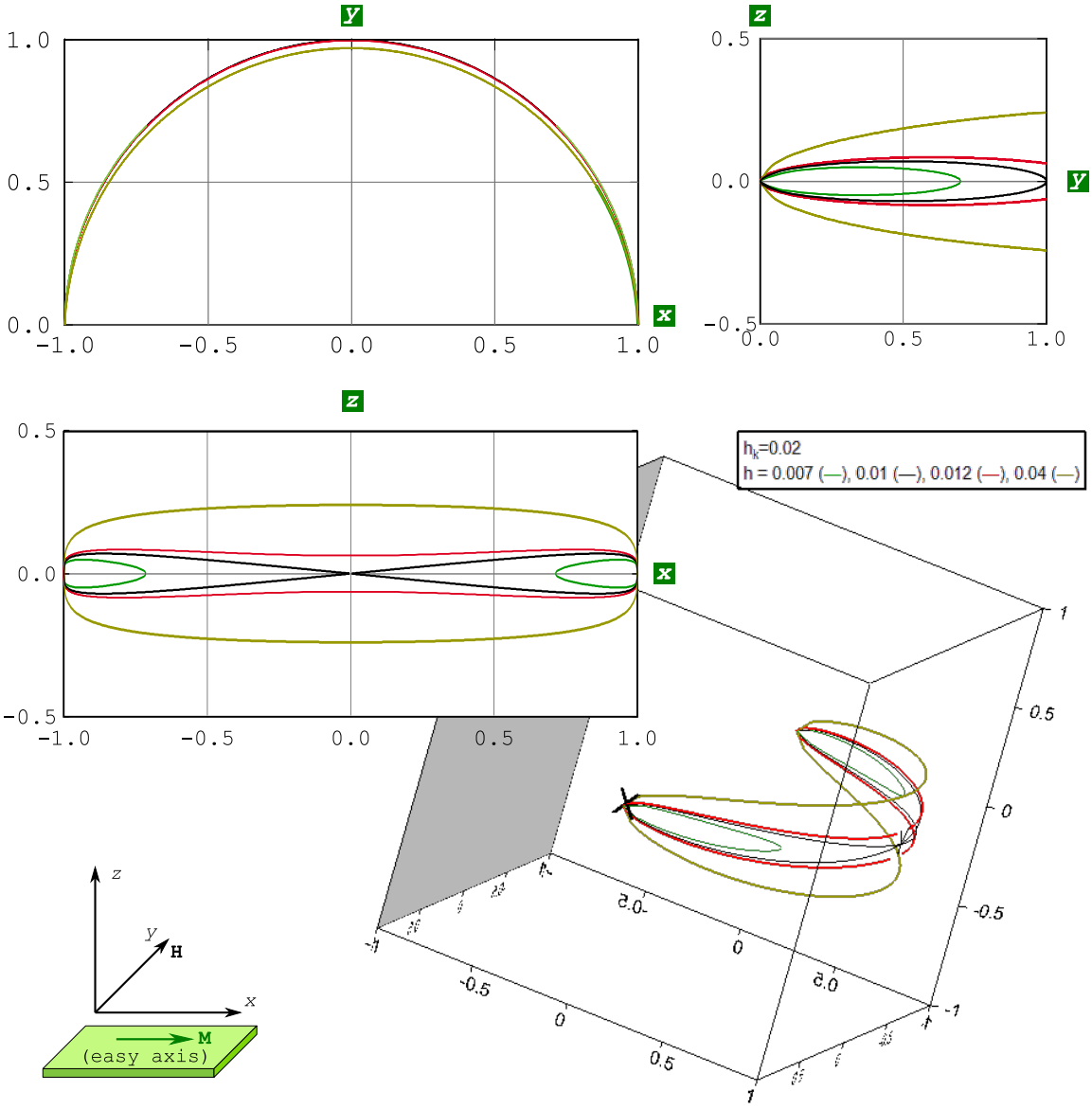

Figure IV.6 – Precessional switching of a thin film with in-plane uniaxial anisotropy (anisotropy field h_K, expressed in M_s units), out-of-plane demagnetizing coefficient 1, and no damping. Trajectories followed by magnetization during switching for various values of applied field h: projection along the three main planes, and three-dimensional view.

is h_K along both the easy and hard axes. The examination of energy profiles provides the answer (Figure IV.7). In the quasistatic picture of Stoner and Wohlfarth, magnetization switching occurs when the local minimum vanishes; we have seen in sec.III.1.1 that this happens at h_K. To the contrary, in the precessional case the system follows an iso-energy path. Thus, magnetization switching may be possible when the starting point $\theta = 0$ and the passing point allowing reversal have an equal energy, which happens to be for $h_K/2$ with the energy maximum being at $\theta = \pi/2$. The disappearance of a local minimum is not relevant because the system does not remain at the bottom of energy wells in the precessional regime; it does so only in the quasistatic regime.

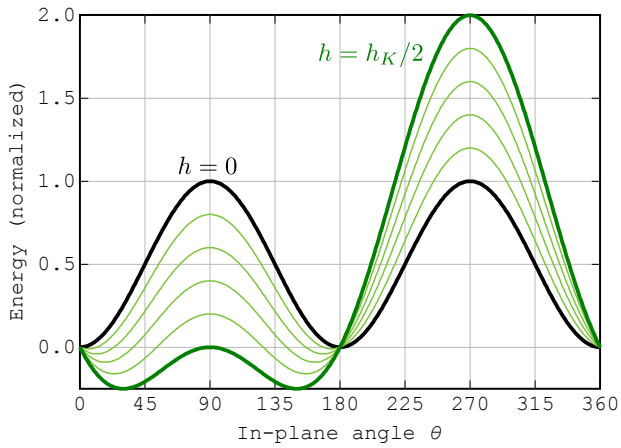

Figure IV.7 – Energy in precessional switching. Energy landscape (uniaxial anisotropy plus Zeeman energy) for the external field applied along $\hat{\boldsymbol{y}}$, *i.e.* the in-plane hard axis along $\theta = 90°$. Landscapes are plotted for field values ranging from zero to half the anisotropy field.

We now discuss the angular frequency when precessional switching is possible, *i.e.* for $h > h_K/2$. While the time-integration of the LLG equations is possible analytically, it involves non-trivial functions and may not be of easy use[150]. As one is interested to switch magnetization at low applied field, an approached scaling law has been derived, for application with high accuracy in the range $h_K/2 < h < h_K$, which is of direct relevance for precessional switching[151]: $\omega_0 \approx 0.847|\gamma_0|\sqrt{M_s(H - H_K/2)}$. Examination of this formula along with the corresponding trajectories brings some understanding (Figure IV.6). For $h \to h_K/2$ the angular frequency vanishes, or in other words the period diverges. The reason is the pinched point of the trajectory at $(m_y, m_z) = (1, 0)$. At this point the anisotropy field is locally parallel to magnetization (or in other words all first-order derivatives of the energy are zero), so that the torque exerted on magnetization vanishes. On the reverse, for increasing field, deviations from this approached formula become noticeable. From the mathematical point of view (*i.e.*, exact however not meaningful for the practical purpose of precessional switching), at high field the precession frequency should follow the slope $|\gamma_0|H$ as for the case of FMR with in-plane magnetization [Eq.(IV.15)], or the free precession of a macrospin with no internal field.

2.3 Practical conditions: finite damping and pulse length

Damping, length and shape of the pulse of applied field all affect the picture developed above. Equations can be solved analytically only to first order for small angle precession of constant magnitude, like for the case described in Pb. 5. In other situations no exact solution can be derived, and approximations must be introduced[150, 151], or numerical integration of the LLG equation performed[152]. Here we only provide a qualitative picture of switching varying damping, pulse duration and pulse shape (Figure IV.8). Magnetization is initially along $-\hat{\boldsymbol{x}}$, and

all directions and magnitudes of the applied field are considered. We call θ_H the angle of the applied field with respect to the direction opposite to the initial direction of magnetization.

Let us first consider the case of a square pulse of field, which was the one we considered analytically in the absence of damping; it is displayed in the first column of Figure IV.8. For a long pulse the switching diagram is the simplest, and can be related to situations previously described:

- Switching occurs for most cases with field globally applied opposite to the initial direction of magnetization, if of sufficient magnitude. The Stoner-Wohlfarth astroid, bounded by the anisotropy field, can be recognized close to the origin. This is consistent with the quasistatic picture.
- Switching does not occur for most fields applied globally parallel to the initial direction of magnetization. This is again consistent with the quasistatic picture.
- In a narrow range around $\theta_H \simeq \pm\pi/2$, switched and non-switched regions alternate regularly. This is consistent with the picture described for precessional switching with no damping and no anisotropy, although here anisotropy is present.

For short pulse duration the diagram of switching is the richest, displaying complex curved stripes. Remember that no reversal in the final state does not mean that significant precession has not occurred, as it can result from an even number of half-turns. A few noticeable facts are the following:

- Stripes are very densely packed close to $\theta_H = 0$. In practice, this means that switching is very sensitive to the initial conditions and to any perturbation or deviations of the material properties.
- No switching occurs for $3\pi/4 < \theta_H < 5\pi/4$. It can easily be shown that the energy barrier cannot be crossed, so precessional switching is not effective.
- The largest pocket allowing switching is located around θ_H. This is consistent with Figure IV.7 which shows that the energy barrier vanishes first for this angle. This highlights that precessional swithing is most efficient at crossed angle.

For intermediate pulse width the features aer intermediate.

The effect of broadening the pulse is to dramatically smoothen the switching diagram, towards the quasistatic features. This is clear in Figure IV.8f which looks like the Stoner-Wohlfarth astroid.

Summary

Precessional switching of macrospins driven by magnetic fields. Precessional magnetization switching, relevant at time scales below typically 1 ns, displays features dramatically different from quasistatic switching. The most efficient switching in terms of magnitude and length of pulse, is when the field is applied at right angle

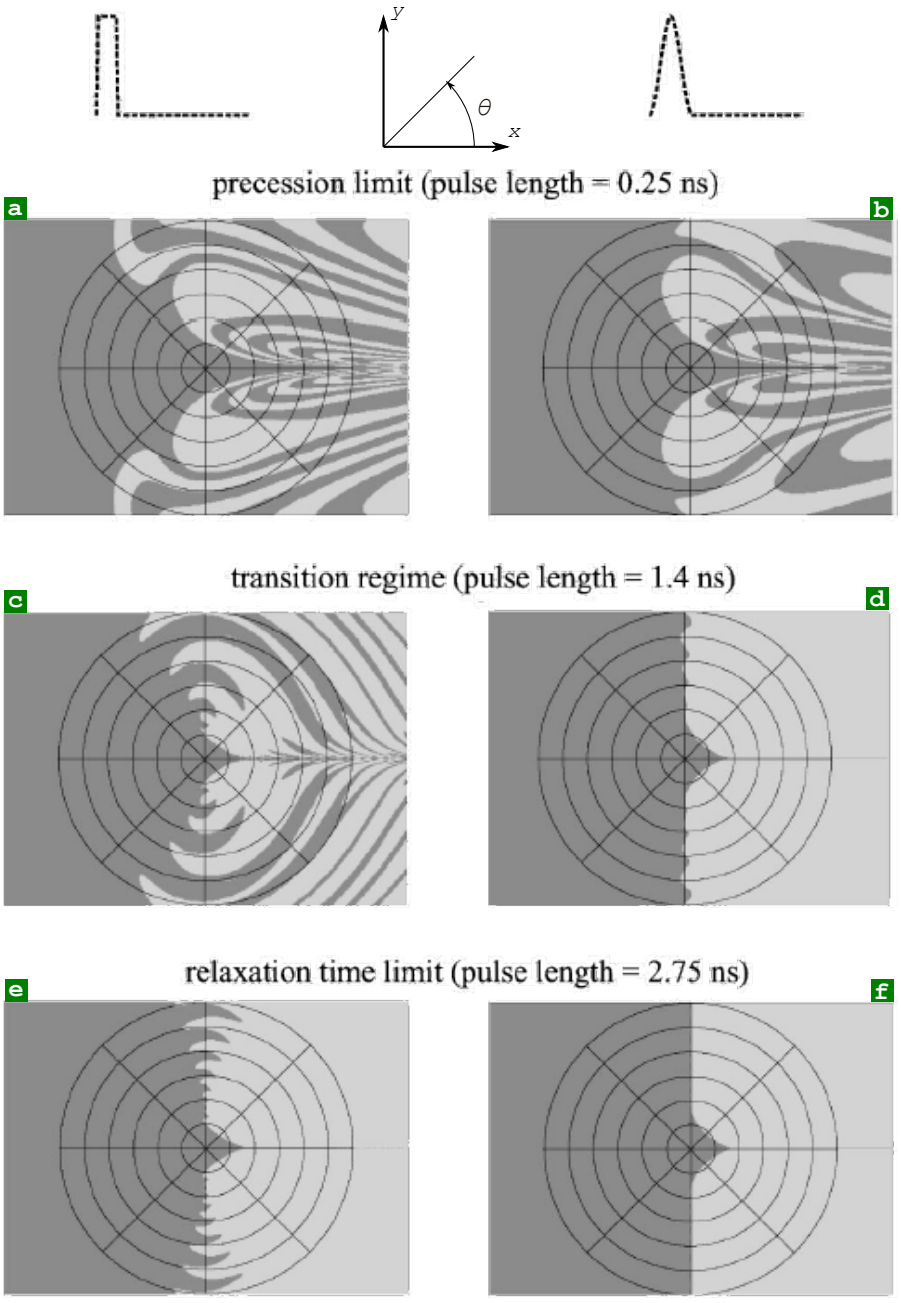

Figure IV.8 – Transition from precessional switching to quasistatic switching. Diagrams of switching versus the components of applied H_x and H_y, based on macrospin precessional simulations of a flat element with demagnetizing factors N_x = 0.008, N_y = 0.012 and N_z = 0.980 and spontaneous magnetization $\mu_0 M_s$ = 1.08 T. This implies and in-plane anisotropy field of 4.32 mT. The damping is α = 0.008. The initial direction of magnetization is along $-\hat{\boldsymbol{x}}$, and light areas mean switching. Each circle designates an increment of field of 2.5 mT.

with the initial direction of magnetization, because the torque driven precession is maximum. However, ringing and multiple precession may occur, which makes the process sensitive to initial conditions and distributions of properties. It is therefore not realistic to implement it as such in devices.

3 Precessional motion of domain walls and vortices driven by a magnetic field

The formalism to describe the precessional nature underlying domain wall motion, is very similar to the one related to magnetization switching, detailed in the previous section. In the following we consider situations with increasing complexity, to introduce the various effects at play one by one.

We consider in all cases a one-dimensional model of domain wall, with magnetization $\mathbf{m}(z)$ varying between two domains aligned along $+\hat{\boldsymbol{z}}$ and $-\hat{\boldsymbol{z}}$ (Figure IV.9). This head-to-head orientation of domains is suitable to describe strips with in-plane magnetization, with magnetization in the domains aligned along the strip length, which we will use as a prototypical case to illustrate this section. Nevertheless, the equations can be transposed to other situations, *e.g.* strips with perpendicular magnetization, or thin films with magnetization perpendicular to $\hat{\boldsymbol{z}}$ in the domains. We will make use of spherical coordinates around this $\hat{\boldsymbol{z}}$ direction to describe the direction of magnetization, with $\theta =< \mathbf{m}, \hat{\boldsymbol{z}} >$, and φ the transverse azimuth of magnetization (Figure **??**). A magnetic field $\mathbf{H}$ will be applied along $\hat{\boldsymbol{z}}$. While the situation may be described more rigorously by considering the entire domain wall, here we will derive most of the physics considering the dynamics at the center of the domain wall. Finally, note that the wall width will be called $\pi\Delta$, defined such that $\mathrm{d}\theta/\mathrm{d}z = 1/\Delta$ at the center of the wall.

Considering the center of the domain wall can be legitimated by the fact that is it where the torque arising from the applied field is the largest. Besides, as the curvature of $\theta(z)$ is zero at this point, there is no exchange contribution to magnetization dynamics. This boils the problem down to considering the domain wall as a macrospin, similar to the situation describing the transition between Bloch and Néel walls in thin films (see p.74).

3.1 Domain walls – The case of azimuthal isotropy

In a first step we disregard any transverse anisotropy, so that magnetic anisotropy may be written $E_a = K_u \sin^2\theta$, *i.e.* with no dependence on φ. At rest the wall width is $\pi\Delta = \pi\Delta_u$. This situation is analogous to that of a cylindrical wire. In the LLG equation the dominating torque is generally the precessional one, because of the low value of α. This torque, due to $\mathbf{H}$ and acting on the core of the domain wall,

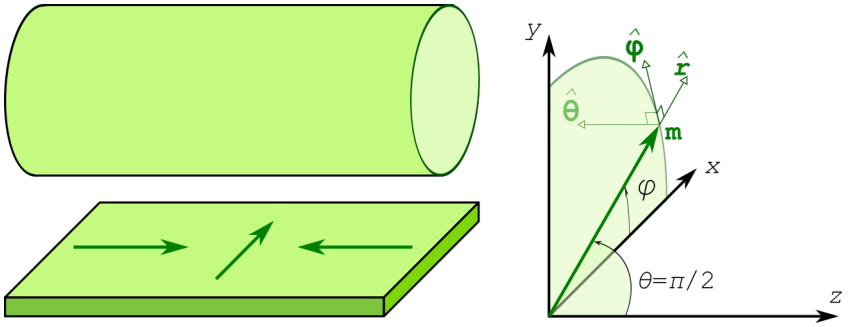

Figure IV.9 – Spherical coordinates to describe domain wall motion. The coordinates apply equally to cylinders and strips, with $\hat{\boldsymbol{z}}$ along the axis. $\hat{\boldsymbol{r}}$, $\hat{\boldsymbol{\theta}}$ and $\hat{\boldsymbol{\varphi}}$ are the local unit vectors related to the spherical coordinates for magnetization along the direction (θ, φ).

yields: $\dot{\mathbf{m}} = -|\gamma_0|\mathbf{m} \times \mathbf{H}$. As $\mathbf{m} = \hat{\boldsymbol{r}}$ and $\mathbf{H} = H\hat{\boldsymbol{z}}$, $\dot{\mathbf{m}} = |\gamma_0|H\hat{\boldsymbol{\varphi}}$. Thus, the variation of $\mathbf{m}$ is purely precessional, with the angular frequency $\dot{\varphi} = \omega_0 = |\gamma_0|H$. At this stage θ remains equal to $\pi/2$, which means that the domain wall does not move.

The absence of forward motion of the domain wall if damping is not considered, can be understood simply. If the domain were to move, this would imply a change of energy of the system, due to the Zeeman energy of the two domains not being equal. This would be a contradiction with the conservation of energy, as no damping is considered.

Let us now consider the damping term as a perturbation to the previous motion, so that $\alpha\mathbf{m} \times \dot{\mathbf{m}}$ can be approximated with $-\alpha|\gamma_0|\mathbf{m} \times (\mathbf{m} \times \mathbf{H})$. Following the above, this torque reads $-\alpha|\gamma_0|\hat{\boldsymbol{r}} \times \hat{\boldsymbol{\varphi}} = \alpha|\gamma_0|H\hat{\boldsymbol{z}}$. As $\mathrm{d}\hat{\boldsymbol{r}}/\mathrm{d}\theta = -\hat{\boldsymbol{z}}$ for $\theta = \pi/2$, the full LLG equation reads: $\dot{\mathbf{m}} = |\gamma_0|H\hat{\boldsymbol{\varphi}} + \alpha|\gamma_0|H\hat{\boldsymbol{z}}$. Identification with $\dot{\mathbf{m}} = \dot{\theta}\hat{\boldsymbol{\theta}} + \dot{\varphi}\hat{\boldsymbol{\varphi}}$ yield $\dot{\theta} = -\alpha|\gamma_0|H$, also showing that the damping torque is orthogonal to the precessional torque. The core of the wall being defined by $\theta = \pi/2$, the variation of θ of this moment initially at the core of the wall, means that the wall is moving. To convert this angular time variation into the domain wall speed, we use the formalism of the particulate derivative of a quantity A:

$$\frac{\mathrm{D}A}{\mathrm{D}t} = \frac{\partial A}{\partial t} + (\mathbf{v} \cdot \boldsymbol{\nabla})A. \tag{IV.24}$$

This equation can be understood in the following manner. $\mathrm{D}A/\mathrm{D}t$ refers to the variation of A in the moving frame of the domain wall. This variation may come both from the time variation of A in the fixed frame (the first term), or the fact that the particle (here the particule is the wall) moves in the spatial field $A(\mathbf{r})$ at speed $\mathbf{v}$, to that the time variation of A in the fixed frame depends also on how A varies along the trajectory of the particle (second term). For $A = \theta$ we have $\mathrm{D}\theta/\mathrm{D}t = 0$ as, by definition, as $\theta \equiv \pi/2$ at the center of the wall. As the model is unidimensional, $\mathbf{v} \cdot \boldsymbol{\nabla} = v\,\partial/\partial z$. Thus, Eq.(IV.24) boils down to: $v\partial\theta/\partial z = -\dot{\theta} = \alpha|\gamma_0|H$. Noticing that by definition $\partial\theta/\partial z = 1/\Delta$, we now have the full description of the dynamics of the domain wall:

$$\dot{\varphi} = |\gamma_0|H \tag{IV.25}$$
$$v = \alpha|\gamma_0|H\Delta \tag{IV.26}$$

Eq.(IV.26) can be rewritten $v = \mu H$ with $\mu = \alpha|\gamma_0|\Delta$ the mobility. The above shows that the main dynamics is azimuthal precession, while the forward motion is only related to damping, yielding a very slow forward motion proportional to α. This one-dimensional model with no azimuthal anisotropy has been validated by numerical simulation of domain wall motion in cylindrical nanowires[153, 154]. While the model is the simplest, the experimental investigation of cylindrical wires requires a bottom-up synthesis method such as electrochemistry performed in the cylindrical pores of a template, followed by the dissolution of the matrix for inspection of single wires. Domain walls in such wires have been imaged only recently[155, 156], and their dynamic features have not been reported yet.

The above may be solved exactly and more quickly based on the Landau-Lifshitz equation, the so-called solved form providing directly the time-derivative of magnetization [Eq.(IV.17)]. However, the effects of precession and damping are not as clearly highlighted as in the above.

3.2 Domain walls – The case of azimuthal anisotropy

Most one-dimensional magnetic conduits investigated so far experimentally, consist of flat strips patterned with lithography and thin-film technology. Still considering soft magnetic materials with in-plane magnetization as an illustration, we call x the in-plane direction transverse to the strip, and y the direction perpendicular to the strip (Figure IV.9). Remaining in the framework of a one-dimensional model, we assume that the domain wall is of transverse type at rest (see Figure II.15, p.88). For $t < 0$ the applied field is zero, while for $t \geq 0$ the applied field is $H\hat{\boldsymbol{z}}$.

We first describe the situation in a handwaving fashion, before deriving formal equations. At $t = 0^+$ the only non-zero torque in the LLG equation is $\boldsymbol{\Gamma}_H$, related to the applied field H, so that Eq.(IV.25) applies, and $\dot{\mathbf{m}}$ is along $\hat{\boldsymbol{\varphi}}$. This onset is similar to azimuthal precession, as described in the previous paragraph. However, at later stages the situation differs because the y component of $\mathbf{m}$ resulting from azimuthal precessional, gives rise to a demagnetizing field $\mathbf{H}_d$ along $-\hat{\boldsymbol{y}}$, around which precession also occurs. This situation is similar to the case of precessional switching of a macrospin (sec.2.1). This implies a torque $\boldsymbol{\Gamma}_d \sim \mathbf{m} \times \hat{\boldsymbol{y}}$ oriented along $\hat{\boldsymbol{z}}$, contributing to the forward motion of the wall. Over time the elevation of $\mathbf{m}$ along $\hat{\boldsymbol{y}}$ keeps increasing, as $\dot{\varphi} > 0$ due to precession around $\mathbf{H}$. In turn, this increases $\mathbf{H}_d$, and the forward motion. Very soon $\boldsymbol{\Gamma}_d$ becomes large, so that the associated damping term $\alpha\mathbf{m} \times \Gamma_d \sim -\alpha\hat{\boldsymbol{\varphi}}$ needs to be considered. This

contribution opposes the one associated with precession around the applied field. It raises with φ, while the latter does not. Thus, after a while the system may reach a stationary state with constant φ, if a balance is found. Below we derive more formal equations, to determine in which case balance occurs or not, and what the resulting speed is.

The torque giving rise to precession around the applied field is:

$$\begin{aligned} \mathbf{\Gamma}_H &= -|\gamma_0|\ \mathbf{m} \times \mathbf{H} \\ &= -|\gamma_0| H\ \hat{\boldsymbol{r}} \times \hat{\boldsymbol{z}} \\ &= |\gamma_0| H\ \hat{\boldsymbol{\varphi}} \end{aligned} \tag{IV.27}$$

The torque giving rise to precession around the demagnetizing field $\mathbf{H}_\mathrm{d} = -M_\mathrm{s} \sin\varphi\ \hat{\boldsymbol{y}}$ is:

$$\begin{aligned} \mathbf{\Gamma}_\mathrm{d} &= -|\gamma_0|\ \mathbf{m} \times \mathbf{H}_\mathrm{d} \\ &= |\gamma_0| M_\mathrm{s} \sin\varphi\ \hat{\boldsymbol{r}} \times \hat{\boldsymbol{y}} \\ &= |\gamma_0| M_\mathrm{s} \sin\varphi \cos\varphi\ \hat{\boldsymbol{z}} \end{aligned} \tag{IV.28}$$

Considering damping as a perturbation $\dot{m} \simeq \mathbf{\Gamma}_H + \mathbf{\Gamma}_\mathrm{d}$, so that the damping term reads:

$$\begin{aligned} \alpha \mathbf{m} \times \dot{\mathbf{m}} &= \alpha\ \hat{\boldsymbol{r}} \times \left[|\gamma_0| H\ \hat{\boldsymbol{\varphi}} + \frac{1}{2} |\gamma_0| M_\mathrm{s} \sin(2\varphi)\ \hat{\boldsymbol{z}} \right] \\ &= \alpha |\gamma_0| \left[H \hat{\boldsymbol{z}} - \frac{1}{2} M_\mathrm{s} \sin(2\varphi)\ \hat{\boldsymbol{\varphi}} \right] \end{aligned} \tag{IV.29}$$

The above three equations can be combined to yield the full LLG equation:

$$\dot{m} = |\gamma_0| \left(\alpha H + \frac{1}{2} M_\mathrm{s} \sin 2\varphi \right)\ \hat{\boldsymbol{z}} + |\gamma_0| \left[H - \frac{1}{2} \alpha M_\mathrm{s} \sin(2\varphi) \right] \hat{\boldsymbol{\varphi}} \tag{IV.30}$$

A steady-state solution for $\dot{\mathbf{m}}$ is characterized with a constant component along $\hat{\boldsymbol{z}}$, and no component along $\hat{\boldsymbol{\varphi}}$ (implying constant φ). This is possible only if there exists an azimuth φ for which $H = (1/2)\alpha M_\mathrm{s} \sin(2\varphi)$, or in other words: $\sin(2\varphi) = 2H/(\alpha M_\mathrm{s})$. In this case the wall speed is determined from the $\hat{\boldsymbol{z}}$ component $|\gamma_0|(\alpha/+ 1/\alpha)H \simeq |\gamma_0| H/\alpha$, so that in the end the wall velocity is:

$$v = \frac{|\gamma_0| H \Delta}{\alpha} \tag{IV.31}$$

The case of strips is drastically different from the one of azimuthal anisotropy, as now the speed is now inversely proportional to damping, which makes a great difference as in most cases $\alpha \ll 1$. The reason is, the smaller the damping, the larger $\sin 2\varphi$ need to be to balance H in the second term of Eq.(IV.30), so larger the elevation is, the demagnetizing field, and hence the precession angular frequency around it.

This remains valid while $H \leq H_W$, with $H_W = \alpha M_s/2$ the so-called Walker field[157]. It is associated with the maximum speed $v_W = |\gamma_0| M_s \Delta/2$, called the Walker speed. Above this threshold $\mathbf{\Gamma}_H$ is too large to be compensated by damping. Azimuthal precessional occurs again as in the case of cylinders, albeit with a non-constant angular velocity due to the difference of energy along the x and y directions. It results in a sharp drop of the wall mobility, a phenomenon called the Walker breakdown. For very large applied fields, it can be shown that the mobility of the wall recovers a scaling law inversely proportional to α.

In the above we named Δ the wall parameter ($\pi\Delta$ is the wall width). While it equals Δ_u at rest, it is no more a constant at later stages. During motion the wall width tends to decrease, to lower the energy of the system as the core of the domain wall is now associated with a significant demagnetizing energy. In practice, this introduces a negative curvature to the initially-expected linear variation of v with H. One may account for it writing $\Delta = \sqrt{A/(K_u + NK_d \sin^2\varphi)}$ where K_u is the magnitude of the transverse hard anisotropy direction, and N the demagnetizing coefficient along y[158]. This also means that the maximum velocity is reduced, compared with the above simplified equations.

In these notes the discussion is restricted to the case of a one-dimensional model. This hypothesis is analogous to the case of magnetization switching described by the Stoner-Wohlfarth model. We have already mentioned that this hypothesis can be too strong, in which case the model may largely overestimate the actual switching field of a realistic sample. Here, for finite-width strips the 1d model overestimates the energy barrier preventing the core of the wall from performing an azimuthal rotation, because of the hypothesis of invariance of magnetization across the strip. Micromagnetic simulations show that a microscopic scenario allows to switch the core of the wall at a threshold much below the Walker field. Starting from a transverse wall, it consists of the nucleation of a vortex or antivortex at the edge of the strip, which progressively inverts the transverse component of the transverse wall by moving towards the opposite edge. Thus, a parallel can be made with the breakdown of the Stoner-Wohlfarth model, when incoherent switching mechanism occur, consisting of nucleation and propagation steps. Here, in a finite-width the magnetization texture has a 2d feature; the transverse component of the wall is a 1d object, which can be switched by the propagation of an essentially 0d object (the core of a vortex or antivortex)

Orders or magnitude are the following. In the 1D model, for $\alpha \simeq 0.01$ and $\mu_0 M_s \simeq 1\,\mathrm{T}$, the Walker field $\mu_0 H_W$ is of the order of a few millitesla, while the Walker speed is of the order of 1 km/s. In finite-width strips the Walker breakdown occurs. In realistic systems these values are somewhat lower, mostly due to the finite-size effect decribed above.

Summary

Domain wall motion driven by magnetic field. We considered the one-dimensional case with a head-to-head domain wall as a model, for which all features of the wall motion can be derived analytically, assuming some reasonable assumptions. For cylinders the main feature is the azimuthal precessional of the wall core around the applied field, while the wall mobility (speed over field) is low because inversely proportional to damping α. To the contrary, for strips (characterized by an azimuthal dependance of the demagnetizing field) the initial mobility is high and proportional to α, before dropping at the so-called Walker field due to the reentrance of azimuthal precession. In real strips, due to the finite width, or even more so in extended thin films, micromagnetic processes are more complex and both the Walker field and the speed are often reduced.

Problems for Chapter IV

Problem 1: Self-testing

1. What is the gyromagnetic ratio γ? What is the difference between γ and γ_0?
2. Write the Landau-Lifshitz-Gilbert equation, including the precessional and the damping terms.
3. What is the expression of the generalized effective field?
4. Describe the trajectory of magnetization for undamped precession: a. of an isolated moment around a fixed magnetic field b. in a body subject to an internal demagnetizing field.
5. What is a spin wave?
6. What is the most efficient direction of applied field to switch magnetization in the precessional regime?
7. Explain why precessional switching can be achieved for a magnitude of applied field lower than that in the Stoner-Wohlfarth model.

Problem 2: Short questions

1. Demonstrate Eq.(IV.1).
2. Following Landau-Lifshitz equations (sec.1.3), a system reaches equilibrium if at any point the effective field is parallel to magnetization. Give an example of a system at equilibrium where the effective field is zero, and one with a non-zero effective field.
3. Explain what happens microscopically for the ferromagnetic resonance of a thin film of soft magnetic material under a static perpendicular field with magnitude smaller than magnetization.
4. In sec.1.1 we introduced the complex variable $Z = \mu_x + i\mu_y$ to solve the simple case of precession of an isolated moment. Which variable should be introduced to address the case of precession under an in-plane static field from Eq.(IV.7)?

5. In Figure IV.8 no switching occurs for $3\pi/4 < \theta_H < 5\pi/4$, whatever the pulse magnitude, width and length. Proove that indeed no switching can occur.

Problem 3: Effective fields

All effective fields affect the precession of magnetization. The formulas given in sec.1.2 are given for simple geometries and external applied field plus dipolar field only. They need to be adapted in case magnetocrystalline anisotropy or exchange energy contribute to internal fields. It is the purpose of this problem to provide a glimpse on these fields and their use. In Eq.(IV.6) we introduced the general form for the total effective field, which we will use in the following.

3.1. Anisotropy fields

1. Consider a uniaxial anisotropy of second order: $E_a = K\sin^2\theta = K(1 - m_z^2)$. Compute the associated effective field H_K, called the anisotropy field. On one single graph, plot the energy and the field versus the direction of magnetization, and comment.
2. Consider now a fourfold anisotropy of second order in the (x, y) plane: $E_a = K_4\sin^4\theta$. Compute the anisotropy field. Plot again energy and field, and comment.

3.2. The exchange field

We consider the exchange energy with volume density $E_{ex} = A\sum_i(\boldsymbol{\nabla} m_i)^2$. Due to the spatial derivative a variational treatment is required. Estimate the impact of an infinitesimal functional variation $\delta\mathbf{m}$ on the total energy $\delta\mathcal{E} = \int_\mathcal{V}\delta E\ \mathrm{d}\mathcal{V}$. Proceeding through identification with $\delta\mathcal{E} = -\mu_0 M_s\int_\mathcal{V}\mathbf{H}_{ex}\cdot\delta\mathbf{m}\,\mathrm{d}\mathcal{V}$, find the form of the exchange field: $H_{ex} = (2A/\mu_0 M_s)\delta\mathbf{m}$

3.3. Cases combining anisotropy and exchange

1. Consider a simple wall such as in sec.I.5. Compute the anisotropy and exchange fields for the simple linear model; comment. Consider the exact wall profile; comment about equilibrium of magnetization at any point.

Problem 4: Precessional switching of magnetization

We consider the precessional dynamics of magnetization in a uniformly-magnetized body and neglect energy losses. We focus on a thin film infinitely extended in the lateral directions (Figure IV.10). We assume a uniaxial anisotropy

of second order with volume density K and easy direction along x. The system is initially at rest with uniform magnetization along $+\hat{\boldsymbol{x}}$. Starting at time $t = 0$ a constant magnetic field of strength $H > 0$ is abruptly applied along $+\hat{\boldsymbol{y}}$.

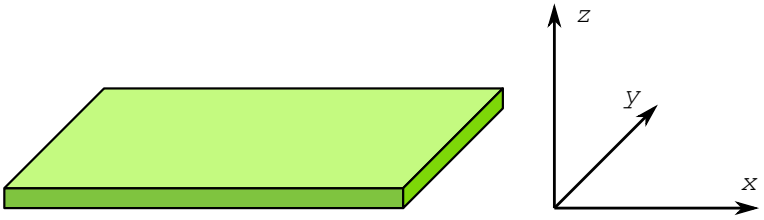

Figure IV.10 – Definition of axes for an extended thin film with normal along $\hat{z}$.

4.1. Energy

Express the volume density of energy E (Zeeman + internal) of the system in terms of all three components of magnetization M_i. Normalizing magnetization **M** and magnetic field **H** with M_s (write these **m** and **h**), and energy densities with $\mu_0 M_s^2$, provide the volume density of energy e in reduced units. We will write h_K the reduced anisotropy field associated with K: $H_K = 2K/(\mu_0 M_s)$.

4.2. Equations of motion

Based on the conservation of energy, provide the equations of the trajectory in the (x, y) plane and in the (y, z) plane. Show that these are equations of ellipses.

4.3. Small angle precession

First consider the case $h \ll h_K$. Based on the above equations sketch the trajectories in the (x, y) and (y, z) planes. To determine the sign of m_y remember that magnetization obeys equation:

$$\frac{\mathrm{d}\mathbf{m}}{\mathrm{d}t} = \gamma \mathbf{m} \times \mu_0 \mathbf{H} \tag{IV.32}$$

where $\gamma < 0$ is the gyromagnetic ratio. Comment.

4.4. Magnetization switching

Precessional switching (magnetization going from initially $+\hat{\boldsymbol{x}}$ to the $-\hat{\boldsymbol{x}}$ direction) may be possible if $m_x = 0$ is reached on the trajectory. Still based on the above equations, determine the value of m_y for which m_x may be zero. Discussing the constraints on m_y, show that this condition is met if $h \geq h_K/2$. Computing e for $m_x = 1$ and $m_y = 1$, explain why switching may be possible under this condition

whereas $h \geq h_K$ is required in the static Stoner-Wohlfarth model.

Problem 5: Damping

We consider precession around a magnetic field of constant magnitude H_0, as in sec.1.1. Being an external field, $\mathbf{H}_0$ does not depend on the direction of magnetization. We will use spherical coordinates, with the z axis chosen along H_0. The unit vectors will be named $\hat{\boldsymbol{r}}$, $\hat{\boldsymbol{\theta}}$ and $\hat{\boldsymbol{\varphi}}$. Damping is accounted for with the LLG equation, with damping parameter α (sec.1.3). We will derive solutions in the limit $\alpha \ll 1$, for which damping effects will be treated pertubatively.

5.1. Damping for free oscillations

1. First neglect damping. Express the rate of change of magnetization $\mathrm{d}\mathbf{m}/\mathrm{d}t$, based on the unit vectors of the spherical coordinates. Deduce $\theta(t)$ and $\varphi(t)$, starting from the state of magnetization $(\theta, \varphi) = (\theta_0, 0)$. We will write $\omega_0 = |\gamma_0| H_0$. Describe the motion and the meaning of ω_0
2. We now consider damping pertubatively, based on the previous result for $\mathrm{d}\mathbf{m}/\mathrm{d}t$. Show that $\mathrm{d}\theta/\mathrm{d}t = -\alpha\omega_0 \sin\theta$
3. Solve the above equation starting from the initial condition $\theta(t_0) = \theta_0$.
4. We first consider small angle precession: $\theta_0 \ll 1$. Simplify the previous equations in that case, and express $\theta(t)$ and $\mathrm{d}\theta/\mathrm{d}t$. What is the typical time scale and number of turns towards the final equilibrium state?
5. We now consider large angle precession. Express $\mathrm{d}\theta/\mathrm{d}t$ for $\theta = \pi/2$. Comment, with respect to the previous result. Provide an estimate of the time needed to approach the equilibrium state starting from θ_0 with an arbitrary value.

5.2. Damping in ferromagnetic resonance

We now consider small-angle resonance ($\theta \ll 1$), sustained by an external excitation. The excitation is considered to be a field of constant magnitude h, rotating in the (x, y) plane at the angular frequency ω. It is easier to seek solutions with the complex notation for vector components in the (x, y) plane, while the component along $\mathbf{u}_z$ is still described by a real number. Thus, any vector $\mathbf{B}$ may be described by the set (β, B_z). As a shortcut we will write: $\mathbf{B} = (\beta, B_z)$. Thus, the excitation field will be written: $\mathbf{h} = (H_0\eta, 0)$ with $\eta = \eta_0 \exp(i\omega t)$ and $\eta \ll 1$. In the limit of small angle precession, the reduced magnetization will be written: $\mathbf{m} = (\mu, 1)$, with $|\mu| \ll 1$

1. Show that $(0, 1) \times (\beta, 1) = (i\beta, 0)$, and: $(\beta, 0) \times (\gamma, 0) = (0, \mathfrak{Im}(i\beta\overline{\gamma}))$ with $\overline{\gamma}$ the complex conjugate of γ. We may write $\mathfrak{Im}(i\beta\overline{\gamma}) = (\beta\overline{\gamma} - \overline{\beta}\gamma)/2$.
2. To get used to the complex notation, express $\mathrm{d}\mathbf{m}/\mathrm{d}t$ with no damping and no excitation. Show that this results in $\mathrm{d}\mu/\mathrm{d}t = -i\gamma_0 H_0 \mu$, and make the link

with the result of free precession described in the previous part. Consider now non-zero damping, and express $\mathrm{d}\mu/\mathrm{d}t$ again. Integrate this differential equation and again make the link with the result of the previous part.

3. Consider now both damping and excitation **h**. We will neglect all second-order terms, *i.e.* those in $\alpha\mu$, $\alpha\eta$ and $\eta\mu$. Apply Eq.(IV.18) and show that this yields: $\mathrm{d}\mu/\mathrm{d}t = (i - \alpha)\omega_0\mu - i\omega_0\eta$.
4. Solve the above equation seeking a solution with the form: $\mu = \mu_0 \exp(i\omega t)$. Express the magnitude and the phase of the response, and make graphs. Calculate the full width at half maximum $\Delta\omega$ of the amplitude signal.
5. Draw and discuss the various torques at play in Eq.(IV.18) at resonance: $\omega = \omega_0$.

Appendices

Symbols

A	Exchange stiffness	Defines the micromagnetic volume density of exchange energy $E_{\text{ex}} = A(\nabla \mathbf{m})^2$, measured in J/m
$\mathbf{B}$	Magnetic induction	Tesla is the unit for $\mathbf{B}$, and $\operatorname{div} \mathbf{B} = 0$ is one of Maxwell's equations.
E_{mc}	Volume density of magnetocristalline anisotropy	
E_{Z}	Volume density of Zeeman energy	Measured with J/m^3.
$\mathcal{E}_{\text{Z}}$	Zeeman energy	Integrated over an entire system, and measured with J.
g	Landé factor	$g = 1$ for magnetic moments of purely orbital origin, and $g \approx 2$ for magnetic moments of purely spin origin.
$\mathbf{H}$	Magnetic field	Measured in A/m. $\mu_0 \mathbf{H}$ is the induction sensed by local magnetic moments giving rise to magnetization.
$\mathbf{H}_{\text{d}}$	Dipolar field, or demagnetizing field	Dipolar field is the general name for magnetic field arising from a distribution of magnetization in space. Demagnetizing field is the name when this field is considered inside the magnetic body itself.
I	Electric current	Measured with A.
$\mathbf{j}$	Volume density of electric current	Measured with A/m^2.
J	Interatomic exchange energy	Example: $\mathcal{E}_{12} = -J\mathbf{S}_1 \cdot \mathbf{S}_2$.
K_{d}	Dipolar constant	$K_{\text{d}} = \frac{1}{2}\mu_0 M_{\text{s}}^2$, measured in J/m^3.
K_{u}	Uniaxial anisotropy constant	For the case of magnetic anisotropy: $E_{\text{a}} = K_{\text{u}} \sin^2 \theta$, measured in J/m^3.

$\mathbf{M}$, M	Magnetization (vector and magnitude)	General definition such as in Maxwell's equations, making no hypothesis in the origin of magnetization, spontaneous or induced (susceptibility).
$\mathbf{m}$	Local unit vector parallel to magnetization.	
$\mathcal{M}$	The total moment of magnetic system	In the case of uniform magnetization, $\mathcal{M} = M_s V$ with V the volume of the system
$\mathbf{M}_s$, M_s	Spontaneous magnetization	Magnetization when it arises from magnetic ordering
N	Demagnetizing coefficient	May be written N_i for the coefficient along a main direction i; or more generally the tensor coefficient N_{ij} such that $\langle \mathbf{H}_d \rangle = -\overline{\overline{\mathbf{N}}} \cdot \mathbf{M}$.
ℓ	An angular momentum	
Q	Quality factor	$Q = K_{mc}/K_d$ for the micromagnetic quantity. Also used with a different meaning in the context of atomic force microscopy.
γ	Gyromagnetic ratio	$\gamma = ge/2m$
Γ_W	Energy of a domain wall, per unit area	
Δ_u	Anisotropy exchange length	$\Delta_u = \sqrt{A/K}$ with A the exchange stiffness and K the anisotropy constant. Also sometimes called: Bloch wall parameter
Δ_d	Dipolar exchange length	$\Delta_d = \sqrt{A/K_d} = \sqrt{2A/\mu_0 M_s^2}$ with A the exchange and M_s the spontaneous magnetization. Also sometimes called: exchange length.
$\boldsymbol{\mu}$, μ	A pinpoint magnetic dipole	
μ_0	Magnetic permeability in vacuum	$\mu_0 = 4\pi \times 10^{-7}$ H/m
ϕ_d	Scalar potential for the dipolar field $\mathbf{H}_d$	$\mathbf{H}_d = -\mathbf{grad}\,\phi_d$
ω_0	Resonance frequency	Used in various context: atomic force microscopy; ferromagnetic resonance.

Acronyms

AFM	Atomic Force Microscopy
EMF	Electromotive force
LL	Landau-Lifshitz (for the equation describing the time evolution of magnetization)

LLG	Landau-Lifshitz-Gilbert (for the equation describing the time evolution of magnetization)
MAE	Magnetic Anisotropy Energy
MFM	Magnetic Force Microscopy
PMA	Perpendicular Magnetic Anisotropy
SEMPA	Scanning Electron Microscopy with Polarization Analysis
SPLEEM	Spin-Polarized Low-Energy Electron Microscopy
SQUID	Superconducting Quantum Interference Device
TXM	Transmission X-ray Microscopy
UHV	Ultra-High Vacuum
VSM	Vibrating Sample Magnetometer

Glossary

creep	Propagation in the creep regime: the domain wall remains most of the time at rest, and moves forward only in the form of discrete jumps, which are thermally activated .
erg	Unit for energy in the cgs-Gauss system. Is equivalent to 10^{-7} J.
Extrinsic	In the context of magnetization processes, an effect related to inhomogeneities, also called defects, such as grains or grain boundaries, multi-phased materials, roughness etc.
Intrinsic	In the context of magnetization processes, an effect related to the material parameters (anisotropy, magnetization, exchange) and the sample shape only.
Macrospin	The model where uniform magnetization is assumed in a system, whose description may thus be restricted to the knowledge of one or two degrees of freedom, the angular directions of a hypothetical spin. When formerly written as a variable, the macrospin may be dimensionless, or have units of A.m^2 for a volume, A.m for magnetization integrated over a surface (*e.g.* that of a nanowire), or A for magnetization integrated along a thickness (*e.g.* that of a thin film).
Micromagnetism	All aspects related the arrangement of magnetization in domains and domain walls, when the latter are resolved (*i.e.*, not treated as a plane with zero thickness nor energy). The term applies to theory, simulation and experiments. Except some rare cases that may be considered as fine points, micromagnetism is based on the description of magnetization by a continuous function of constant and homogeneous magnitude equal to the spontaneous magnetization M_s.

Nanomagnetism — Broadly speaking, all aspects of magnetism at small length scale, typically below one micrometer. This concerns ground-state (intrinsic) properties such as magnetic ordering and magnetic anisotropy, as well as magnetization configurations and magnetization reversal at these small scales. Notice that some persons restrict the meaning of Nanomagnetism to the former.

Bibliography

[1] S. Blundell, Magnetism in condensed matter, Oxford University Press, 2001, a basic however clear and precise review of magnetism in condensed matter. Definitely a major reference.

[2] R. Skomski, Simple models of magnetism, Oxford, 2008, an excellent entry point for magnetism, especially nanomagnetism. Simple and hand-waving presentations, with references for readers seeking a deeper insight.

[3] J. M. D. Coey, Magnetism and magnetic materials, Cambride University Press, 2010, an excellent book about magnetism. Of particular interest for reviewing properties of various types of materials and compounds. To read absolutely.

[4] C. L. Dennis, R. P. Borges, L. D. Buda, U. Ebels, J. F. Gregg, M. Hehn, E. Jouguelet, K. Ounadjela, I. Petej, I. L. Prejbeanu, M. J. Thornton, The defining length scales of mesomagnetism: a review, J. Phys.: Condens. Matter 14, R1175–R1262 (2002).

[5] R. Skomski, Nanomagnetics, J. Phys.: Condens. Matter 15, R841–896 (2003), review: overview of fundamental and micromagnetic aspects (static and dynamic) of growth and artificial magnetic nanostructures.

[6] A. Hubert, R. Schäfer, Magnetic domains. The analysis of magnetic microstructures, Springer, Berlin, 1999, micromagnetic theories and experimental results, imaging techniques.

[7] A. P. Guimaraes, Principles of Nanomagnetism, Springer, 2009.

[8] F. Cardarelli, Encyclopedia of Scientific units, weights and measures, Springer, London, 2003, comprehensive reference about units: systems, conversions, and incredible set of units in all fields of physics and beyond.

[9] Bureau International des Poids et Mesures.
URL http://www.bipm.org/

[10] J. STÖHR, H. C. SIEGMANN, Magnetism – From fundamentals to nanoscale dynamics, no. 152 in Springer series in Solid-State Sciences, Springer, Heidelberg, 2006, comprehensive review book on Magnetism. Slightly annoying with respect to the choice of defining $\mathbf{B} = \mu_0\mathbf{H} + \mathbf{M}$.

[11] W. F. BROWN, Theory of the Approach to Magnetic Saturation, Phys. Rev. 58, 736–743 (1940).

[12] A. HUBERT, W. RAVE, Systematic Analysis of Micromagnetic Switching Processes, Phys. Stat. Sol. (b) 211 (2), S815–829 (1999).

[13] E. C. STONER, The demagnetization factors for ellipsoids, Philos. Mag. 36, 803–821 (1945).

[14] P. RHODES, G. ROWLANDS, Demagnetizing energies of uniformly magnetized rectangular blocks, Proc. Leeds Phil. Liter. Soc. 6, 191 (1954), demagnetizing factor in rectangular blocks.

[15] A. AHARONI, Demagnetizing factors for rectangular ferromagnetic prisms, J. Appl. Phys. 83 (6), 3432–3434 (1998).

[16] G. ROWLANDS, Magnetising energies and domain structures in ferromagnetics, Ph.D. thesis, University of Leeds, Leeds (1956).

[17] D. A. GOODE, G. ROWLANDS, The demagnetizing energies of a uniformly magnetized cylinder with an elliptic cross-section, J. Magn. Magn. Mater. 267, 373–385 (2003).

[18] B. BORCA, O.FRUCHART, E.KRITSIKIS, F.CHEYNIS, A.ROUSSEAU, PH.DAVID, C.MEYER, J. TOUSSAINT, Tunable magnetic properties of arrays of Fe(110) nanowires grown on kinetically grooved W(110) self-organized templates, J. Magn. Magn. Mater. 322 (2), 257 (2010).

[19] G. ROWLANDS, On the calculation of acoustic radiation impedance of polygonal-shaped apertures, J. Acoust. Soc. Am. 92 (5), 2961–2963 (1992).

[20] M. BELEGGIA, M. DE GRAEF, On the computation of the demagnetization tensor field for an arbitrary particle shape using a Fourier space approach, J. Magn. Magn. Mater. 263, L1–9 (2003).

[21] M. BELEGGIA, M. DE GRAEF, Y. T. MILLEV, Magnetostatics of the uniformly polarized torus, Proc. Roy. Soc. Lond. A 465, 3581 (2009).

[22] J. C. MAXWELL, A Treatise on Electricity and Magnetism, 3rd Edition, Vol. 2, Clarendon, Oxford, 1872.

[23] B. A. LILLEY, Energies and widths of domain boundaries in ferromagnetics, Philos. Mag. 41 (7), 401–406 (1950).

[24] J. P. JAKUBOVICS, Comments on the definition of ferromagnetic domain wall width, Philos. Mag. B 38 (4), 401–406 (1978).

[25] A. A. THIELE, Steady-State Motion of Magnetic Domains, Phys. Rev. Lett. 30 (6), 230–233 (1973).

[26] P. BRUNO, Geometrically Constrained Magnetic Wall, Phys. Rev. Lett. 83 (12), 2425 (1999).

[27] Y. ZHU (Ed.), Modern techniques for characterizing magnetic materials, Springer, Berlin, 2005, `covers many characterization techniques, including microscopies.`

[28] H. HOPSTER, H. P. OEPEN (Eds.), Magnetic Microscopy of Nanostructures, Springer, 2005.

[29] H. KRONMÜLLER, S. S. P. PARKIN (Eds.), Handbook of magnetism and advanced magnetic materials, Wiley, 2007, `several thousands of pages of review articles dedicated to many topics in Magnetism. Always to be checked when you search for something.`

[30] J. STÖHR, Exploring the microscopic origin of magnetic anisotropies with X-ray magnetic circular dichroism (XMCD) spectroscopy, J. Magn. Magn. Mater. 200, 470–497 (1999).

[31] E. BAUER, Low energy electron microscopy, Rep. Prog. Phys. 57, 895–938 (1994).

[32] E. BAUER, Surface Microscopy with Low Energy Electrons, Springer, New-York, 2014.

[33] J. VOGEL, S. CHERIFI, S. PIZZINI, F. ROMANENS, J. CAMARERO, F. PETROFF, S. HEUN, A. LOCATELLI, Layer-resolved imaging of domain wall interactions in magnetic tunnel junction-like trilayers, J. Phys.: Condens. Matter 19, 476204 (2007).

[34] P. FISCHER, T. EIMÜLLER, G. SCHÜTZ, G. DENBEAUX, A. PEARSON, L. JOHNSON, D. ATTWOOD, S. TSUNASHIMA, M. KUMAZAWA, N. TAKAGI, M. KÖHLER, G. BAYREUTHER, Element-specific imaging of magnetic domains at 25 nm spatial resolution using soft x-ray microscopy, Rev. Sci. Instr. 72 (5), 2322 (2001).

[35] R. BELKHOU, S. STANESCU, S. SWARAJ, A. BESSON, M. LEDOUX, M. HAJLAOUI, D. DALLE, HERMES: a soft X-ray beamline dedicated to X-ray microscopy, J. Synchro. Radiat. 22 (4), 968–979 (2015).

[36] P. EATON, P. WEST, Atomic force microscopy, Oxford, 2010.

[37] R. WIESENDANGER, Spin mapping at the nanoscale and atomic scale, Rev. Mod. Phys. 81, 1495 (2009).

[38] W. WULFHEKEL, J. KIRSCHNER, Spin-polarized scanning tunneling microscopy on ferromagnets, Appl. Phys. Lett. 75 (13), 1944 (1999).

[39] J. A. FISCHER, L. M. SANDRATSKII, S.-H. PHARK, S. OUAZI, A. A. PASA, D. SANDER, S. S. P. PARKIN, Probing the spinor nature of electronic states in nanosize non-collinear magnets, Nat. Commun. 7, 13000 (2016).

[40] K. VON BERGMANN, S. HEINZE, M. BODE, E. VEDMEDENKO, G. BIHLMAYER, S. BLÜGEL, R. WIESENDANGER, Observation of a Complex Nanoscale Magnetic Structure in a Hexagonal Fe Monolayer, Phys. Rev. Lett. 96, 167203 (2006).

[41] L. GERHARD, T. K. YAMADA, T. BALASHOV, A. F. TAKACS, R. J. H. WESSELINK, M. DANE, M.FECHNER, S. OSTANIN, A. ERNST, I. MERTIG, W. WULFHEKEL, Electrical Control of the Magnetic State of Fe, IEEE Trans. Magn. 47 (6), 1619 (2011).

[42] M. S. GRINOLDS, S. HONG, P. MALETINSKY, L. LUAN, M. D. LUKIN, R. L.WALSWORTH, A. YACOBY, Nanoscale magnetic imaging of a single electron spin under ambient conditions, Nat. Phys. 9, 215 (2013).

[43] O. FRUCHART, A. MASSEBOEUF, J. C. TOUSSAINT, P. BAYLE-GUILLEMAUD, Growth and micromagnetism of self-assembled epitaxial fcc(111) cobalt dots, J. Phys.: Condens. Matter 25, 496002 (2013).

[44] T. TANIGAKI, Y. TAKAHASHI, T. SHIMAKURA, T. AKASHI, R. TSUNETA, A. SUGAWARA, D. SHINDO, Three-Dimensional Observation of Magnetic Vortex Cores in Stacked Ferromagnetic Discs, Nano Lett. 15, 1309 (2015).

[45] R. ALLENSPACH, Modern Techniques for Characterizing Magnetic Materials, Kluwer, Boston, 2005, Ch. Spin-polarized microscopy scanning electron microscopy, pp. 327–360.

[46] G. STEIERL, G. LIU, D. IORGOV, J. KIRSCHNER, Surface domain imaging in external magnetic fields, Rev. Sci. Instr. 73 (12), 4264 (2002).

[47] R. FRÖMTER, H. P. OEPEN, J. KIRSCHNER, A miniaturized detector for high-resolution SEMPA, Appl. Phys. A 76, 869–871 (2003).

[48] E. BAUER, Modern Techniques for Characterizing Magnetic Materials, Kluwer, Boston, 2005, Ch. Spin-polarized low energy electron microscopy (SPLEEM), pp. 361–379.

[49] N. ROUGEMAILLE, A. K. SCHMID, Magnetic imaging with spin-polarized low-energy electron microscopy, Europhys. J.: Appl. Phys. 50, 20101 (2010).

[50] F. BLOCH, Zur Theorie der Austauschproblems und der Remanenzerscheinung der Feromagnetika, Z. Phys. 74, 295 (1932).

[51] G. A. T. ALLAN, Critical temperatures of Ising Lattice Films, Phys. Rev. B 1 (1), 352–357 (1970).

[52] U. GRADMANN, Magnetism in ultrathin transition metal films, in: K. H. J. BUSCHOW (Ed.), Handbook of magnetic materials, Vol. 7, Elsevier Science Publishers B. V., North Holland, 1993, Ch. 1, pp. 1–96, review: Magnetic fundamental properties in continuous thin films: methods, magnetic anisotropy, temperature dependance of magnetization, ground state properties (interface magnetization), metastable phases.

[53] L. ONSAGER, Crystal Statistics. I. A Two-Dimensional Model with an Order-Disorder Transition, Phys. Rev. 65, 117–149 (1944).

[54] H. E. STANLEY, T. A. KAPLAN, Possibility of a Phase Transition for the Two-Dimensional Heisenberg Model, Phys. Rev. Lett. 17, 913 (1966).

[55] R. P. ERIKSON, D. L. MILLS, Anisotropy-driven long-range order in ultrathin ferromagnetic films, Phys. Rev. B 43, 11527 (1988).

[56] P. GAMBARDELLA, A. DALLMEYER, K. MAITI, M. C. MALAGOLI, W. EBERHARDT, K. KERN, C. CARBONE, Ferromagnetism in one-dimensional monoatomic metal chains, Nature 416, 301–304 (2002).

[57] J. BANSMANN, S. BAKER, C. BINNS, J. BLACKMAN, J.-P. BUCHER, J. DORANTES-DÀVILA, V. DUPUIS, L. FAVRE, D. KECHRAKOS, A. KLEIBERT, K.-H. MEIWES-BROER, G. M. PASTOR, A. PEREZ, O. TOULEMONDE, K. N. TROHIDOU, J. TUAILLON, Y. XIE, Magnetic and structural properties of isolated and assembled clusters, Surf. Sci. Rep. 56, 189–275 (2005), review of a European project on the subject, mainly focused on clusters.

[58] A. J. COX, J. G. LOUDERBACK, L. A. BLOOMFIELD, Experimental observation of magnetism in rhodium clusters, Phys. Rev. Lett. 71 (6), 923–926 (1993).

[59] A. J. COX, J. G. LOUDERBACK, S. E. APSEL, L. A. BLOOMFIELD, Magnetism in 4d-transition metal clusters, Phys. Rev. B 49 (17), 12295–12298 (1994).

[60] U. GRADMANN, J. MÜLLER, Flat ferromagnetic exitaxial 48Ni/52Fe(111) films of few atomic layers, Phys. Stat. Sol. 27, 313 (1968).

[61] M. T. JOHNSON, P. J. H. BLOEMEN, F. J. A. DEN BROEDER, J. J. DE VRIES, Magnetic anisotropy in metallic multilayers, Rep. Prog. Phys. 59, 1409–1458 (1996).

[62] M. DUMM, B. UHL, M. ZÖLFL, W. KIPFERL, G. BAYREUTHER, Volume and interface magnetic anisotropy of $Fe_{1-x}Co_x$ thin films on GaAs(001), J. Appl. Phys. 91 (10), 8763 (2002).

[63] D. T. D. LACHEISSERIE, Magnetostriction - Theory and Applications of Magnetoelasticity, CRC Press, 1993.

[64] W. A. JESSER, D. KUHLMANN-WILSDORF, On the theory of interfacial energy and elastic strain of epitaxial overgrowth in parallel alignment on single crystal substrates, Phys. Stat. Sol. 19 (1), 95–105 (1967), `first model for` $1/t$ `strain relaxation in thin films related to misfit dislocations.`

[65] C. CHAPPERT, P. BRUNO, Magnetic anisotropy in metallic ultrathin films and related experiments on cobalt films, J. Appl. Phys. 64 (10), 5336–5341 (1988), `first application of the theory of strain relaxation in thin films to the ambiguity if interface and magnetoelastic anisotropy.`

[66] D. SANDER, R. SKOMSKI, A. ENDERS, C. SCHMIDTHALS, D. REUTER, J. KIRSCHNER, The correlation between mechanical stress and magnetic properties of ultrathin films, J. Phys. D: Appl. Phys. 31, 663–670 (1998).

[67] G. BERTOTTI, I. D. MAYERGOYZ, C. SERPICO, M. DIMIAN, Comparison of analytical solutions of Landau-Lifshitz equation for 'damping' and 'precessional' switchings, J. Appl. Phys. 93 (10), 6811–6813 (2003).

[68] C. CHAPPERT, H. BARNAS, J. FERRÉ, V. KOTTLER, J.-P. JAMET, Y. CHEN, E. CAMBRIL, T. DEVOLDER, F. ROUSSEAUX, V. MATHET, H. LAUNOIS, Planar patterned magnetic media obtained by ion irradiation, Science 280, 1919–1922 (1998).

[69] L. NÉEL, énergie des parois de Bloch dans les couches minces, C. R. Acad. Sci. 241 (6), 533–536 (1955).

[70] K. RAMSTÖCK, W. HARTUNG, A. HUBERT, The phase diagram of domain walls in narrow magnetic strips, Phys. Stat. Sol. (a) 155, 505 (1996).

[71] A. E. LABONTE, Two-dimensional Bloch-type domain walls in ferromagnetic thin films, J. Appl. Phys. 40 (6), 2450–2458 (1969).

[72] A. HUBERT, Stray-field-free magnetization configurations, Phys. Stat. Sol. 32 (519), 519–534 (1969).

[73] S. FOSS, R. PROKSCH, E. DAHLBERG, B. MOSKOWITZ, B. WALSCH, Localized micromagnetic perturbation of domain walls in magnetite using a magnetic force microscope, Appl. Phys. Lett. 69 (22), 3426–3428 (1996).

[74] H. JOISTEN, S. LAGNIER, M. VAUDAINE, L. VIEUX-ROCHAZ, J. PORTESEIL, A magnetic force microscopy and Kerr effect study of magnetic domains and cross-tie walls in magnetoresistive NiFe shapes, J. Magn. Magn. Mater. 233, 230 (2001).

[75] W. DÖRING, Point singularities in micromagnetism, J. Appl. Phys. 39 (2), 1006 (1968).

[76] C. KITTEL, Physical theory of ferromagnetic domains, Rev. Mod. Phys. 21 (4), 541–583 (1949).

[77] H. A. M. VAN DEN BERG, A micromagnetic approach to the constitutive equation of soft-ferromagnetic media, J. Magn. Magn. Mater. 44 (1-2), 207–215 (1984).

[78] H. A. M. VAN DEN BERG, Self-consistent domain theory in soft-ferromagnetic media. II. Basic domain structures in thin-film objects, J. Appl. Phys. 60, 1104 (1986).

[79] R. DANNEAU, P. WARIN, J. P. ATTANÉ, I. PETEJ, C. BEIGNÉ, C. FERMON, O. KLEIN, A. MARTY, F. OTT, Y. SAMSON, M. VIRET, Individual Domain Wall Resistance in Submicron Ferromagnetic Structures, Phys. Rev. Lett. 88 (15), 157201 (2002).

[80] M. HEHN, K. OUNADJELA, J. P. BUCHER, F. ROUSSEAUX, D. DECANINI, B. BARTENLIAN, C. CHAPPERT, Nanoscale Magnetic Domains in Mesoscopic Magnets, Science 272, 1782–1785 (1996).

[81] M. DONAHUE, D. PORTER, Interagency Report NISTIR 6376, Tech. rep., National Institute of Standards and Technology, Gaithersburg, MD (1999).

[82] http://math.nist.gov/oommf/.
URL http://math.nist.gov/oommf/

[83] P. O. JUBERT, R. ALLENSPACH, Analytical approach to the single-domain-to-vortex transition in small magnetic disks, Phys. Rev. B 70, 144402/1–5 (2004).

[84] A. THIAVILLE, D. TOMAS, J. MILTAT, On Corner Singularities in Micromagnetics, Phys. Stat. Sol. 170, 125 (1998).

[85] W. RAVE, K. RAMSTÖCK, A. HUBERT, Corners and nucleation in micromagnetics, J. Magn. Magn. Mater. 183, 329–333 (1998).

[86] M. A. SCHABES, H. N. BERTRAM, Magnetization processes in ferromagnetic cubes, J. Appl. Phys. 64 (3), 1347–1357 (1988).

[87] R. P. COWBURN, M. E. WELLAND, Analytical micromagnetics of near single domain particles, J. Appl. Phys. 86 (2), 1035–1040 (1999).

[88] R. DITTRICH, A. THIAVILLE, J. MILTAT, T. SCHREFL, Rigorous micromagnetic computation of configurational anisotropy energies in nanoelements, J. Appl. Phys. 93 (10), 7891–7893 (2003).

[89] A. FERT, J. L. PIRAUX, Magnetic nanowires, J. Magn. Magn. Mater. 200, 338–358 (1999).

[90] R. MCMICHAEL, M. DONAHUE, Head to Head Domain Wall Structures in Thin Magnetic Strips, IEEE Trans. Magn. 33, 4167 (1997).

[91] E. C. STONER, E. P. WOHLFARTH, A Mechanism of Magnetic Hysteresis in Heterogeneous Alloys, Phil. Trans. Roy. Soc. Lond. A 240, 599–642 (1948).

[92] E. C. STONER, E. P. WOHLFARTH, reprint of 1948 'A Mechanism of Magnetic Hysteresis in Heterogeneous Alloys', IEEE Trans. Magn. 27 (4), 3469–3518 (1991).

[93] J. C. SLONCZEWSKI, Theory of magnetic hysteresis in films and its applications to computers, Tech. Rep. RM 003.111.224, IBM Research Center, Poughkeepsie, NY (1956).

[94] A. THIAVILLE, Extensions of the geometric solution of the two dimensional coherent magnetization rotation model, J. Magn. Magn. Mater. 182, 5–18 (1998).

[95] B. BORCA, O. FRUCHART, C. MEYER, Magnetic properties of self-organized lateral arrays of (Fe,Ag)/Mo(110) nanostripes, J. Appl. Phys. 99, 08Q514 (2005).

[96] O. FRUCHART, P. O. JUBERT, C. MEYER, M. KLAUA, J. BARTHEL, J. KIRSCHNER, Vertical self-organization of epitaxial magnetic nanostructures, J. Magn. Magn. Mater. 239, 224–227 (2002).

[97] A. TAMION, M. HILLENKAMP, F. TOURNUS, E. BONET, V. DUPUIS, Accurate determination of the magnetic anisotropy in cluster-assembled nanostructures, Appl. Phys. Lett. 95, 062503 (2009).

[98] A. TAMION, E. BONET, F. TOURNUS, C. RAUFAST, A. HILLION, O. GAIER, V. DUPUIS, Efficient hysteresis loop simulations of nanoparticle assemblies beyond the uniaxial anisotropy, Phys. Rev. B 85, 134430 (2012).

[99] W. F. J. BROWN, Criterion for uniform micromagnetization, Phys. Rev. 105, 1479 (1957).

[100] E. H. FREI, S. SHTRIKMAN, D. TREVES, Critical Size and Nucleation Field of Ideal Ferromagnetic Particles, Phys. Rev. 106, 446 (1957).

[101] S. SHTRIKMAN, D. TREVES, The coercive force and rotational hysteresis of elongated ferromagnetic particles, J. Phys. Rad. 20, 286 (1959).

[102] A. AHARONI, Angular dependence of nucleation by curling in a prolate spheroid, J. Appl. Phys. 82, 1281 (1997).

[103] W. C. UHLIG, J. SHI, Systematic study of the magnetization reversal in patterned Co and NiFe Nanolines, Appl. Phys. Lett. 84 (5), 759 (2004).

[104] K. J. KIRK, J. N. CHAPMAN, C. D. W. WILKINSON, Switching fields and magnetostatic interactions of thin film magnetic nanoelements, Appl. Phys. Lett. 71 (4), 539–541 (1997).

[105] R. P. COWBURN, D. K. KOLTSOV, A. O. ADEYEYE, M. E. WELLAND, Lateral interface anisotropy in nanomagnets, J. Appl. Phys. 87 (9), 7067 (2000).

[106] P. BRYANT, H. SUHL, Thin-film magnetic patterns in an external field, Appl. Phys. Lett. 54, 78 (1989).

[107] P. BRYANT, H. SUHL, Micromagnetic below saturation, J. Appl. Phys. 66, 4329 (1989).

[108] A. DESIMONE, R. V. KOHN, S. MÜLLER, F. OTTO, R. SCHÄFER, Two-dimensional modeling of soft ferromagnetic films, Proc. Roy. Soc. Lond. A 457, 2983–2991 (2001).

[109] A. DESIMONE, R. V. KOHN, S. MÜLLER, F. OTTO, R. SCHÄFER, Low energy domain patterns in soft ferromagnetic films, J. Magn. Magn. Mater. 242-245, 1047–1051 (2002).

[110] A. DESIMONE, R. V. KOHN, S. MÜLLER, F. OTTO, A reduced theory for thin-film micromagnetics, Comm. Pure Appl. Math. 55 (11), 1408–1460 (2002).

[111] P. O. JUBERT, J. C. TOUSSAINT, O. FRUCHART, C. MEYER, Y. SAMSON, Flux-closure-domain states and demagnetizing energy determination in sub-micron size magnetic dots, Europhys. Lett. 63 (1), 132–138 (2003).

[112] M. T. BRYAN, D. ATKINSON, R. P. COWBURN, Experimental study of the influence of edge roughness on magnetization switching in Permalloy nanostructures, Appl. Phys. Lett. 85 (16), 3510 (2004).

[113] F. CAYSSOL, D. RAVELOSONA, C. CHAPPERT, J. FERRÉ, J. P. JAMET, Domain Wall Creep in Magnetic Wires, Phys. Rev. Lett. 92, 107202 (2004).

[114] R. D. MCMICHAEL, J. EICKE, M. J. DONAHUE, D. G. PORTER, Domain wall traps for low-field switching of submicron elements, J. Appl. Phys. 87 (9), 7058 (2000).

[115] T. TANIYAMA, I. NAKATANI, T. YAKABE, Y. YAMAZAKI, Control of domain structures and magnetotransport properties in patterned ferromagnetic wires, Appl. Phys. Lett. 76 (5), 613 (2000).

[116] K. SHIGETO, T. SHINJO, T. ONO, Injection of a magnetic domain wall into a submicron magnetic wire, Appl. Phys. Lett. 75 (18), 2815 (1999).

[117] Y. YOKOYAMA, Y. SUZUKI, S. YUASA, K. ANDO, K. SHIGETO, T. SHINJO, P. GOGOL, J. MILTAT, A. THIAVILLE, T. ONO, T. KAWAGOE, Kerr microscopy observations of magnetization process in microfabricated ferromagnetic wires, J. Appl. Phys. 87 (9), 5618 (2000).

[118] L. THOMAS, R. MORIYA, C. RETTNER, S. S. P. PARKIN, Dynamics of Magnetic Domain Walls Under Their Own Inertia, Science 330, 1810 (2010).

[119] S. MIDDELHOEK, Domain Walls in Thin Ni-Fe Films, J. Appl. Phys. 34 (4), 1054–1059 (1963).

[120] A. V. POHM, C. S. COMSTOCK, 0.75, 1.25 and 2.0 μm wide M-R transducers, J. Magn. Magn. Mater. 54, 1667–1669 (1986).

[121] A. V. POHM, J. M. DAUGHTON, C. S. COMSTOCK, H. Y. YOO, J. HUR, Threshold properties of 1, 2 and 4 μm multilater M-R memory cells, IEEE Trans. Magn. 23, 2575–2577 (1987).

[122] A. V. POHM, J. M. DAUGHTON, K. E. SPEARS, A high output mode for submicron M-R memory cells, IEEE Trans. Magn. 28, 2356–2358 (1992).

[123] N. KIKUCHI, S. OKAMOTO, O. KITAKAMI, Y. SHIMADA, Vertical bistable switching of spin vortex in a circular magnetic dot, J. Appl. Phys. 90 (12), 6548 (2001).

[124] A. THIAVILLE, J. M. GARCÌA, R. DITTRICH, J. MILTAT, T. SCHREFL, Micromagnetic study of Bloch-point-mediated vortex core reversal, Phys. Rev. B 67, 094410 (2003).

[125] F. CHEYNIS, A. MASSEBOEUF, O. FRUCHART, N. ROUGEMAILLE, J. C. TOUSSAINT, R. BELKHOU, P. BAYLE-GUILLEMAUD, A. MARTY, Controlled Switching of Néel Caps in Flux-Closure Magnetic Dots, Phys. Rev. Lett. 102, 107201 (2009).

[126] R. BECKER, Elastic tensions and magnetic characteristics, Phys. ZS 33, 905 (1932), `first mention of connexion of coercivity to pinning forces related to inhomogenities of strain.`

[127] E. KONDORSKI, On the nature of coercive force and irreversible changes in magnetisation, Phys. Z. Sowjetunion 11, 597 (1937).

[128] A. A. IVANOV, V. A. ORLOV, A Comparative Analysis of the Mechanisms of Pinning of a Domain Wall in a Nanowire, Phys. Sol. State 53 (12), 2441 (2011).

[129] A. AHARONI, Reduction in Coercive Force Caused by a Certain Type of Imperfection, Phys. Rev. 119 (1), 127–131 (1960).

[130] G. W. RATHENAU, J. SMIT, A. L. STUYTS, Ferromagnetic properties of hexagonal iron-oxide compounds with and without a preferred orientation, Z. Phys. 133, 250 (1952), `local region with zero anisotropy in the framework of a Kondorski model. Comes prior to AHA1960, however just value of nucleation field, not shape of wall.`

[131] D. SUESS, J. FIDLER, G. ZIMANYI, T. SCHREFL, P. VISSCHER, Thermal stability of graded exchange spring media under the influence of external fields, Appl. Phys. Lett. 92, 173111 (2008).

[132] R. H. VICTORA, Predicted time dependence of the switching field for magnetic materials, Phys. Rev. Lett. 63, 457–460 (1989).

[133] G. D. CHAVES-O'FLYNN, G. WOLF, J. Z. SUN, A. D. KENT, Thermal Stability of Magnetic States in Circular Thin-Film Nanomagnets with Large Perpendicular Magnetic Anisotropy, Phys. Rev. Appl. 4 (2), 024010 (2015).

[134] O. FRUCHART, J.-P. NOZIÈRES, W. WERNSDORFER, D. GIVORD, F. ROUSSEAUX, D. DECANINI, Enhanced coercivity in sub-micrometer-sized ultrathin epitaxial dots with in-plane magnetization, Phys. Rev. Lett. 82 (6), 1305–1308 (1999).

[135] O. FRUCHART, J. C. TOUSSAINT, B. KEVORKIAN, Micromagnetic model of non-collective magnetization reversal in ultrathin magnetic dots with in-plane uniaxial anisotropy, Phys. Rev. B 63 (17), 174418 (2001).

[136] S. LEMERLE, J. FERRÉ, C. CHAPPERT, V. MATHET, T. GIAMARCHI, P. L. DOUSSAL, Domain Wall Creep in an Ising Ultrathin Magnetic Film, Phys. Rev. Lett. 80, 849–842 (1998).

[137] G. HERZER, Grain size dependence of coercivity and permeability in nanocrystalline ferromagnets, IEEE Trans. Magn. 26 (5), 1397 (1990).

[138] G. HERZER, Nanocrystalline soft magnetic materials, J. Magn. Magn. Mater. 112, 258–262 (1992).

[139] R. BECKER, W. DÖRING, Ferromagnetismus, Springer, 1939, `first model of strong pinning of a Bloch domain will a delta-like defect.`

[140] D. D. STANCIL, A. PRABHAKAR, Spin waves. Theory and applications, Springer, New-York, 2009.

[141] J. H. E. GRIFFITHS, Anomalous high-frequency resistance of ferromagnetic materials, Nature 158, 670 (1946), `first report of FMR in ferromagnetic bodies.`

[142] C. KITTEL, Interpretation of Anomalous Larmor Frequencies in Ferromagnetic Resonance Experiment, Phys. Rev. 71 (4), 270–271 (1947).

[143] J. SMIT, H. G. BELJERS, Philips Res. Rep. 10, 113 (1955).

[144] L. BASELGIA, M. WARDEN, F. WALDNER, S. L. HUTTON, J. E. DRUMHELLER, Y. Q. HE, P. E. WIGEN, M. MARYSKO, Derivation of the resonance frequency from the free energy of ferromagnets, Phys. Rev. B 38 (4), 2237 (1988).

[145] M. FARLE, Ferromagnetic resonance of ultrathin metallic layers, Rep. Prog. Phys. 61, 755–826 (1998), `review: methods, theory and experiments (anisotropy, magnetic order).`

[146] M. BAILLEUL, D. OLLIGS, C. FERMON, Propagating spin wave spectroscopy in a permalloy film: A quantitative analysis, Appl. Phys. Lett. 83 (5), 972 (2003).

[147] D. A. GARANIN, Fokker-Planck and Landau-Lifshitz-Bloch equations for classical ferromagnets, Phys. Rev. B 55, 3050 (1997).

[148] I. RADU, K.VAHAPLAR, C. STAMM, T.KACHEL, N. PONTIUS, H. , T. A. OSTLER, J. BARKER, R. L. EVANS, R. W. CHANTRELL, A. TSUKAMOTO, A. ITOH, A. KIRILYUK, T. RASING, A. V. KIMEL, Transient ferromagnetic-like state mediating ultrafast reversal of antiferromagnetically coupled spins, Nature 472, 205 (2011).

[149] C. H. BACK, R. ALLENSPACH, W. WEBER, S. S. P. PARKIN, D. WELLER, E. L. GARWIN, H. C. SIEGMANN, Minimum Field Strength in Precessional Magnetization Reversal, Science 285, 864–867 (1999).

[150] C. SERPICO, I. D. MAYERGOYZ, G. BERTOTTI, Analytical solutions of Landau-Lifshitz equation for precessional switching, J. Appl. Phys. 93 (10), 6909–6911 (2003).

[151] T. DEVOLDER, C. CHAPPERT, Precessional switching of thin nanomagnets: analytical study, Europhys. J. B 36, 57–64 (2003), `a step-by-step paper on the analytical description of precessional switching. Written by experimentalists, easy to read.`

[152] M. BAUER, J. FASSBENDER, B. HILLEBRANDS, Switching behavior of a Stoner particle beyond the relaxation time limit, Phys. Rev. B 61 (5), 3410 (2000).

[153] H. FORSTER, T. SCHREFL, W. SCHOLZ, D. SUESS, V. TSIANTOS, J. FIDLER, Micromagnetic simulation of domain wall motion in magnetic nano-wires, J. Magn. Magn. Mater. 249, 181 (2002).

[154] R. HERTEL, Computational micromagnetism of magnetization processes in nickel nanowires, J. Magn. Magn. Mater. 249, 251 (2002).

[155] N. BIZIERE, C. GATEL, R. LASSALLE-BALIER, M. C. CLOCHARD, J. E. WEGROWE, E. SNOECK, Imaging the Fine Structure of a Magnetic Domain Wall in a Ni Nanocylinder, Nano Lett. 13, 2053 (2013).

[156] S. DA COL, S. JAMET, N. ROUGEMAILLE, A. LOCATELLI, T. O. MENTES, B. S. BURGOS, R. AFID, M. DARQUES, L. CAGNON, J. C. TOUSSAINT, O. FRUCHART, Observation of Bloch-point domain walls in cylindrical magnetic nanowires, Phys. Rev. B 89, 180405 (2014).

[157] N. L. SCHRYER, L. R. WALKER, The motion of 180ř domain walls in uniform dc magnetic fields, J. Appl. Phys. 45 (12), 5406–5421 (1974).

[158] A. THIAVILLE, Y. NAKATANI, Spin dynamics in confined magnetic structures III, Vol. 101 of Topics Appl. Physics, Springer, Berlin, 2006, Ch. Domain-wall dynamics in nanowires and nanostrips, pp. 161–206.